Scalable and Rate Adaptive Wireless Multimedia Multicast

Dissertation

zur Erlangung des Grades des

Doktors der Ingenieurwissenschaften (Dr.-Ing.)

der Naturwissenschaftlich-Technischen Fakultäten
der Universität des Saarlandes

vorgelegt von

Jochen Miroll

Eidesstattliche Versicherung

Hiermit versichere ich an Eides statt, dass ich die vorliegende Arbeit selbstständig und ohne Benutzung anderer als der angegebenen Hilfsmittel angefertigt habe. Die aus anderen Quellen oder indirekt übernommenen Daten und Konzepte sind unter Angabe der Quelle gekennzeichnet. Die Arbeit wurde bisher weder im In- noch im Ausland in gleicher oder ähnlicher Form in einem Verfahren zur Erlangung eines akademischen Grades vorgelegt.

Saarbrücken, 18. September 2013

_____

Jochen Miroll

Kurzzusammenfassung

Die in vorliegender Arbeit aufgezeigten Methoden der paketbasierten drahtlosen digitalen Kommunikation ermöglichen es, Fernsehinhalte, aber auch audio-visuelle Datenströme im Allgemeinen, bei hoher Effizienz an beliebig große Gruppen von Empfängern zu verteilen. Im Fokus dieser Arbeit steht damit die Punkt- zu Mehrpunktübertragung bei begrenzter Ende-zu-Ende Verzögerung. Ein grundlegender Unterschied zur Punkt-zu-Punkt Verbindung zwischen genau zwei miteinander kommunizierenden Sender- und Empfängerstationen liegt in der Übermittlung der Information über erfolgreichen oder nicht erfolgreichen Paketempfang auf Seite der Empfänger. Da die zu übertragende Information am Sender vorliegt, die Information über den Erfolg der Übertragung jedoch ausschließlich beim jeweiligen Empfänger, muss eine Erfolgsmeldung auf dem Rückweg von Empfänger zu Sender erfolgen. Diese Information wird dann zum Beispiel zur einfachen Paketwiederholung im nicht erfolgreichen Fall genutzt, oder aber um die Übertragungsrate an die Kapazität des Kanals anzupassen, oder beides. Grundsätzlich beschäftigt sich diese Arbeit mit der einmaligen, gleichzeitigen Übertragung von Information (einschließlich Wiederholungen) an mehrere Empfänger, wobei ein Vergleich zu an mehrere Empfänger sequentiell redundant übertragenden Systemen (Simulcast MIMO) angestellt wird.

In dieser Arbeit ist die Betrachtung bezüglich eines Rückkanals auf Zeitduplexsysteme beschränkt. In diesen Systemen wird der Kanal für Hin- und Rückweg zeitlich orthogonalisiert. Damit steht für die Übermittlung der Erfolgsmeldung eine beschränkte Zeitdauer zur Verfügung. Je mehr an Kanalzugriffszeit für die Erfolgsmeldungen der potentiell vielen Empfänger verbraucht wird, desto geringer wird die Restzeit, in der dann entsprechend weniger audio-visuelle Nutzdaten übertragbar sind, was sich direkt auf die Dienstqualität auswirkt. Ein in der Literatur weniger ausführlich betrachteter Ansatz ist die gleichzeitige Übertragung von Rückmeldungen mehrerer Teilnehmer auf gleicher Frequenz und bei identischer Bandbreite, sowie unter Nutzung gleichartiger Signale (hier: orthogonale Frequenzmultiplexsignalformung). Das Schema wird in dieser Arbeit daher als zeitliche Aggregation von Rückmeldungen, engl. *feedback aggregation*, bezeichnet. Dabei wird, unabhängig von der Anzahl der Empfänger, eine konstante Zeitdauer für Rückmeldungen genutzt, womit auch der Datendurchsatz durch zusätzliche Empfänger nicht notwendigerweise sinkt. Diese Eigenschaft ist aus statisch konfigurierten und für einen einzigen Zweck konzipierten Systemen, wie z. B. der terrestrischen Fernsehübertragung, bekannt. In dieser Arbeit werden im Gegensatz dazu jedoch am Beispiel von WLAN Mehrzweck- und Mehrbenutzersysteme betrachtet. Es handelt sich in derartigen Systemen zur digitalen Datenübertragung dabei um einen entscheidenden Vorteil, unabhängig von der Empfängeranzahl zu bleiben, da es sonst unweigerlich zu Einschränkungen in der Güte der angebotenen Dienstleistung der allgegenwärtigen digitalen Vernetzung kommen muss.

Vorliegende Arbeit zeigt in diesem Zusammenhang auf, welche Datenraten unter Benutzung von *feedback aggregation* in der Verteilung an mehrere Empfänger und in verschiedenen Szenarien zu erreichen sind. Hierbei zeigt sich, dass das Schema im Zusammenspiel mit einer Adaption der Datenrate an den Übertragungskanal inhärent einen Datenratengewinn durch Mehrbenutzerempfang zu erzielen vermag, wenn ein überlagerter idealer Paketauslöschungsschutz-Code angenommen wird. Des weiteren wird bei der Übertragung mit zeitlich begrenzter Ausführungsdauer, z. B. dem sogenannten *Live*-Fernsehen, aufgezeigt, wie sich die erreichbare Datenrate reduziert und welche Restfehlertoleranz an die Übertragung gestellt werden muss. Hierbei wird ebenso aufgezeigt, wie sich durch Verbesserung der Ratenadaption erstere erhöhen und zweitere verringern lässt. An einem auf handelsüblichen Computer-Systemen realisiertem Prototypen zur Live-Fernsehübertragung können die hierin beschriebenen Mechanismen zu großen Teilen gezeigt werden.

Abstract

The methods that are described in this work enable highly efficient audio-visual streaming over wireless digital communication systems to an arbitrary number of receivers. In the focus of this thesis is thus point-to-multipoint transmission at constrained end-to-end delay. A fundamental difference as compared to point-to-point connections between exactly two communicating sending and receiving stations is in conveying information about successful or unsuccessful packet reception at the receiver side. The information to be transmitted is available at the sender, whereas the information about successful reception is only available to the receiver. Therefore, feedback about reception from the receiver to the sender is necessary. This information may be used for simple packet repetition in case of error, or adaptation of the bit rate of transmission to the momentary bit rate capacity of the channel, or both. This work focuses on the single transmission (including retransmissions) of data from one source to multiple destinations at the same time. A comparison with multi-receiver sequentially redundant transmission systems (simulcast MIMO) is made.

With respect to feedback, this work considers time division multiple access systems, in which a single channel is used for data transmission and feedback. Therefore, the amount of time that can be spent for transmitting feedback is limited. An increase in time used for feedback transmissions from potentially many receivers results in a decrease in residual time which is usable for data transmission. This has direct impact on data throughput and hence, the quality of service. In the literature, an approach to reduce feedback overhead which is based on simultaneous feedback exists. In the scope of this work, simultaneous feedback implies equal carrier frequency, bandwidth and signal shape, in this case orthogonal frequency-division multiplex signals, during the event of the herein termed *feedback aggregation* in time. For this scheme, a constant amount of time is spent for feedback, independent of the number of receivers giving feedback about reception. Therefore, also data throughput remains independent of the number of receivers. This property of audio-visual digital transmission is taken for granted for statically configured, single purpose systems, such as terrestrial television. In the scope of this work are, however, multi-user and multi-purpose digital communication networks. Wireless LANs are a well-known example and are covered in detail herein. In suchlike systems, it is of great importance to remain independent of the number of receivers, as otherwise the service of ubiquitous digital connectivity is at the risk of being degraded.

In this regard, the thesis at hand elaborates at what bit rates audio-visual transmission to multiple receivers may take place in conjunction with feedback aggregation. It is shown that the scheme achieves a multi-user throughput gain when used in conjunction with adaptivity of the bit rate to the channel. An assumption is the use of an ideal overlay packet erasure correcting code in this case. Furthermore, for delay constrained transmission, such as in so-called *live* television, throughput bit rates are examined. Applications have to be tolerant to a certain level of residual error in case of delay constrained transmission. Improvement of the rate adaptation algorithm is shown to increase throughput while residual error rates are decreased. Finally, with a consumer hardware prototype for digital live-TV re-distribution in the local wireless network, most of the mechanisms as described herein can be demonstrated.

Acknowledgments

Contents

Acronyms

syms/s/Hz	symbols per second per Hz
3GPP	Third Generation Partnership Project
AC	access category
ACK	acknowledgement
AIFS	arbitration inter-frame space
AP	access point
ARQ	automated repeat-request
AV	audio/visual
AWGN	additive white Gaussian noise
BA	block acknowledgement
BCH	Bose-Chaudhuri-Hocquengham
BEP	bit error probability
BPSK	binary phase shift keying
BSS	basic service set
cdf	cumulative distribution function
CDMA	code-division multiple access
CNR	carrier-to-noise ratio
CP	cyclic-prefix
CQI	channel quality indication
CRC	cyclic redundancy check
CSI	channel state information
CSMA/CA	carrier sense multiple access with collision avoidance
CTS	clear-to-send
CW	contention window
dB	decibel
DBPS	data bits per symbol
DCF	distributed coordination function
DCT	discrete cosine transform
DFT	discrete Fourier transform
DIFS	DCF inter-frame space
DLNA	Digital Living Network Alliance
DTIM	delivery traffic indication message
DTV	digital television
DVB	Digital Video Broadcast
EDCA	enhanced distributed channel access
EIFS	extended inter-frame space
ES	elementary stream
EVM	error vector magnitude
FCS	frame check sequence
FDMA	frequency-division multiple access

FEC	forward error coding
FFT	fast Fourier transform
FIR	finite impulse response
FLUTE	"file delivery over unidirectional transport"
fps	frames per second
GCR	groupcast with retries
GI	guard interval
GOP	group of pictures
HARQ	hybrid automated repeat-request
HCF	hybrid coordination function
HDTV	high definition television
HLBP	hybrid leader based protocol
HT	IEEE 802.11n high throughput
HTTP	hyper-text transfer protocol
i.i.d.	independent and identically distributed
ICI	inter-carrier interference
IDFT	inverse discrete Fourier transform
IEEE	Institute of Electrical and Electronic Engineers
IETF	Internet Engineering Task Force
IFFT	inverse fast Fourier transform
IFS	inter-frame space
IP	Internet Protocol
IPTV	Internet protocol television
ISI	inter-symbol interference
ISO	International Standards Organization
ITU	International Telecommunication Union
LAN	local area network
LBP	leader based protocol
LDPC	low density parity check
LOS	line-of-sight
LTE	Long-Term Evolution
MAC	medium access control
MAN	metropolitan area network
MATLAB®	*The MathWorks*®Matrix Laboratory
MBMS	multimedia broadcast multicast service
MBSFN	multicast/broadcast single frequency network
MCS	modulation and coding scheme
MDS	maximum distance separable
MIMO	multiple-input multiple-output
MPE	DVB multiprotocol encapsulation
MPEG	Moving Pictures Experts Group
MTU	maximum transmission unit
MU-MIMO	multi-user multiple-input multiple-output
MUDiv	multi-user diversity
NACK	negated acknowledgement
NAL	network abstraction layer
NAV	network allocation vector
nHT	pre-802.11n/ac non high throughput
nL	non-leader receiver
OBO	power amplifier output back-off
OFDM	orthogonal frequency division multiplex
OFDMA	orthogonal frequency division multiple access

OSI	open systems interconnection
PAM	pulse amplitude modulation
PAPR	peak-to-average power ratio
PC	personal computer
PCF	point coordination function
PCR	program clock reference
pdf	probability density function
PEP	packet error probability
PES	packetized elementary stream
PHY	physical layer
PLCP	physical layer convergence procedure
PLL	phase-locked-loop
PRRT	predictably reliable real-time transport
PS	program stream
psd	power spectral density
QAM	quadrature amplitude modulation
QoS	quality of service
QPSK	quarternary phase shift keying
RA	rate adaptation
RFC	request for comments
rms	root-mean-square
RRC	root-raised-cosine
RSSI	received signal strength indication
RTCP	real-time transport control protocol
RTP	real-time transport protocol
RTS	request-to-send
RTSP	real-time streaming protocol
RV	random variable
SC-FDMA	single-carrier frequency division multiple access
SDTV	standard definition television
SFN	single frequency network
SIFS	short inter-frame space
SINR	signal-to-interference-plus-noise ratio
SIR	signal-to-interference ratio
SISO	single-input single-output
SNR	signal-to-noise ratio
STA	wireless station
SU-MIMO	single-user multiple-input multiple-output
TCP	transmission control protocol
TDMA	time-division multiple access
TGaa	IEEE 802.11 task group aa
TGn	IEEE 802.11 task group n
TS	transport stream
TV	television
TXOP	transmit opportunity
UDP	user datagram protocol
UMTS	Univeral Mobile Telecommunications System
UTRA	UMTS Terrestrial Radio Access
VCXO	voltage controlled crystal oscillator
VHT	IEEE 802.11ac very high throughput
VLC	variable-length coding
WLAN	wireless local area network
WSSUS	wide-sense stationary uncorrelated scattering

List of Figures

List of Tables

Overview

Motivation

Distribution of one or more audio/visual (AV) signals to more than one receiver is ubiquitous. Television (TV) may be the most well-known example, video telephony including multiple participants, classroom scenarios and tiled display-wall applications are others. When we speak of "TV" in a classical sense, we refer to a broadcast system designed for *live* audio-visual signal transmission. Assume an event being captured by some recording device (e.g. microphone or camera) is broadcast at the time of recording. In this context, the term "live" implies a constant time delay between an event happening in front of the camera and the captured footage being reproduced e.g. on a *television set*. Within this work, the term "live" is used in this sense, as opposed to the definition of the term *real-time*. In real-time systems a strict delay requirement is given. For example, the International Telecommunication Union (ITU) recommends an upper limit in digital telephony[1] mouth-to-ear delay of less than 400 ms, whereas a satisfying quality of service is achieved below 300 ms. Within this context, in both live and real-time systems, each sink is necessarily consuming content at the exact same rate at which it is produced. The focus in this work is on how to efficiently transmit wireless multicast streams at different delay requirements. The term "live streaming" is herein used for digital AV data transmitted with some delay requirement.

One of the enabling technologies for digital television (DTV) clearly has been video coding. Digital video data rates, measured in bits per second (bps), are considered very high. For example, at a video frame rate of 25 frames per second (fps), uncoded (raw) video data rates are about 124 Mbps for standard definition television (SDTV) and up to 830 Mbps for high definition television (HDTV). These are reduced to a fraction in the order of 10 Mbps or less by digital video coding. In DTV all over the world [1], the Moving Pictures Experts Group (MPEG) family of standards is used for this kind of source coding. Video coding for live streaming is subject to a reduced efficiency as compared to redundancy reduction in pre-recorded sequences. As mentioned above, live content is broadcast at the time of production, hence a source coding algorithm is restricted in the average amount of time it may spend per coding unit. Nevertheless, data rates of digital audio-visual bit streams encoded for live TV can be in the order of several Mbps and can thus be transmitted over satellite, terrestrial and wired television systems, utilizing spectral bandwidth in the order of several megahertz to several ten megahertz.

Broadband Internet access networks, such as Long Term Evolution and Fiber To The Home, or Digital Subscriber Line (DSL) in combination with wireless local area network (WLAN), may achieve data rates that are well in the order of coded live TV requirements. Consequently, they are in principle suited for distribution thereof. HbbTV[2] and dynamic broadcast [2] aim at usage of the plurality of digital communications systems available to the end user, in order to provide an improvement in quality of service and a more rich feature set, as well as a reduction in broadcast transmit power consumption. Internet protocol television (IPTV), as provided by broadband Internet access networks, introduces the possibility of bidirectional communication,

---

[1] ITU-T Recommendation G.114 – One-way transmission time
[2] Hybrid Broadcast Broadband TV, www.hbbtv.org

which is rather unusual for classical television. Internet transport of television however also introduces the problem of shared access to the transmission medium, as opposed to the exclusive use of time and spectrum in classical broadcast.

With respect to the number of users receiving a broadcast program, typically we do not assume any limitation. This important aspect, which we are used to in classical broadcast, is motivation for the work presented herein: Can AV streams be transmitted efficiently to a very large number of receivers via Internet protocols and especially when relying on multi-purpose and best-effort service provided by systems, such as wireless broadband or local area networks?

WLANs according to the Institute of Electrical and Electronic Engineers (IEEE) 802.11 standards (802.11 for short) typically offer limited *broadcast/multicast*, i.e. point-to-multipoint services. Similar to classical wireless television broadcast, Internet Protocol (IP) based 802.11 wireless multicast is an efficient way of distributing multimedia content such as live TV to more than a single receiver. Any data that is transmitted by the base station of a WLAN may be received by any other wireless station associated to this base station (subject to distance, received power, receiver sensitivity and scrambling). In multicast, data shall be received by the group of receivers, i.e. a specific multicast group, that is e.g. subscribed to the same television program. In a strict point-to-point (unicast) scenario, receivers of the exact same data will receive individual copies of the data (i.e. simulcast), resulting in an overhead of at least $n - 1$ for n receivers. Hence, multicast is a promising solution for efficient distribution of television via wireless networks, especially when the number of receivers is large. For a quantification of the term "large", multicast may be compared to simulcast using multiple antennas at sender and receiver terminals. In theory, with i antennas at the sender and o antennas at the receivers, an $i \times o$ multiple-input multiple-output (MIMO) system may increase throughput by a factor of $min(i, o)$ as compared to single antenna systems. The smaller number of antennas and transmit or receive circuitry at either side[3] – sender or receiver – determines the achieveable MIMO throughput. Consequently, multicast will outperform simultaneous unicast (simulcast) MIMO when the number of receivers exceeds the number of practically realizable number of antennas at either side. In WLANs according to amendment 802.11n, a typical number of base station antennas is 4, whereas handheld terminals may be limited to lower numbers due to size constraints.

One reason why some communication system may offer only limited multicast service is the problem of feedback implosion. When data is transmitted to multiple receivers simultaneously, feedback messages issued immediately after data frame reception will arrive at the sender at the same time – in absence of coordination. The problem does not apply to unicast and simulcast, in which only a single receiver may issue feedback at a time for each pre-defined unit of received data. In absence of feedback, however, there is no knowledge at the sender about the state at the receiver. In the most simple case this is a binary state of either success or failure of reception. Unidirectional communication systems, such as broadcast television, are so-called open loop systems, in which an imagined feedback loop is not closed, as feedback is issued by none of the receivers. This has also been the case for 802.11 WLAN multicast, which has changed in 2012 by ratification of amendment 802.11aa. The scheme for multicast feedback and retransmission management specified therein is termed *groupcast with retries (GCR)*. The work at hand deals with multicast feedback schemes for 802.11 WLANs that are avoiding feedback implosion, such as GCR and its alternatives.

The digital communication system that has become the predominant source of *pre-recorded* audio-visual content, as opposed to *live* audio-visual *streaming*, is the Internet. The Internet is a multipoint-to-multipoint bidirectional and shared communication system. In a typical home, corporate or public Internet access scenario, the last hop for Internet protocol packet traversal between source (typically one or multiple *servers)* and sink (typically a *personal computer* or e.g. a so-called smart-TV) may be a WLAN or a mobile broadband network. Due to the set of transmission parameters of these wireless systems not being fixed but potentially variable over time (as opposed to e.g. conventional television, which uses a fixed parameter set once

---

[3]Assuming $min(i, o)$ distinct and uncorrelated channels

deployed), distribution of *live* TV over these kinds of systems becomes a challenging problem. Transmission parameters are variable due to the high dynamic range of wireless communication. In modern wireless networks a number of modulation and coding schemes (MCSs) are defined. Any such MCS combination achieves some bit error probability (BEP) at some given signal-to-noise ratio (SNR). With sophisticated error correction coding this results in MCS-dependent achieveable bit rates, whereas transmission takes place free of error above a lower SNR threshold. Efficient transmission takes place close to the Shannon [3] additive white Gaussian noise (AWGN) channel capacity, a rate of $C = B \cdot log_2(1 + SNR)$ bits per second. As the achievable link-SNR is variable, the bit rate has to be adapted to varying channel conditions by MCS selection. In a multicast scenario, receivers are located at different spatial positions and thus observe a different momentary SNR for the same transmission from a single source. This thesis deals with multicast rate adaptation in orthogonal frequency division multiplex (OFDM) based wireless systems. Consequently, bounds on wireless communication as well as propagation effects and receiver impairments producing the major part of transmit errors are described in the following. Scalable multicast rate adaptation for Internet protocol based audio-visual streaming is evaluated by example of the current prevalent WLAN standard IEEE 802.11. OFDM is used in many different telecommunications systems, such as DSL, WLAN, WiMAX, LTE and DVB, and is becoming the predominant transmit technique in nowadays wireless systems. For this reason, a detailed discussion of OFDM and an overview of different usage models in some of the above named systems are included herein. Furthermore, synchronization is addressed in this work. Generally, a source is emitting a signal at some speed, whereas due to local clock deviation at the sink, the signal would be perceived at a different speed in absence of synchronization. Frequency synchronization is fundamental for avoiding errors due to phase rotation in physical transmission, live streaming and playback.

Contribution

It is shown herein that a leader-based wireless multicast protocol based on positive versus negative feedback jamming by aggregation of feedback from all receivers within the same time slot can be incorporated into the currently most widespread wireless local area networking standard IEEE 802.11. The focus is on the OFDM based variants[4] due to the increasing prevalence of OFDM as a physical layer transmit module in wireless systems. Apart from a description of a possible implementation of the above named scalable multicast mechanisms, the proposal is shown to outperform other approaches to WLAN multicast. Furthermore, it is elaborated how existing algorithms for unicast link adaptation are applicable to multicast rate adaptation.

It is well known that wireless multicast introduces the opportunity to exploit a multicast throughput gain. An increase in multicast throughput may further be achieved by multi-user multiple-input multiple-output (MU-MIMO). Both strategies imply the necessity for non-binary feedback from all receivers, as channel state information is required at the sender. Feedback aggregation multicast may achieve a good portion of the multicast throughput gain without explicit channel state information feedback. Consequently, multicast distribution of e.g. television is efficient and scalable with increasingly large numbers of receivers, outperforming practically feasible multi-antenna simulcast systems. Nevertheless, the proposed mechanisms are supplementary to simulcast MIMO and MU-MIMO multicast.

---

[4]802.11a (5 GHz), 802.11g (2.4 GHz), 802.11n ("high throughput", MIMO) and future 802.11ac ("very high throughput", multi-user MIMO)

Introduction

2.1   Use Cases

As the focus in this work is on multimedia streaming over wireless multicast broadband Internet Protocol (IP) networks, this chapter shall provide an overview over potential use cases, encoding of the content that is transmitted, its formats and properties. With an upper boundary a constant delay is a requirement for live television, bidirectional audio-visual communication or real-time transmission in general. We may thus also speak of *delay constrained* transmission of audio-visual content. In the following, two use cases within the scope of this work are described.

Use Case 1: Local Re-Distribution of Digital Television

The combination of at least one digital (stereo) audio and one digital video signal at a low delay between recording (or playback of pre-recorded material), transmission (e.g. wireless to any arbitrary place within some terrestrial or satellite coverage area) and reproduction (e.g. on a television (TV) set at home) is what we refer to as digital television (DTV). In the case of a video camera recording events as they happen and nearly immediate display on television, we explicitly speak of *live* television. For some recording that was made in the past and of which a (typically redundancy reduced) digital copy is available, playback at some arbitrary point in time after recording may be possible, among other things such as random access, trick-mode (fast-forward and backward) as well as pausing playback. By contrast, live TV is designated to broadcast present events and thus requires the time delay between an event happening in front of the camera and its display on a TV set to be constant over time.

In general, TV broadcast is a mix of live and previously recorded *footage* (i.e. film sequence). A conventional DTV system such as the ones according to the Digital Video Broadcast (DVB) standards family [4] are typically deployed as unidirectional point-to-multipoint digital transmission systems with fixed parameters, resulting in deterministic and, for each stationary receiver, constant delay.

A use case within the scope of this work is the local wireless re-distribution of DTV as depicted in figure 2.1. This case is covered in joint specifications of Digital Living Network Alliance (DLNA) and DVB *services in home networks phase 1* [5] (DVB-HN). According to the aforementioned, multimedia streaming in the home network may optionally be protected by forward error coding (FEC) as described in section 2.5.5.

Use Case 2: Audio-Visual Group Communication

Another important use case in the scope of multimedia broadcast multicast service (MBMS) is bidirectional audio/visual (AV) group communication. An example would be voice and video teleconferencing as depicted in figure 2.2. An important difference to use case 1 is observable with respect to wireless multicast. Here, streaming is done in both directions. In the unidirectional streaming case, a certain level of quality of service (QoS) as provided by the wireless access to the shared medium may be achieved by prioritized downlink medium access scheduling. In the
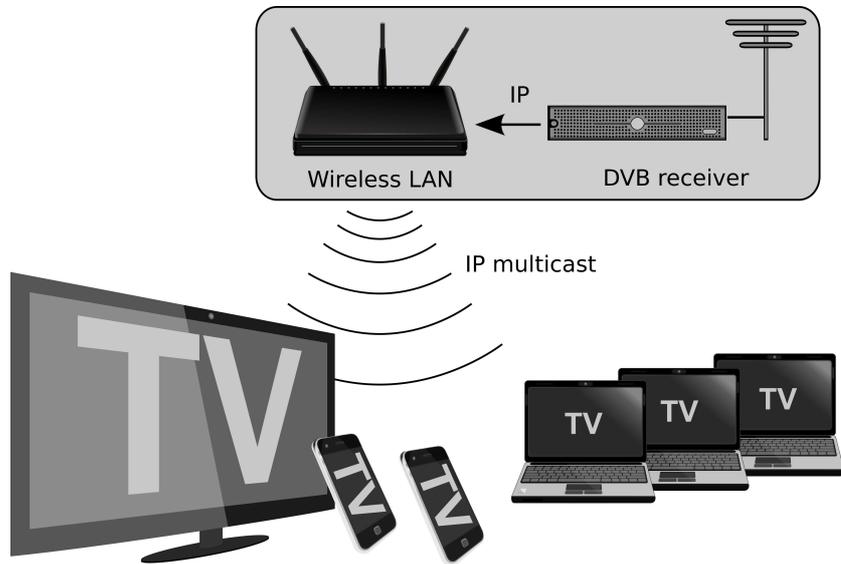
Figure 2.1: Digital television redistribution use case. For example, a DVB receiver may provide one or more individual TV programs via IP to the wireless gateway. Efficient distribution thereof is done in WLAN multicast.
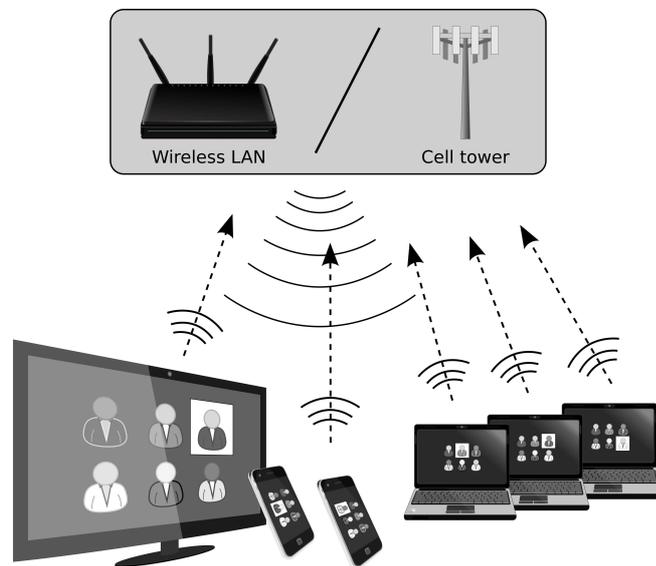
Figure 2.2: Audio-visual group communication use case. For example, a WLAN access point or cellular network base station may relay audio/visual streams received by users back to the users efficiently by multicast. While all user terminals can communicate with the same base station, inter-terminal communication may be impeded.

case of bidirectional streaming, medium access coordination and prioritization of traffic flows at each station (for uplink and downlink) becomes of importance. In the scope of this work, a decentralized scheme as defined in IEEE 802.11e [6, 7] for wireless local area networks (WLANs) is feasible (cf. section 5.3.4.1).

An overview of existing audio-visual coding algorithms for the various fields of application is out of the scope of this work. In the following, an introduction to source coding and transport of digital video streams is given by example of live television.

2.2 Digital Video Sampling and Quantization

In this section, a brief introduction to the requirements of audio-visual transmission under delay constraints with respect to video coding, packetization, as well as clock synchronization is given. In general, audio plays a less important role due to its comparatively low bandwidth requirement. It is merely important to present the audio stream lip-synchronous to the respective video stream.

Research and development of video source coding has been key to the success of digital television. Audio and video signals are typically captured (sampled) at equi-distant intervals. Furthermore, for digital representation of the captured amplitude value at some time instant, a sample is quantized. The sampling rate, for video the so-called frame or refresh rate, is measured in Hz, or frames per second (fps). The rate should satisfy the human auditory or visual sense in a way that the time domain sampling of the real signal is unnoticed. For audio, the required sampling rate is reciprocally proportional to the highest frequencies the human ear can capture, while for video, the visual reproduction at the video frame rate shall be perceived as smooth in case of motion in the visual content. Typically, video signals are sampled at $23-25$ fps [1]. Spatial sampling of video determines a maximum sharpness related to the size of the screen on which video is reproduced. It is e.g. done at resolutions of 720×576 (digital PAL standard definition TV) or 1920×1080 (high definition TV) with square or stretched pixels (resulting in different aspect ratios). Color sampling depends on the color representation. Useful representations are RGB (red, green and blue) and YCbCr. Latter separates luminance from two chrominance channels (blue-yellow and red-green). Moving Pictures Experts Group (MPEG) has specified use of YCbCr with chroma subsampling. Chrominance channels are subsampled according to the "4:2:0" or "4:2:2" patterns. Assuming an RGB image as captured by a digital camera is quantized at $8+8+8=24$ bits per pixel (bpp) and consequently converted to YCbCr, "4:2:0" results in $8+2+2=12$ bpp on average, while "4:2:2" results in $8+4+4=16$ bpp on average.

In digial PAL SDTV systems with a frame rate of 25 fps, a video signal fed into an MPEG video encoder exhibits a bit rate of $720 \cdot 576 \cdot 25 \,\text{Hz} \cdot 12 \,\text{bit} = 124.42$ Mbps. HDTV signals at "4:2:2" chrominance subsampling have a bit rate of $1920 \cdot 1080 \cdot 25 \,\text{Hz} \cdot 16 \,\text{bit} = 829.44$ Mbps. Target bit rates for HEVC[1] encoded HDTV material are between 1 Mbps and 6 Mbps [8]. Redundancy and irrelevancy reduction by two orders of magnitude is achieved in MPEG by a combination of still-image coding and image sequence processing. Still-image coding irrelevancy reduction is achieved by two-dimensional frequency domain quantization. Image sequence processing aims at finding redundant information in consecutive images, such as static background.

2.3 Video Source Coding

Digital video capturing by sampling reduces video entropy as irrelevant information is omitted in the aforementioned domains, time, 2D image plane and color. Video source coding further reduces entropy by redundancy reduction in the time and planar frequency domains. Still image redundancy is reduced by frequency domain quantization and subsequently, by variable-length coding (VLC) of the quantized values. This is depicted by example in figure 2.4. Differential image coding is done in intra or inter modes. Intra frame prediction exploits similarity within

---

[1] MPEG high efficiency video coding, successor to advanced video coding

original image block

DCT representation

Quantization table

Reduced and scaled (8/Q/scale) DCT

Quantized DCT

iDCT of quantized DCT

original image block

-117	-107	-97	-93	-97	-107	-117	-123
-101	-78	-55	-45	-55	-78	-101	-117
-78	-34	9	27	9	-34	-78	-107
-55	9	71	98	71	9	-55	-97
-45	27	98	128	98	27	-45	-93
-55	9	71	98	71	9	-55	-97
-78	-34	9	27	9	-34	-78	-107
-101	-78	-55	-45	-55	-78	-101	-117

DCT representation

-299	128	-329	-51	-11	-4	-6	-1
-128	-23	58	9	2	1	1	0
-329	-58	149	23	5	2	3	1
51	9	-23	-4	-1	-1	0	0
-11	-2	5	1	0	0	0	0
4	1	-2	-1	0	-1	0	0
-6	-1	3	0	0	0	0	0
1	0	-1	0	0	0	0	1

Quantization table

8	16	19	22	26	27	29	34
16	16	22	24	27	29	34	37
19	22	26	27	29	34	34	38
22	22	26	27	29	34	37	40
22	26	27	29	32	35	40	48
26	27	29	32	35	40	48	58
26	27	29	34	38	46	56	69
27	29	35	38	46	56	69	83

Reduced and scaled (8/Q/scale) DCT

-30	6	-14	-2	0	0	0	0
-6	-1	2	0	0	0	0	0
-14	-2	5	1	0	0	0	0
2	0	-1	0	0	0	0	0
0	0	0	0	0	0	0	0
0	0	0	0	0	0	0	0
0	0	0	0	0	0	0	0
0	0	0	0	0	0	0	0

Quantized DCT

-300	120	-333	-55	0	0	0	0
-120	-20	55	0	0	0	0	0
-333	-55	163	34	0	0	0	0
55	0	-33	0	0	0	0	0
0	0	0	0	0	0	0	0
0	0	0	0	0	0	0	0
0	0	0	0	0	0	0	0
0	0	0	0	0	0	0	0

iDCT of quantized DCT

-116	-107	-95	-89	-93	-103	-114	-120
-101	-80	-55	-46	-58	-81	-102	-114
-78	-37	12	30	6	-40	-81	-103
-57	4	77	106	74	6	-58	-93
-50	19	103	139	106	30	-46	-89
-59	-1	70	103	77	12	-55	-95
-78	-44	-1	19	4	-36	-80	-107
-93	-78	-59	-50	-57	-78	-101	-116

fx

fy

"2-D Gaussian": 64 DCT chrominance coefficients

-30	-6	-14	-2	0	0
6	-1	2	0	0	
14	-2	5	1		
2	0	-1			
0	0				
...					

Coefficients in "zig-zag" ordering:

-30	-6	6	14	-1	-14	-2	...	0...0

45x

DCT coefficient (8bit)

# of following zeros (6bit)

-30	0	...	0	-2	2	5	4	1	0	-1	45

8x

RLE 2-tuple (coeff,zeros)

8 bit per pixel:	64 * 8bit	=512bit
Quantised DCT and RLE:	13 * (8+6)bit	=182bit

Figure 2.3: Discrete cosine transform (DCT) and redundancy reduction by quantization and variable length coding of a "2-D Gaussian".
Top left: Six gray scale representations of image data, transform, quantization table and quantization, normalization and inverse transform.
Top right: number representation of the process.
Bottom: The zig-zag scan pattern is used in standards prior to HEVC.

a single image, while inter frame prediction estimates motion between consecutive frames and compensates for similar portions of two or more images when similarity is found within some motion estimation search range.

Wiegand et al. [9] as well as Puri et al. [10] provide overview of currently standard video coding according to MPEG H.264. In the scope of this work is, to a large extent, live television and thus video source coding under a delay constraint. An MPEG video stream consists two fundamentally different kinds of pictures: Pictures that can be decoded independently (I) and
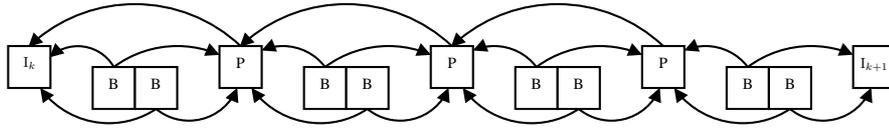
Figure 2.4: Coded picture inter-dependencies within MPEG group of pictures k of fixed length 12, according to DVB

inter predicted pictures. Single direction predicted pictures (P) are depending on a previously decoded picture. P pictures are transmitted as motion compensated difference signals. Furthermore, bidirectionally predicted (B) pictures may depend on previous and future frames, which implies re-ordering of frames for transmission. When a new independently coded picture is inserted into the stream of pictures, a group of pictures (GOP) has passed. A maximum channel switching delay in television implies the requirement to switch from one set of live audio-visual streams to another within a specific period of time. For this reason, DVB mandates fixed size groups of pictures of length 12. At 25 fps it is thus possible to switch between channels within 480 ms.

Compared to stored video streams, this can be a significant difference. Here a GOP size limitation does not exist and hence the source coder may distribute the targeted bitrate over a larger period of time. This typically results in greater efficiency in terms of coded bitrate at equal video quality or conversely, in a quality improvement at equal bitrate. A clear benefit of variable GOP size is the possibility of detection of scene changes within the video. Naturally, a picture should be independently coded when previous pictures differ greatly, while following pictures differ less. Furthermore, referencing frames of significant temporal difference (in the order of seconds), but strong similarity (e.g. due to an intermittently inserted, largely different scene) is only possible with dynamic GOPs. Lastly, the possibility to re-iterate the encoding process multiple times (multi-pass encoding) enables the encoder to refine the result with respect to bit rate or video quality.

Consequently, stored audio-visual streams can be assumed to consume less bits per second at equal quality when compared to encoding on-the-fly. With MPEG audio-visual streams, mixed use of live broadcast and pre-coded material is feasible and yields a gain in transmit efficiency [2].

2.4 Program Multiplex

MPEG-2 systems [11] defines encapsulation and packetization of individual program elements. Elementary streams (ESs) are bytestreams of audio, video or any other arbitrary data. Each elementary stream is independently decodable of any other one, or any other signaling. Pixel dimensions, frame rate, aspect ratio and copy protection scrambling, among others, are signaled in the ES header. In another layer, packetized elementary streams (PESs) form the basic unit of program multiplex. A start code prefix marks the beginning of a PES packet. The following header contains, among others, packet length information and optional decoding and presentation timestamps. The content may thus be e.g. a coded picture or block of audio samples. In case of video however, it is not signaled in the PES header of what type the coded picture (I,B,P) is.

Each PES contains a logically connected set of data and as such may be multiplexed into either program stream (PS) or transport stream (TS). Latter are multiplex variants in MPEG designed for file storage or broadcast, respectively.

2.4.1 MPEG-2 Transport Streams

In the case of elementary streams multiplexed for broadcast, an MPEG-2 transport stream (MPEG-TS) is composed. The program multiplex for broadcast is comprised of a number of tables for association of elementary streams with a TV program. Furthermore, network, ser-

Table 2.1: MPEG-2 transport stream multiplex according to DVB (two elementary streams)

Program ID	Program element
$0x00$	Program Association Table (PAT)
$0x10$	Network Information Table (NIT)
$0x11$	Service Description Table (SDT)
$0x12$	Event Information Table (EIT)
defined in PAT	Program Map Table (PMT)
defined in PMT	Video elementary stream
defined in PMT	Audio elementary stream

vice and event information may be contained. Each such transport stream program element is identified by a unique program identifier (PID). A transport stream containing two audio-visual streams is given in table 2.1. The table shows that at least a program map table and a program association table are mandatory.

End-to-End Synchronization

Due to the continuous broadcast of DTV, receivers need to decode and playback audio-visual content at the exact same rate at which it is generated and transmitted. Independent of their actual capacity, audio and video buffers are a finite resources and thus buffer limits will be exceeded if playback and broadcast rate differ. Audio/visual data would have to be dropped in case of buffer overflow. Conversely, buffer underrun occurs when playback is too fast, resulting in image judder and audio dropout. With receiver clock speed difference, one or the other will eventually happen. Therefore, receiver clocks must be synchronized to that of the broadcast station, which is accomplished by a generator-locking (GenLock) mechanism. By some phase-locked-loop (PLL) implementation, a DTV receiver constantly monitors and adapts its frequency and phase as compared to a reference clock signal provided by the broadcast sender.

DTV broadcast according to e.g. DVB is transmitted as an MPEG TS multiplex into which reference timestamps are inserted at an interval of less than 100 ms. They comprise the so-called program clock reference (PCR) elementary stream. Presentation as well as decoding timestamps (PTS, DTS) are further provided relative to the PCR. Each PCR timestamp represents a clock tick counter value of a clock running at 27 MHz. The receiver likewise deduces its local system frequency from a 27 MHz quartz. According to DVB, receivers shall incorporate crystal oscillators with less than ±30 ppm (parts per million) frequency deviation. The actual frequency offset of the specific receiver oscillator is typically compensated by a PLL and voltage controlled crystal oscillator (VCXO) combination.

2.4.2   Network Abstraction Layer

As compared to MPEG-2 systems, with advanced video coding (AVC) the concept of network abstraction layer (NAL) units was introduced. H.264/AVC packetized elementary stream packets contain a single access unit (AU), which in turn contains one or more NAL units. In broadcast using MPEG-2 systems, the PES syntax may be seen as the container necessary for TS multiplex, and it provides decoding timestamps for synchronization. As such, the NAL/AU/PES concept is similar to ES/PES, whereas former provides greater flexibility. For example, a video stream may be comprised of several views (cf. multi-view video coding) to support e.g. stereoscopic reproduction. A decoder may however be incapable of decoding multiple views. The NAL/AU structure enables low complexity demultiplexing of a single view from multiple coded views. Decoding of a single access unit results in a single picture (a set of hierarchical pictures in case of multi-view). A single NAL unit on the other hand may be comprised of a whole picture (I,P or B) or a so-called *slice* thereof. Redundancy coded picture NALs within the same AU may be

used to compensate for transmission errors but remain undecoded in absence of errors, which is useful in the scope of this work as live streaming implies a residual error rate.

With respect to scrambling for copy protection, which is an important aspect of television, compared to MPEG-2 elementary streams the NAL/AU structure has an important benefit: All stream information is external to the coded (and potentially scrambled) audio, visual, or auxiliary data. For video this includes picture dimensions, timing information and picture type, among others. Picture type information enables seeking a stream of NAL units for the next I picture without actual decoding/descrambling of intermittent pictures, which implies a large reduction in complexity [10]. Concerning digital video recording this is beneficial for trick mode (fast forward and reverse) playback.

MPEG-2 systems for television differ greatly from IP based architectures, while requirements pertaining to the container structure of stored digital video may differ greatly from that of real-time video conferencing services. The NAL unit flexibility is tailored for heterogeneous environments within which digital video may be transmitted and stored. It is important to note that within the scope of this work there is no limitation regarding transport of any of the above mentioned data formats. Hence, methods as described herein are multimedia encapsulation protocol agnostic.

2.5 Internet Protocol Streaming

The focus of this work is on downlink audio-visual streaming over multi-user Internet protocol based networks. Latest generation dedicated TV distribution according to DVB supports carriage of IP packets by generic stream encapsulation (GSE) [12]. This may be used for audio-visual streaming data delivery in a dedicated broadcast setup, which is out of the scope of this work. As the predominant application in the context of Internet protocol television (IPTV), an overview of Internet transport is given in the following.

2.5.1 Network Layering

Two different models are frequently used to describe a layering structure in computer networks: the TCP/IP model and the International Standards Organization (ISO) open systems interconnection (OSI) reference model. Both are depicted in figure 2.5. Two protocols predominantly used in IP networking, the user datagram protocol (UDP) and the transmission control protocol (TCP), represent very different packet oriented transmission paradigms. Both are expressed in terms of the TCP/IP model, in which they are classified as *Transport Layer* protocols. The ISO/OSI classification is rarely used, in particular the higher layers termed *Session* and *Presentation* are not represented in the TCP/IP model. Following the notion of Tanenbaum [13, 14], a hybrid layering model is used herein, but extended by the Session layer, cf. figure 2.5 on the following page. The TCP/IP model does not define the lowest ISO/OSI layers *data link* and *physical* layer. Consequently, the hybrid model includes them. In the following, any reference to network layers is made to the hybrid model.

Physical Layer   The physical layer establishes a communication channel over a physical, wired or wireless medium. The unit exchanged is bits, while in terms of analog representation of binary data, the notion of symbols (carrying one or multiple bits) is applicable. Medium characteristics and sources for bit flips may be fundamentally different e.g. for guided media, i.e. wired transmission as compared to wireless transmission. Therefore, different physical layer specifications for various fields of application exist in the available digital communication standards, some of which have been mentioned above. In any case, the physical layer may not be assumed reliable. In information theoretic terms, both remaining equivocation and noise would need to be zero for perfect reliability, i.e. any transmitted binary 1 not being interpreted as 0, and vice versa, at the receiver. Shannon [3] stated that perfect reliability is impossible with a finite amount of
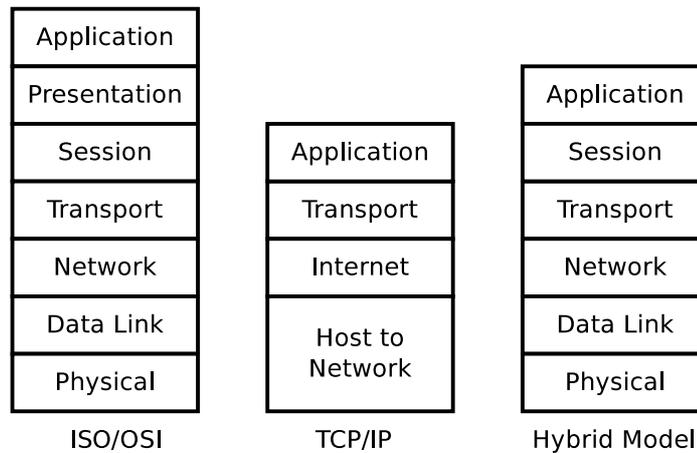
Figure 2.5: OSI, TCP/IP and a hybrid network layer model

time for error correction. The physical layer thus deals with digital to analog (and vice versa) conversion, bit to symbol (and vice versa) mapping and error control.

Data Link Layer The data link layer provides reliability on the basis of blocks of bits. The unit exchanged is thus termed a link layer *frame*. Data from higher layers is grouped into frames. Some form of checksum over this set of data is provided with the data as part of the frame. Error recovery may be achieved e.g. by having a receiver acknowledge error-free reception of each frame. A repetition is performed by the sender in absence of thereof. Errors are detected by checksum comparison at the receiver and provided to upper layers only in case checksums match. Consequently, the data link layer is seen as a frame erasure channel by upper layers. Its service has to be regarded as *best effort*, as it will provide error recovery within finite time and thus only up to a certain extent (subject to a retransmission limit).

Network Layer Controlling packet traversal from one host via possibly many intermediate hosts to one or multiple destination host(s) is done at the network layer. A protocol defined at the network layer is the Internet Protocol (IP). The unit of data exchange is packets. Within the IP family of protocols, each packet is provided with a source and destination address (protected by a header checksum) and forwarded to the data link layer. Furthermore, routing tables may define forwarding rules for packets between source and destination. Multicast and broadcast services are realized by address space reservations. The network layer provides the higher layers with a packet erasure channel as packets may be dropped for any reason, such as memory overflows due to congestion.

Transport Layer Applications running on different hosts are connected by transport layer protocols. In the TCP/IP model, transport layer protocols define port numbers for transport layer multiplex. Each transport layer bit stream is extracted from the incoming network layer traffic by transport layer unit port number matching. Different transport layer protocols may provide different kinds of transport services. A suitable protocol is consequently chosen by the application programmer. A transport layer protocol may provide an abstraction for a bit pipe of some continuous throughput, reliability to a certain extent or a limited end-to-end delay. The transmission control protocol is a widely used reliable transport layer protocol which includes network congestion control[2]. On the other hand, the user datagram protocol supports multicast

---

[2]IETF RFC 2581 – TCP Congestion Control

and does not abstract the characteristics of the underlying layers except for the size of the unit exchanged at each layer.

Session and Application Layer   An application communicates via a *network socket* by registering a port number on the host the application is executed. Use of potentially multiple different transport layer protocols via pre-defined ports for an application's potentially multiple tasks is left to the application and depends on the application requirements. Session layer protocols can be assumed as conventions on application layer for setting up a session, such as a voice call. The real-time transport protocol (RTP)[3] and hyper-text transfer protocol (HTTP)[4] families are prominent examples.

Maximum Transmission Unit Size

A problem with layering is the abstracted size of exchange units of the next lower layer. Data integrity below the transport layer is only maintained if complete units (or integer multiples thereof) are contained in the respective lower layer unit. For example, if a single UDP transport layer unit exceeds the size of a network layer unit, it is split up (i.e. *fragmented*) into at least two network layer units. If one of them is lost, the rest has to be discarded, too. However, a loss may remain undetected up to the application layer, as e.g. the user datagram protocol does only include a header checksum. Conversely, the transmission control protocol guarantees data integrity and the described case results in reduced efficiency at the transport layer. It is a convention on the Internet to use a maximum transmission unit (MTU) at the transport layer of 1500 Bytes. Implementations of underlying layers shall at least be able to transport this size without fragmentation in order not to compromise integrity or efficiency unnecessarily. An application may consequently assume this size, the exact value of which it may typically query from the host operating system, as the maximum payload unit size. As this size may however not be assumed to provide integrity or maximum efficiency (in case of packet loss) via the transmission channel as a whole, the current end to end path MTU may be tested by forcing the lower layers not to fragment a payload unit. The size at which lower layers do not discard payload units, following the order not to fragment them, is determined by sending multiple test packets of different size for the momentary path configuration (subject to change). This form of inter-layer communication is done by the transmission control protocol by *path MTU discovery*[5]. As there is only a limited number of existing lower layer implementations, a reasonable value may be found in reasonable time.

2.5.2   Bidirectionality, Adaptivity and Multiplex

A key difference of IPTV as compared to classical television broadcast is the bidirectional nature of IP networks. A more simple form of error correction as compared to FEC can be implemented by providing cyclic redundancy check (CRC) checksums with individual data units on multiple layers as elaborated above. Upon mismatch of the provided checksum with a locally computed checksum over the same parts of the data, the receiver may request the sender to repeat the transmission of this part of the data. Feedback which is issued by the receiver is binary, as transmit success or failure thereof is signaled. Checksum mismatch occurs due to bit flips in the received data. Furthermore, individual data units may not reach their destination at all due to the switching nature of bidirectional networks. Intermediate network nodes may have to refuse to accept or forward a data unit due to processing limits. This kind of error correction is termed automated repeat-request (ARQ). It requires sequence numbers on transmit units in order to distinguish repetitions from original transmissions. On several of the above described network layers, ARQ is implemented. For example, wired lower layers typically use *stop-and-wait* ARQ,

---

[3]IETF RFC 3550 – RTP: A Transport Protocol for Real-Time Applications
[4]IETF RFC 2068 – Hypertext Transfer Protocol – HTTP/1.1
[5]IETF RFC 4821 – Packetization Layer Path MTU Discovery, see also RFC 1981, RFC 1191

while more error prone wireless lower layers implement *selective repeat*. TCP implements *go back n* ARQ, which is a sliding-window approach. They are defined as follows:

Stop-and-wait. After a unit of data is sent, the sender waits for positive acknowledgement (ACK) from the receiver before transmitting the next data unit. If no negative ACK is defined in the stop-and-wait protocol, the sender will retransmit the same data after some pre-defined period of time has elapsed (referred to as *timeout*). In case no sequence numbering is available, duplicate data at the receiver may occur due to potential ACK loss.

Go-back-n enables multiple (w) data units in transit until the algorithm waits for a positive acknowledgment for the first time. In absence of an ACK after a timer has expired, the sender repeats all w data units. Otherwise, the receiver has signaled the range of data units it has consecutively received from the beginning ($w - n$), upon which the sender repeats the last n data units. When some of those n have previously been received, duplicate data is introduced. TCP, as an example for *go back n* ARQ, therefore uses sequence numbering for duplicate detection and removal. Adaptivity to the current network conditions is achieved by varying the window size w.

Selective-repeat may similarly transmit multiple data units in a burst as in go-back-n, but further extends the signaling capability of positive acknowledgments. For example, one bit per transmitted data unit may be reserved in the ACK message in order to signal individual data unit transmit success. The sender repeats only those packets that are signaled as missing. This introduces additional complexity at the receiver when the correct order of data units needs to be re-established.

2.5.3 IP Multicast

In the network layer provided by the *Internet Protocol, Version 4* (IPv4) according to the Internet Engineering Task Force (IETF) request for comments (RFC) 719[6], by definition all network hosts may be reached via the reserved broadcast address *255.255.255.255*. Alternatively, by for example using a 24 bit network mask, all local area network hosts subject to this mask may be reached by *xxx.xxx.xxx.255/24*. In practice, however, the possibility of reaching all Internet hosts is not a desirable network feature, as it would easily lead to congestion. The successor to the IETF RFC 791 defined IPv4 is the *Internet Protocol Version 6* (IPv6)[7]. Apart from an increase in network address field size etc., broadcast is replaced by multicast. In multicast, a *multicast group* is defined prior to transmission. By example of IPv4, valid multicast addresses[8] range from *224.0.0.0* to *239.255.255.255*. There are permanently established multicast groups reserved for special purposes. All other multicast groups are temporarily defined by their address and subnet mask combination and are managed by the Internet Group Management Protocol (IGMP)[9]. Multicast capability is a transport layer feature. Without exception, IP based multicast transport protocols as described below make use of IGMP for multicast group setup and management. TCP is the only below mentioned strictly point-to-point unicast transport protocol. Medium access control (MAC) layer MBMS makes use of IGMP for MAC address group setup as well (cf. section 5.3.1). Within the scope of this work, the wireless link used for multicast is assumed as multicast capable with respect to IP based transport, whereas multicast traffic is broadcast by a base station to the set of wireless terminals associated to it. A detailed description of multicast addressing and routing is thus out of the scope of this work.

---

[6]IETF RFC 791 – Internet Protocol, see also RFC 1349, RFC 2474, RFC 6864
[7]IETF RFC 2460 – Internet Protocol, Version 6 (IPv6) Specification
[8]IETF RFC 1112 – Host Extensions for IP Multicasting
[9]IETF RFC 3376 – Internet Group Management Protocol

2.5.4 Transport Protocols

2.5.4.1 User Datagram Protocol

Under the user datagram protocol[10], communication is established between exactly two transport layer end points. A UDP packet is sent from a *source port* to a *destination port* e.g. via IP to a unicast or multicast destination. Apart from packet length and checksum, they are the only UDP header fields. Relying on the underlying layers to forward packets from one network host to another, UDP functionality is limited to port multiplex on the receiver host. For bidirectional communication, the source port of an incoming UDP packet may be used as a return port, but no guarantee is given that the sending application accepts incoming packets on that same port. Typically, destination port numbers are pre-defined, while source port numbers on the communicating hosts are chosen randomly from a pool of currently unused port numbers.

2.5.4.2 Transmission Control Protocol

TCP[11] is the predominant protocol used in the Internet. It has been mentioned above that TCP provides perfect reliability by go-back-n ARQ. As it is further limited to point-to-point transmission, multicast and broadcast is unsupported with TCP. Detailed discussion of TCP is available in the literature [13] and is out of the scope of this work. However, in order to elaborate why live streaming using TCP is infeasible, it's behavior can be sketched as follows. In the so-called "slow-start" phase of TCP only few IP packets are transmitted per received ACK. The number of unacknowledged packets in transit is increased exponentially during this initial phase, which increases throughput by decreasing the number of periods during which the sender has to wait for an ACK. After the slow-start phase the go-back-n window size w is increased only linearly by *additive increase* (AI). Upon packet loss, it is reset and slow-start is initiated again. The point at which a transition is made from slow-start to additive increase is *multiplicatively decreased* (MD) by a factor of 1/2 after packet loss. In conclusion, TCP adapts to the network by AI-MD and reacts with decreasing byte rate in case of packet loss due to either network congestion or transmission errors. Specifically, TCP implements no mechanisms to provide timely delivery in case of multimedia streams, also referred to as *inelastic flows* in this context, as compared to the elasticity of TCP.

2.5.4.3 Real-Time Transport Protocol

Using the network socket and port syntax of UDP/IP networking for stream multiplex, in the transport of audio-visual streams, end-to-end synchronization is required. With the real-time transport protocol (RTP) this is achieved by additional headers providing payload type information, sequence numbers and timestamps on top of UDP. As opposed to MPEG-TS multiplex, RTP makes use of the multiplexing mechanisms provided by IP based transport by instantiating a separate RTP session via UDP/IP packet streams per elementary stream. RTP may further be used to encapsulate MPEG-TS packets. Carriage of H.264 video in RTP is done by encapsulation of one or more NAL units (cf. section 2.4.2) per RTP packet, subject to the IP fragmentation threshold (cf. section 2.5.1).

As depicted in figure 2.6, accompanying protocols are the real-time streaming protocol (RTSP) and the real-time transport control protocol (RTCP). Initiation of streaming sessions is done via RTSP. It provides means for service description, such as the number of streams, content types and IP port numbers, to name a few. After session initialization, RTSP may be used for playback control.

RTP accounts for the fact that on e.g. personal computer (PC) systems, audio and video streams are played back at individual and independent clock speeds (sound card clock and graphics card clock) by enabling different time bases and synchronization sources e.g. for audio and

---

[10]IETF RFC 768 – User Datagram Protocol
[11]IETF RFC 793 – Transmission Control Protocol
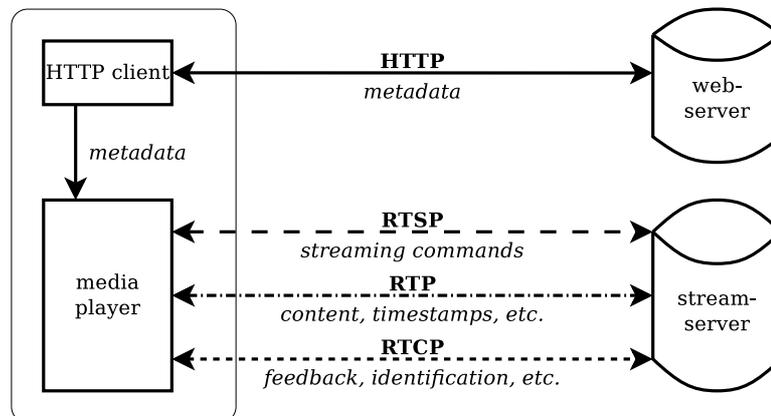
Figure 2.6: Real-time transport protocol streaming and RTSP, RTCP control

video. However, it is not guaranteed that playback on a PC based audio visual sink is possible at the exact same clock speed as compared to the clock speed at the capture source. Synchronization in RTP is thus not based on a reference clock elementary stream but based on external synchronization sources, such as network time protocol (NTP) servers. Nevertheless, it enables inter-stream synchronous ("lip-synchronous") playback, potentially subject to re-sampling. By means of sender and receiver reports, RTCP is used to link the *synchronization source identifier* of each RTP packet to an NTP time source. RTP timestamps are interpreted on this time-line.

2.5.4.4 Transport Protocol Alternatives

Design of an alternative transport protocol can be regarded as a complex task. Performance and improvement thereof, in whatever regard, depends at least on sender and receiver behavior, as well as the network in between, with varying and potentially highly dynamic traffic conditions. As of today, TCP is the predominant transport protocol for user data transmission in IP based networks, regardless of the transmitted content and although different proposals exist. An alternative which adds multi-homing and multi-streaming capabilities to reliable transport is the stream control transmission protocol[12] (SCTP) [15]. It is used for various types of backhaul signaling traffic in Long-Term Evolution (LTE). A well studied unreliable transport layer protocol which adds congestion control mechanisms to UDP is the datagram congestion control protocol[13] (DCCP) [16]. In this work the focus is on wireless medium access and multicast transmission. These mechanisms are transport protocol agnostic but require multicast capabilities. In the following, it will be elaborated that multiple combinations of upper layer protocols are feasible. The RTP protocol family comprises application and session layer protocols. An evaluation of multicast enabled multi-view 3D-TV streaming using RTP/DCCP/IP has been done by Tekalp et al. [17]. A predictably reliable real-time transport (PRRT) protocol has been proposed by Gorius et al. [18, 19, 14], in which a tradeoff between timely delivery and upper bounded residual error is achieved by adaptive hybrid error correction with variable error tolerance. This protocol is multicast capable and provides negated acknowledgement based retransmissions in multicast, combined with flexible FEC coding configurations on the transport protocol layer, as well as end-to-end synchronization similar to RTP.

---

[12]IETF RFC 4960 – Stream Control Transmission Protocol
[13]IETF RFC 4340 – Datagram Congestion Control Protocol

2.5.5 DVB-IPTV

Carriage of MPEG-2 transport stream multiplex (MPEG-TS) over IP is specified by *DVB-IPTV Phase 1* [20]. This approach does not rely on the inherently existing multiplexing capabilities of IP networking through port numbers. Instead, the receiver needs to parse the provided transport stream for each individual audio or visual stream to be played back, as well as extract the clock reference stream (cf. section 2.4.1). A benefit of this is compatibility with DTV. With available network connectivity they are capable of processing broadcast identical transport streams that are received via Internet protocols in the same way as via terrestrial or satellite interfaces with low additional effort. In DVB-IPTV, three different methods of transmission are defined:

- Unprotected unicast and multicast UDP streaming transport

- Application layer FEC (AL-FEC) protected RTP transport

- RTP with retransmissions (RET)

In its most simple form, a number[14] of MPEG-TS packets of constant size (188 Bytes) are accumulated into one UDP packet and transmitted immediately to a unicast or multicast destination. A drawback of this mechanism is the lack of packet sequence numbers. As re-ordering of IP packets may occur, this may be indistinguishable from packet loss.

AL-FEC protected unicast and multicast streaming is thus only possible via RTP/UDP/IP and may use rateless Raptor [21] codes as deployed in mobile communication networks Univeral Mobile Telecommunications System (UMTS) and LTE for MBMS [22] (cf. section 6.5), or a more simple *XOR* parity code or a combination of both. The rateless Raptor code is a Fountain [23] code with error correction capabilities at a non-vanishing probability of failure. As such, it is not perfectly reliable and its performance has been studied [24] within the scope of DVB-IPTV in a unidirectional Internet connected home network scenario. Additionally (and alternatively), DVB-IPTV supports retransmissions (RET) to recover from packet loss. The DVB-IPTV RET feature is defined in multiple variants with respect to the provision of redundancy by packet repetition. In each variant, retransmissions are requested by the receiver(s) via RTCP feedback. The streaming server may provide redundancy by repetition in one of the follwing three variants:

1. Repetition upon request by use of the original multicast streaming RTP session for both feedback and retransmissions.

2. Repetition upon request, whereas individual unicast session(s) are used for retransmissions based upon feedback received via the original session.

3. An additional multicast streaming session is used for retransmissions, while feedback remains to be transmitted via the original session. Retransmissions are provided upon request or a-priori. The additional multicast session is used for sender reports in RTCP messages. This way, feedforward feedback suppression is achieved when receivers refrain from requesting feedback knowing that feedback is scheduled for transmission anyhow.

Consequently, Internet transport of DTV according to DVB-IPTV incorporates methods and algorithms on top of best-effort networks and thus differs from classical television according to DVB. Bidirectionality may be utilized and forward error correction is adapted to the non-dedicated IP based transmission medium. Program multiplex is flexible by the possibility of using either MPEG-TS exclusively or individual RTP sessions per TV program and multicast receiver group. In wireless multicast, as will be elaborated further herein, there is room for improvement by leveraging cross-layer communication and MAC layer multicast feedback.

---

[14]At the typical Internet MTU size (cf. section 2.5.1), 7 MPEG-TS packets are used

Direct NAL-unit encapsulation

A broadcast compatible multiplex of several individual streams, such as audio, video, timing and program information, is encapsulated as MPEG-TS/UDP or MPEG-TS/RTP in DVB-IPTV. A drawback of this is a possible overlap of information boundaries (e.g. video frame start) and IP packet boundaries. In case of IP packet loss, direct NAL-unit encapsulation in variable size RTP or PRRT packets is therefore more error resilient than use of the additional MPEG-TS encapsulation. A single MPEG-TS packet may contain data of multiple information elements (e.g. video frames) and even of multiple elementary streams (e.g. audio and video). Hence, more than one information element or elementary stream may be damaged by isolated IP packet loss. An IP packet furthermore contains multiple MPEG-TS packets, resulting in redundancy due to multiple MPEG-TS headers. Conversely, for NAL units encapsulated as RTP payload[15] this is not the case. Each payload unit may contain data of exactly one information element, whereas each RTP/UDP/IP stream carries a single elementary stream.

Timing information is necessary to synchronize playback of audio visual streams. In RTP, a single timestamp is conveyed within an RTP header field. MPEG-TS on the other hand provides possibilities to convey two timestamps, indicating a decoding and a presentation time instant. A reference clock signal is conveyed in-band within the MPEG-TS multiplex, while RTP relies on bidirectional out-of-band RTCP signaling for the same purpose. Both MPEG-TS and the combination of RTP and RTCP provide mechanisms for synchronous TV playback. Further description of benefits and drawbacks of one method of encapsulation over the other is out of the scope of this work. Neither method is excluded from this scope, as live streaming capabilites are provided in both cases.

2.6 Requirements and Summary

In conclusion of the above description of systems and mechanisms for the distribution of delay-constrained audio-visual streams, a number of requirements can be deduced:

- a multiplexing mechanism for transmission of a mix of audio, video and auxiliary signals.

- an upper bounded delay of transmission from source to receiver(s).

- mechanisms for end-to-end clock synchronization.

- error correction subject to error tolerance.

In the following chapters it will be elaborated to which extent the distribution over wireless broadband networks can meet the given requirements. Audio/visual IP streams are received by a group of receivers in a wireless network, such as LTE and WLAN. The focus is on orthogonal frequency division multiplex (OFDM) based WLANs according to IEEE 802.11. Multicast and delay constraints prohibit the use of reliable protocols. TCP is thus out the scope of this work. Protocols such as RTP/UDP and PRRT on the other hand are equally suited in this regard. Delay constrained services such as IPTV are what this work aims at providing in an efficient manner over shared wireless networks. Furthermore, regarding non-delay-constrained content such as pre-recorded, stored AV streams, a treatment of achievable multicast throughput is given. Some redundancy may be assumed for transport according to DVB-IPTV as compared to RTP, especially in case of carriage of H.264 (and its successors). Nevertheless, both may be used in the scope of this work, since above named requirements for live streaming are met.

However, it should be noted that in an IP network, guarantees with respect to delay and bitrate cannot be given due to the multi-purpose nature of IP and the shared nature of multi-user wireless networks. In both domains, over-provisioning to some extent may be necessary. The remainder of this work deals with the wireless last hop in multicast with the focus on multicast feedback and multicast rate adaptation.

---

[15]IETF RFC 3984 – RTP Payload Format for H.264 Video

3

Fading Channels and Wireless Impairments

Propagation in radio communication is subject to a large number of effects. Most notably, thermal noise due to random molecular motion, *Brownian* motion, limits communication speed in terms of bits/second at a given transmit power and distance. Noise is naturally present in any wired or wireless system. The universal law of conservation of energy implies signal strength attenuation as a function of distance, while absorption of an electromagnetic wave using an antenna introduces frequency dependence. Fading channels can be grouped into two main categories: a) both sender and receiver are situated indoors; b) at least the sender is located outdoors. Consequently, indoor and outdoor channels differ in existence and severity of effects. At frequencies above 10 GHz, oxygen absorption becomes important. Using typical radio frequencies well below 10 GHz, in e.g. terrestrial and land-mobile satellite channels, other effects are predominant. The effect of radio wave propagation via multiple propagation paths (multipath) has to be considered in the presence of objects between and around sender and receiver(s), whereas reflection, diffraction and scattering may occur at these objects. Multipath propagation introduces the potential for cancellation by summation of phase shifted copies of the same signal (destructive interference), but also for constructive interference. Signal strength enhancing wave-guiding effects have been reported for corridors when sender and receiver are placed at respective opposite ends.

Furthermore, motion has to be considered, introducing temporal channel variations. Fixed base station outdoor communication faces receiver speeds of up to several hundred km/h with mobile handsets. Car-to-car communication for example implies mobility at both ends. Models for indoor channels typically assume stationarity of sender and receiver during communication, while motion of surrounding objects is considered. These three possibilities result in different statistical or discrete Doppler characteristics.

Obstruction of a line of sight between sender and receiver may occur, introducing significant shadowing, diffraction and scattering. Human body shadowing of a strong multipath signal component is considered in handheld mobile cellular telephony and clearly affects indoor propagation with people moving in the vicinity. Additionally, electromagnetic interference from electrical devices in the vicinity, such as fluorescent lights and microwave ovens, is likely to affect system performance indoors. Finally, with ubiquitous wireless technology, interference from different wireless systems as well as co-channel interference by spatial frequency reuse and adjacent channel interference is present.

Wireless transmission is in any realistic case subject to fading, which may at times be adverse or gainful. Literature distinguishes between slow and fast fading, which implies temporal variability of the received signal strength. Other effects are impairments that may be permanent, temporal, location dependent or frequency dependent. A core topic in this work is feedback aggregation. Its performance depends on received signal strength of multiple concurrent signals. Therefore, it is necessary to investigate the fading characteristics of wireless channels. The focus will be on indoor propagation as the predominant scenario for wireless local area networks. Indoor channels are typically characterized by rich scattering, i.e. a large number of multipath components, but an upper bounded excess delay due to building geometry.

3.1 Noise and Interference

Signal-to-noise ratio (SNR) is a performance measure of any communications system. Thermal noise is ubiquitous and defined by its two-sided constant power spectral density (psd) $N_0/2 = k_B T_{abs}/2 \, [\text{W/Hz}]$ (below $10^{12} \, \text{Hz}$) and autocorrelation $N_0/2 \cdot \delta(t)$, where $k_B = 1.38 \cdot 10^{-23}$ Joule/Kelvin is Boltzmann's constant and T_{abs} is the absolute temperature. At room temperature of 290 Kelvin[1], the thermal noise floor for two-sided digital communication is $-174 \, \text{dBm}$.

White Noise

Noise is assumed as a random variable (RV) uncorrelated with the transmitted signal. It is of high bandwidth and constant over frequency ("white") and assumed as a superposition of many independent noise sources. According to the central limit theorem, it is thus Gaussian distributed with zero mean and further referred to as additive white Gaussian noise (AWGN). When observed over time, AWGN is assumed a stationary ergodic random process and the received signal $r(t)$ is thus expressed by the sent signal $s(t)$ and the noise $n(t)$ as

$$r(t) = s(t) + n(t)$$

The symbol average SNR γ is given as the expected value of the ratio of symbol energy E_s over noise energy

$$E_s = \int_0^\infty |s(t)|^2 \, dt$$
$$\gamma = \text{E}\left[\frac{2E_s}{N_0}\right].$$

AWGN signal-to-noise ratio is an important performance measure for constant channel conditions, thus frequently termed "AWGN channels". In case the channel exhibits a time varying gain (due to fading, see below), the instantaneous SNR γ is a random variable with probability density function (pdf) $p_\gamma(\gamma)$ and the average fading SNR is

$$\bar{\gamma} = \int_0^\infty \gamma \cdot p_\gamma(\gamma) d\gamma. \tag{3.1.1}$$

It is important in evaluating system performance when transmitting over fading channels.

Receiver Imperfectness

An incoming signal is amplified at the receiver. The receiver noise figure is the amount of noise that is added by the sum of active elements in the receiver circuit. Digital systems in general are subject to quantization error. Any digital representation of an analog signal is quantized, hence a digital receiver needs to quantize the amplitude of the incoming analog signal. Quantization noise is a function of quantization step size and probability distribution of the amplitude. In case of digital multicarrier transmission, quantization affects both transmitted and received signal [25].

Artificial Noise: Interference

Microwave ovens and fluorescent lights are examples for the introduction of artificial noise during transmission. Harmonic interference may be introduced by electrical circuits in the vicinity of the receiver, but is also introduced by transmitter power amplifier non-linearity or any other non-linear system component. In frequency-division multiple access (FDMA) systems, adjacent

---

[1] A value of 290 Kelvin = 16.85° Celsius = 62.33° Fahrenheit is typically assumed as room temperature in the literature
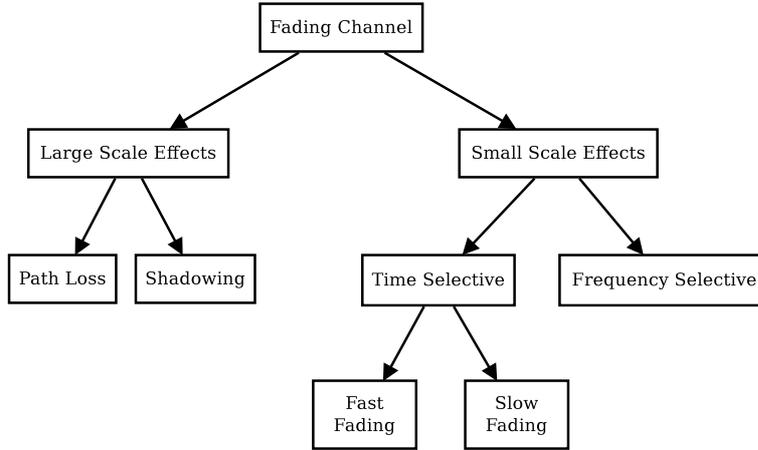
Figure 3.1: Taxonomy of fading channels regarding the scope of this work.
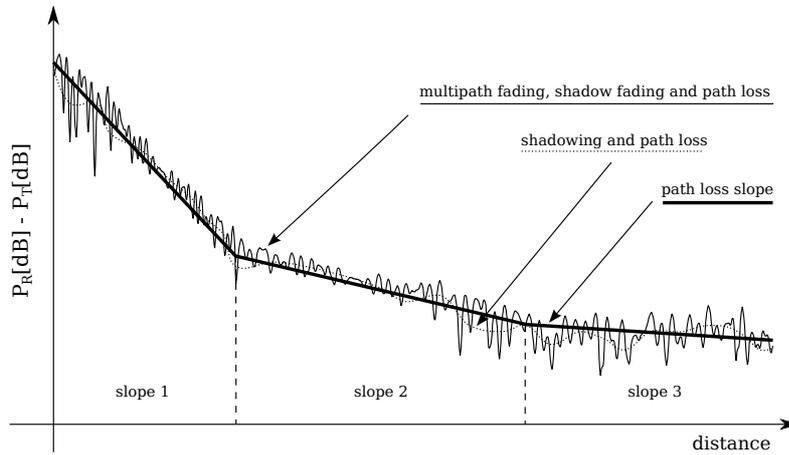
Figure 3.2: Path loss and fading channel effects

channel interference is present when frequency domain channels are closely spaced. Multiple access interference is introduced due to frequency re-use at different spatial locations, while interference is introduced in general when the same frequency band is used in the vicinity of the receiver.

3.2 Taxonomy of Fading Channels

Wireless fading channels are described by large scale and small scale effects. While large scale effects may result from significant changes in sender-receiver distance or significant obstruction of sender-receiver line-of-sight (LOS), small scale effects result from multipath and motion. Herein, motion is qualified either as being mainly due to the mobility of the receiver within a multipath environment or as motion in the vicinity of the stationary transmitter and receiver(s). A widely accepted [26, 27] taxonomy of fading channels is given in figure 3.1. An abstract example of the superposition of small scale and large scale effects is depicted in figure 3.2. In the following, a subset of said effects is considered for simplicity.

3.2.1 Large Scale Effects

3.2.1.1 Free Space Path Loss

Path loss in free space is assumed in vacuum where the electromagnetic waves are emitted from a point source. This results in isotropic radiation, i.e. the transmitted power is distributed over the area of a sphere of radius r around the point source. Consequently, quadratic path loss is given

$$L_{\text{fs}} = \left(\frac{4\pi r f}{c} \right)^2$$

whereas L_{fs} is the free space path loss, c is the speed of light and f is the radio frequency. It is said that the free space path loss exponent is 2. Assuming non-isotropic antennas at sender and receiver, with the antenna gains G_{t} and G_{r} for transmitter and receiver due to directional radiation/absorption, respectively, the received power P_{r} is typically expressed as

$$P_{\text{r}} = \frac{P_{\text{t}} G_{\text{t}} G_{\text{r}}}{L_{\text{fs}}}$$

whereas P_{t} is the transmit power at the sender.

3.2.1.2 Piecewise Log-linear Path Loss

Empirical distance dependent mean path loss prediction models assume [28, 29, 30]

$$P_{\text{t}}/\overline{P_{\text{r}}} = \overline{L}(d) \propto \left(\frac{d}{d_0} \right)^n$$

where the mean path loss $\overline{L}$ at the transmitter-receiver distance d is dependent on the mean path loss exponent n. Herein d_0 is a reference distance, in the following referred to as the *breakpoint* distance. A piecewise linear (in dB) path loss model is depicted in figure 3.2 in which path loss over transmitter-receiver distance d is subdivided into three slopes with different path loss exponent n each.

3.2.1.3 Shadowing

Propagation environments are subject to shadowing, i.e. permanent or sporadic strong attenuation due to obstructions in the dominant propagation path (LOS). Sporadic shadowing results in so-called *burst errors*, i.e. signal loss for the duration of a longer sequence of transmitted symbols as opposed individual symbol errors, and is very common e.g. in mobile communications systems. Therefore, these systems typically employ (outer) FEC coding and interleaving. For example, the aforementioned DVB-T/T2 are such systems. In its first generation an outer Reed-Solomon block code in conjunction with a convolutional interleaver to correct burst errors is used, while in its second generation, low density parity check (LDPC) and Bose-Chaudhuri-Hocquengham (BCH) codes are used.

Body shadowing may occur when the receiving device is close to the human body, as may be the case for mobile cellular networks. For indoor scenarios, it may occur due to people walking through the LOS between the base station and the user terminal station. A number of measurements have been conducted and are available in the literature. Villanese et al. [31] find up to $36\,\text{dB}$ body shadowing fading depths in a $150\,\text{m}^2$ open plan environment with pedestrian traffic. Ziri-Castro et al. [32] report $5 - 10\,\text{dB}$ attenuation due to body shadowing at $5\,\text{GHz}$ in offices and corridors. We have measured up to $10\,\text{dB}$ attenuation at $5\,\text{GHz}$ when a single person crosses the LOS in indoor home scenarios [33].

3.2.2 Small Scale Effects

3.2.2.1 Doppler

Doppler shifts on monochromatic signals appear due to a difference in velocity of sender and receiver (here: velocity v) in a non-orthogonal vector component. The Doppler frequency shift is defined as

$$f_{\mathrm{d}}(f) = \frac{v \cdot f}{c} cos(\alpha) \quad f > 0$$

As a special case, assuming motion directly towards or away from the source, i.e. orthogonal to the wave front, the maximum Doppler shift is experienced and given as

$$f_{\mathrm{D}}(f) = \pm \frac{v \cdot f}{c} \quad f > 0$$

As Doppler is frequency dependent, the spectrum of a non-monochromatic signal will be distorted by an increasing shift with increasing frequency f. In multipath propagation, i.e. when multiple reflections arrive at the receiver antenna from different directions, any two distinct directions α_1, α_2 are subject to different Doppler shifts. Multipath and mobility thus result in a *Doppler spread* of the transmitted signal. The way in which a signal is spread is further depending on the distribution of Doppler shifts on multiple reflected paths. The Doppler spread shape depends on the wave incident at the antenna and thus on its geometry: for strictly planar (2-D) limited field incident (Clarke's model [34]), the so-called *Jakes / classical* "bathtub" shaped Doppler spread curve may be found as given in equation 3.3.4, while for half-spheroid field incident it is found to be a box function [35]. Indoor transmission is typically simulated with "bell" shaped Doppler spread shape [36].

In the following, Doppler spread assumptions will be made in a way that Doppler is location independent (although Doppler occurs due to motion). In this case, the received signal spectrum $R(f)$ appears as a "smeared" version of the sent signal spectrum $S(f)$. Motion during transmission results in a limited time coherence T_{coh} of the channel, cf. section 3.3.3.

3.2.2.2 Multipath

Multipath propagation results in *frequency selectivity*, as opposed to a *frequency-flat* channel when there is single-path propagation. The coherence bandwidth is finite in case of multipath and is a measure for the coherence of the channel in the frequency domain. Any real transmission implies some non vanishing bandwidth, hence a multipath channel may influence frequency components within the used bandwidth differently. Coherence bandwidth is defined as the frequency difference Δf over which the channel may be assumed constant in the frequency domain. A measure of the channel being approximately frequency-flat is typically assumed as the $\pm 3 \, \mathrm{dB}$ coherence bandwidth B_{coh}, i.e. the Δf beyond which the frequency response of the channel differs by 50% relative to the center frequency. Practical examples for coherence bandwidth are given in section 3.3.3.

In the scope of this work is wideband transmission by OFDM. Due to the properties of OFDM, finite coherence bandwidth due to frequency selectivity, however, is not an issue (cf. section 4.2). While a channel may not be frequency flat, OFDM transmits via narrow bandwidth individual subcarriers, for which the channel may then be assumed frequency flat. Thus, it suffices to know the average multipath fading gain over the OFDM symbol bandwidth to approximate the performance of OFDM. Since the number of subcarriers is a design parameter in OFDM, frequency selectivity within the bandwidth of a subcarrier can be avoided.

3.2.2.3 Speed of Fading

Fading is experienced at the receiver due to multipath propagation. Multiple paths may interfere constructively or destructively, as they arrive at the receiver via different trajectories in space

and hence at different phase shifts. Multipath fading may thus result in so-called "deep fades", during which the signal strength is close to or equal zero. Fading channels are characterized in terms of *coherence time* T_{coh}. This is defined as the time during which the channel remains approximately constant, once the channel is accessed. Typically, coherence time is defined as the time after which the channel differs by 50% ($\pm 3\,\mathrm{dB}$), compared to the channel fading gain at the time instant of first access. The speed of fading (fast/slow) is thus related to the duration of channel access. If latter is assumed constant, a fixed symbol duration is given, as is typical in digital communication. With respect to the scope of this work considering symbol based multi-carrier transmission, fast fading is assumed if the duration of channel access is in the order of the coherence time of the channel, or even above. Slow fading is assumed if the duration of channel access is well below the coherence time.

Both fast and slow fading arise from time-selectivity (cf. figure 3.1), which is due mobility in a multipath propagation environment. Mobility during transmission implies the presence of the Doppler effect and in case of multiple signal paths, Doppler spread in the frequency domain. Slow fading may however be superimposed with an increase of transmitter-receiver distance and other large-scale effects, such as obstruction of a strong multipath component. The scope of this work comprises slow fading under the assumption that there is no superposition with large-scale effects.

3.3   Stochastic Channel Description

Mobile wireless channels can be described as linear time-variant systems by a time-variant impulse response $h(t, \tau)$ or alternatively by its respective Fourier transform in delay time τ, the time-variant transfer function

$$T(t, f) = \mathcal{F}_\tau \left\{ h(t, \tau) \right\} = \int_0^\infty h(t, \tau) e^{-j2\pi f\tau} d\tau.$$

With an input $x(t)$, the system responds at its output with

$$y(t) = h(t, \tau) * x(t) = \int_0^\infty h(t, \tau) x(t - \tau) d\tau.$$

In the following, it will be elaborated how multipath fading channels are described stochastically in general and an important properties of a simplified stochastic channel description are introduced.

3.3.1   Tapped Delay Line Channel Model

Let the impulse response $h(t, \tau)$ be the output of the channel for an impulse at time t. The signal at the output of the transmitter arrives at the input of the receiver after passing through the channel. The signal at the receiver input is represented as a sum of delayed copies of the transmitted signal due to multipath propagation. At each point in time of transmission, each copy may arrive at different amplitude, phase and Doppler shift. The tapped delay line channel model impulse response is thus given as (cf. figure 3.3)

$$h(t, \tau) = \sum_{n=0}^{N-1} c_{\mathrm{n}}(t)\, \delta\left(\tau - \tau_{\mathrm{n}}(t)\right).$$

Herein, $\tau_{\mathrm{n}}(t)$ is the delay of the n-th copy (multipath component) at time t . When discrete time simulation of this channel model is done in the complex baseband, the impulse response is sampled at equi-distant intervals. Bandwidth of this discrete time system is then limited to $|f| < B/2$, with the sampling frequency B. Independent of the sampling frequency, any two path
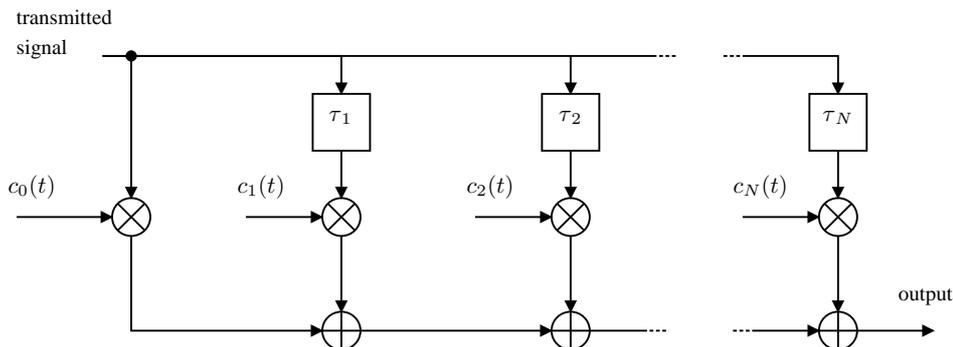
Figure 3.3: Tapped delay line channel model

delays may differ in $\Delta\tau \ll B$. Under the assumption that $\Delta\tau \in \mathbb{R}$, the resolution of the sampled impulse response is limited in practice. In the tapped delay line channel model, paths arriving approximately at the same time are accumulated as one channel tap at some delay $\tau_{\mathrm{n}}(t)$. Hence, the channel tap properties are not discrete but require stochastic description.

Complex magnitude and phase of one undersampled accumulated path may be assumed independently distributed. Resulting magnitude of each delay line channel-coefficient is then typically assumed Rayleigh or Rician distributed, cf. section 3.3.2, while delay τ is given in the granularity of the model's sampling frequency. The individual channels $c_{\mathrm{n}}(t)$ can be independently modeled and are frequency non-selective, while the compound impulse response of the channel is frequency selective in case $N > 1$.

Assuming a stationary process in τ, without loss of generality, τ can be set to zero, hence the time-variant impulse response becomes time-invariant

$$h(t,0) = \sum_{\mathrm{n}=0}^{N-1} c_{\mathrm{n}}(t)\delta\left(0 - \tau_{\mathrm{n}}(t)\right).$$

For a single channel tap, this simplifies to

$$h(t,0) = c_0(t)\delta\left(0 - \tau_0(t)\right).$$

With stationarity in t, the single channel-coefficient c_0 is a RV and the delay τ_0 may be assumed as a constant. In this case, the channel is reduced to a weighting coefficient, i.e. the fading gain of the channel. Popular assumptions for the statistical properties of this coefficient are Rayleigh and Rician distributions. In a digital transmission system that can perfectly compensate multipath propagation, such as OFDM with cyclic-prefix guard interval (cf. section 4.2.3), multipath fading may be reduced to fading gain RV simulation in case of slow fading (cf. section 3.2.2.3).

The tapped delay line model is one possibility for simulation of fading channels. Especially in multi carrier systems like OFDM, another option is simulation of a set of correlated fading subchannels, one for each subcarrier.

3.3.2 Distributions Rayleigh and Rice

A popular assumption for the magnitude distribution of one channel tap is *Rayleigh*. Let X and Y be independent Gaussian RVs with equal variance $\sigma^2 = \bar{P}/2$. In this case it can be shown that the random variable $Z = \sqrt{X^2 + Y^2}$ is Rayleigh distributed. Furthermore, as a measure for power, Z^2 is exponentially distributed. By change of variables, from the pdf of the Rayleigh distribution

$$p_{\mathrm{Z}}(x) = \frac{x}{\sigma^2}e^{-(x/\sigma)^2/2}$$

one obtains the "Rayleigh power pdf" or chi-squared distribution

$$p_{Z^2}(P) = 1/\bar{P} \cdot e^{-P/\bar{P}}. \tag{3.3.1}$$

When comparing fading channel measurements to this analytical model, it is important to consider the respective fading cumulative distribution function (cdf). In case of Rayleigh fading, the cdf of the chi-squared distribution is [27] $cdf_{Z^2}(P) = 1 - exp(-P)$. In case a dominant multipath component exists, e.g. the line-of-sight path, a Rician amplitude distribution is assumed. As will be elaborated later, these assumptions have proven to be realistic for both indoor and outdoor communication.

The "Rician power pdf" is given by the non-central chi-squared distribution [37]

$$\begin{aligned} p_{Z^2}(P, K) &= 1/\bar{P} \cdot (1 + K) \, e^{-K-(K+1)P/\bar{P}} \\ &\quad \cdot I_0 \left(2\sqrt{\frac{K(K+1)P}{\bar{P}}} \right) \end{aligned} \tag{3.3.2}$$

where I_0 is the zeroth-order modified Bessel function of the first kind [38], and the Rician dominant path factor $K \geq 0$ is defined as

$$K = P/\bar{P}.$$

In the special case of $K = 0$, the Rayleigh power distribution is obtained as the exponential distribution

$$p_{Z^2}(P, 0) = 1/\bar{P} \cdot e^{-P/\bar{P}}$$

Typical values for $K > 0$ in indoor communication environments are $0\,\text{dB} - 6\,\text{dB}$ [36]. The cdf of the non-central chi-squared distribution can be approximated numerically.

3.3.3 WSSUS

A simplified description of linear time variant channels is obtained by two assumptions [39]

- Uncorrelated scattering (US)

- Wide-sense stationarity (WSS)

The US assumption holds when multipath contributions at different arrival times are uncorrelated. WSS is a weak form of stationarity, whereas first and second order moments of the process are independent of absolute time, but dependent on time difference. An example for a stationary channel is a constant channel, which naturally implies no movement. In case of movement, Doppler occurs if motion is not orthogonal to the direction of wave propagation. It has been elaborated above that Doppler introduces time selectivity.

A wide-sense stationary uncorrelated scattering (WSSUS) channel is thus completely characterized by a 2-dimensional impulse response in delay τ and time difference Δt, i.e. the *time-variant impulse response* of the channel. It is valid at any absolute point in time (due to WSS) and as it is a finite impulse response (FIR), it decays over τ. The following notation in describing WSSUS channels is inherited from the literature [39, 26, 40]. Function plots are omitted herein, as they are widely available in the literature [40].

The time-variant impulse response $h(t, \tau)$ and the time-variant transfer function $T(t, f)$ and their Fourier relationship have been introduced above. By respective inverse Fourier transform in f and f_d, the four *Bello* [39] functions are obtained:

- *time-variant impulse response* $h(t, \tau) = \mathcal{F}_\mathrm{f}^{-1} \{T(t, f)\} = \mathcal{F}_\mathrm{f_d}^{-1} \{S(f_\mathrm{d}, \tau)\}$ with cross correlation

$$\phi_\mathrm{h}(t_1, t_2, \tau_1, \tau_2) = \mathrm{E}\left[h^*(t_1, \tau_1) h(t_2, \tau_2)\right]$$

- *time-variant transfer function* $T(t, f) = \mathcal{F}_\tau \{T(t, f)\} = \mathcal{F}_\mathrm{f_d}^{-1} \{H(f_\mathrm{d}, f)\}$ with cross correlation

$$\phi_\mathrm{T}(t_1, t_2, f_1, f_2) = \mathrm{E}\left[T^*(t_1, f_1) T(t_2, f_2)\right]$$

- *Doppler-variant impulse response* $S(f_\mathrm{d}, \tau) = \mathcal{F}_\mathrm{t} \{h(t, \tau)\} = \mathcal{F}_\mathrm{f}^{-1} \{H(f_\mathrm{d}, f)\}$

$$\phi_\mathrm{S}(f_\mathrm{d1}, f_\mathrm{d2}, \tau_1, \tau_2) = \mathrm{E}\left[S^*(f_\mathrm{d1}, \tau_1) S(f_\mathrm{d2}, \tau_2)\right]$$

- *Doppler-variant transfer function* $H(f_\mathrm{d}, f) = \mathcal{F}_\tau \{S(f_\mathrm{d}, \tau)\} = \mathcal{F}_\mathrm{t} \{T(t, f)\}$

$$\phi_\mathrm{H}(f_\mathrm{d1}, f_\mathrm{d2}, f_1, f_2) = \mathrm{E}\left[H^*(f_\mathrm{d1}, f_1) H(f_\mathrm{d2}, f_2)\right]$$

It can be shown [40] that the channel properties coherence time (T_coh), coherence bandwidth (B_coh), and delay spread (T_ds) can be deduced from the following four functions under the WSSUS assumptions, whereas capital Φ indicates the WSSUS version of the respective lowercase ϕ cross correlation functions:

- *delay cross power spectral density* $\Phi_\mathrm{h}(\Delta t, \tau)$

- *time frequency correlation function* $\phi_\mathrm{T}(\Delta t, \Delta f)$

- *Doppler cross power spectral density* $\Phi_\mathrm{H}(f_\mathrm{d}, \Delta f)$

- *Doppler delay cross power spectral density* $\Phi_\mathrm{S}(f_\mathrm{d}, \Delta f)$

They are independent of absolute time and frequency and are related by Fourier theory, whereas $\bullet\!\!-\!\!\circ$ denotes the Fourier transform, as follows:

$$
\begin{array}{ccc}
\Phi_\mathrm{h}\left(\Delta t, \tau\right) & \bullet\!\!\xrightarrow{\tau}\!\!\circ & \phi_\mathrm{T}\left(\Delta t, \Delta f\right) \\
\phi_\mathrm{T}\left(\Delta t, \Delta f\right) & \bullet\!\!\xrightarrow{\Delta t}\!\!\circ & \Phi_\mathrm{H}\left(f_\mathrm{d}, \Delta f\right) \\
\Phi_\mathrm{H}\left(f_\mathrm{d}, \Delta f\right) & \circ\!\!\xrightarrow{\tau}\!\!\bullet & \Phi_\mathrm{S}\left(f_\mathrm{d}, \tau\right) \\
\Phi_\mathrm{S}\left(f_\mathrm{d}, \tau\right) & \circ\!\!\xrightarrow{\Delta t}\!\!\bullet & \Phi_\mathrm{h}\left(\Delta t, \tau\right)
\end{array}
$$

WSSUS channels can thus be classified as

- *frequency flat* if invariant over Δf, i.e. monochromatic in τ.

  otherwise, a channel is referred to as *frequency selective*

- *time non-selective* if is invariant over Δt, i.e. monochromatic in f_d.

  otherwise, a channel is referred to as *time selective*

3.3.4 Single-Path Rayleigh Fading

The Rayleigh fading assumptions according to Clarke [34] are

- a very large number of planar waves arriving at the receiver antenna

- independent phases of uniform phase distribution between 0 and 2π

This results in the envelope of the received signal being Rayleigh distributed. The delay cross power spectral density function of a single channel tap Rayleigh fading channel, under the assumption of strictly planar wave incident, is [34]

$$\Phi_{\mathrm{h}}(\Delta t, \tau) = c_0(\Delta t, \tau) = J_0\left(2\pi f_{\mathrm{D}}\Delta t\right)\delta\left(\tau - \tau_0\right) \qquad (3.3.3)$$

where J_0 is the zeroth-order Bessel function of the first kind [38]. By the Dirac $\delta(\tau - \tau_0)$, the single path Rayleigh fading time variant impulse response is monochromatic in τ. The Dirac only positions the single received Rayleigh faded path in the delay domain. Hence, Rayleigh fading is frequency flat. The shape of $\Phi_{\mathrm{h}}(\Delta t, \tau)$ in Δt is independent of the delay and it can be immediately seen that it is also not changing with introduction of multiple reflected paths. Thus, the time delay autocorrelation function, in any case, is $\Phi_{\mathrm{h}}(\Delta t) = J_0\left(2\pi f_{\mathrm{D}}\Delta t\right)$ while for single path fading and $\tau_0 = 0$, the parameter τ can be omitted. Fourier transform by Δt of autocorrelation function results in the Doppler spread spectrum of a monochromatic (narrowband) signal

$$\Phi_{\mathrm{H}}(f_{\mathrm{d}}, \Delta f) = \frac{1}{\pi f_{\mathrm{D}}\sqrt{1 - (f_{\mathrm{d}}/f_{\mathrm{D}})^2}} \qquad |f_{\mathrm{d}}| \leq f_{\mathrm{D}} \qquad (3.3.4)$$

Consequently, the Rayleigh fading channel is time selective. The probability density function in (3.3.4) is the so-called "classical" or *Jakes* Doppler spectrum.

The coherence bandwidth is infinite for single path Rayleigh fading. From equation 3.3.3 the $-3\,\mathrm{dB}$ coherence time, T_{coh}, is obtained as

$$T_{\mathrm{coh}} = \arg\min_{|\Delta t|}\left\{J_0\left(2\pi f_{\mathrm{D}}\Delta t\right) \leq 0.5\right\} \approx \frac{3}{4\pi f_{\mathrm{D}}}$$

since in that case, $\Phi_{\mathrm{h}}\left(T_{\mathrm{coh}}\right) = J_0(3/2) \approx 0.51 > 0.501 \approx -3\,\mathrm{dB}$. As an example, for $f_{\mathrm{D}} = 1\,\mathrm{Hz}$, Rayleigh fading coherence time is $T_{\mathrm{coh}}|_{\mathrm{f_D=1}} \approx 0.239\,\mathrm{s}$.

3.3.5 Single-Path Rician Fading

In single channel tap Rician fading a dominant path component is introduced. It is assumed that a constant Doppler shift f_{k} occurs on this component. Thus, the Doppler spread (assuming $\tau_0 = 0$) is described as [40]

$$\Phi_{\mathrm{H}}(f_{\mathrm{d}}) = \frac{1}{1+K}\cdot\frac{1}{\pi f_{\mathrm{D}}\sqrt{1 - (f_{\mathrm{d}}/f_{\mathrm{D}})^2}} + \frac{K}{1+K}\delta(f_{\mathrm{d}} - f_{\mathrm{K}}) \quad |f_{\mathrm{d}}| \leq f_{\mathrm{D}}$$

where compared to Rayleigh, the dominant component is located at Doppler shift f_{K}. The power is distributed by the Rician K-factor among the uncorrelated Rayleigh scatterers and the dominant component.

The delay cross power spectral density function of a single path Rician fading channel is thus obtained by inverse Fourier transform over Δt as follows, omitting the τ domain as elaborated above

$$\Phi_{\mathrm{h}}\left(\Delta t\right) = c_0(\Delta t) = \frac{1}{1+K}J_0\left(2\pi f_{\mathrm{D}}\Delta t\right) + \frac{K}{1+K}exp(j2\pi f_{\mathrm{K}}\Delta t) \qquad (3.3.5)$$

This shows two things: the dominant path introduces a non-zero mean and the phase depends on the Doppler shift of the dominant component. Consequently, the $\pm 3\,\mathrm{dB}$ coherence time T_{coh} may become infinitely large due a significantly increased mean. It is e.g. for $K = 1$ and $f_{\mathrm{D}} = 1\,\mathrm{Hz}$

$$T_{\mathrm{coh}}|_{\mathrm{K}=1,\mathrm{f_D}=1} = \underset{|\Delta t|}{\arg\min}\left\{ J_0\left(2\pi\Delta t\right) = 0 \right\}$$

which can be found numerically to yield $T_{\mathrm{coh}}|_{\mathrm{K}=1,\mathrm{f_D}=1} \approx 0.879\,\mathrm{s}$.

3.3.6 Rayleigh Fading with Exponential Decay

Important in evaluation of indoor propagation is an exponential decay of individual channel taps $h_{\mathrm{n}}(t,\tau)$ over τ, cf. section 3.5.1. Again assuming a classical Doppler spectrum, the exponential decay over τ of single path Rayleigh fading is assumed Poisson distributed [40]

$$\Phi_{\mathrm{h}}(\Delta t,\tau) = c_0(\Delta t,\tau) = J_0\left(2\pi f_{\mathrm{D}}\Delta t\right)\frac{1}{T_{\mathrm{ds}}}exp\left(-\tau/T_{\mathrm{ds}}\right) \quad \tau > 0$$

with normalization of the power delay profile $\Phi_{\mathrm{h}}\left(0,\tau\right)$ of

$$\int_0^\infty \Phi_{\mathrm{h}}\left(0,\tau\right)d\tau = 1.$$

Then the average delay spread and the root-mean-square (rms) delay spread are defined as [26]

$$\begin{aligned}
\bar{\mu} &= \frac{\int_0^\infty \tau\Phi_{\mathrm{h}}\left(0,\tau\right)d\tau}{\int_0^\infty \Phi_{\mathrm{h}}\left(0,\tau\right)d\tau} \\
\mu_{\mathrm{rms}} &= \sqrt{\frac{\int_0^\infty \left(\tau-\bar{\mu}\right)^2\Phi_{\mathrm{h}}\left(0,\tau\right)d\tau}{\int_0^\infty \Phi_{\mathrm{h}}\left(0,\tau\right)d\tau}}
\end{aligned} \tag{3.3.6}$$

which results for the example of Poisson distributed profile in $\bar{\mu} = \mu_{\mathrm{rms}} = T_{\mathrm{ds}}$.

This channel is both time and frequency selective. In order to evaluate coherence time and coherence bandwidth at the same time, the envelope of the time frequency correlation function of the channel, $|\phi_{\mathrm{T}}(\Delta t,\Delta f)|$, is of interest and obtained by Fourier transform of the delay cross power spectral density over the delay τ

$$\mathcal{F}_\tau\left\{\Phi_{\mathrm{h}}(\Delta t,\tau)\right\} = \phi_{\mathrm{T}}(\Delta t,\Delta f) = \frac{J_0\left(2\pi f_{\mathrm{D}}\Delta t\right)}{1 + j2\pi\Delta f T_{\mathrm{ds}}}.$$

Coherence time is identical to the Rayleigh fading case, thus only

$$|\phi_{\mathrm{T}}\left(0,\Delta f\right)| = \frac{1}{\sqrt{1 + \left(2\pi\Delta f T_{\mathrm{ds}}\right)^2}}$$

is of interest and coherence bandwidth is given as

$$\begin{aligned}
B_{\mathrm{coh}} &= \underset{|\Delta f|}{\arg\min}\left\{\left[1 + \left(2\pi\Delta f T_{\mathrm{ds}}\right)^2\right]^{-1/2} = 0.5\right\} \\
&= \frac{\sqrt{3}}{2\pi T_{\mathrm{ds}}}.
\end{aligned}$$

Delay spread μ_{rms} in indoor environments is reported in the literature between $2\,\mathrm{ns}$ and $150\,\mathrm{ns}$ [41, 42, 36]. When the delay spread is $T_{\mathrm{ds}} < 100\,\mathrm{ns}$, which may be the case for indoor transmission, accordingly, $B_{\mathrm{coh}} > 2.76\,\mathrm{MHz}$.

3.4 Mobile Radio

Mobile radio implies that there is a fixed base station located outdoors and a number of mobile stations. A channel is termed *land-mobile* when both base and mobile station(s) are situated outdoors, and *indoor-mobile* when latter are indoors. The Nakagami fading model has been shown to accurately model the characteristics of both of the above mentioned mobile radio channels [43]. The Nakagami-m fading distribution is given as

$$p_\gamma(\gamma) = \frac{\gamma^{m-1}}{\Gamma(m)} (m/\bar{\gamma})^m e^{-m\gamma/\bar{\gamma}} \quad \gamma \geq 0 \tag{3.4.1}$$

where m is the Nakagami fading parameter ($m \geq 1/2$), and $\Gamma(.)$ is the gamma function [38]. For $m = 1/2$ it yields the one-sided Gaussian distribution, which is a more severe fading with even higher outage probability as compared to Rayleigh. Nakagami-m yields latter distribution for $m = 1$. It can be shown that a good approximation of a Rician distribution is obtained with $m > 1$. With $m \to \infty$ the Nakagami-m distribution converges to a non-fading AWGN channel. It is thus very flexible and widely used for mobile radio channels.

3.5 Indoor Attenuation

Indoor transmission is the case when both communication ends are located indoors. Typically, there is a wall mounted base station and a number of stationary user terminals within the same room, a room on the same floor or on another floor. Typically, low mobility in the order of one to several km/h is assumed in the environment. A simple indoor path loss prediction model including the attenuation of walls and floors is given as [30, 44]

$$P_\mathrm{t}/\overline{P_\mathrm{r}} = \beta_0 - n \cdot 10 \cdot log_{10}\left(\frac{d}{d_0}\right) - \sum_\mathrm{p} WAF(p) - \sum_\mathrm{q} FAF(q)$$

whereas β_0 is a reference path loss at the breakpoint distance d_0 and WAF and FAF are empirically determined wall and floor attenuation factors, respectively. Regarding the fact that multiple floors may contribute non-linearly [29], this is a simplified model.

According to Haykin et al. [44], the international telecommunications union recommends in ITU-R P.1238-2 for 5GHz indoor transmission

$$P_\mathrm{t}/\overline{P_\mathrm{r}} = 41dB + 31 \cdot log_{10}d - \sum_\mathrm{p} WAF(p) - \sum_\mathrm{q} FAF(q)$$

in which the path loss exponent is fixed to 3.1 and a number of p walls and q floors attenuate the signal linearly (in dB). The breakpoint distance is $d_0 = 1\,\mathrm{m}$. With respect to attenuation due to building structure, there is a wide variety of different measurement results due to different materials and transmit frequency used. For example, WAF of concrete walls is reported between 7 and 27dB [41].

3.5.1 Ray-Cluster Model

The Saleh-Valenzuela [45] (S-V) ray-cluster model is a tapped delay line model with exponential decay. The power delay profile $\Phi_\mathrm{h}(0, \tau)$ is Poisson distributed. The model is based on the observation that indoors, electromagnetic waves arrive in clusters (groups) of rays (multipath components). The building structure forms clusters, while rays are formed due to rich scattering at objects in the vicinity of sender and receiver.

Let T_l be the arrival time of cluster l and let the arrival time of a ray in cluster l, measured from T_l, be $\tau_\mathrm{k,l}$. Furthermore, let $\beta_\mathrm{k,l}$ be the gain and $\theta_\mathrm{k,l}$ be the phase of the ray with index (k, l). Then the S-V ray-cluster model is defined as [45]
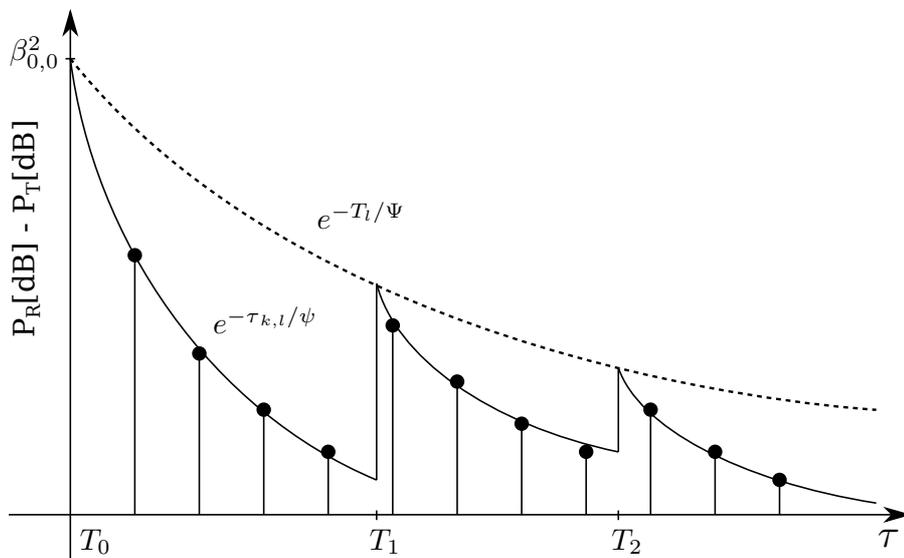
Figure 3.4: Indoor ray-cluster model according to Saleh and Valenzuela [45]. Here: Equi-distant channel taps, three clusters and eleven "channels" (samples).

$$h(t,\tau) = \sum_{k=0}^{\infty} \sum_{l=0}^{\infty} \beta_{k,l} \cdot e^{j\theta_{k,l}} \cdot \delta(\tau - T_l - \tau_{k,l}).$$

With $\overline{\beta_{0,0}^2}$ defined as the average power gain of the first cluster, the $\beta_{k,l}$ are defined as

$$
\begin{aligned}
\overline{\beta_{k,l}^2} &= \overline{\beta^2(T_l, \tau_{k,l})} \\
&= \overline{\beta_{0,0}^2} \cdot e^{-T_l/\Psi} \cdot e^{-\tau_{k,l}/\psi}
\end{aligned}
$$

where Ψ, ψ are normalization constants. The ray-cluster phases $\theta_{k,l}$ are independent uniformly distributed random variables over $[0, 2\pi)$. By the WSSUS assumptions, T_0 is set to zero.

The model can thus be characterized as clusters decaying with $exp(-T_l/\Psi)$ and multipath components within a cluster decaying with $exp(-\tau_{k,l}/\psi)$ (cf. section 3.3.6). It is important to note that clusters may overlap in delay time. Sampling $h(t,\tau)$ at equidistant intervals results in discrete time channel taps that are a superposition of multiple clusters, starting from T_1. This is depicted in figure 3.4.

3.6 IEEE 802.11 Channel Model

3.6.1 Large Scale Modeling

For modeling variations in the transmitter-receiver distance, a piecewise log-linear path loss model is assumed for simulation of 802.11n/ac. Furthermore, shadow fading with varying standard deviation is assumed. IEEE 802.11n channel model B [36] models a transition in path loss and shadow fading jointly at a breakpoint distance of 5 m. At this distance, there is also a transition from LOS to non-LOS (NLOS) conditions. Model B is derived from measurements of residential area indoor intra-room and room-to-room communication. Before the breakpoint, path loss is assumed as free-space with path loss exponent of 2. After the breakpoint, path loss exponent becomes 3.5. At the same point, the shadow fading std. dev. changes from 3 dB to 4 dB.
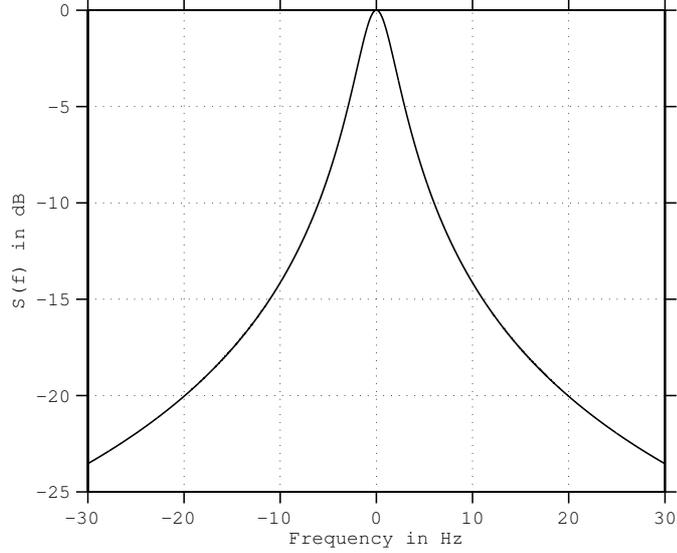
Figure 3.5: Bell shaped Doppler spectrum at $6\,\mathrm{Hz}$ maximum Doppler shift.

3.6.2 Small Scale Modeling

As an example of ray-cluster channel modeling, IEEE 802.11n [36] *model B* defines two clusters. A simplification therein compared to S-V is that clusters and rays are on sampled delay times, whereas S-V models Poisson distributed arrival times. Sampling frequency of the channel model is $100\,\mathrm{MHz}$, resulting in channel taps in steps of $10\,\mathrm{ns}$. For simulation, the two clusters composed of five and seven rays are superimposed, whereas the second cluster is delayed by two samples. The individual channel taps are modeled as Rayleigh distributed, while for LOS conditions, the first channel tap, i.e. at $\tau_{0,0}$, is modeled as Rician distributed with $K = 1 = 0\,\mathrm{dB}$. The delay spread according to eq. 3.3.6 in this model is $\mu_{\mathrm{rms}} = 15\,\mathrm{ns}$. Correlation of fading gains over time is due to "bell shaped" Doppler spectrum

$$\Phi_{\mathrm{H}}\left(f_{\mathrm{d}}\right) = \frac{1}{1 + \left(\frac{\sqrt{A}}{f_{\mathrm{D}}} f_{\mathrm{d}}\right)^2} \cdot \sqcap\left(\frac{f_{\mathrm{d}}}{10 f_{\mathrm{D}}}\right)$$

with $A = 9$ to satisfy

$$\Phi_{\mathrm{H}}\left(f_{\mathrm{d}}\right)|_{\mathrm{f_d=f_D}} = 0.1.$$

The Doppler cross power spectral density $\Phi_{\mathrm{H}}\left(f_{\mathrm{d}}\right)$ is plotted in figure 3.5. The inverse Fourier transform results in the scaled and band limited double sided exponential autocorrelation function

$$\Phi_{\mathrm{h}}\left(\Delta t\right) = \frac{\pi f_{\mathrm{D}}}{\sqrt{A}} exp\left(-\left|\frac{2\pi f_{\mathrm{D}}}{\sqrt{A}}\Delta t\right|\right) * 10 f_{\mathrm{D}} \cdot sinc\left(10 f_{\mathrm{D}}\Delta t\right)$$

Required for autocorrelation functions is $\Phi_{\mathrm{h}}\left(0\right) \overset{!}{=} 1$, hence a normalization constant $\zeta = \frac{\sqrt{A}}{\pi f_{\mathrm{D}}}$ is introduced. The band limitation of $\zeta \cdot \Phi_{\mathrm{H}}\left(f_{\mathrm{d}}\right)$ to $\pm 5 f_{\mathrm{D}}$ results in a convolution with a narrow *sinc* in the Δt domain. For finding the coherence time, it can approximated by a Dirac–$\delta(\Delta t)$. The autocorrelation function is thus rewritten as

$$\Phi_{\mathrm{h}}\left(\Delta t\right) = exp\left(-\frac{2\pi f_{\mathrm{D}}}{\sqrt{A}}|\Delta t|\right) \quad f_{\mathrm{D}} > 0$$
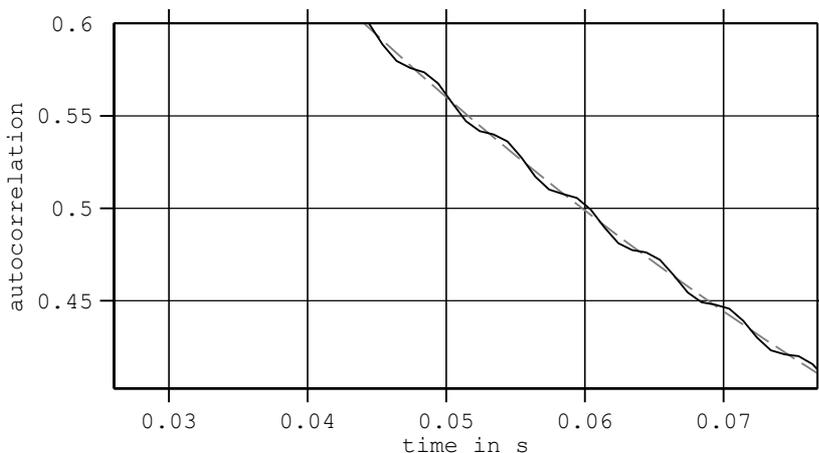
Figure 3.6: Autocorrelation of IEEE 802.11 channel models B–E and F (NLOS), latter with ripple due to 40 km/h vehicle.

and the coherence time is consequently found as

$$T_{\mathrm{coh}}(f_{\mathrm{D}}) = \frac{\sqrt{A}}{2\pi f_{\mathrm{D}}} ln\,(2)$$

which results in $T_{\mathrm{coh}}(2.7\,\mathrm{Hz}) \approx 125\,\mathrm{ms}$ at 2.4 GHz and $T_{\mathrm{coh}}(5.6\,\mathrm{Hz}) \approx 60\,\mathrm{ms}$ at 5 GHz for walking speeds of up to 1.2 km/h [36]. Computing coherence time as in the examples using a classical Doppler shape [34] (cf. section 3.3.3), at 1 Hz Doppler spread the coherence time becomes $T_{\mathrm{coh}}(1\,\mathrm{Hz}) \approx 330\,\mathrm{ms}$.

Independent of LOS or NLOS conditions, in channel model F a spike in the Doppler spectrum is added to model effects of a moving car at the speed of 40 km/h. The Doppler spectrum is thus set to

$$\Phi_{\mathrm{H}}{}^{F}\left(f_{\mathrm{d}}\right) = \zeta_{\mathrm{F}} \left[\frac{1}{1 + 9\left(\frac{f_{\mathrm{d}}}{f_{\mathrm{D}}}\right)^2} + \frac{1}{2}\frac{1}{1 + B\left(\frac{f_{\mathrm{d}} - f_{\mathrm{v}}}{f_{\mathrm{v}}}\right)^2} \right] \cdot \sqcap\left(\frac{f_{\mathrm{d}}}{2f_{\mathrm{max}}}\right)$$

with $f_{\mathrm{max}} = f_{\mathrm{v}}(1 + 5(0.02/2)) + 5f_{\mathrm{D}}$ and B set to 90 000 [36]. At 2.4 GHz this results in $f_{\mathrm{v}} \approx 89\,\mathrm{Hz}$ and with normalization

$$\zeta_{\mathrm{F}} = \frac{\zeta}{1 + \zeta \frac{2\sqrt{B}}{\pi f_{\mathrm{v}}}}$$

the autocorrelation function is found as

$$|\Phi_{\mathrm{h}}\left(\Delta t\right)| \quad = \quad \zeta_{\mathrm{F}}\left(\frac{\pi f_{\mathrm{D}}}{\sqrt{A}}e^{-\frac{2\pi f_{\mathrm{D}}}{\sqrt{A}}|\Delta t|} + \left|\frac{\pi f_{\mathrm{v}}}{2\sqrt{B}}e^{-\frac{2\pi f_{\mathrm{v}}}{\sqrt{B}}|\Delta t|}e^{j2\pi f_{\mathrm{v}}\Delta t}\right|\right).$$

This introduces a ripple in the autocorrelation function as depicted for the case of non-LOS conditions (NLOS) in figure 3.6.

In standardization of 802.11ac [46], the channel model developed for the standard 802.11n by IEEE 802.11 task group n (TGn) was adopted. Doppler spread has been re-investigated [47] by indoor measurements. Following those new measurements, the 802.11ac channel model slightly modifies the 802.11n channel model by setting the default maximum environmental speed for simulation to 0.089 km/h for stationary devices, resulting in an increased channel coherence time of about 800 ms at 5 GHz.

OFDM-QAM Wireless Digital Transmission

OFDM is a digital transmission scheme that is characterized by a number of important benefits. Modern wired and wireless communication systems [48, 7, 49] make use of OFDM due to its ease of implementation by inverse fast Fourier transform (IFFT) digital signal processing. In the scope of this work, multicast throughput of an OFDM based wireless system, the wireless LAN according to the IEEE 802.11 set of standards, is evaluated. Furthermore, feedback aggregation in wireless multicast is advocated herein, due to which a focus is on the physical layer (PHY) of transmission. With respect to this, the focus is on OFDM feedback aggregation. The purpose of this section is thus to give an overview of the characteristics of OFDM based transmission.

4.1 Spectral Efficiency

Digital transmission implies sampling in the time domain. From Fourier theory follows that a discrete time signal has an infinite, at $1/T_s$ periodically repeated spectrum, whereas T_s is the sampling period. Let the signal be band-limited, then the spectrum is determined by the one-sided signal bandwidth W (positive or negative non-zero spectral width). In general, the spectrum may be two-sided. For example, real valued samples have an even spectrum, i.e. the Fourier transform is two-sided (Hermitian symmetry). Clearly, if $1/T_s \gg 2W$, there is no overlap in the spectral replicas due to sampling. Shannon first postulated that at a sampling rate of $1/T_s = 2W$ the original signal can still be reconstructed perfectly from the samples – though not in practice, as the effort would be infinite[1].

Transmission of digital signals requires conversion from the digital domain to an analog, electrical signal. However, the resulting analog signal shape, the *pulse shape* $g_T(t)$, is undetermined in this process. In pulse amplitude modulation, multiple binary symbols are transmitted in a pulse train, whereas individual symbols are spaced by T_s. At the receiver, a finite time recording aperture $g_R(t)$ is used and this is again sampled at a rate of $1/T_s$. It can be shown that *matched filtering,* i.e. use of identical signals as pulse shape and recording aperture, maximizes the SNR in the presence of white noise. The output of the matched filter is the input to the sampler at the receiver and further denoted as $x(t) = g_T(t) * g_R(t)$, whereas $*$ denotes the convolution operator.

This however introduces the problem of inter-symbol interference (ISI): The time domain response of $x(t)$ must decay and have zeros at the sampling point of the next (and previous) symbols in order not to interfere with other symbols. In other words, the first *Nyquist* criterion shall be fulfilled. It is commonly termed the *pulse shaping criterion* or *Nyquist condition for zero ISI*. It is fulfilled if after sampling the output of the matched filter $x(t)$ at the receiver at the rate $1/T_s$

$$x\left(t = nT_s\right) = \begin{cases} 1 & n = 0 \\ 0 & n \neq 0 \end{cases}$$

---

[1] A limited spectrum implies infinite temporal spread.

which in the frequency domain corresponds to

$$\sum_{n=-\infty}^{\infty} X\left(f + \frac{n}{T_s}\right) = T_s \tag{4.1.1}$$

whereas $X(f)$ is the Fourier transform of $x(t)$. For eq. (4.1.1) to become true, there are several possibilities. Clearly, if $1/T_s > 2W$, where W is the one-sided spectral width of $X(f)$, spectral replica of $X(f)$ due to sampling of $x(t)$ never overlap. For other values of T_s, eq. (4.1.1) may become true.

The second criterion is fulfilled if the matched filter output of several consecutive symbols interferes destructively at $t - T_s/2$ and $t + T_s/2$. Then the so-called *vertical eye-opening* is maximized, which simplifies implementation. A pulse shape fulfilling both criteria is the modified *raised cosine*, which is evenly split into *root-raised* cosine pulses at sender and receiver respectively (matched filter). The raised cosine is defined as

$$\chi_{rc}(x, r) = \begin{cases} 1 & 0 \leq |x| \leq \frac{1-r}{2} \\ cos^2\left(\frac{\pi}{r}\left(|x| - \frac{1-r}{2}\right)\right) & \frac{1-r}{2} \leq |x| \leq \frac{1+r}{2} \\ 0 & |x| < \frac{1+r}{2} \end{cases} \tag{4.1.2}$$

and the modified raised cosine in the frequency domain $\chi_{rc}^m(f, r)$ fulfilling both criteria is defined as

$$\begin{aligned} \chi_{rc}^m(f, r) &= T_s \cdot \chi_{rc}(fT_s, r) \\ &= \begin{cases} T_s & 0 \leq |f| \leq \frac{1-r}{2T_s} \\ T_s \cdot cos^2\left(\frac{\pi T_s}{r}\left(|f| - \frac{1-r}{2T_s}\right)\right) & \frac{1-r}{2T_s} \leq |f| \leq \frac{1+r}{2T_s} \\ 0 & |f| < \frac{1+r}{2T_s} \end{cases} \end{aligned}$$

The roll-off factor r determines the excess bandwidth above $1/2T_s$ as well as the vertical eye opening. With $r = 1$ the eye opening is maximized as described above (the 2nd criterion is fulfilled). The excess bandwidth however is also maximized, thus bandwidth efficiency, measured in symbols per second per Hz (syms/s/Hz), is minimized. From this it can be concluded that using a pulse shape conforming to the *Nyquist criteria*, ISI free[2] digital transmission is possible at < 2 syms/s/Hz. However, the chosen frequency response $X(f) = \chi_{rc}$ also determines the interference introduced at adjacent channel usage. Interference thus needs to be considered. To reduce interference, spectral masks are defined in wireless transmission systems and guard bands are introduced.

4.2 Orthogonal Frequency Division Multiplex

For pulse amplitude modulation (PAM) it has been shown in section 4.1 that in single carrier transmission using matched root-raised-cosine (RRC) filters, spectral efficiency of less than 2 syms/s/Hz is realizable. For OFDM, symbol rate is equal to used bandwidth (neglecting spectral side lobes at both upper and lower band limits), hence OFDM spectral efficiency is 1 sym/s/Hz [51].

---

[2]Non ISI free transmission such as controlled ISI [50] is out of the scope of this work.

4.2.1 Inverse Discrete Fourier Transform

The complex baseband representation of an OFDM signal is defined using orthogonal signals sine and cosine at integer multiples of frequencies:

$$\hat{y}(t) \quad = \quad \sum_{n=0}^{N-1} \left[a_n(t) + jb_n(t) \right] e^{j2\pi nt/T} e^{-j\pi(N-1)t/T} \tag{4.2.1}$$

with $a_n(t)$ (and similarly, $b_n(t)$) defined as

$$a_n(t) \quad = \quad a_n \cdot s_c \left(t - \frac{T}{2} \right)$$

Let $s_c(t) = \sqcap(t)$, then the discrete time representation after sampling at a rate of N/T is found as

$$\hat{y}[i] \quad = \quad \sum_{i} \sum_{n=0}^{N-1} \left[a_n \left(\frac{iT}{N} \right) + jb_n \left(\frac{iT}{N} \right) \right] e^{j2\pi ni/N} e^{-j\pi(N-1)i/N}$$

In order to avoid aliasing, subcarriers at the edges remain unused all of the time, providing space for the low pass filter frequency domain rise and fall regions. Let $\hat{d}_n$ be a complex data symbol on subcarrier n. Without loss of generality, the discrete time representation of one multicarrier symbol can be written as

$$\hat{y}[i] \quad = \quad \sum_{n=0}^{N-1} \hat{d}_n e^{j2\pi ni/N}, \, 0 \leq i \leq N-1$$

This definition is identical to that of the inverse discrete Fourier transform (IDFT). Due to availability of IDFT hardware realizing the numerical approximate IFFT [52] in an efficient manner in practice, OFDM is generated in the complex baseband by IFFT, i.e. it is inherently sampled at a sampling rate of $T_s = N/T$ and consequently exhibits spectral repetitions at $1/T_s$. When the spectrum is centered as given in eq. 4.2.1, i.e. it is two-sided, $1/T_s < 2W$ does not strictly hold, but may be achieved by discarding some of the out most subcarriers. The number of unused or inactive carriers depends on implementation considerations in the digital to analog conversion stage.

4.2.2 Frequency Domain Considerations

As described above, OFDM is subject to self-interference by the spectral overlap due to sampling when generated by the IFFT. For $s_c(t) = \sqcap(t)$, Fourier transform thereof yields

$$\mathcal{F}_t \left\{ s_c(t) \right\} = \frac{sin(\pi f)}{\pi f} = sinc(f)$$

Hence, the spectrum of each OFDM subcarrier is not band-limited and consequently, that of IFFT-OFDM is not band-limited. If all subcarriers were used, the out most subcarriers would interfere with each other significantly, reducing the achievable SNR. In order to reduce distortion due to spectral overlap, the guard band is introduced. Figure 4.1 shows the use of guard band in single-carrier and multi-carrier transmission. While in the first case, a band gap is defined between two frequency bands, IFFT-OFDM with guard band permanently sets the out most subcarriers to zero. Without loss of generality, the IFFT-OFDM signal can be written as

$$\hat{y}_{gb}[i] \quad = \quad \sum_{n=0}^{N_u-1} \hat{d}_n e^{j2\pi ni/N}, \, 0 \leq i \leq N-1 \tag{4.2.2}$$
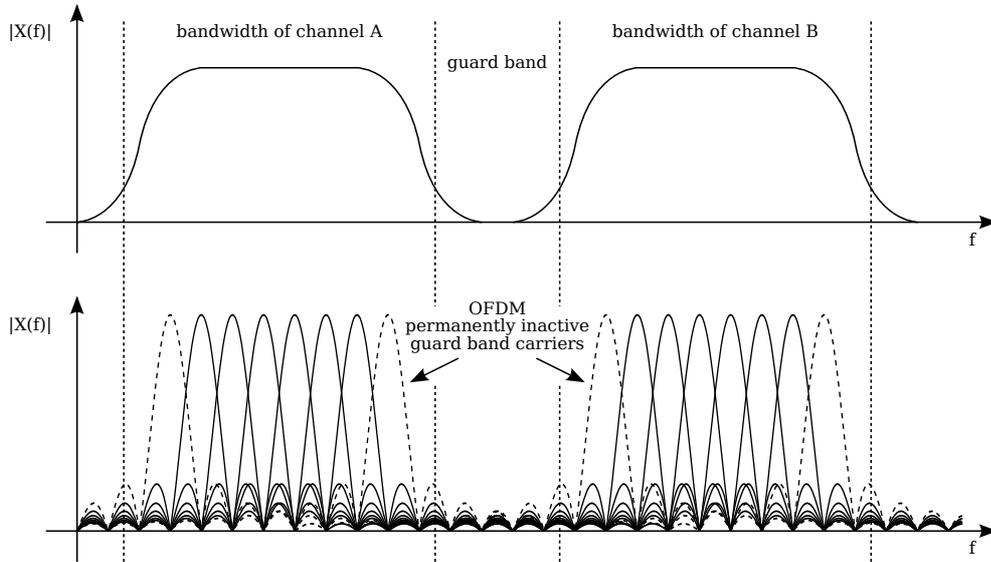
Figure 4.1: Top: Frequency division multiplex with guard band; Bottom: OFDM guard band by inactive carriers at the edges of the spectrum.

where $N_u < N$ is the number of used subcarriers. From eq. 4.2.1 it can further be seen that eq. 4.2.2 may also be obtained with integer multiples $k \cdot N$ and k/T_s, i.e. oversampling the IFFT.

When OFDM is subject to noise with constant psd $N_0/2$, using less than N carriers over the bandwidth $1/T_s$ results in an increase in SNR per subcarrier as compared to the SNR per OFDM symbol. With N_{GB} permanently inactive guard band carriers, the SNR is increased by less than N/N_{GB}.

4.2.3 Time Domain Considerations

The time domain representation of an OFDM symbol is given by the IFFT as derived above. A guard interval (GI) is beneficial concerning sampling time synchronization in OFDM. An OFDM transmission will typically be continuous, i.e. the individual symbols are transmitted back-to-back. Assuming the receiver being perfectly in sync with the sender in frequency and phase, the receiver still has to compute the fast Fourier transform (FFT) per symbol over the correct samples, i.e. over those of exactly one OFDM symbol. This can be visualized by means an OFDM eye-diagram [25].

Cyclic prefix is a guard interval solution with distinct benefits. The cyclic extension of an OFDM symbol at its beginning increases the symbol duration, whereas the added information is completely redundant. As can be seen from figure 4.2, the OFDM symbol can be detected at identical SNR for a duration that is equal to the guard interval when cyclic prefix is used and in absence of echoes. In the presence of echoes, OFDM with cyclic prefix guard interval preserves orthogonality as long as the latest echo arrives and decays within the guard interval.

With a cyclic prefix of $P \leq N$ samples, the discrete time representation of one OFDM symbol can be written as

$$\hat{y}_{gb,cp}[i] = \sum_{n=0}^{N_u-1} \hat{d}_n e^{j2\pi ni/N}, \quad -P \leq i \leq N-1$$

If chosen properly, the cyclic prefix guard interval makes OFDM much less sensitive with respect to required sampling time accuracy as compared to non-OFDM systems. According to
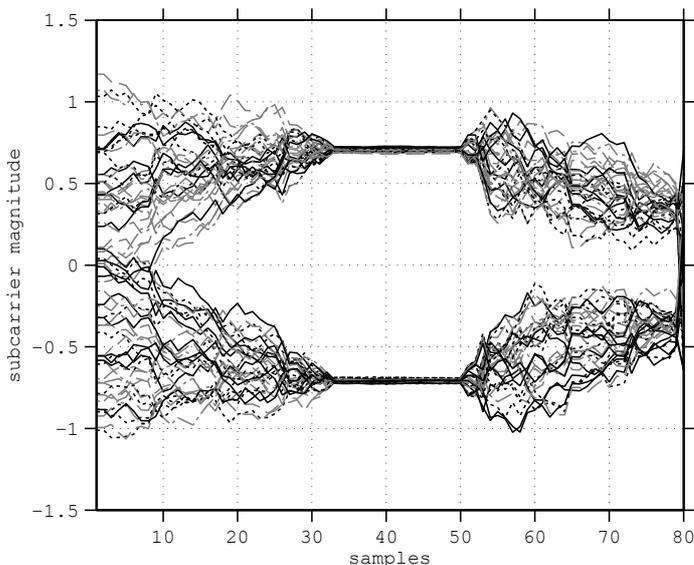
Figure 4.2: OFDM eye diagram with cyclic prefix. Individual curves represent one BPSK subcarrier each. The OFDM symbol consists of 64 IFFT samples plus 16 GI samples. A plateau of duration T_{GI} is visible during which the FFT is evaluated within the OFDM symbol duration $(T_{\mathrm{sym}} + T_{\mathrm{GI}})$. The symbol is zero padded at both ends and the FFT is computed 80 times.

Schmidt [25], an upper bound of $1/T_{\mathrm{sym}}$ sampling time jitter would be necessary in single carrier transmission in order to reach bitrates of OFDM systems.

Due to the redundancy introduced by the GI, there is a reduction in efficiency. Expressed in terms of signal power, the SNR is reduced by transmitter-receiver filter mismatch ν_{g}^2 [25]. Let $h(t)$ and $g(t)$ be the impulse responses of the transmit and receive filters, respectively, then

$$
\begin{aligned}
\nu_{\mathrm{g}}^2 \;&=\; \frac{\left[\int_{-\infty}^{\infty} h(\tau) \cdot g\left(-\tau\right) d\tau\right]^2}{\int_{-\infty}^{\infty} |h(t)|^2 \; \mathrm{dt} \cdot \int_{-\infty}^{\infty} |g(t)|^2 \; \mathrm{dt}} \\
&=\; 1 - \frac{T_{\mathrm{GI}}}{T_{\mathrm{sym}} + T_{\mathrm{GI}}}
\end{aligned}
$$

For example, when $T_{\mathrm{GI}}/T_{\mathrm{sym}} = 0.25$, the loss in SNR due to the GI is approximately $1\,\mathrm{dB}$.

4.2.4   Power Spectral Density

The psd of an OFDM signal, including the guard interval, can be simulated. During the simulation, it may however not be completely evident whether the shape of the psd is due to OFDM and e.g. a cyclic-prefix guard interval, or due to some simulation parameter, such as the chosen FFT size and windowing filters. Waterschoot et al. [53] have derived analytical expression for the psd of cyclic-prefix and zero-padding OFDM signals. An example plot of an OFDM psd is given in figure 5.6 on page 56.

4.3 OFDM Performance Impairments

4.3.1 Peak-to-Average Power Ratio

For the discrete time signal s_n at the IFFT output, peak-to-average power ratio (PAPR) is defined as

$$PAPR = \frac{max\,|s_\mathrm{n}|^2}{\mathrm{E}\left[|s_\mathrm{n}|^2\right]}$$

It can be easily shown that with equal magnitude on all subcarriers, the maximum power for an OFDM symbol with $N - N_\mathrm{GB} = N_\mathrm{u}$ used carriers is N_u^2 while the average power is N_u. For an OFDM system using e.g. $N_\mathrm{u} = 52$ of $N = 64$ carriers, PAPR is $10 \cdot log_{10}(52) = 17.2\,\mathrm{dB}$. As maximum power N_u^2 may not be achieved when the information on the subcarriers is assumed random, peak-to-average power ratio is typically less than N_u.

4.3.2 Power Amplifier Nonlinearity

Consideration of power amplifier nonlinearity is important in case of OFDM due to high PAPR. This is especially true for OFDM systems that do not include algorithms for PAPR reduction, such as the IEEE 802.11 OFDM systems (cf. chapter 5).

   The model used herein is the popular Rapp PA model, which is limited to amplitude distortion. An output back-off (OBO) is defined as a quantity relative to the maximum output power and thus typically given in dB. OBO is the ratio of maximum to average output power. The signal amplitude Rapp model is given as

$$y(t) = \frac{G \cdot x(t)}{\left(1 + \left|\frac{x(t)}{V_\mathrm{sat}}\right|^{2p}\right)^{1/2p}}$$

in which the input voltage is $x(t)$, the amplifier output voltage is $y(t)$ and v_sat is output at the saturation point (i.e. an input voltage higher than v_sat does not result in an increase in output voltage). The output power of the amplifier is calculated as

$$P_\mathrm{out} = \int_0^\infty |y(t)|^2\,dt$$

An iterative algorithm controlling the input gain G is required to achieve an OBO in practice. The average output power may e.g. be computed over one transmitted symbol. If the symbol is composed of n samples, the average output power over one symbol is given in dB as

$$P_\mathrm{out}[\,\mathrm{dB}] = 20 \cdot log_{10}\left(\frac{1}{n}\sum_{\mathrm{k}=1}^n |y[k]|\right)$$

$$OBO = P_\mathrm{sat}[\,\mathrm{dB}] - P_\mathrm{out}[\,\mathrm{dB}]$$

The average output power of an OFDM symbol is unknown in general, hence it is estimated per transmitted OFDM symbol.

   For simulation of OFDM based wireless LAN, a recommendation [54] is to set $p = 3$ and the power amplifier output back-off to

$$OBO = 25dBm - 17dBm = 8dB$$

It can be assumed that small-scale power amplifier technology is evolving and improving with respect to non-linear distortion. However, it can be concluded that a reduction in transmit power with respect to the maximum tolerated power, as will be relevant in the course of this work, may result in reduced distortion.

4.3.3 Carrier Frequency Offset and Phase Noise

In a real system, transmitter and receiver use independently running oscillators to generate the carrier frequency. They are subject to frequency deviation and phase noise. Furthermore, in Rician fading a dominant LOS path (cf. section 3.3.5) with deterministic Doppler contributes to carrier frequency offset (CFO). While there are multiple approaches to frequency synthesis for carrier frequency modulation and demodulation, frequency offset between sender and receiver will cause distortion if it is not compensated. A frequency tracking algorithm in conjunction with a VCXO is one possibility for frequency offset compensation.

Multi carrier transmission via orthogonal subcarriers can be assumed more sensitive to frequency offset, as it introduces inter-carrier interference due to loss of orthogonality. Pollet et al. [55] have derived an approximation of OFDM degradation in the presence of frequency error and phase noise (PN). While for single carrier transmission, the degradation due to frequency error Δf is proportional with $(\Delta f)^2$, for OFDM it is proportional with $\gamma (N\Delta f)^2$, where γ is the symbol average SNR. For an oscillator linewidth[3] of β, the degradation of single carrier is proportional with $\beta\gamma$ and that of OFDM is proportional with $\beta\gamma N$. Consequently, with increasing number of subcarriers, the system is increasingly sensitive to frequency and phase errors.

Stephens et al. [54] specified a frequency offset at the receiver, with respect to the transmitter, of $|\Delta f| < 13.675$ ppm in a comparison criteria specification document for the development of the 802.11n and 802.11ac standards. Residual carrier frequency offset and phase noise of specific OFDM receiver structures are out of the scope of this work. Herein, it is assumed that CFO and PN are zero.

4.4 OFDM in Fading Channels

4.4.1 Sensitivity to Frequency Selectivity

Ultra wideband fading channels are characterized by large delay spreads, i.e. $T_{ds} \gg 1/B$. Then, the bandwidth B of the signal is large compared to $1/T_{ds}$, and echoes of the original signal may be decoded individually and combined using e.g. maximum ratio combining (cf. code-division multiple access (CDMA)). Narrowband fading conversely implies $T_{ds} \ll 1/B$, i.e. very small B compared to $1/T_{ds}$, and thus the channel is regarded as frequency non-selective (flat). Consequently, frequency selectivity occurs in-between the above two extremes.

In a single carrier system using a bandwidth B, a frequency domain equalizer is required in case of frequency selectivity due to multipath propagation. In multi carrier systems of the same overall bandwidth B however, frequency selectivity may affect individual subcarriers differently. As an example, assume a discrete two ray multipath channel in which the delayed component arrives at the receiver with the same power as the first component. This will result in cancellation of some frequency components by destructive interference, while some other frequency components will experience constructive interference. For OFDM transmission, attenuation and amplification of individual subcarriers may be experienced, resulting in an increase of SNR on some subcarriers and decrease on others. Thus, OFDM as such is highly sensitive to frequency selectivity. A frequency domain equalizer is implicitly incorporated in the OFDM itself (FFT at the receiver). However, frequency domain equalization on a per subcarrier basis is not strictly required, as a frequency domain interleaving of the bits transmitted over the different subcarriers of appropriate dimension will sufficiently decouple the errors on low SNR subcarriers. In

---

[3]One-sided 3 dB linewidth of the phase noise psd of the free-running carrier frequency oscillator

systems like DVB-S/T as well as WLAN, this is solved by (inner) convolutional FEC coding error protection followed by (inner) interleaving. In the scope of this work, frequency selectivity is considered. Its influence, however, is summarized under a complex channel fading gain and the influence on the SNR is averaged over a burst of OFDM symbols.

4.4.2 Sensitivity to Time Selectivity

As elaborated above, the Doppler effect introduces time selectivity. In case of Doppler spread, as opposed to a simple shift, a monochromatic signal is spread in the frequency domain according to the Doppler spread psd, which in turn is determined by geometry. In the case of OFDM, depending on the subcarrier distance, this may introduce non-negligible inter-carrier interference (ICI). For a multiple reflection Rayleigh fading channel, assuming a classical Doppler psd, with exponential decay of the individual multipath components (reflections), ICI has been derived by Choi et al. [56]. Their analytical solution is normalized and thus independent of multipath delays and magnitudes, assuming the excess delay is smaller than the OFDM guard interval.

The time-varying multipath channel with transfer function $T(t, f)$ and time frequency correlation function $\phi_T(\Delta t, \Delta f)$ introduces a time-varying complex factor $\phi_T[n, k]$ for every OFDM subcarrier k at discrete time n. Defining $\phi_T[k]$ as the arithmetic mean over all discrete time instants n during the OFDM symbol results in a complex gain per subcarrier k. The expected value of its squared magnitude is used as a power normalization constant:

$$
\mathrm{E}\left[|\phi_T|^2\right] \quad = \quad \frac{1}{N^2}\left[N + 2\sum_{n=1}^{N}(N-n)\, J_0\left(\frac{2\pi f_D T_{sym} n}{N}\right)\right]
$$

Furthermore, Choi et al. derive the ICI power $\mathrm{E}\left[|a_k|^2\right]$ on subcarrier k due to the time selective channel as

$$
\mathrm{E}\left[|a[k]|^2\right] \quad = \quad \frac{1}{N^2}\sum_{m=0,m\neq k}^{N_u}\left[N + 2\sum_{n=1}^{N}(N-n)\right.
$$
$$
\left. \cdot J_0\left(\frac{2\pi f_D T_{sym} n}{N}\right)\cos\left(\frac{2\pi n\,(m-k)}{N}\right)\right]
$$

where N_u is the number of used carriers, and the normalized ICI power as

$$
\sigma_{\mathrm{ICI}}^2[k] = \frac{\mathrm{E}\left[|a[k]|^2\right]}{\mathrm{E}\left[|\Phi_T|^2\right]}
$$

One observes that ICI power on subcarrier k as introduced by a single subcarrier $m \neq k$ thus is

$$
\sigma_{\mathrm{ICI}}^2[k, m] \quad = \quad \frac{N + 2\sum_{n=1}^{N}(N-n)\, J_0\left(\frac{2\pi f_D T_{sym} n}{N}\right)\cos\left(\frac{2\pi n(m-k)}{N}\right)}{N + 2\sum_{n=1}^{N}(N-n)\, J_0\left(\frac{2\pi f_D T_{sym} n}{N}\right)}
$$

As an example, figure 4.3 plots $\sigma_{\mathrm{ICI}}^2[k]$ for a normalized maximum Doppler shift of $f_D T_{sym} = 4 \cdot 10^{-4}$, where T_{sym} is the OFDM symbol duration. The normalized ICI power is about -65.8 dB on the used carriers N_u except for a decrease of less than 3 dB at the out most left and right subcarriers. It is independent of the number of subcarriers when $N \geq 64$ [56]. Note that this amount of maximum normalized Doppler is experienced for example at 20 km/h at a center subcarrier frequency of 5 GHz and $T_{sym} = 4\,\mu$s. As data on the individual subcarriers is assumed uncorrelated, this results in an SNR per subcarrier due to time selectivity of more than 66 dB for Doppler speeds below 100 Hz at an OFDM symbol duration of $4\,\mu$s.

For low mobility, the coherence time may be well above an OFDM burst transmission duration. In that case, ICI due to Doppler is negligible.
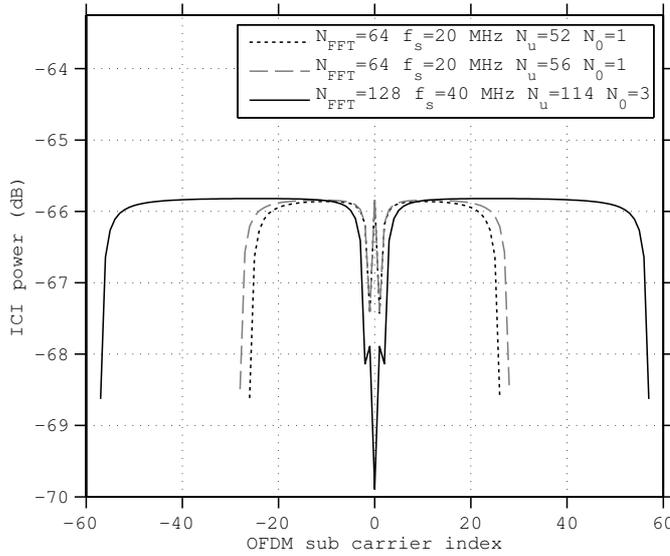
Figure 4.3: OFDM inter-carrier interference power due to $f_D = 100\,\text{Hz}$ maximum Doppler shift at $T_{\text{sym}} = 4\,\mu\text{s}$ (normalized Doppler $f_D \cdot T_{\text{sym}} = 0.0004$) for different OFDM configurations applying no data on N_0 center carriers.

4.5 Subcarrier Modulation

In this section the notation of signal-to-noise ratio per PSK/QAM symbol ($E_s/N_0 = \gamma_s$) and signal-to-noise ratio per bit ($E_b/N_0 = \gamma_b$) will be used. Their relation is

$$\frac{E_b}{N_0} = \frac{1}{ld(M)} \frac{E_s}{N_0}$$

with $ld(M)$ being the number of bits per PSK/QAM symbol and $\frac{1}{2}N_0$ is AWGN noise power per Hertz. For OFDM transmission, this should not be mixed up with the SNR on the channel, SNR_c, which may be due to AWGN and is a measure for the distortion of an OFDM symbol. The relation with SNR_c is given as

$$SNR_c = \frac{1}{B_n T_{\text{sym}}} \frac{E_s}{N_0}$$

for complex baseband signals, in which B_n is the bandwidth of noise acquisition. In a discrete time OFDM simulation for the sake of simplicity $B_n = 1/T_s/N$ is assumed and the SNR is further decreased by ν_g^2 (cf. section 4.2.3).

The passband (analog) signal is a real signal and thus has a symmetric spectrum. After demodulation, positive and negative parts of the spectrum are combined. Noise in both parts (bandwidth) is uncorrelated, hence its spectrum (psd) is non-symmetric. Noise with constant psd (white noise) of $N_0/2$ affects the real signal and thus becomes complex valued with constant psd of N_0 in the demodulated complex baseband signal representation. A scatterplot of quarternary phase shift keying (QPSK) constellation points on subcarriers of an OFDM symbol, averaged over a large number of symbols, and in the presence of 10 dB AWGN is depicted in figure 4.4.

Of ultimate interest is the bit error probability (BEP) at a given channel SNR, i.e. $P_b(SNR_c)$. The BEP is an important performance measure, especially in case of binary coding, where an input BEP is linked to an output BEP after decoding.
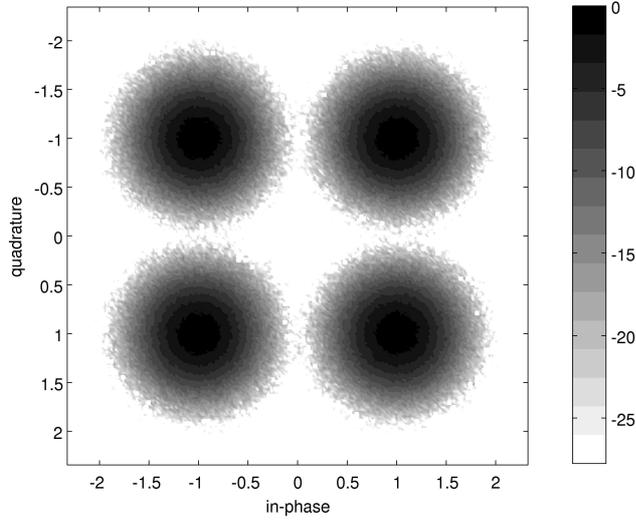
Figure 4.4: Logarithmic density scatterplot of OFDM-QPSK over an AWGN channel at $10\,\mathrm{dB}$ SNR at the receiver ($11.4\,\mathrm{dB}$ per used subcarrier, as measured).

4.6 Bit Error Probability

In digital transmission, bit error probability (BEP) is expressed by the Q function. This is either a Gaussian-Q function (coherent detection) or a Marcum-Q function (non or partially coherent detection) [57]. As OFDM transmission schemes typically use pilot symbols, frequency and phase synchronization can be assumed. Therefore, the focus herein is on coherent detection, thus

$$Q(x) = \frac{1}{\sqrt{2\pi}} \int_{x}^{\infty} exp\left(-\frac{x^2}{2}\right) dx = \frac{1}{2}erfc\left(\frac{x}{\sqrt{2}}\right)$$

Binary Phase Shift Keying For BPSK, the BEP can be given exactly and it is identical to the symbol error probability

$$P_{\mathrm{b}}^{BPSK} = P_{\mathrm{s}}^{BPSK} = Q\left(\sqrt{2\gamma_{\mathrm{s}}}\right)$$

Quadrature Phase Shift Keying Assuming the direct neighbors to only differ by one bit (Gray coding), the BEP of QPSK is exactly [51]

$$P_{\mathrm{b}}^{QPSK} = Q\left(\sqrt{\gamma_{\mathrm{s}}}\right) = Q\left(\sqrt{2\gamma_{\mathrm{b}}}\right)$$

The BEP per γ_{b} of BPSK and QPSK are identical. An approximate $3\,\mathrm{dB}$ degradation in BEP performance of QPSK as compared to BPSK concerning γ_{s} is due to the more closely spaced signal points, i.e. the magnitude of the complex phasors for BPSK $d_{\mathrm{BPSK}} = 2$ and for QPSK $d_{\mathrm{QPSK}} = \sqrt{2}$ under an equal transmit power assumption, here $E_{\mathrm{s}} = 1$. This shows that the BEP per γ_{b} is not a useful performance measure.

M-ary Quadrature Amplitude Modulation An approximation for Gray coded symbols is $P_{\mathrm{b}} = P_{\mathrm{s}}/ld(M)$, but only valid for high SNR values as non-direct neighbor errors are neglected. Exact derivation of QAM BEP is considered irrelevant in the scope of this work, as rate adaptation is done in bidirectional wireless networks. In that regard, knowledge about a lower limit

in SNR of a given modulation is of interest, which is obtained by evaluation at high SNR with respect to the modulation order. An approximate M-ary QAM BEP can be found as

$$P_{\mathrm{b}}^{QAM} \approx \frac{2\left(1 - \sqrt{1/M}\right)}{ld\left(M\right)} Q\left(\sqrt{\frac{3\,ld\left(M\right)}{M-1}\frac{\bar{\gamma}_{\mathrm{s}}}{ld(M)}}\right)$$

where the average constellation point energy is again normalized to $\bar{E}_{\mathrm{s}} = 1$. Exact BEP derivation for higher order modulations can be found in a publication by Peng et al. [58].

4.7 Bit Error Probability under Fading

It has been elaborated above how OFDM with frequency domain interleaving is robust against frequency selective fading when the delay spread is less than the guard interval duration. However, the average SNR per subcarrier may be degraded. For time non-selective channels, i.e. the coherence time of the channel is significantly larger than the duration of (an OFDM symbol burst) transmission, the BEP is determined instantaneously and approximately by the average AWGN SNR. In time-selective channels, ICI and AWGN both influence system performance. When the coherence time of the channel is in the order of the OFDM symbol time, it has been shown that a significant additive noise term from ICI is obtained. Due to the transmitted data being quasi random (e.g. due to scrambling in WLAN, cf. section 5.2.2), this can be assumed as another AWGN term. The resulting carrier-to-noise ratio (CNR) definition holds in any case:

$$CNR = \frac{\mathrm{E}\left[P_{\mathrm{carrier}}\right]}{P_{\mathrm{ICI}} + N_0 \cdot \Delta_{\mathrm{f}}} \tag{4.7.1}$$

Herein $\mathrm{E}\left[P_{\mathrm{carrier}}\right]$ consists of the average channel gain per subcarier due to multipath and the transmit power. However, from 4.7.1 it can bee seen that one or the other noise term may be negligible.

Detailed analysis of convolutional FEC coding performance over non-Gaussian distributed noise channels has been done in the past [50]. Influence of e.g. an additional Rayleigh or Rician fading RV is considered in case the probability density of constellation point errors is indeed influenced by the additional RV. Under fast fading, transmission is impaired by AWGN with variable complex gain. This gain is then e.g. assumed Rayleigh distributed. In general, it has a pdf of $p_\gamma(\gamma)$. The average bit error rate is obtained by averaging the instantaneous AWGN BEP over the distribution of the SNR γ

$$\overline{P_{\mathrm{b}}} \quad = \quad \int_0^\infty P_{\mathrm{b}}(\gamma)p_\gamma(\gamma)\,\mathrm{d}\gamma \tag{4.7.2}$$

For OFDM, the result yields the error rates averaged over a burst of OFDM symbols in case the symbol time is smaller than the coherence time but the burst duration is multiples of the coherence time (with the RV being properly represented during the burst transmission). This assumes quasi constant conditions during one OFDM symbol and thus an average white noise SNR, averaged over the subcarriers. For packet based transmission in which the packet duration is smaller than the coherence time, and with multiple modulation and coding scheme (MCS) combinations to adapt to the time-varying channel conditions, eq. 4.7.2 is not directly applicable. For each avaliable quadrature amplitude modulation (QAM) signal constellation, a $\overline{P_{\mathrm{b,QAM}}}$ can be computed, and consequently including FEC, for each available MCS. Bit rate adaptation to the channel, however, is typically done on a per packet basis or per block of packets, consisting of multiple OFDM symbols. Packet error rate consideration as given in 5.4 is more feasible in this regard, and is thus the primary focus of this work. $\overline{P_{\mathrm{b}}}$ is directly applicable in fixed rate transmission, such as open-loop WLAN multicast (cf. section 7.1) and wireless DVB subject to multipath fading.

Table 4.1: Coefficients for BPSK and M-QAM error probabilities

	c_1	c_2
BPSK/QPSK	$1/2$	1
M-QAM	$\frac{2(\sqrt{M}-1)}{\sqrt{M}ld(M)}$	$\frac{3ld(M)}{2(M-1)}$

4.7.1 Rayleigh fading

Rayleigh fading channel gain by definition of a Rayleigh distributed RV R is introduced into eq. 4.7.2 such that the instantaneous SNR is replaced by a faded $\gamma_f = R^2 \cdot \bar{\gamma}_b$, whereas $\bar{\gamma}_b$ is the average AWGN SNR per bit. Focusing on Gaussian-Q function analysis as elaborated in section 4.6, the bit error probability is of the form

$$P_b\left(R^2\right) \quad \propto \quad Q\left(R^2 \frac{\bar{E}_b}{N_0} c_2\right)$$

where c_2 is a modulation dependent parameter as given in table 4.1. With this, the mean BEP becomes [51]

$$\bar{P}_b \quad = \quad E\left[P_b(R^2)\right] = \int_0^\infty P_b(x) f_{R^2}(x) dx$$

where $f_{R^2}(x)$ is the pdf of a Chi-squared distributed RV, i.e. the distribution of the power of a Rayleigh faded magnitude of eq. 3.3.1. It can be shown that this integral can be transformed and solved in closed form as [51]

$$E\left[P_b(R^2)\right] \quad = \quad \frac{2c_1}{\pi} \int_0^{\pi/2} \frac{sin^2(\Theta)}{sin^2(\Theta) + c_2 \cdot \bar{\gamma}_b} d\Theta$$

$$\bar{P}_b^{Ray} \quad = \quad c_1\left(1 - \sqrt{\frac{c_2 \cdot \bar{\gamma}_b}{1 + c_2 \cdot \bar{\gamma}_b}}\right)$$

where coefficients c_1 and c_2 are given in table 4.1. With $\bar{\gamma}_b = \bar{\gamma}_s / ld(M)$ and above given approximation for M-QAM, exact results can be given immediately for BPSK and QPSK

$$\bar{P}_{b|BPSK}^{Ray} \quad = \quad \frac{1}{2}\left(1 - \sqrt{\frac{2 \cdot \bar{\gamma}_s}{1 + 2 \cdot \bar{\gamma}_s}}\right)$$

$$\bar{P}_{b|QPSK}^{Ray} \quad = \quad \frac{1}{2}\left(1 - \sqrt{\frac{\bar{\gamma}_s}{1 + \bar{\gamma}_s}}\right)$$

For M-ary QAM a nearest neighbor approximation can be found as [51]

$$\bar{P}_{b|M-QAM}^{Ray} \approx 2\frac{\sqrt{M}-1}{\sqrt{M}ld(M)}\left(1 - \sqrt{\frac{3\bar{\gamma}_s}{2(M-1) + 3\bar{\gamma}_s}}\right)$$

4.7.2 Rician fading

Similarly, the Rician fading average BEP can be found by taking $f_R(x)$ from eq. 3.3.2. For the resulting integral

$$\bar{P}_b^{Rice} \quad = \quad \frac{2c_1}{\pi} \int_0^{\pi/2} \frac{(1+K)sin^2(\Theta)}{(1+K)sin^2(\Theta) + c_2\bar{\gamma}_b}$$
$$\cdot exp\left(\frac{K \cdot c_2\bar{\gamma}_b}{(1+K)sin^2(\Theta) + c_2\bar{\gamma}_b}\right) d\Theta$$

there is no known closed form solution. Numerical results for BPSK, QPSK, 16-QAM and 64-QAM with Rician $K = 10$ are depicted in figure 4.5.
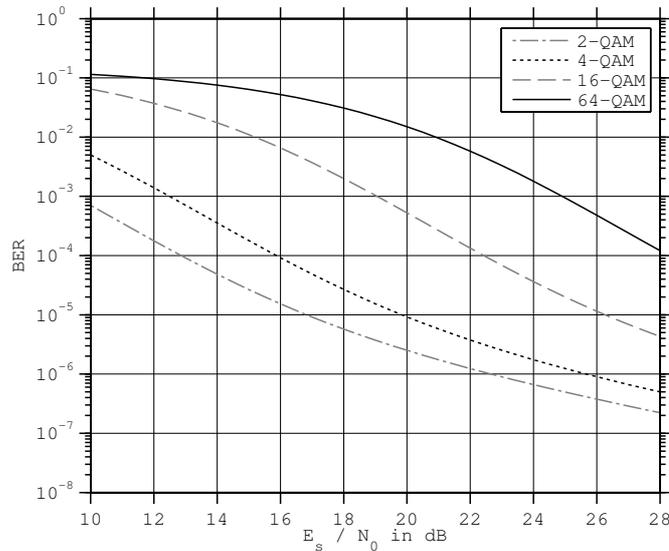
Figure 4.5: Rician fading BERs with LOS component 10 times as strong as the sum of the scattering components ($K = 10$)

4.8 OFDM Link Budget

Apart from transmit power and receiver distance, several factors influence the range of communication. Some of them are due to the environment, while some are OFDM specific.

It has been shown that large scale effects, such as human body shadowing and building structure (walls, floors) play an important role. Small scale effects due to multiple reflected path propagation result in fast or slow fading of the signal and a fading margin, e.g. with respect to the average depth of fades, has to be considered. This is especially true for broadcast systems transmitting at a fixed MCS defined bitrate.

Specifically in case of OFDM, reduction of transmit power due to a required power amplifier back-off reduces the available link budget. At the receiver, the receiver design (from analog front end to soft/hard Viterbi decoding) and its implementation noise figure determine its sensitivity, whereas lowering sensitivity results in an increase in link budget. Use of the OFDM guard interval has been shown to be a necessity, however, the achievable SNR is lowered by the transmitter-receiver filter mismatch. Due to the OFDM being inherently sampled when created by an IFFT, silent guard band subcarriers at the spectral edges are required, reducing spectral efficiency.

The highly flexible structure of OFDM with respect to the number of subcarriers and the easily configurable and potentially adaptive cyclic-prefix guard interval allows adaptation of an OFDM system to a multitude of propagation scenarios and system requirements. Reduction of the PAPR in OFDM can be achieved by a number of pre-coding schemes, whereas building highly linear and efficient power amplifier designs is ongoing research. Consequently, an OFDM link budget can only be roughly approximated. In this work, for a subset of effects, conservative estimates will be used, whereas the focus is on OFDM transmission over fading channels.

4.9 OFDM in Modern Wireless Systems

The focus of this work is on OFDM based communications systems due to the fact that OFDM has become the predominant digital transmission technique. It lends itself to being used in a variety of ways other than in a monolithic way. Variability of the guard interval introduces flexibility of deployment in multipath fading channels with largely different delay spreads. In "evolved

Table 4.2: OFDM parameters of some established wireless systems

	DVB-T2 [48]	IEEE 802.11 [7]	3GPP LTE [49]
OFDM technology	OFDM with rot. const.	OFDM	OFDMA (downlink), SC-FDMA (uplink)
Occupied bandw. B [MHz]	1.7, 5 − 8, 10	16.6 − 156.6	$2^i \cdot 1.25$, $i \in \{1, 2, 3, \log_2(12), 4\}$
Sampling frequency [MHz]	$\frac{8}{7} \cdot B$	20 − 160	$k \times 3.84$, $k \in \left\{\frac{1}{2}, 1, 2, 3, 4, 5, 6, 7, 8\right\}$
FFT size	$2^{10} - 2^{15}$	64 − 256	128 − 2048, 4096*
Used data carriers (approx.)	83 %	75 % − 91 %	59 %
Subcarrier spacing [KHz]	0.279 − 8.929	312.5	7.5*, 15
Cyclic-prefix GI [μs]	7 − 512	0.8 / 0.4	4.69, 7.29, 16.67, 33.34*
Determines GI duration	bandwidth	fixed	bandwidth, MBSFN*
Minimum constellation	QPSK	BPSK	QPSK
Maximum constellation	256-QAM	256-QAM	64-QAM

* used only in LTE evolved MBMS SFN (MBSFN) for mobile TV

MBMS" as specified by the Third Generation Partnership Project (3GPP) on the LTE mobile communication standard, an extended GI is used in multicast/broadcast single frequency networks (MBSFNs). In frequency selective channels, implementing some form of correlation among subcarriers may be reasonable and is easily achieved e.g. by interleaving and *rotated constellations* as used in DVB-T2 [48]. This combination further achieves decoupling of I/Q-components by the rotation of the constellation patterns. Furthermore, subcarriers of a single OFDM symbol may be shared among wireless stations. This kind of frequency division multiple access by allocation of different OFDM subcarriers for different users is termed orthogonal frequency division multiple access (OFDMA). It is applied in "evolved UMTS Terrestrial Radio Access (UTRA)" networks at the base station for downlink transmission, while single-carrier frequency division multiple access (SC-FDMA) is used by user terminals in the uplink [49]. SC-FDMA is a discrete Fourier transform (DFT) pre-coded variant of OFDMA. Due to the DFT operation on a subset of subcarriers, these subcarriers are used as a single carrier while maintaining OFDM orthogonality. As the PAPR is reduced by SC-FDMA as well [59], it is used in mobile terminal devices in order to reduce power consumption of uplink transmission. Table 4.2 provides a comparison of currently established wireless systems using differently parameterized OFDM as well as different variants of OFDM(A). Results presented in this work are obtained by evaluating 802.11 wireless LAN. Due to an observable convergence in new generations of wireless systems towards being implemented using OFDM, portability of the results to other OFDM based systems is given. For a better understanding of the herein presented results, a detailed description of OFDM in 802.11 is given in the following.

5

IEEE 802.11 Wireless LAN

The purpose of this chapter is to elaborate on the frame transmission process in IEEE 802.11 wireless LAN, as MAC layer *frames* are used for data transmission and feedback in this work. With respect to the theoretical results as provided in this work as well as a prototype implementation (cf. chapter 10), relevant parts of WLAN are discussed in the following, whereas the focus is on MAC and physical layers.

5.1 Architectural Overview

A working group of the IEEE 802 project among the local area network (LAN) and metropolitan area network (MAN) groups, identified as 802.11, defines the architecture and the service of what is referred to as wireless local area network (WLAN). For some of the IEEE 802 standards, among those 802.11, the open systems interconnection data link layer and the physical layer (cf. section 2.5.1) are subdivided into two sublayers each. The data link layer is divided into the logical link control (LLC) layer (cf. 802.2-1989) and the MAC layer. LLC enables coexistence of different network layer protocols, such as IP and IPX[1]. IEEE 802.11 appears to LLC as a wired LAN. Therefore, its MAC incorporates ARQ by means of a stop-and-wait protocol for frame loss compensation in order to meet the reliability assumption that LLC makes about lower layers. The PHY layer is subdivided into the physical layer convergence procedure (PLCP) and the physical medium dependent sublayer (PMD). Latter defines transmission over a physical medium, such as OFDM, as depicted in figure 5.1 on the following page. Another PMD variant, among others, is direct sequence spread spectrum [60] (DSSS). Each PMD sublayer defines a unique PLCP to enable mixed operation of different PMD variants in the same frequency band, such as unimpaired mixed DSSS-OFDM operation. For this, a DSSS PLCP preamble is used to synchronize channel access while data is transmitted as OFDM symbols at higher data rates [61]. The PLCP of purely OFDM based 802.11a [62] is depicted in figure 5.2 on page 52.

IEEE 802 standards families share the same address space conventions, in which three different kinds of addresses are defined: unicast, multicast and the broadcast (wildcard) address. The address space is of cardinality 2^{48}. Every IEEE 802 device is uniquely identified within this address space by pre-defined, vendor assigned addresses. While data destined to the broadcast address is processed by any device on the network, no multicast group management protocol is defined. IEEE 802 networks are multicast capable (cf. section 5.3.1) but rely on upper layer multicast protocols (cf. section 2.5.3). Broadcast on the other hand is used e.g. for MAC management frames, such as the WLAN *beacon* frame, which is a periodically transmitted message sent by access points (APs) exclusively, announcing WLAN service to potential clients. Broadcast may also be used for data transmission by applications. However, in wireless networks a wireless LAN broadcast data frame shall only be initiated by an AP. By definition, any terminal that is associated to an AP may receive broadcast data frames from this AP, while broadcast frames initiated by any other terminal may not be received by all associated terminals within the AP range. Consequently, the same holds true for multicast.

---

[1]Novell, Inc., "Advanced NetWare V2.1 Internetwork Packet Exchange Protocol (IPX)"
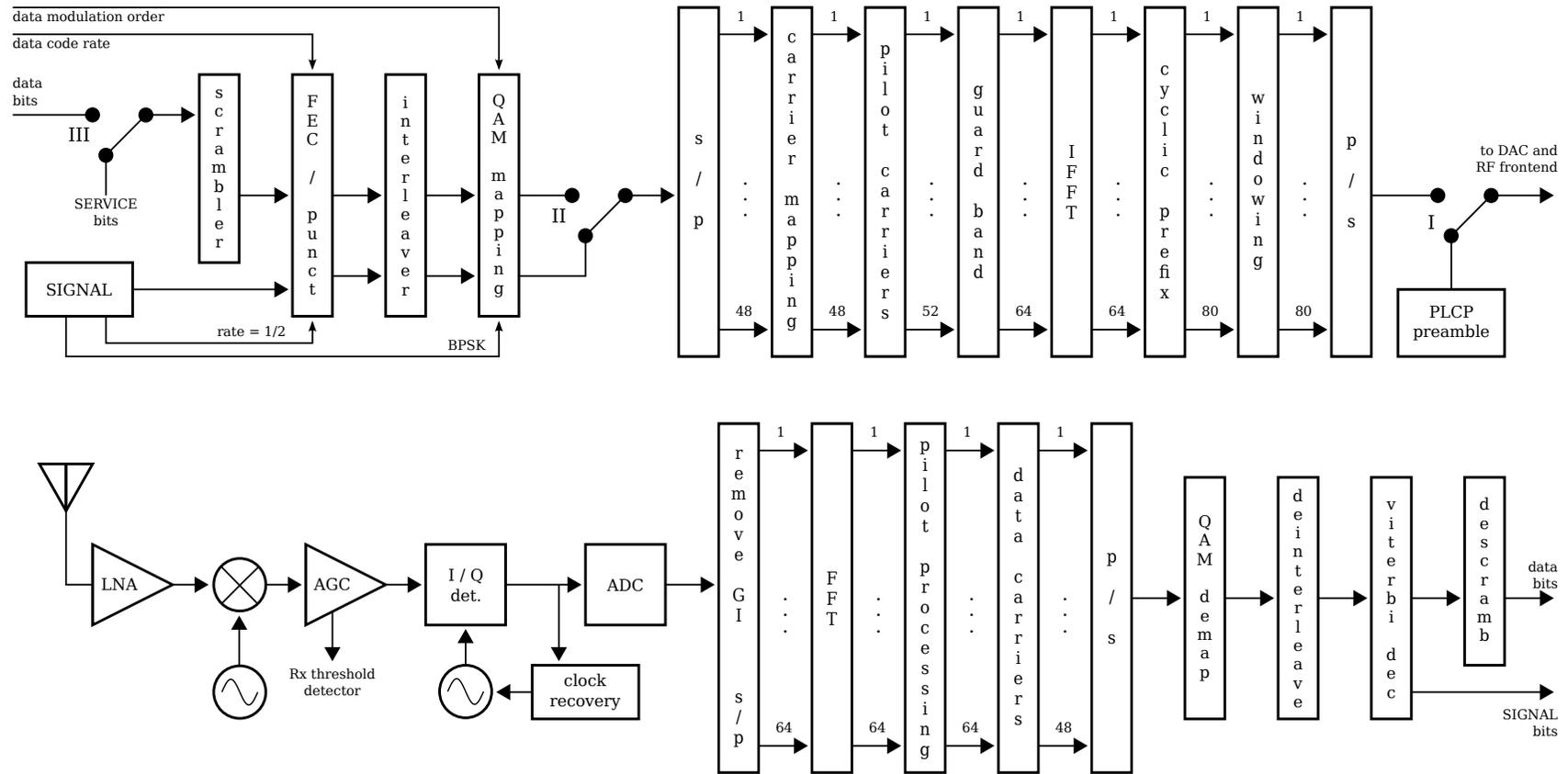
Figure 5.1: IEEE 802.11 OFDM transmit (top) and receive (bottom) block diagram. In the transmitter, the switches I, II and III are switched in their lexicographical order for every 802.11a/g OFDM frame (sequence of OFDM symbols).
Top: baseband transmit structure, *bottom:* complete receiver structure

Table 5.1: IEEE 802.11a/g/n/ac OFDM parameters

Parameter set	non-HT	HT	HT	VHT	VHT
Sampling frequency	20 MHz	20 MHz	40 MHz	80 MHz	160 MHz
N: FFT size	64	64	128	256	512
Guard band (GB)$^+$	$6_\mathrm{L} + 5_\mathrm{R}$	$4_\mathrm{L} + 3_\mathrm{R}$	$6_\mathrm{L} + 5_\mathrm{R}$	$6_\mathrm{L} + 5_\mathrm{R}$	$6_\mathrm{L} + 5_\mathrm{R}$
Null carriers (incl. GB)	12	8	14	14	28
N_u: Used carriers	52	56	114	242	484
Pilot carriers	4	4	6	8	16
Data carriers	48	52	108	234	468
Δ_f: Subcarrier spacing	312.5 kHz	312.5 kHz	312.5 kHz	312.5 kHz	312.5 kHz
T_FFT: IFFT duration	3.2 μs	3.2 μs	3.2 μs	3.2 μs	3.2 μs
T_GI: Symbol GI*	0.8 μs	0.4 μs	0.4 μs	0.4 μs	0.4 μs
T_sym: Symbol interval*	4 μs	3.6 μs	3.6 μs	3.6 μs	3.6 μs
T_P: PLCP preamble*	16 μs	8 μs	8 μs	8 μs	8 μs
T_GI2: Preamble GI*	1.6 μs	0.8 μs	0.8 μs	0.8 μs	0.8 μs
T_sig: Signal field*	4 μs	8 μs	8 μs	8 μs	8 μs

$^+$ $_\mathrm{L}$ and $_\mathrm{R}$ indicate left/right of center (carrier) frequency
$*$ minimum values

5.2 OFDM Physical Layer

5.2.1 Parameters

Table 5.1 provides an overview of OFDM parameters as specified by IEEE 802.11a/g/n/ac. Three sets of available 802.11 OFDM parameters are distinguished, referred to as pre-802.11n/ac non high throughput (nHT), IEEE 802.11n high throughput (HT) [63] and IEEE 802.11ac very high throughput (VHT) [46]. At the time of writing, latter is in the process of being standardized. In the following, those parameters relevant in the scope of this work are discussed.

The physical layer convergence procedure (PLCP) as defined in IEEE 802.11 specifies the general form of any transmitted signal, denoted as $s_\mathrm{plcp}(t)$, as follows:

$$s_\mathrm{plcp}(t) = s_\mathrm{preamble}(t) + s_\mathrm{signal}\left(t - T_\mathrm{P}\right) + s_\mathrm{data}\left(t - T_\mathrm{P} - T_\mathrm{sig}\right) \tag{5.2.1}$$

It is divided into a fixed and a variable part. Both primary terms are of fixed duration, whereas the *preamble* part $s_\mathrm{preamble}(t)$ is additionally of fixed structure. The *data* part $s_\mathrm{data}(t)$ is of variable duration. The preamble is of duration T_P and the *signal* symbol $s_\mathrm{signal}(t)$ is of duration T_sig. For example, $T_\mathrm{P} + T_\mathrm{sig} = 16\,\mu\mathrm{s} + 4\,\mu\mathrm{s}$ for 20 MHz nHT OFDM operation, whereas $T_\mathrm{P} + T_\mathrm{sig} = 8\,\mu\mathrm{s} + 8\,\mu\mathrm{s}$ for mixed 20 MHz/40 MHz HT operation. Any OFDM symbol is generated as described in section 4.2 according to

$$s_\mathrm{ofdm}(t) = \sqcap(t/T_\mathrm{FFT} - 0.5) \sum_{\mathrm{k}=-N_\mathrm{u}/2}^{N_\mathrm{u}/2} C_\mathrm{k} e^{j2\pi k \Delta_\mathrm{f} t / T_\mathrm{FFT}} \tag{5.2.2}$$

in which C_k are complex information symbols and N_u is the number of subcarriers used, whereas a subset thereof, so-called *pilot carriers* are permanently set to either ± 1 or 0. The subcarriers are spaced in the frequency domain by Δ_f and T_FFT is the OFDM core symbol duration. The individual parameters are specified as given in table 5.1 for 802.11a/g/n and as proposed for 802.11ac by the IEEE task group TGac.

Guard Band

The OFDM WLAN guard band is realized by permanently inactive subcarriers at the spectral edges, depending on the number of subcarriers in total. In table 5.1 the number of guard band carriers is given in the format $a_\mathrm{L} + b_\mathrm{R}$, indicating that at the left (L) and right (R) edges of the overall spectrum, a and b carriers, respectively, remain unused all of the time.
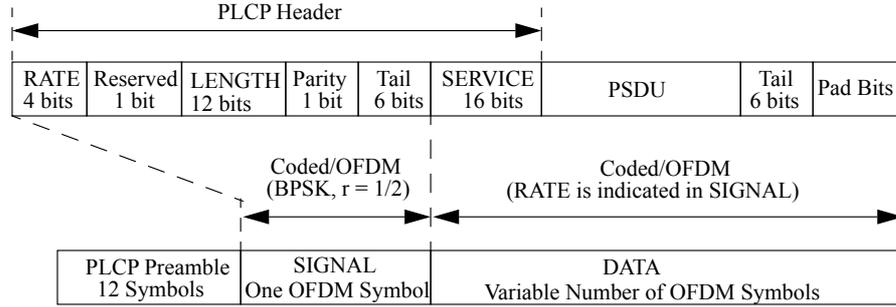
Figure 5.2: 802.11a OFDM physical layer frame format with physical layer convergence procedure (PLCP) header [62]

Guard Interval

An OFDM guard interval is required in multipath propagation channels. As 802.11 is mainly designed for indoor operation, it is consequently realized as a *cyclic prefix* (cf. section 4.2.3). Thus the guard interval is taken by copying the back end of the symbol and appending it at the front, which can be defined in the time domain as follows:

$$s_{\text{guard}}(t) = \sqcap\left(\frac{t - T_{\text{FFT}} + T_{\text{GI}}}{T_{\text{GI}}} - 0.5\right) s_{\text{ofdm}}(t).$$

5.2.2 Symbol Structure

With cyclic prefix guard interval extension, the resulting prolonged OFDM symbol is further weighted by $w_{\text{T}}(t)$ for spectral shaping as elaborated in section 5.2.4. The final OFDM symbol can be written as

$$s_{\text{symbol}}(t) = w_{\text{T}}(t) \cdot (s_{\text{ofdm}}(t - T_{\text{GI}}) + s_{\text{guard}}(t + T_{\text{FFT}} - T_{\text{GI}})).$$

For pure OFDM based IEEE 802.11 WLAN transmission, $s_{\text{plcp}}(t)$ is composed of a sequence of back-to-back OFDM symbols, whereas $s_{\text{preamble}}(t)$ and $s_{\text{data}}(t)$ in eq. 5.2.1 are composed as defined by $s_{\text{symbol}}(t)$, in which only C_{k} of $s_{\text{ofdm}}(t)$ varies with transmitted data.

The SIGNAL symbol As depicted in figure 5.2, the length and MCS (RATE bits) of the following sequence of OFDM frames containing payload data is signaled in the *SIGNAL* symbol. In single-input single-output (SISO) OFDM modes it is always transmitted at the most robust rate (BPSK and FEC rate 1/2 on all subcarriers), resulting in 6 Mbps raw throughput, and is not scrambled. Thus the receiver can immediately predict the duration of transmission even if it is unable to decode the transmission successfully. This is useful for determining the point in time of next channel access which is recorded as the network allocation vector (NAV) in case the frame is not destined to this very station. As part of the clear channel assessment (CCA) functionality, the NAV stores the time until which the channel is going to be idle.

Scrambling Parts of the transmitted data are scrambled before transmission in order to assure pseudo-random signal characteristics even in case of long sequences of ones or zeros. Figure 5.3 shows the 802.11a/g binary convolutional scrambling by the generator polynomial $x^7 + x^4 + 1$. Consequently, the *SERVICE* field in the PLCP header contains seven zeros for initialization of the scrambler.
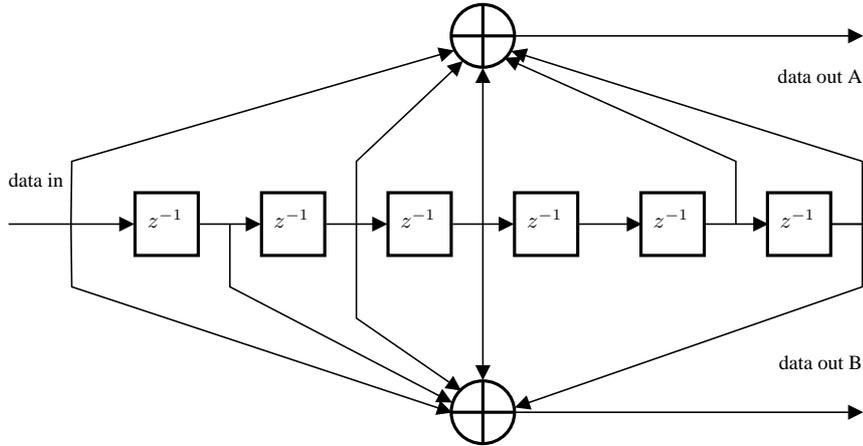
Figure 5.4: 802.11a/g convolutional coder $133, 171|_o$ of rate $1/2$
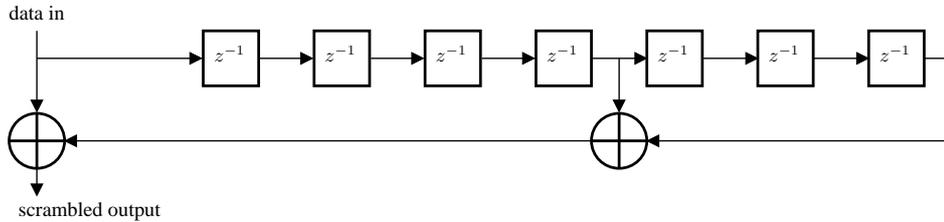
Figure 5.3: 802.11a/g scrambler $x^7 + x^4 + 1$

Forward Error Coding Convolutional FEC is employed using two generator polynomials, $133|_o$ and $171|_o$. Thus, the code is of rate $1/2$ and realized as shown in the shift register diagram of figure 5.4. A state diagram of the encoder is omitted due to its size of 128 states. For each input bit, the bit at data output "A" shall be output before the bit at data output "B". Higher rates of $2/3$, $3/4$ and $5/6$ [64] are achieved by puncturing, for which the puncturing matrices can be given as

$$\mathbf{P}_{2/3} = \begin{pmatrix} 1 & 1 \\ 1 & 0 \end{pmatrix}$$

$$\mathbf{P}_{3/4} = \begin{pmatrix} 1 & 1 & 0 \\ 1 & 0 & 1 \end{pmatrix}$$

$$\mathbf{P}_{5/6} = \begin{pmatrix} 1 & 1 & 0 & 1 & 0 \\ 1 & 0 & 1 & 0 & 1 \end{pmatrix}$$

The Hamming distance of this code is $d_{1/2} = 10$ for rate $1/2$ while it is $d_{2/3} = 6$ and $d_{3/4} = 5$ for the punctured rates. A sequence of $\lfloor \frac{d-1}{2} \rfloor$ erroneous bits can be corrected by this code (4 or 2, respectively). Even though the QAM mapper ensures that direct neighbors in the constellation diagram differ by only one bit (Gray coding), it is obvious that bit interleaving is required in low SNR situations. The performance of Viterbi decoding under different propagation scenarios is elaborated in section 4.6. Further error recovery in unicast 802.11 WLAN is done by retransmissions. Depending on the capabilities of the two participating stations, this can be either stop-and-wait ARQ or block acknowledgements (BAs), a form of go-back-n ARQ (cf. section 2.5.2). Starting with 802.11n [63] and in what followed [7, 46], WLAN supports optional

Table 5.2: 802.11a/g receiver sensitivity requirements (20 MHz channels) [64]

Data rate [Mbit/s]	6	9	12	18	24	36	48	54
Modulation type	BPSK		QPSK		QAM			
Modulation order	2	2	4	4	16	16	64	64
Code rate	1/2	3/4	1/2	3/4	1/2	3/4	2/3	3/4
S_{RX} [dBm]	-82	-81	-79	-77	-74	-70	-66	-65

use of LDPC codes. These block codes of coded block lengths 81, 162, or 243 bytes are defined at the same code rates as given above. A gain of 1.5 dB to 3 dB [65] in SNR can be achieved with LDPC codes as compared to binary convolutional codes. As LDPC is not mandatory of any IEEE 802.11 standard at the time of writing and lower level channel coding is out of the scope of this work, the reader is referred to the respective literature.

Interleaving   The binary sequence is interleaved before groups of bits are mapped to QAM constellation points on the OFDM subcarriers. OFDM transmission in frequency selective channels requires frequency domain interleaving and thus a first interleaving stage ensures that neighboring bits will not be mapped to neighboring subcarriers. A second interleaving stage ensures that neighboring bits are mapped to front and back bit positions of the individual QAM symbols. Both interleaving stages use block interleaving. The first interleaving stage maps a bit index $k \in [0, N_{\mathrm{CBPS}} - 1]$, where N_{CBPS} is the number of coded bits per OFDM symbol, to a bit index $i \in [0, N_{\mathrm{CBPS}} - 1]$

$$i = \frac{N_{\mathrm{CBPS}}}{16}(k \bmod 16) + \left\lfloor \frac{k}{16} \right\rfloor$$

and in the 2nd interleaving stage, i is mapped to $l \in [0, N_{\mathrm{CBPS}} - 1]$

$$l = s \left\lfloor \frac{i}{s} \right\rfloor + \left[\left(i + N_{\mathrm{CBPS}} - \left\lfloor \frac{16i}{N_{\mathrm{CBPS}}} \right\rfloor \right) \bmod s \right]$$

where $s = \max\left(log_2(M)/2, 1\right)$ and M is the QAM symbol modulation order.

5.2.3   Receiver Sensitivity

The IEEE 802.11 [7] standard defines minimum input level sensitivity figures for the OFDM receiver that hold for both 2.4 GHz and 5 GHz operational modes as given in table 5.2 for 20 MHz channel width. Receiver sensitivity figures for 40 MHz, 10 MHz and 5 MHz bandwidths are bandwidth proportional, i.e. $+3$ dB, -3 dB and -6 dB respectively. To arrive at these figures, the assumptions made are a receiver noise figure of $NF = 10$ dB and an implementation margin of $I = 5$ dB between the receiver antenna and analog-to-digital conversion. Minimum sensitivity is specified as 10 % packet loss for 1 kB packet length.

The federal communications commission (FCC) of the United States of America permits U-NII[2] devices in the $5.15 - 5.25$ GHz band to use a maximum transmit power of 50 mW and a peak psd of 2.5 mW/MHz. For 802.11a/g/n SISO OFDM transmission, assuming the transmit spectrum to be ideally flat, the psd requirement is a limiting factor. This results in a maximum transmit power of 17 dBm when all OFDM subcarriers are active. For 802.11a/g configurations using e.g. $52/64 \cdot 20$ MHz $= 16.25$ MHz (neglecting spectral sidelobes) this results in a maximum transmit power of 40.6 mW $= 16.1$ dBm.

The thermal noise floor, again assuming full bandwidth usage, is given as (cf. section 3.1)

$$-174 \, \mathrm{dBm/Hz} \cdot 20 \, \mathrm{MHz} \approx -101 \, \mathrm{dBm}$$

---

[2]Subpart E: Unlicensed National Information Infrastructure Devices (15.401-15.407)

Table 5.3: Lower 802.11a/g SNR limits (20 MHz, 10% PER, 1 kB)

Data rate [Mbit/s]	6	9	12	18	24	36	48	54
γ_{req} [dB]		4	5	7	9	12	16	20	21

The available link budget down to this noise floor is thus

$$L_{\mathrm{B}} = 17\,\mathrm{dBm} - (-101\,\mathrm{dBm}) = 118\,\mathrm{dB}$$

while the same result is achieved for less active carriers. For each given MCS one may thus compute the required SNR under the above assumptions for the modulation and coding parameters:

$$\gamma_{\mathrm{req}}(\mathrm{MCS}) = L_{\mathrm{B}} - (P_{\mathrm{t}} - S_{\mathrm{RX}}(\mathrm{MCS}) + NF + I)$$

Resulting values for 802.11a/g defined OFDM-QAM with convolutional FEC coding MCSs are given in table 5.3. As a side note, it can be seen that some of the punctured rates (9, 18, and > 36) and their respective non-punctured counterparts are closely spaced.

5.2.4 Spectral Shaping

In 802.11 OFDM, multiple channels are defined by their center carrier frequency and they may be directly adjacent (or even overlapping). When the digital OFDM signal is converted to analog at the transmitter, in order to achieve a reasonable level of adjacent channel interference (ACI), it is required to apply spectral shaping. A possible windowing function for spectral sidelobe control is the following

$$
\begin{aligned}
w_{\mathrm{T}}(t) &= \chi_{\mathrm{rc}}\left(\frac{t - \frac{1}{2}T_{\mathrm{sym}} + t_{\mathrm{RC}}}{T_{\mathrm{sym}}}, r_{\mathrm{w}}\right) \\
&= \begin{cases}
sin^2\left(\frac{\pi}{2}\left(\frac{1}{2} + \frac{t}{t_{\mathrm{RC}}}\right)\right) & -\frac{1}{2}t_{\mathrm{RC}} < t < \frac{1}{2}t_{\mathrm{RC}} \\
1 & \frac{1}{2}t_{\mathrm{RC}} < t < T_{\mathrm{sym}} - \frac{1}{2}t_{\mathrm{RC}} \\
sin^2\left(\frac{\pi}{2}\left(\frac{1}{2} - \frac{(t - T_{\mathrm{sym}})}{t_{\mathrm{RC}}}\right)\right) & T_{\mathrm{sym}} - \frac{1}{2}t_{\mathrm{RC}} < t < T_{\mathrm{sym}} + \frac{1}{2}t_{\mathrm{RC}}
\end{cases}
\end{aligned}
$$

with configurable rise time and fall time $t_{\mathrm{RC}} = 2T_{\mathrm{s}}$. This is a cosine roll-off in the time domain with roll-off factor

$$r_{\mathrm{w}} = \frac{t_{\mathrm{RC}}}{T_{\mathrm{sym}}}$$

which is $2 \cdot 50\,\mathrm{ns}/3.2\,\mu\mathrm{s} = 3.125\,\%$ for 20 MHz nHT operation and may be $1.5625\% < r_{\mathrm{w}} < 12.5\%$ for a 40 MHz HT configuration with reduced GI duration while not exceeding the GI ($t_{\mathrm{RC}} \leq T_{\mathrm{GI}}$), cf. table 5.1 on page 51. The corresponding discrete time filter (windowing function) for 20 MHz, $N = 64$ (nHT) is thus given in 802.11 [62] with $t_{\mathrm{RC}} = 100ns$ as

$$
w_{\mathrm{T81}}[n] = w_{\mathrm{T81}}(nT_{\mathrm{s}}) = \begin{cases}
1 & 1 \leq n \leq 79 \\
1/2 & n = 0,\, 80 \\
0 & else
\end{cases}
$$

which spans 81 discrete time samples. An implementation would overlap the last sample of symbol m with the first sample of symbol $m + 1$ to restore the original number of samples $T_{\mathrm{sym}} \cdot T_{\mathrm{s}} = 80$ per symbol. The effect of this time domain spectral shaping however, in which the sender uses an IFFT implementation of minimum order and hence $N_{\mathrm{i}} = N$, is limited [25, (4.2.2)]. However, an OFDM sender can be implemented with higher order IFFT such that
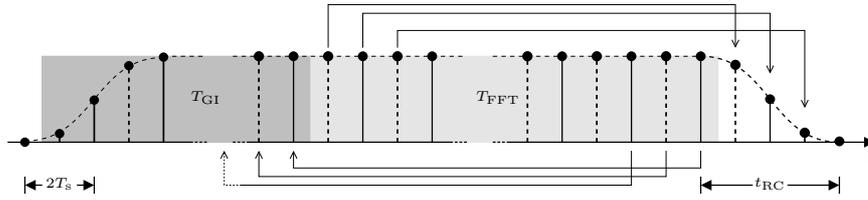
Figure 5.5: 802.11 OFDM time domain spectral shaping ($T_s = 25$ ns; $N_i = 2 \cdot N = 128$; $r_w = 1/32$). Note: Dashed samples are due to oversampling.
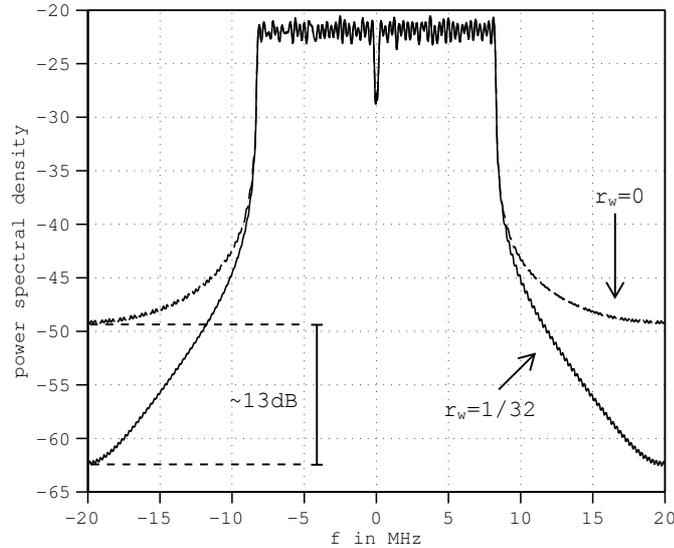

Figure 5.6: 802.11 OFDM baseband transmit spectrum with and without windowing ($T_s = 25$ ns; $N_i = 2 \cdot N = 128$; $r_w = 1/32$). Note: Curves are averaged to expose the effect of spectral shaping.

$N_i > N$. Wireless LAN interfaces according to 802.11n are capable of up to 40 MHz (160 MHz for 802.11ac) channel bandwidth, and can thus be assumed to use higher order IFFT when operating in 20 MHz 802.11a/g mode. Figure 5.5 depicts the process spectral shaping by weighting with $w_{T163}[n]$ ($N_i = 128$) after cyclic suffix extension by $t_{RC} = 4T_s = 100ns$, as well as of GI construction by cyclic prefix. Figure 5.6 depicts the spectrum of this signal with and without windowing. At the center of the next non-overlapping 20 MHz channel, the spectral side lobe reduction achieves roughly 13 dB attenuation. Furthermore, it can be shown that this amount of spectral side lobe reduction does not influence the OFDM eye pattern significantly [25, (4.2.2)]. Consequently, across the used part the spectrum can be considered as "white" independently of whether it is generated by oversampling or not. Therefore, it is further assumed that multiple 802.11 OFDM transmitters increase the additive white Gaussian noise (AWGN) when signals are transmitted at the same time.

5.2.5 Frame Synchronization

Synchronization of receiver circuitry in OFDM-based wireless LANs according to IEEE standards is two-fold: a synchronization sequence is generated prior to any data transmission, while during data transmission, pilot symbols are incorporated in the frequency domain. The periodic repetitive structure in both cases can be used for frequency oscillator synchronization at the

receiver in order to consume the transmitted data at the speed at which it is being emitted.

Synchronization Preamble

As stated above, the PLCP preamble is prefixed to the OFDM data symbols and is used for synchronization during signal reception. The structure of $s_{\mathrm{preamble}}(t)$ is not specifically relevant in the scope of this work. By example of SISO OFDM based WLAN, the initial *short preamble* is used for amplifier gain control and timing synchronization, the succeeding *long preamble* may be used for frequency estimation and frequency selective channel estimation and compensation by means of maximum mean-squared error or zero forcing [65].

As OFDM is sensitive to frequency and phase error (cf. section 4.3.3), for reception of a burst of back-to-back OFDM data symbols it is in a first step necessary to detect the start of such a burst. The deterministic structure of the PLCP preamble is used in this context. Detection can be regarded increasingly difficult with decreasing signal-to-interference-plus-noise ratio (SINR). In the scope of this work, reception at SINR close to 0 dB is considered. When two OFDM symbol bursts of the same kind are transmitted at the same time, due to identical PLCP preambles at the receiver, they may appear as echoes subject to frequency offset. At a typically achieved frequency deviation of two transmitting stations in wireless LAN of less than 17 ppm [54], a phase difference after simultaneous transmission of 802.11a PLCP preambles of less than 0.5 % (here: 16 μs) is assumed negligible for signal detection. During reception of bursts of OFDM data symbols, the additional phase noise introduced by the interference of multiple non-synchronous signals can be assumed beneficial with respect to intentionally simultaneous transmission for the purpose of signal jamming (cf. section 7.3).

Another aspect of using deterministic preambles is the possibility of quannel quality estimation due to the known preamble signal structure at the receiver. Within the scope of this work, the channel information can be used for rate adaptation according to the receiver-side estimation thereof. Furthermore, the preamble can be used for receiver antenna selection for multi-antenna employing a single receiver chain. With respect to SNR estimation (cf. section 5.5.1), the preamble subcarrier modulation is of interest. By example of 802.11a, subcarriers are quadrature amplitude modulated by C_{k} in eq. 5.2.2 according to

$$C_{\mathrm{k,short}} = \sqrt{13/6} \cdot \begin{cases} 1+j & k \in \{\pm 24, \pm 16, -4, 12, 20\} \\ -1-j & k \in \{-20, -12, \pm 8, 4\} \\ 0 & else \end{cases}$$

in the short preamble, whereas BPSK with zero center carrier is used in the long preamble portion, resulting in $C_{\mathrm{k,long}} \in \{-1, 0, 1\}$.

Pilot Carriers   Another aspect of synchronization in 802.11a/g/n are pilot carriers inserted in each OFDM data symbol. The center carrier as well as the pilot carriers as given in table 5.1 form the set of pilot symbols. DC is permanently set to zero, while latter are BPSK and thus of unit magnitude. Frequency tracking and synchronization can be achieved by observing DC offset on the center carrier and phase rotation on the pilot carriers.

An overview of synchronization techniques with preambles and solely based on multiple auto-correlation and cross-correlation metrics has been done by Morelli et al. [66].

5.2.6   Achievable Throughput

Single carrier transmission has been shown to be possible at a rate of less than 2 syms/s/Hz, hence for binary PAM the Shannon upper bound on spectral efficiency is $C < 2$bit/s/Hz. Furthermore, it has been shown that OFDM when generated by the IFFT is inherently sampled and thus e.g. at 20 MHz, in the time domain 20 Msyms/s are transmitted. When e.g. 48 of 64 carriers are used (as done in legacy non-HT 802.11a/g), this numerically reduces to 15 Msyms/s and with FEC of
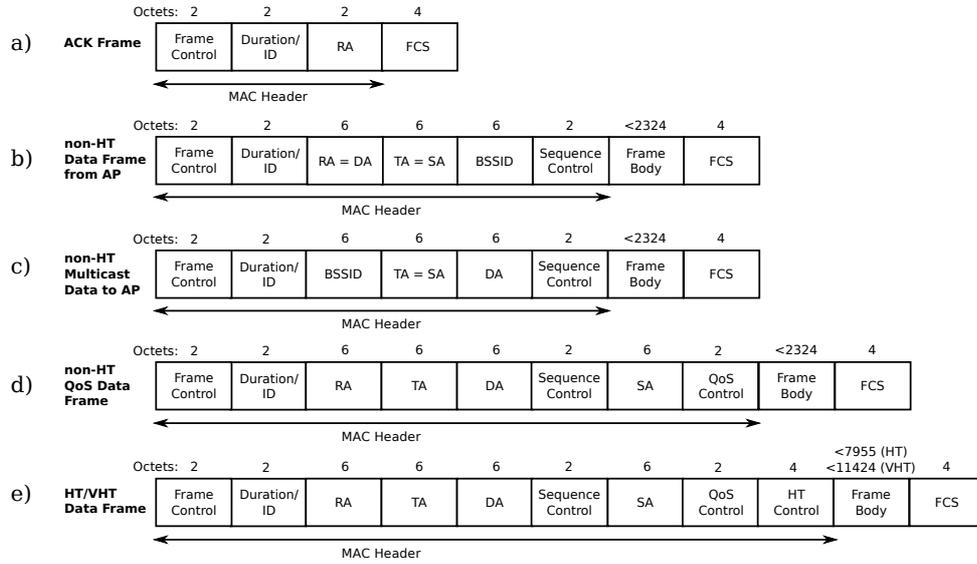
Figure 5.7: a–d) 802.11a/b/g (legacy) MAC layer frame formats [7]. a) 802.11 immediate feedback acknowledgment frame; b) non-QoS data frame; c) non-QoS multicast data frame as unicast addressed from station, will be relayed as b) by the AP; d) general QoS data frame format; e) 802.11n/ac [63, 46] frames

rate 1/2, 7.5 Msyms/s remain. The corresponding GI of 20% further reduces this to 6 Msyms/s. Hence, for the lowest MCS of 6 Mbps the throughput capacity is $R = 0.3$ bit/s/Hz, while for 54 Mbps it is at most $R = 2.7$ bit/s/Hz.

5.3   Medium Access Control Layer

In this work, a system is proposed relying on jamming of unmodified MAC layer frames by simultaneous transmission of suchlike frames. An overview of the MAC framing structure in 802.11 is therefore elaborated in the following. Framing formats relevant in the scope of this work are given and MAC layer multicast functionality is described (cf. address fields).

5.3.1   Frame Formats

Multiple destination address fields enable multicast over wireless LAN, in which multicast frames are transmitted by the access point. The AP is not necessarily the origin of the multicast stream. Sequence numbers enable MAC layer retransmissions in case of erroneous reception. Latter is detected by frame checksum matching, as the frame check sequence enables error detection by comparison with a locally computed checksum over the received data. In the most recently published version of the 802.11 standards [7] at the time of writing, the IEEE 802.11n high throughput control field adds a vehicle for fast link adaptation feedback (cf. section 5.5.2.2). Figure 5.7 depicts general frame formats for different types of MAC layer frames with the following frame header fields:

Frame Control   Consists of bit masked sub-fields to describe (among other things) the type and subtype of the frame, the direction and destination of the frame (which influences the interpretation of the address fields) and information on fragmentation of frames.

- *Protocol version* field

- *Type* and *Subtype* fields

- *To* and *from distribution system* flags. If the former is set to 1, this indicates that the frame will be relayed by the AP, cf. figure 5.7c)

- *More fragments* flag

- *Retry* flag indicating a previous transmission of the same frame

- *Power management* flag indicating a station's power safe mode after this frame

- *More data* flag indicating whether a station should stay powered on after this frame

- *Protected frame* flag indicating whether this frame is encrypted

- *Order* flag indicating that the frame ordering has to be strictly maintained, even in mixed unicast multicast traffic

Duration/ID For non-fragmented data frames this field is set to the time in microseconds required to transmit one ACK frame plus one Short Inter- frame Space (SIFS) interval.

1-4 Address fields In various configurations, these fields indicate the basic service set (BSS) identifier, source address (SA), destination address (DA), transmitting station address (TA) and receiving station address (RA). Depending on the frame type only a subset of address fields is used. Each address field contains a 48-bit address as defined in IEEE Std 802-1990, Section 5.2. This may be an individual/unicast address or a group address. Group addresses may either be transmitted as MAC multicast with the group bit of the MAC address set to 1, or alternatively broadcast with all bits set to 1 [67]. Association of a station to a multicast group is out of the scope of IEEE 802.11. It is typically done via the Internet group management protogol (cf. section 2.5.3), whereas IP multicast addresses can be mapped[3] to Ethernet MAC addresses. Stations associated to a multicast group forward the frames directed to this multicast address to upper layers. The distinguished broadcast address is a special form of a multicast address that always denotes the set of all stations associated with this BSS.

Sequence Control Data frames of each unicast connection are assigned a unique sequence counter. The sequence number is incremented for every complete data frame as well as data frame fragments in case of IP or MAC layer fragmentation. Broadcast, multicast, management and control frames share a dedicated single sequence counter.

QoS Control This field only exists if a QoS subtype is set for data frames in the frame control field. It describes the QoS class of this frame which specifies its priority by means of the access category (AC). Different ACs result in differently prioritized channel access (cf. section 5.3.4.2).

HT Control as of IEEE 802.11n, the high throughput (HT) control field contains, among others, information for link adaptation in case of SISO, multiple-input multiple-output (MIMO) and multi-user multiple-input multiple-output (MU-MIMO) (cf. 802.11ac).

Frame Body Variable length payload of the MAC layer frame. Control and management frames omit this field. With increasing physical layer throughput and thus decreasing symbol duration, the maximum frame body payload length has been increased from $2,324$ Byte for 64-QAM 20 MHz SISO (legacy 802.11a/g) to $7,955$ Byte for 64-QAM 40 MHz MIMO (802.11n) and to $11,424$ Byte for 256-QAM 160 MHz MU-MIMO (802.11ac).

---

[3]IETF RFC 1112 – Host Extensions for IP Multicasting

FCS A frame check sequence (checksum) to verify data integrity at the receiver is appended to any 802.11 frame.

5.3.2 Retransmissions

The frame check sequence (FCS) in 802.11 frames is a CRC value that is provided by the transmitter and used at the receiver to determine if the frame is received in error. The binary nature of this error detection code by either checksum match or mismatch, as well as the predominance of IP packet based transmission results in the property of the WLAN channel being conceived as a packet erasure channel from the point of view of upper layers (cf. section 2.5.1). As opposed to some transport layer protocols (cf. e.g. TCP), there is a probability of frame loss, even in unicast, although a stop-and-wait ARQ is employed. A standard defined limit of 7 repetitions per frame (or 4 repetitions, depending on the transmitted frame type [7]) is the reason for this.

5.3.3 Frame Durations

All OFDM based 802.11 variants define usage of either BPSK, QPSK or M-ary QAM across all active subcarriers and without changing the modulation scheme for the payload data part of one OFDM frame, comprised of a number of OFDM symbols (symbol burst). Furthermore, FEC coding rates 1/2, 2/3, 3/4 and 5/6 can be used. With fixed preamble signaling times $T_{\mathrm{P}} + T_{\mathrm{sig}}$, the frame duration T_{frame} depends on the number of data bits N and the number of data bits per symbol (DBPS) N_{DBPS} and is given as

$$T_{\mathrm{frame}}(N, N_{\mathrm{DBPS}}) \quad = \quad T_{\mathrm{P}} + T_{\mathrm{sig}} + \left\lceil \frac{N + 16 + 6}{N_{\mathrm{DBPS}}} \right\rceil \cdot T_{\mathrm{sym}}$$

For example, in 802.11a, transmitting at a rate of 6 Mbps (BPSK, code rate $R = 1/2$, $N_{\mathrm{DBPS}} = 24$) this yields for 14 Bytes

$$\begin{aligned} T_{\mathrm{frame}}(14\,\mathrm{B}, 24) \quad &= \quad 16\,\mu\mathrm{s} + 4\,\mu\mathrm{s} + \left\lceil \frac{14 \cdot 8 + 16 + 6}{24} \right\rceil \cdot 4\,\mu\mathrm{s} \\ &= \quad (11 \cdot 4\,\mu\mathrm{s}) = 44\,\mu\mathrm{s} = T_{\mathrm{ACK,6M}} \end{aligned}$$

which is the frame duration for the base rate ACK frame. With respect to this work it it is important to note that according to above standards, the ACK may also be transmitted at higher rates while not exceeding the rate of the immediately preceding data frame. By example of 802.11n (HT), the ACK frame of again 14 Bytes may thus even be transmitted at 65 Mbps (64-QAM, code rate $R = 3/4$, $N_{\mathrm{DBPS}} = 234$, short GI of 400 ns). This results in a lower frame duration of

$$\begin{aligned} T_{\mathrm{frame}}(14\,\mathrm{B}, 234) \quad &= \quad 8\,\mu\mathrm{s} + 8\,\mu\mathrm{s} + \left\lceil \frac{14 \cdot 8 + 16 + 6}{234} \right\rceil \cdot 3.6\,\mu\mathrm{s} \\ &= \quad 19.6\,\mu\mathrm{s} = T_{\mathrm{ACK,65M}} \end{aligned}$$

Table 5.4 on the facing page lists all mandatory and all possible 802.11a rates, as well as some SISO 802.11n (HT) rates and the maximum 802.11ac (VHT) single-user multiple-input multiple-output (SU-MIMO) single stream rate, along with minimum frame durations for each rate given.

Table 5.4: Some IEEE 802.11a/g/n/ac data rates and frame durations for 20 MHz SISO channels. Max. Payload is $2,324$ B, $7,955$ B (HT) and $11,424$ B (VHT)

Modulation	R	N_DBPS	Data rate [Mbps] (T_sym)	Min. frame duration T_frame [μs]		
				ACK 14 B	Data payload 1500 B	max.
BPSK	1/2	24	$6^\dagger$	44	2024	3172
	1/2	26	6.5*	40	1868	9856 (HT)
	1/2	26	7.2 (3.6 μs)	37.6	1682.8	8872 (HT)
	3/4	36	9	36	1356	2124
QPSK	1/2	48	$12^\dagger$	32	1024	1596
	1/2	52	13*	28	944	4936 (HT)
	3/4	72	18	28	688	1072
	3/4	78	19.5*	24	636	3296 (HT)
16-QAM	1/2	96	$24^\dagger$	28	524	808
	1/2	104	26*	24	480	2476 (HT)
	3/4	144	36	20	356	548
	3/4	156	39*	20	328	1656 (HT)
64-QAM	2/3	192	48	20	272	416
	2/3	208	52*	20	248	1248 (HT)
	3/4	216	54	20	244	372
	3/4	234	58.5*	20	224	1112 (HT)
	3/4	234	65 (3.6 μs)	19.6	203.2	998.8 (HT)
	5/6	260	65*	20	204	1000 (HT)
	5/6	260	72.2 (3.6 μs)	19.6	185.2	901.6 (HT)
256-QAM	3/4	312	86.7 (3.6 μs)‡	19.6	156.4	1070.8 (VHT)

‡ 802.11ac (VHT) SISO mandatory MCS

* 802.11n (HT) SISO mandatory MCS

† 802.11a/g/n mandatory MCS

5.3.4 Medium Access Coordination

5.3.4.1 Distributed Coordination

The basic and solely mandatory channel access method in 802.11 is distributed and summarized under the term distributed coordination function (DCF). Under distributed coordination, each station executes the same randomized back-off procedure in case the wireless medium is sensed as non-idle. In the resulting carrier sense multiple access with collision avoidance (CSMA/CA) protocol, from a set of back-off slots defined by the *contention window* size, each station with pending transmission randomly picks a slot. The result of this RV determines the time of deferral from medium access. It has been shown by Bianchi [68] that independent of the selected MCS at any wireless station, in case of complete saturation[4], each station will achieve the same throughput under the DCF. It is thus regarded as "fair" under the given assumptions. Figure 5.8 shows a slightly simplified flow diagram of DCF based collision avoidance at a wireless stations. Centralized coordination by means of the point-coordination function (PCF) is out of the scope of this work as it is rarely used in practice.

The aspect of decentralized coordination is important in the scope of this work. Whenever medium access is not perfectly managed, i.e. access scheduling is not centrally coordinated, there is a probability of medium access collision. In the event of a collision, it may be that any of the data frames accidentally transmitted in parallel can not be received correctly at the respective receiver due to SINR degradation. It is important to note that in typical wireless networks, it is impossible for wireless stations to both transmit and sense another stations transmission at the same time. The event of collision may thus remain unnoticed to the affected stations. As such,

---

[4]In saturation, each station has data pending for transmission at any time and thus all stations are in permanent contention for medium access
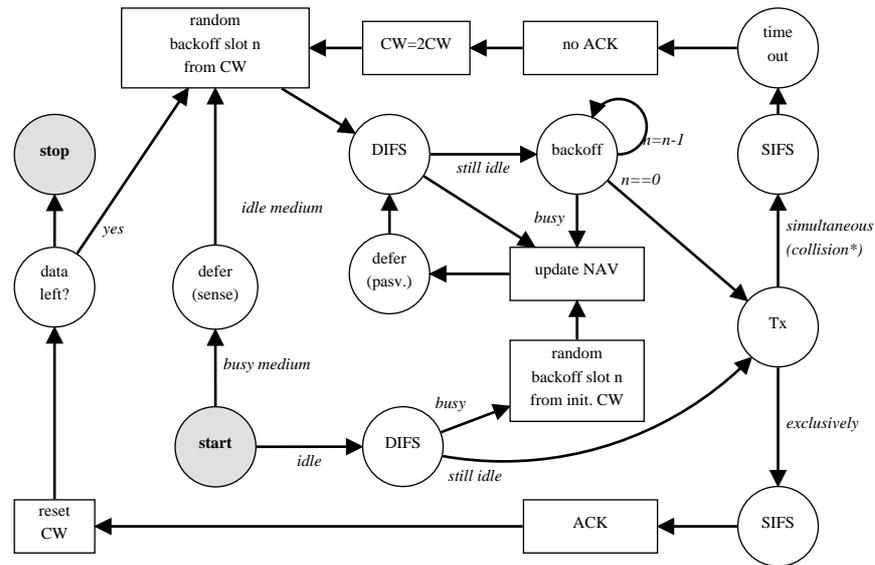
Figure 5.8: DCF based collision avoidance (local). Note: Frame and acknowledgement (ACK) decoding failure as well as EIFS handling are omitted for simplicity. *Event of collision is assumed upon absence of an ACK.*

medium access collision at data frame transmission is undesirable as it may result in transmit error. With respect to multicast, a collision among multicast and non-multicast data frames may result in joint loss at the multicast receivers. Concerning simultaneous feedback in a leader based protocol (LBP) for multicast feedback and error correction, however, joint data frame loss, as opposed to disjunct loss, is regarded as beneficial concerning the reliability of feedback (cf. section 8.1).

EIFS. In case a station senses a data frame (or part thereof) but fails to correctly receive it (indicated by FCS failure) due to e.g. far exceeded transmitter-receiver distance for the used MCS, it shall defer for the duration of the extended inter-frame space (EIFS). This period of deferral includes the duration of a possible ACK frame from an even further away station this data frame was originally destined to. An improved collision avoidance is achieved by compensating for an otherwise overheard ACK during contention. However, it is herein assumed relevant only in the evaluation of medium access layer throughput. The reason for this is the data frame transmission to multiple receivers (broadcast/multicast) and rate adaptation for the group of receivers.

Virtual carrier sensing. As stated above, upon reception of a valid *SIGNAL* symbol, the NAV is updated and the channel assessment procedure declares the channel as idle for the duration signaled in the *SIGNAL* symbol. Furthermore, request-to-send (RTS) and clear-to-send (CTS) frames can be used to ensure collision free transmission. The RTS/CTS exchange is done prior to data frame transmission destined for the AP and the duration is set to encompass RTS, CTS and data frame duration. Any station in the vicinity of the AP will thus assume the channel as busy for that period of time.

Collision detection. Another part of clear channel assessment (CCA) during medium sensing as depicted in figure 5.8 is the detection of medium access collision when a transmitting station senses the channel as busy immediately after it has completed its own transmission. Especially in case of the access point being the transmitter, a high probability of frame loss at the receiver(s)

Table 5.5: IEEE 802.11a/g/n/ac medium access timing parameters

Parameter	802.11a	802.11g	802.11n/ac
Slot time T_{slot} [μs]	9	9, 20*	9
SIFS T_{SIFS} [μs] (tolerance)	16 ($\pm 0.1 T_{\text{slot}}$)	16, 10*	16 ($\pm 0.1 T_{\text{slot}}$)
DIFS [μs]	34	28, 50*	34
AIFS	$T_{\text{SIFS}} + c \cdot T_{\text{slot}}, \;\; c \in \{2, 3, 7\}$		

* in the presence of 802.11b devices

can be deduced from a busy state at this point in time. In case of multicast, a subsequent positive acknowledgement could be identified as false positive concerning the whole receiver group. Multicast packet error probability (PEP) considering false positives is elaborated further in section 8.1.

Frame capture. In wireless time-division multiple access (TDMA) systems, such as 802.11, the so-called *capture effect* has an influence on throughput. In case a transmitted frame is received and correctly decoded, it is said to have captured the receiver. With respect to achievable throughput under distributed coordination the probability of collision is evaluated with non-zero capture probability. 802.11 DCF throughput analysis, if capture is not considered [68], has been shown to underestimate throughput [69, 70, 71] as collisions do not necessarily result in definite loss of the colliding frames. While data frame capture is out of the scope of this work, feedback frame capture is considered in section 7.4 in the scope of multicast feedback aggregation.

5.3.4.2 Enhanced Distributed Channel Access

The basic distributed coordination of channel access is extended by content dependent prioritization by the enhanced distributed channel access (EDCA). Its access parameters may be provided and updated in the EDCA parameter-set information element, which is e.g. present in periodic beacons broadcast by the AP. Stations associated to the the BSS of this AP use the last seen version of the parameters. The AP may adjust the parameters over time. Table 5.6 on the next page lists the default parameters which shall be used by all stations in case the AP does not provide a different set of parameters. Different levels of prioritization (i.e. levels of quality of service) are achieved by channel access parameters modified according to different channel access categories. An arbitration inter-frame space (AIFS) is added in EDCA which is identical to DCF inter-frame space (DIFS) in legacy 802.11. Furthermore, distributed randomized back-off contention window (CW) minimum and maximum values are modified per AC as to increase the chance of real-time media stream packets in AC Video and AC Voice to gain channel access before AC Bulk and AC Best Effort traffic, cf. figure 5.9 which is based upon figure 5.8 on the facing page.

Enhanced distributed channel access inherits the probability of medium access collisions from DCF, as opposed to centralized point coordination function (PCF) and hybrid coordination function (HCF). From the author's experience, latter non-distributed mechanisms are rarely used in consumer wireless networks and are therefore excluded from further considerations.

TXOP. Transmit opportunity (TXOP) is another mechanism of EDCA to prioritize media traffic channel access. It is a bounded period during which a station may transfer data uninterruptedly, i.e. in *bursts,* without changing the traffic access category. According to table 5.6, a station transmitting in either AC *Video* or AC *Voice* may transmit a sequence of frames, separated only by a fixed time short inter-frame space (SIFS) interval, up to the amount of medium access time as specified for this AC. A TXOP is *obtained* by a station by means of the channel access procedure with parameters for the particular AC, i.e. back-off slot countdown from CW(AC) and AIFS(AC). In the absence of a TXOP limit, such as for ACs *Bulk* and *Best Effort,* only a single frame may be transmitted before contending for channel access again. This QoS
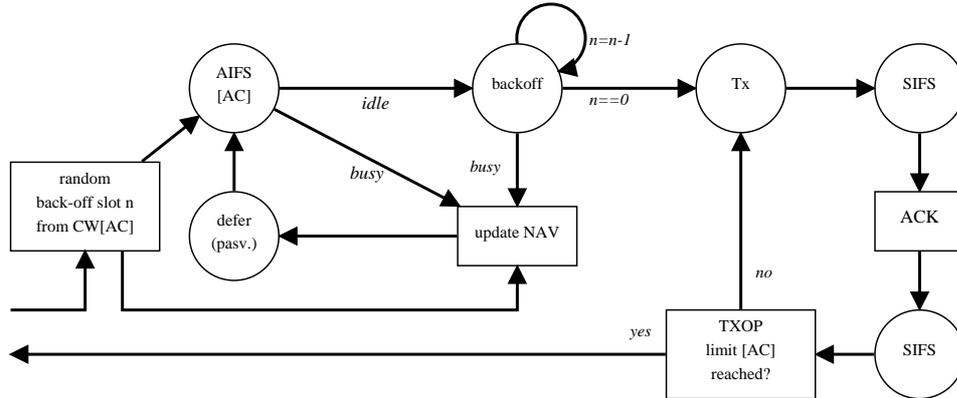
Figure 5.9: EDCA based collision avoidance introduces unfairness of channel access by multiple access categorys (ACs) as well as transmit time fairness within some of the ACs.

Table 5.6: IEEE 802.11a/g/n EDCA and DCF parameters with TXOP limits

Access category	Contention window		AIFS c	TXOP
	Minimum	Maximum		
Bulk (BK)	31	1023	7	-
Best Effort (BE)	31	1023	3	-
Video (VI)	15	31	2	3.008 ms
Voice (VO)	7	15	2	1.504 ms
legacy DCF	15	1023	DIFS$\widehat{=}$ 2	-

concept enables resource fairness rather than throughput fairness within the same AC. Stations contending for medium access will on average receive the same amount of channel holding time for traffic in that AC as opposed to DCF in which even contending stations with different MCS will receive the same throughput on average, cf. section 5.3.4.1.

TXOP Collision Detection. In carrier sense multiple access with collision avoidance using either EDCA or legacy DCF, the virtual carrier sense mechanism by deferral according to the network allocation vector (NAV) is only used in case an alien transmission has started before the back off counter decrementing collision avoidance mechanism has reached a back off count of zero. However, burst transmission of multiple frames within a TXOP period may increase the loss of air time in case of medium access collision under some circumstances. Therefore, collision detection by means of an RTS/CTS exchange or a single Data/ACK exchange is mandatory at the beginning of a TXOP. The frame duration signaled in any of these *collision detect* exchanges is consequently set to the targeted burst duration, equal to or smaller than the maximum TXOP duration, for other stations to defer for the whole burst sequence.

5.3.4.3 Distributed prioritized channel access by example

Assuming that no collision has previously occurred, the random back-off contention window is at its initial value *CWmin*. Using default EDCA parameters as given in table 5.7, the probability that packets of some AC are transmitted when at the same time packets of the other three ACs are pending for transmission can be deduced. When queues of the four access categories are saturated, the probability that the AC Video (VI) randomly chooses an earlier slot than the AC Voice (VO) is $\frac{1}{3} \cdot \frac{2}{7} + \frac{1}{3} \cdot \frac{1}{7} = \frac{1}{7}$. Similarly, the probability that Best-Effort (BE) is scheduled earlier than VO is $\frac{1}{45}$. Background (BG) traffic will never contend with VO since its AIFS offset is larger

Table 5.7: Distributed prioritized channel access in 802.11 with default EDCA parameters.

AC	AIFS offset and contention window (CW) time slots	CWmin
BG	AIFS=7	15
BE	3	15
VI	2	7
VO	2	3

than the largest slot the AC Voice could possibly choose. Thus, VO packets are transmitted at a probability of $1 - \frac{1}{7} - \frac{1}{45} - \frac{1}{7} \cdot \frac{1}{45} = 0.83$.

5.3.5 Broadcast and Multicast

According to IEEE 802.11-2007 [64, (9.2.7)], in broadcast and multicast data frame transmission, no RTS/CTS is done prior to transmission and no ACK is issued by the receivers after successful reception. This is important in the scope of this work and further covered in section 7.1. For multicast and broadcast data frames sent by a non-AP station, the ToDS flag (a frame control *subtype* subfield flag, cf.5.3.1) is set and the destination address is the address of the AP. This indicates that those multicast frames are transmitted as unicast from the multicast origin and are consequently relayed by the AP to the multicast group members. Any non individual addressed frames are buffered at the AP and transmitted at pre-defined times. At an interval specified by the delivery traffic indication message (DTIM) period, multicast frames are transmitted after the access point *Beacon* frame by the AP. A DTIM period of 2 e.g. indicates broadcast and multicast frames are transmitted by the AP after every other Beacon. This enables power saving for stations receiving multicast traffic. A power saving station will be awake during Beacon transmission and stays awake whenever this Beacon indicates unicast frames destined to this station are buffered at the AP, or if this is a DTIM period and this station is part of a multicast group.

Overhead by Number of Receivers

In the scope of this work, multicast receiver groups in double figures are targeted. It is thus of interest whether WLAN supports such large numbers of stations associated to the same AP. Mishra et al. [72] as well as Raghavendra et al. [73] have investigated into limiting factors of association of with increasing number of stations. Their conclusion is that active probe requests (used by stations to find another AP of better signal strength) can significantly degrade performance. While this is an open problem, in the scope of this work it is assumed that this is going to be solved in IEEE 802.11 in the future. Apart from said probing request flooding, no other limiting factor is known to the author prohibiting increasingly large multicast receiver groups.

5.4 Packet Loss

Average Coded Bit Error Probability

For BPSK (M=2) and QPSK (M=4) it has been shown that the BEP is typically expressed by

$$P_{\mathrm{b}}(M) = \frac{1}{2} erfc\left(\sqrt{\frac{\gamma_{\mathrm{s}}}{ld(M)}} d\right) \ (M = 2, 4)$$

802.11 FEC on the MAC layer uses the above introduced $(133, 171)|_{\mathrm{o}}$ binary convolutional code of rate 1/2 with puncturing rates 2/3 and 3/4. The PEP for AWGN can be computed from the average coded BEP according to [74, 75, 76] as follows. For hard decision decoding, i.e. the

operation on QAM demodulated bits, the probability for the Viterbi decoder to select a wrong path in the trellis at distance d, denoted $P_{\mathrm{p}}(d)$, is [76]

$$
P_{\mathrm{p}}(d) = \begin{cases} \sum_{\mathrm{k}=(\mathrm{d}+1)/2}^{d} \binom{d}{k} P_{\mathrm{b}}^{k} (1 - P_{\mathrm{b}})^{d-k} & odd\ d \\ \frac{1}{2}\binom{d}{d/2} P_{\mathrm{b}}^{d/2} (1 - P_{\mathrm{b}})^{d/2} + \\ \qquad \sum_{\mathrm{k}=\mathrm{d}/2+1}^{d} \binom{d}{k} P_{\mathrm{b}}^{k} (1 - P_{\mathrm{b}})^{d-k} & even\ d \end{cases}
$$

where P_{b} is the BEP for the modulation scheme in use, which may be subject to fading. Distance profiles of convolutional codes can be obtained from tables as provided in the literature [76], also for punctured rates [75]. Assuming an all-zero sequence is the correct decoding result, the sum of the pairwise error probabilities $P_{\mathrm{p}}(d)$ over all possible paths that merge with the all-zero path at the given node are given as the union bound on bit error probability by summing up the wrong path probabilities multiplied by their Hamming weights c_{d} [58]

$$
P_{\mathrm{p}}^{u} < \frac{1}{n_{\mathrm{c}}} \sum_{\mathrm{d}=\mathrm{d}_{\mathrm{free}}}^{\infty} c_{\mathrm{d}} P_{\mathrm{p}}(d) \tag{5.4.1}
$$

where n_{c} is the numerator of the (potentially punctured) rate

$$
r = \frac{n_{\mathrm{c}}}{\mathrm{denom.}}
$$

This shows that an exact BEP for convolutional coded OFDM-QAM systems is not easily obtained analytically. Simulation thereof is possible, as depicted in figure 5.10. For said figure, per subcarrier identical M-ary QAM OFDM transmission is simulated at the given average SNR values. Soft decision decoding, in which the QAM de-mapper feeds log-likelihood estimates of constellation points (subject to quantization) into the soft decision Viterbi decoder, performs nearly $2\,\mathrm{dB}$ better with respect to SNR.

Packet Error Probability

The Viterbi decoder either takes the correct path in the trellis or, in case of decoding failure, picks one of the other paths, i.e. a wrong path. Bit errors at the output of the Viterbi decoder are not independent but dependent due to the path. Thus, a PEP may not be computed from the average BEP as given above. The sum in eq. 5.4.1 extends to infinity, thus numerical approximation results in truncation of the union bound. Truncation is addressed by Lassing et al. [77]. Depending on the channel model (e.g. AWGN or Rayleigh), a lower bound on the SNR for a given PEP exists and an upper bound on the probability of packet error is [74, 78]

$$
\rho_{\mathrm{u}} < 1 - \left(1 - P_{\mathrm{p}}^{u}\right)^{8 \cdot L} \tag{5.4.2}
$$

with L is the number of transmitted bytes. See figure 5.11 for example thresholds at $PER = 10^{-3}$. Figure 5.11 depicts the union bound PER performance of hard decision Viterbi decoding at full traceback with truncation at $d_{\mathrm{free}} \leq d \leq d_{\mathrm{free}} + 10$ (cf. eq. 5.4.1) of 802.11a/g MCSs in the presence of AWGN only. It can be seen that *mode 2, i.e. BPSK $r = 3/4$ and mode 3* are spaced very closely. Consequently, *mode 2* has been removed as of 802.11n [63].

The union bound approximation for hard decision decoding is valid only for long packets (e.g. 1000 Bytes) [74] . To relax the assumption of uncorrelated bit errors at the decoder output and thus obtain results for shorter packets, simulation of ρ_{ref} can be done for a length $L_{\mathrm{ref}} > 1\,\mathrm{kB}$, while for another length L the PEP can be found as

$$
\rho_{\mathrm{L}} = 1 - (1 - \rho_{\mathrm{ref}})^{L_{\mathrm{ref}}/L} \tag{5.4.3}
$$

In case the independent BEP is known exactly, an 802.11 OFDM data frames is lost if at least one of two conditions hold true. Firstly, the signal field of the preamble (BSPK modulated at FEC
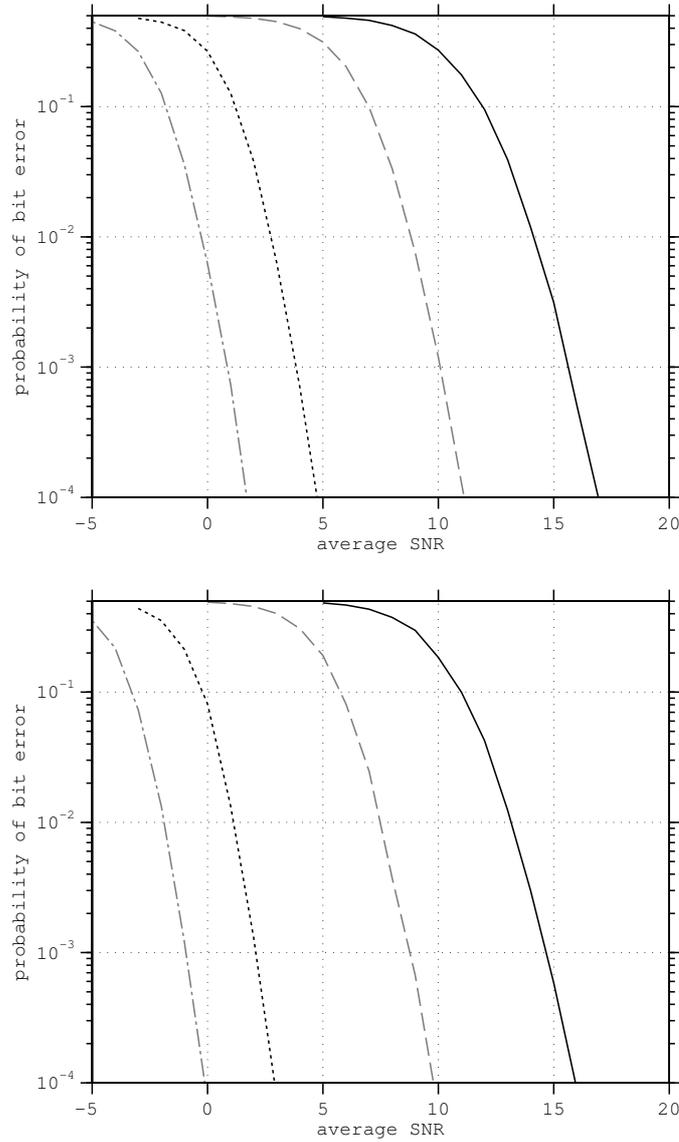
Figure 5.10: Exact bit error probability of $r = 1/2$ convolutional coded M-QAM ($M = 2, 4, 16, 64$) as simulated on 48/64 OFDM subcarriers over AWGN channel (*top:* hard decision; *bottom:* soft decision, 4 bit quantization; *both:* Viterbi state traceback length 48)
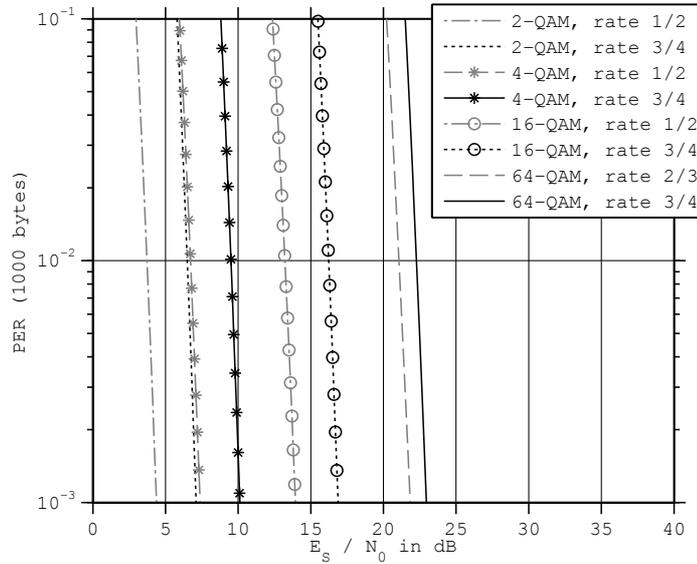
Figure 5.11: packet error probability for the eight modulation and coding schemes of 802.11a/g and thresholds for $\rho = 10^{-3}$ due to AWGN (hard decision upper bound, full traceback)

rate r=1/2, i.e. at *mode 1*) may be decoded incorrectly and hence the following payload MCS properties may be misinterpreted, or the payload length field is interpreted wrongly. Secondly, the OFDM symbols carrying the payload data may be subject to bit errors resulting in checksum mismatch. With the probability of bit error at MCS *mode m*, $P_{b,m}$, this results in the PEP of

$$\rho = 1 - \left[1 - P_{b,1}\right]^{8 \cdot 24} \left[1 - P_{b,m}\right]^{8 \cdot L}$$

This shows that a BEP of less than $P_{b,m} \approx 1.32e - 5$ is required to achieve a PEP of less than 10% for $L \approx 1\,\text{kB}$.

Other Packet Erasure Causes

From eq. 5.4.3 it can be seen how a difference in packet length has an influence on the packet error probability. For example, when the packet length is halved the error probability is approximately halved. In terms of SNR, an approximately 3 dB improvement in PEP performance is observed. It is further important to note that with increased packet length, the increased probability of sporadic interference during a long packet increases the observed packet erasure rate. Frequency drift at the receiver due to imperfect synchronization will affect long packets more severely than short packets. Furthermore, the coherence time of the channel is an externally defined value, and for long packets, the MCS chosen by rate adaptation may become infeasible when the fast fading channel degrades during packet transmission.

5.5 Unicast Link Rate Adaptation

Due to the high dynamic range of received signal strength in wireless communications, wireless networks typically define a set of modulation and coding schemes (MCSs), resulting in a list of achievable raw throughput bitrates. Selection of a suitable rate for the current wireless channel condition is termed link adaptation, whereas for multicast, the term *rate adaptation* seems more suitable. In this work it is shown how rate adaptation can be employed for leader based multicast, while existing unicast algorithms as found in the literature may be immediately re-used.
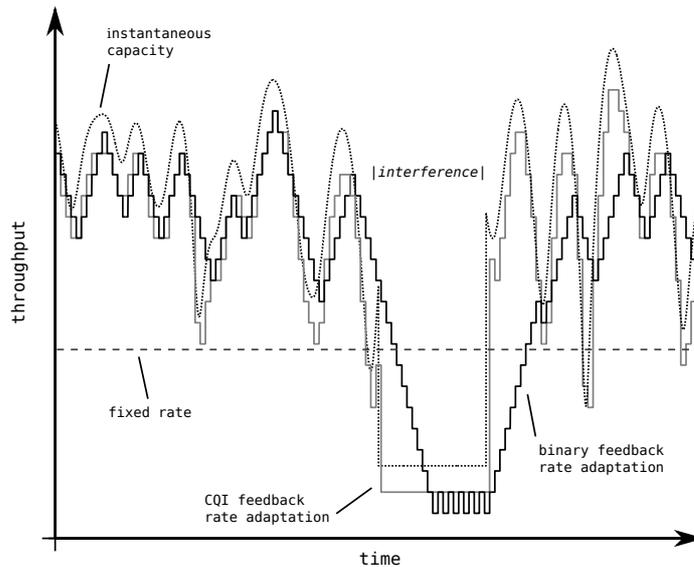
Figure 5.12: Bit rate adaptation to a fading channel over time using different metrics. In case of interference, adaptation can be fast with channel quality information available at the sender. The fixed rate may achieve a long-term PER identical to a short-term PER of any of the other adaptation schemes, however, its throughput is potentially lower.

Unicast rate adaptation may be based upon several metrics, such as channel quality, transmit failure and average frame erasure rate. Any channel state information (CSI) metric on the other hand requires CSI feedback, which itself is subject to noise and feedback loss. With an immediate ACK policy (as e.g. in 802.11), and thus immediate knowledge at the sender about transmit failure in absence of the acknowledgement, transmit failure is a prominent metric for rate adaptation. Typically, after some number of successful transmissions, a less robust bitrate is chosen, while after e.g. one unsuccessful transmission, a more robust bitrate is chosen. A metric based on average frame erasure rate is infeasible for sporadic traffic, but can be used with saturated elastic and inelastic traffic flows. As with immediate channel quality information, receiver individual transmit success statistics are available at each receiver, but unavailable at the sender.

As shown above, modulation and coding scheme combinations create steep packet error probability curves in AWGN conditions. Therefore, channel and threshold aware adaptivity is possible. The instantaneously ideal MCS is perfectly decodeable at the receiver while using up the least amount of time for a number of transmitted bits. Rate adaptation by MCS selection ideally follows the instantaneous channel capacity over time, while it is insensitive to sporadic interference, such as medium access collisions. In case of collision induced loss there is no reason to switch to a more robust rate, as no implication can be deduced for the next transmission (cf. IEEE 802.11 collision avoidance as described in section 5.3.4.1). In case of loss due to low SNR on the other hand, some level of correlation in channel quality can be assumed for the next transmission.

Use of an immediate positive ACK after each data frame transmission is a form of binary feedback. In the presence of external sporadic interference, non-binary knowledge about channel quality can be beneficial, as shown in figure 5.12. However, this introduces additional complexity at the receiver and increases the feedback signaling overhead.
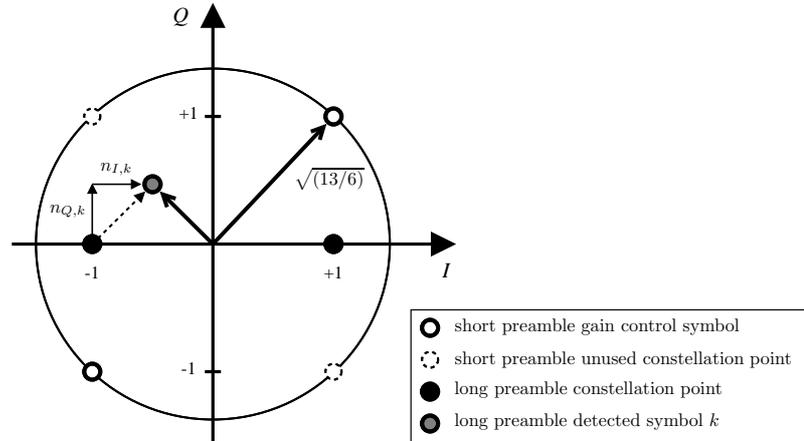
Figure 5.13: WLAN OFDM-QAM error vector magnitude (EVM) in the synchronization preamble. *Short symbols* are used for gain control and timing, *long symbol* BPSK subcarrier symbols for EVM estimation.

5.5.1 Receiver Signal-to-Noise Ratio Measurement

When channel quality at the receiver shall be used for rate adaptation, not only does this information need to be fed back, it needs to be acquired in the first place. Therefore, a brief overview of how this can be done in OFDM based IEEE 802.11 wireless LANs is provided in the following.

In 802.11, the way consumer wireless LAN cards measure *signal strength* is not specified by any standard, but all implementations known to the author report it (or a similar indication of channel quality) to the host operating system. The standard does however mandate the received signal strength indication (RSSI) to be determined during the preamble [64, (17.2.3.2)]. It is further specified how this measurement value as an indicator of channel quality is signaled to the MAC layer management entity (MLME). What is more, the standard specifies a *transmit modulation accuracy test* [64, (17.3.9.7)]. The error vector magnitude (EVM) shall be measured as shown in figure 5.13. When this is done during the preamble of an 802.11a/g OFDM frame (cf. 5.2.5), the long preamble can be used, as it is composed of two regular[5] OFDM symbols (including the GI) and thus of $K = 2 \cdot N_\mathrm{u} = 104$ BPSK [64] symbols. The EVM can then be written as

$$\mathrm{EVM_K} = \frac{\frac{1}{K} \sum_{\mathrm{k}=1}^{K} |n_{\mathrm{I,k}}|^2 + |n_{\mathrm{Q,k}}|^2}{P_\mathrm{long}}$$

whereas $n_{\mathrm{I,k}}$ and $n_{\mathrm{Q,k}}$ are the noise components per symbol k on the in-phase and quadrature-phase components, respectively, and P_long is the mean power of the long preamble. With $K \to \infty$, $\mathrm{EVM_K} \to 1/SNR$. The SNR measured by 802.11a/g devices during the preamble is thus an approximation of the average SNR. With increasing length of OFDM frames, it can be assumed as increasingly erroneous under non-static channel conditions. Furthermore, channel quality indication (CQI) in terms of an approximate SNR is forwarded from WLAN receiver frontend to operating system, subject to noise due to quantization.

Measurements using 802.11a consumer hardware have shown the SNR to be inconsistently reported [79] over the set of different MCS. SNR reports have been evaluated at a single receiver by reception of back-to-back OFDM frames transmitted at alternating MCSs while introducing motion below 1 km/h in the scenario. As depicted in figure 5.14, SNR values as reported by network interface cards upon frame reception at different MCSs should be assumed inaccurate in

[5]The corresponding short preamble is composed of 10 repetitions of 1/4 of an OFDM symbol in order to achieve distinct time domain properties beneficial for signal detection
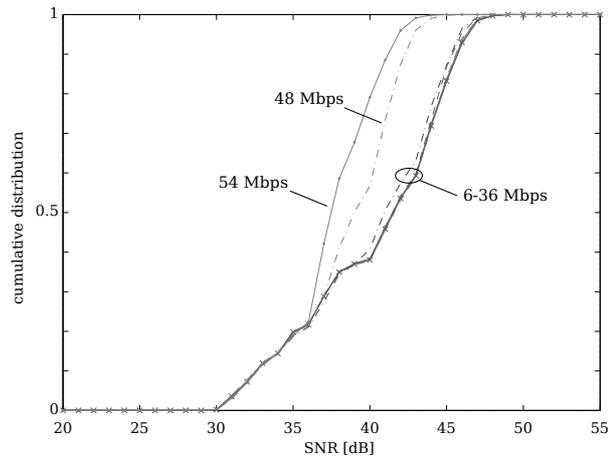
Figure 5.14: Reported SNR during accuracy measurement

absence of calibration[6]. When SNR is used as a channel quality indication for rate adaptation, Camp et al. [80] propose feedback of SNR measurements from the receiver to the sender to be done by four-way handshake in order to mitigate measurement error. Observation of the average error rate per reported quantized SNR value and other RA strategies have been evaluated and are found as lacking robustness under varying coherence times [80].

In case of distributed channel access coordination (cf. section 5.3.4.1), channel quality may unknowingly be estimated during medium access collision, i.e. in the presence of interference. Hence, a SINR is measured instead, adversely affecting rate adaptation. As in the case of binary feedback in the event of medium access collision, preamble based SNR figures are generally not a valid measure for channel quality. With respect to IEEE 802.11 WLAN, a Kalman filter approach to distinguish collision loss from loss due to low SNR has been studied by Tinnirello et al. [81]. The focus in this work is on binary feedback, as to why will be elaborated in detail in the following.

5.5.2 Existing Algorithms

This section provides an overview of related work with respect to rate adaptation for point-to-point unicast. The overview is separated into two categories: binary feedback and non-binary feedback based algorithms. In the latter case, channel quality may be obtained by the receiver at data frame reception, by the sender at ACK reception or by any other additional means of measurement and feedback.

5.5.2.1 Binary Feedback Based Algorithms

Immediate data transmit success based rate adaptation operates on past information about transmit success exclusively, while the information is acquired via binary feedback. Success is signaled by an ACK which is immediately returned after data frame transmission, whereas a state of failure is taken in absence of this positive feedback. These kinds of schemes are described in the following. A widely used simple version may provide insight into potential drawbacks.

Auto Rate Fallback (ARF). The ARF [82] algorithm is a binary feedback, reactive rate adaptation algorithm. It has been used in pre-802.11 wireless networking products referred to as *WaveLAN*®. These devices featured a set of five distinct MCSs (1, 2, 5, 8, and 10 Mbps) to

---

[6]The reason for inaccuracy of reported SNR at 48 Mbps and 54 Mbps is unknown to the author.

adapt to the current channel quality between two communicating stations. The ARF algorithm is based on a-posteriori transmit success observations and is typically described as follows:

- Whenever a (default $a = 10$) consecutive data frames have been transmitted successfully or after transmitting successfully for at least a pre-defined duration of time at the same MCS, the sender immediately switches the MCS to the next less robust rate (if available), effective for the next data frame with identical destination. The *consecutive* success requirement implies no intermediate need for retransmissions.

- Transmit success of the first data frame transmitted after adapting the original MCS to a more robust rate is required for the sender to maintain the new MCS. In case of failure, the original MCS is restored. This is further referred to as a *rate probing* transmission.

- Whenever b (default $b = 2$) consecutive data frames have not been transmitted successfully at the same MCS, the sender immediately adapts the MCS to the next more robust level (if available).

ARF has been adopted for many IEEE 802.11 wireless implementations in SISO unicast. Implicitly, ARF assumes that two consecutive transmission failures are unlikely to happen due to channel access collisions. This aspect makes ARF sensitive to the number of contenders for the wireless medium, as this directly influences the collision probability (cf. section 5.3.4.1). Typically the number of wireless stations and thus medium access contenders is not strictly limited and thus cannot be foreseen. Consequently, choice of proper b for the current number of wireless stations, if known, may be necessary. The same holds for the number of successful transmissions a required for a rate switch upwards at some MCS. As the channel usage time for a transmissions at different MCSs differs, the time duration during which the channel may be assumed rather constant is of importance. In a non-congested situation but with varying channel conditions due to mobility, a value of $a = 10$ could be overly conservative. The algorithm would be unable to follow the the channel variations, assuming the coherence time being less than the duration of transmitting a data frames. On the other hand, in a congested scenario, a number of consecutive successful transmissions equal to a may not be possible to achieve at all.

Given stationary channel conditions and an SNR approximately constant within a range that enables transmission at some rate A, ARF exhibits another weakness. When transmission at the next more robust MCS A_{next} is impossible (at close to zero transmit success probability), throughput achieved with ARF suffers from loss of the above mentioned rate probing transmission. Not only is the rate probing transmission at rate A_{next} wasted, further overhead is added by its retransmission at the MCS A. This problem is solved when ARF is applied to multicast, as elaborated in section 10.3.

Adaptive Auto Rate Fallback (AARF). With fixed parameters as described above, ARF does not adapt to varying fading speeds. An Adaptive Auto Rate Fallback (AARF) algorithm has been proposed [83] to overcome this. In this approach the ARF parameter a (successful transmissions before switching to a higher rate) is adapted to the currently estimated channel conditions. While adaptation to fast channel changes is not improved, loss due to rate adaptation probing transmissions at fixed intervals is reduced in static scenarios. To achieve this, the next rate probing transmission is done at some increased value of a whenever the previous rate probing transmission had to be compensated by a retransmission.

Adaptive Multi Rate Retry (AMRR). As proposed by Lacage et al. [83], AMRR is a parametrization of a distinct hardware feature of *madwifi*-compatible[7] wireless LAN adapters. These devices can be configured for some hierarchical retransmission sequence in order to provide

---

[7]Madwifi is an outdated Linux WLAN driver for Atheros devices

flexibility of rate adaptation without compromising latency. For retries (retransmissions) at different rates, the parameters c_k, r_k, $k \in \{0, 1, 2, 3\}$ are available. When a data frame transmission fails, the hardware will retransmit it $c_0 - 1$ times at rate r_0. If still unsuccessful, the data frame is repeated c_1 times at rate r_1, and so forth, until it has been tried $\sum_{k=0}^{3} c_k$ times.

SampleRate. Bicket [84] proposes a rate adaptation algorithm that introduces the concept of random rate probing transmissions. At periodic packet intervals, SampleRate transmits the following data packet at a random rate different to the current one, under some conditions. A condition is that collected statistics of frame transmit durations indicate shorter channel holding time for the selected MCS. The algorithm operates wireless interface card agnostic as it measures the time the wireless LAN card takes to transmit a packet at some MCS. This may include retransmissions which the card initiates autonomously and also includes the event of transmit failure due to hitting a retransmission limit. Another condition of selecting a random rate for the probing transmission is the collected frame loss rate statistic.

5.5.2.2 Channel Quality Feedback Based Algorithms

Receiver Based Auto Rate (RBAR). Holland et al. [85] proposed RBAR in which sender and receiver exchange information about the receiver determined SNR of previous data transmission. The use of modified RTS/CTS frames prior to transmission enable the sender to adapt to the requirements of the receiver. During reception of the initial RTS the SNR is measured at the receiver. The receiver feeds back its desired MCS to the sender via the subsequent CTS.

Collision-Aware Rate Adaption (CARA). Medium access collision detection is implemented in a proposal similar to RBAR. In CARA, Kim et al. [86] note that the initial RTS/CTS exchange is highly robust in the presence of noise, thus failure thereof is assumed to be caused by collision. Furthermore, collision is assumed also if the channel is sensed as busy by the transmitter immediately after it has completed data frame transmission. In this case, if the reason for the channel being busy is not an acknowledgment from the receiver, it is assumed that a third station is still transmitting (cf. CCA in section 5.3.4.1). In both cases, collision is distinguished from channel quality induced loss. With CARA, the RTS/CTS exchange is used only in case a rate adaptation decision is pending, reducing the RTS/CTS overhead. A similar approach was taken by Maguolo et al. [87].

Robust Rate Adaption Algorithm (RRAA). As proposed by Wong et al. [88], RRAA is based on short term packet loss rate observations at the transmitter. The PER is averaged over the observation history of several tens of transmitted packets. Additionally, RTS/CTS is selectively enabled upon individual packet loss and disabled upon success. By combination of both, a collision probability is approximated and rate adaptation is performed when the short term PER exceeds a threshold defined for upwards or downwards switching, respectively. The authors claim that their approach significantly outperforms ARF, AARF and SampleRate with respect to throughput.

Fast Link Adaptation (FLA). IEEE 802.11n [63] is the first wireless LAN standard to specify a vehicle for rate adaptation. In the standard, the term link adaptation is chosen as the set of available MCSs comprises of SISO and MIMO configurations, including transmit beamforming. Hence, FLA involves MCS adaptation and antenna configuration. Using the HT control field (cf. section 5.3.1), the receiver may provide the transmitter with feedback about a desired MCS. How this is derived at the receiver is out of the scope of the standard. The transmitter may combine the receiver's feedback with local knowledge e.g. about power amplifier back-off [65] (cf. section 4.3.2). It is not mandated that the transmitter must follow the MCS as provided by the receiver. The transmitter may ignore the receiver's suggestion if it observes (by missing

acknowledgments) that it would results in an increase of frame erasure rate. As such, MCS feedback in fast link adaptation is a form of non-binary channel quality indication (CQI).

Multicast Throughput

Modern communication systems provide multiple modulation and coding scheme (MCS) defined bit rates in order to adapt to varying channel conditions. In physical layer (PHY) time-division multiple access (TDMA) wireless multicast, multiple receivers experience different channel conditions at the same time. The question is thus: Which is the optimum rate to use in multicast. In telecommunications, throughput maximization (minimization of transmission overhead) is of interest and the problem extends to choice of the optimum rate at any point in time. For example, a media stream with an average bit rate of 4 Mbps is transmitted in multicast and there are two MCSs available, providing 6 Mbps and 9 Mbps, respectively. In this case, both MCSs are feasible. The transmitter could permanently use 9 Mbps physical layer bit rate to care for potential bandwidth variations in the media stream. The faster MCS further results in greater medium idle time that can be used otherwise. On the other hand, a more conservative choice may be the slower 6 Mbps mode, as it may be received by a larger set of receivers. Maximizing both range and bandwidth efficiency is achieved by rate adaptation.

In point-to-point (unicast) TDMA, for each unicast *connection* (defined by a source and destination pair) a transmission bit rate suitable for the current channel condition may be chosen dynamically, independent from any other unicast connection. In multicast, logically there is only one connection: a base station transmits data destined to a set of receivers (the multicast group) using a common bit rate. When there is no channel information at the sender, the options are either to permanently use the lowest commonly available MCS or any arbitrary one out of the set of the available rates, e.g. if required due to a given broadcast service data rate.

In this work, the focus lies on exclusive point-to-multipoint transmission by TDMA without cooperation (relaying) at receiver side. Therefore, the k-user parallel interference channel [89, 90], in which multiple point-to-point connections are active at the same time, is outside the scope of this work. Other channels are described as follows. In the following, multicast throughput is evaluated and compared with alternative multi-user transmit techniques.

6.1 Multicast i.i.d. Channels

In a multicast group consisting of more than one receiver, there may be receivers in the vicinity of the sender and some may be farther away. Typically, one of the receivers experiences the least amount of signal power among all receivers, and it may be denoted as the "worst" receiver. It may seem that whenever the "worst" receiver in a multicast group can only receive the multicast signal at some MCS resulting in a rate R or less, say, $R = 6$ Mbps, then the maximum throughput for the multicast transmission is 6 Mbps on average. However, this is only true for channels assumed as constant, as will be discussed below.

In case of slow fading, i.e. there is time-variance in channel gain, multicast throughput may be significantly larger than R. For ease of assessing the multicast performance with non-static channel conditions, independent and identically distributed (i.i.d.) fading assumes no fading correlation between any two receivers but identical statistical properties of fading parameters at all receivers, an example of which is depicted in figure 6.1. Note that the mean value differs in
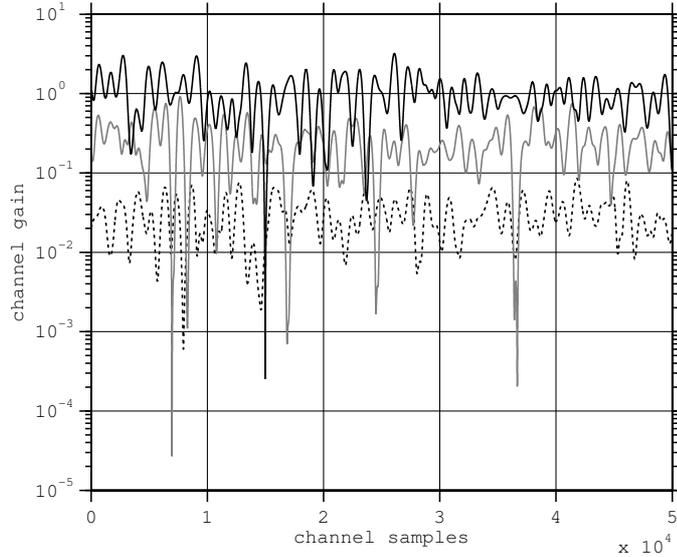
Figure 6.1: Three receivers experiencing i.i.d. fading in a Rician fading scenario at $K = 6\,\text{dB}$ each. Mean value is $1/6$, $1/2$ and 1, respectively, for better visibility.

order to improve visibility. Equal mean i.i.d. SISO fading channels are in the focus of this work, whereas alternatives to SISO multicast are introduced in the following.

6.2 Simulcast MIMO

Use of multiple antennas at base and receiver terminals is termed multiple-input multiple-output (MIMO) [91, 92]. In unicast, MIMO enables multiple spatial streams to be transmitted, or SNR enhancement by exploiting orthogonal channels due to reflections in rich scattering environments. Consequently, in the presence of independent channels, multiple antennas may increase throughput significantly. Multimedia broadcast multicast service (MBMS) is an efficient way of transmitting the same data to more than a single receiver. With advances in multi-antenna research and technology it may be questionable whether multicast is still reasonable when compared to simulcast MIMO, i.e. the case in which each of the n users receives its individual copy of the same MBMS stream. Naturally, this is a question of the number of users provided with this same data in either way. It has been elaborated above that e.g. 802.11 networks support a maximum number of receivers that is far larger than a reasonable number of transmit and receiver antennas. Assume an MBMS transmitted at a constant rate of R and received by n users. Compared to *simulcast*, the gain for multicast is simply equal to n. Now, let the simulcast transmissions be MIMO but the multicast be SISO[1] per receiver. Then, a MIMO gain m is of interest for comparison with achievable multicast throughput.

In case of MIMO, the normalized deterministic *log-det-capacity* in the frequency-flat fading case (single cluster) and with equal transmit power P_T on all N_T transmit antennas at the receiver is given as

$$C_\text{u} = log_2 \left(det \left[\mathbf{I}_{N_\text{R}} + \mathbf{N}^{-1} \mathbf{H} \frac{P_\text{T}}{N_\text{T}} \mathbf{I}_{N_\text{T}} \mathbf{H}^* \right] \right) \tag{6.2.1}$$

where $\mathbf{H}^*$ is the complex conjugate transpose of $\mathbf{H}$, and $\mathbf{N}$ is the receiver antenna noise matrix. Herein, $min\,(N_\text{T}, N_\text{R})$ is the maximum number of degrees of freedom (non-vanishing Eigenvalues)

---

[1]Multicast with multiple antennas at the receiver (SIMO) may benefit from spatial diversity by an improved link-budget of $3\,\text{dB}$ when doubling the number of receive antennas
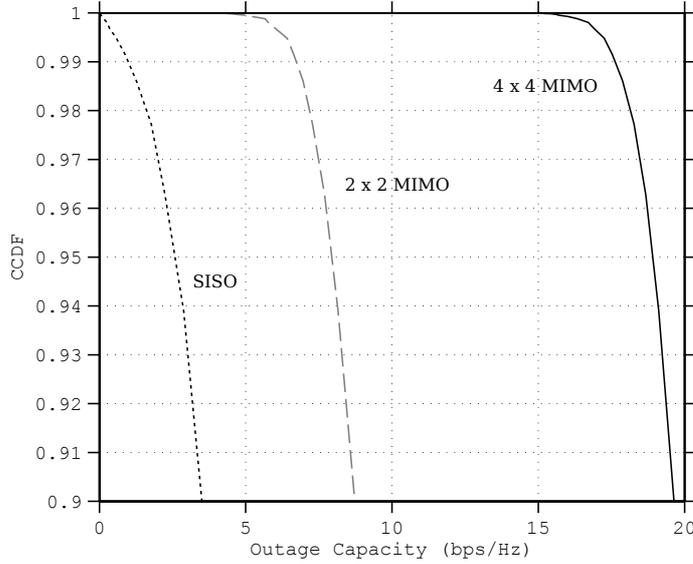
Figure 6.2: Capacity comparison of 4×4 MIMO, 2×2 MIMO and SISO for Rayleigh fading at 20 dB mean SNR.

of $\mathbf{HH}^*$, and thus MIMO sub channels, with increasing signal-to-noise ratio. The maximum MIMO gain in ergodic channel capacity is the number of degrees of freedom. For example, of a 3×4 MIMO system the maximum gain compared to the SISO case is up to $min\,(N_\mathrm{T} = 3, N_\mathrm{R} = 4) = 3$.

For MIMO antenna weighting[2], a channel sounding procedure is required. As weighting is done at the transmitter, CSI is required at the transmitter and a power water-filling algorithm is applied. In case of antenna weighting by $\mathbf{A}_\mathrm{w}$, i.e. allocating different transmit power to individual sub channels the capacity becomes

$$C_\mathrm{w} = \max_{Tr(\mathbf{A}_\mathrm{w})=N_\mathrm{T}} log_2\left(det\left[\mathbf{I}_{N_\mathrm{R}} + \mathbf{N^{-1}HA_wH^*}\right]\right) \tag{6.2.2}$$

which yields an increase in the low average SNR range and consequently, a higher MIMO gain. Weighted MIMO is thus used for range improvement (cf. IEEE 802.11n [63]). In case the MIMO channel is not deterministic but a random variable, the ergodic capacity [91] is given by the expected values of the deterministic capacities $\mathrm{E}\,[C_\mathrm{u}]$, $\mathrm{E}\,[C_\mathrm{w}]$.

Rayleigh fading

In fading environments, *outage capacity* [26] is typically considered as opposed to ergodic capacity. In figure 6.2 both 4×4 and 2×2 MIMO systems are compared to SISO in single channel Rayleigh fading at 20 dB mean SNR with full rank of $\mathbf{H}$ each, perfect CSI at the receiver and no CSI available at the transmitter. Depicted complementary cumulative density function (CCDF) of channel capacity includes outage due to considering Rayleigh distributed RV channel gain that can take values of zero. Consequently, whenever perfect reliability is considered the outage capacity becomes zero. However, e.g. at 95 % probabiliy the 2×2 MIMO system achieves around three times the SISO capacity [65]. Herein it is assumed that with $\mathbf{h}$ being a vector composed of the columns of $\mathbf{H}$ the MIMO channel correlation matrix

$$\mathbf{R_{hh}} = \mathrm{E}\,[\mathbf{hh}^*]$$

---

[2]Frequently termed "transmit beamforming", not to be confused with phased array antenna radiation pattern modification, i.e. "beam steering"

77

can be separated into correlation matrices for sender and receiver, respectively (Kronecker model). To give a literature example for practical evaluation of this and other models, Zimmermann et al. [93] have shown this assumption to be weak for indoor environments where strong non-LOS paths are present.

Effective degrees of freedom

In frequency selective channels with two clusters of scattering components (cf. section 3.5.1), it has been shown experimentally by Schumacher et al. [94] that 4×4 MIMO converges to an effective degree of freedom (EDOF) [92] of $EDOF_{4\times4} = 3$. Indoor measurements at $5.2\,\text{GHz}$ indicate a number of up to nine significantly distinguishable clusters to be realistic [95].

IEEE 802.11n

At the time of writing, 802.11n [63] is a well established standard and thus a good example for MIMO. 802.11n features a maximum antenna configuration of 4×4 MIMO and defines a set of 72 fixed MIMO MCSs, depending on the average SNR of the individual MIMO subchannels. Using all rate improving features (cf. section 5.2) and at the same bandwidth, 802.11a/g multicast for six or more users is more efficient in terms of raw bitrate[3]. This does not directly translate to throughput, as will be elaborated later on.

Above example can be assumed to be biased to the benefit of MIMO by full rank of $\mathbf{H}$ for all simulcast receivers, as the number of EDOF is typically smaller. Furthermore, it will be elaborated below how it is also biased to the detriment[4] of multicast by neglecting spatial diversity. In conclusion, MIMO performance gains are hard to quantify realistically in wireless propagation environments. With the figures as given above however, it can be stated that multicast will become superior to simulcast MIMO when $n \gg m$. A realistic figure for the number of terminal antennas in hand-held or notebook devices can be assumed in the range of $1 \leq N_R \leq 4$ due to a minimum antenna spacing of $\lambda/2$ (e.g. $\approx 6.3\,\text{cm}$ at $2.4\,\text{GHz}$) in practical MIMO systems [63, 46].

6.3 Multi-User MIMO

While in SU-MIMO as described above, each MIMO spatial stream is destined to a single multiantenna receiver, in MU-MIMO (e.g. as proposed for standardization in 802.11ac [46]), independent spatial streams for multiple single-antenna or multi-antenna receivers are transmitted at the same time. The corresponding transmitted mixture of individual signals is orthogonalized spatially by maximization of signal power at the targeted location while at the same time minimizing power at non-targeted locations (i.e. respective other users), for each individual signal (user), respectively. As such, MU-MIMO requires channel knowledge at the transmitter in order to apply appropriate MIMO weighting. A special case of MU-MIMO is MIMO transmission of the same information to multiple receivers by utilizing multiple antennas at the sender and the joint number of antennas at multiple receivers. This special case is termed MU-MIMO broadcast or *downlink MU-MIMO*.

While a LOS in SU-MIMO greatly affects diversity due to increased correlation in antenna angle of arrival of incident waves, MU-MIMO reduces the LOS impact on MIMO by exploiting spatial diversity due to differences in receiver locations. Individual receivers are typically spaced much less close than antenna elements of a single multi-antenna receiver, thus increasing spatial diversity. Likewise, MU-MIMO introduces the MIMO paradigm for single-antenna receivers, in which linear sum capacity scaling figures may be achieved similar to SU-MIMO [96]. Figure 6.3 depicts downlink single and multi-user MIMO with four transmit antennas and four spatial

---

[3]20 MHz channels, comparing raw 289 Mbps of 802.11n to 54 Mbps of 802.11a/g
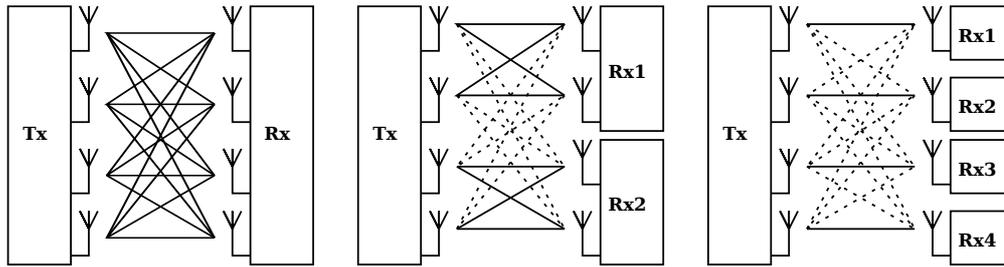[4]In case of non-static channels and if low-delay is not the system target

Figure 6.3: Comparison of SU-MIMO (left) and downlink MU-MIMO for two (center) and four (right) receivers with four transmit antennas each. In the special case of downlink MU-MIMO multicast, all spatial streams for all receivers are identical. Dotted lines indicate spatial zero channels.

streams for a single user, two spatial streams for two users each and one spatial stream for each of four receivers. For insight on respective coding for MU-MIMO, the reader is referred to the literature dealing with space-time coding for MIMO multicasting [97].

An important common limitation of weighted MIMO, such as MU-MIMO, is the requirement for CSI feedback. Depending on the environmental and receiver motion and Doppler spread (cf. section 3.3.3), more or less frequent CSI feedback from multiple receivers is necessary. Measurement results from office buildings reveal that a weighted SU-MIMO gain (cf. equation 6.2.2) may be retained for $100 - 200 \, \text{ms}$ [47] without intermediate CSI update. Within the scope of this work concerning large receiver groups, MU-MIMO gain may vanish with increasing group size due to the requirement of frequent feedback from all receivers. Another important aspect with increasing number of receivers in some distinct scattering environment are increasingly correlated channels among the receivers.

In this work, multicast feedback aggregation is advocated. Channel state information feedback from multiple (e.g. MU-MIMO) receivers (e.g. by means of feedback of an immediate acknowledgement with CSI update information) is infeasible, as aggregation results in destruction of feedback information and hence can only be binary. However, CSI feedback may also be estimated and transmitted by the receiver at some interval typically related to the coherence time T_{coh} of the channel by an explicit sounding procedure [63]. As the interval is decided upon by either sender (polled CSI) or receiver (pushed CSI), MIMO CSI signaling is done out-of-band and consequently unicast (subject to signal and error correction coding that is out of the scope of this work). In conclusion, multicast using feedback aggregation by jamming and downlink MU-MIMO multicast are not mutually exclusive. Evaluation of a potential benefit of using MU-MIMO in conjunction with feedback aggregation for immediate acknowledgments is left for future work.

6.4 Overlay FEC

Wireless digital communication typically requires some form of FEC. In order to increase data rate, m-ary modulation is used, resulting in many possible modulation and coding scheme (MCS) combinations, of which each provides some bit rate. IEEE 802.11 wireless LAN provides a set of different MCSs for operation under different channel conditions. In first approximation, signal power decays with increasing link distance, resulting in decreasing SNR at reception of the signal. With decreasing SNR, wireless link adaptation shall reduce throughput, and vice versa, by respective MCS selection. However, multicast transmission implies existence of more than one receiver and thus multiple wireless links. Initially, let some MCS be pre-configured for multicast. Hence, due to typically independent fading channel conditions at the receivers (different locations and interferences), each frame transmitted at this rate may be correctly received by all, none,

or any other subset of receivers. When this subset is not permanently empty and changing over time during multiple frame transmissions, after some time all receivers have received a subset of transmitted frames. In such cases it is reasonable to deploy *overlay forward error coding*, which is a form of error correcting code concatenation using some additional code on top of another one. For example, overlay FEC is applied to systems that are already protected by FEC in order to increase transmission reliability at the expense of additional coding complexity. It is well known that code concatenation can yield significant performance gains with respect to coming closer to the Shannon limit. Turbo codes and the combination of inner and outer code (and interleaving) in DVB are examples.

In absence of receiver feedback, an overlay FEC system remains an open-loop system (in anticipation of section 7.1). In IP networks, the overlay may incorporate its own feedback mechanisms or make use of out-of-band feedback available e.g. in WLAN multicast according to 802.11v [98] (cf. multicast diagnostics reports). By feedback of residual error rates as measured at the receivers, former is a vehicle for adapting the overlay FEC code rate. In general, two levels of overlay FEC can be defined in the context of IP packet based transmission as follows.

Byte level overlay FEC may e.g. be used in 802.11 WLAN unicast as well as multicast. In section 5.2 it has been elaborated that WLAN applies an $133, 171|_o$ convolutional forward error coding error correcting code. Bit errors that remain uncorrected by this code are detected by a CRC code. In the literature [99], block codes on the Galois-Field $GF\left(2^3\right)$ have been applied on top of convolutional forward error coding in wireless LANs. In order to make this work, the medium access control layer CRC has to be disabled. From a channel coding point of view, the CRC code is replaced by a more powerful, bit error correcting code. This kind of concatenation may be reasonable in some situations, e.g. in which deep fades or shadowing occur during a single channel access (cf. section 3.2.2.3).

Packet level overlay FEC on the other hand applies overlay FEC spanning several packets. Assuming that packets sent to a multicast destination address may be lost at multicast receivers independently due to fading as elaborated above, this kind of concatenation of codes is especially well suited e.g. in WLAN multicast. In packetised TDMA systems, individual packet loss at each receiver may be compensated at another time by overlay FEC redundancy packets. Examples for packet level codes are maximum distance separable (MDS) codes such as the non-binary Reed-Solomon code as e.g. fostered by Rizzo et al. [100] and Gorius [14]. Code word lengths can be chosen in the order of typical IP packet lengths ($> 1\,\mathrm{kB}$) by a *virtual interleaving technique* (cf. section 10.2.2) as defined by DVB multiprotocol encapsulation (MPE) FEC [101] and as used in DVB-H [102]. Rateless codes, such as the Luby-Transform and Raptor [21] codes, are alternatives. The important common property of such block codes is their capability to recover from a loss of any m packets (with proper interleaving, else: symbols) out of a block of $k + m + \epsilon = n$ packets. For MDS codes the ϵ is equal to zero, whereas in case of rateless[5] codes, the coding scheme introduces an $\epsilon > 0$. For a systematic code, the original data is transparently part of the coded data. In case of non-rateless systematic codes this results in the capability to compensate for each lost data packet with exactly one of m redundancy packets. In case of MBMS this is highly beneficial as packets may be assumed independently lost. Assuming for example two different data packets lost at two receivers, a single redundancy packet, if received by both, will compensate for their individual and different loss.

With respect to overlay FEC the focus herein is on packet level FEC, as indoor transmission and transmission at low mobility is assumed, resulting in slowly fading AWGN channels. Channel fluctuations and thus deep fades that are faster than a single packet are consequently out of the scope of this work.

---

[5]The "rateless" property is due to k being defined in advance, while n is not due to the variable ϵ, hence the code rate $R = k/n$ is undefined.

Packet level FEC algorithms are typically distinguished by different variants of hybrid automated repeat-request (HARQ) error correction.

1. Proactive FEC carousel. The sender supplies the whole FEC block of $k + m + \epsilon$ packets proactively. If this is insufficient for decoding, retransmissions are initiated by negative feedback from the receiver(s). A special case of this is termed *chase combining*, in which $k = 1$ and $m + \epsilon = 0$ and thus no overlay FEC code is applied. The receiver(s) obtain copies of the original data and combine received versions of those copies, increasing the SNR.

2. Incremental redundancy FEC carousel. The sender gathers feedback after transmission of k packets and transmits one out of the $m + \epsilon$ in case of negative feedback. Feedback cardinality is binary in this case. When parity is exceeded, retransmissions are initiated.

3. Incremental redundancy with non-binary feedback FEC carousel. As compared to 2., this scheme differs in the non-binary cardinality of the acquired feedback. Non-binary information is used to transmit as much parity packets as required. The receiver(s) may indicate the required amount of parity or the exact set of missing packets within feedback messages after evaluating which packets out of the k transmitted are missing.

4. Open loop FEC. Due to the absence of feedback, the scheme is subject to potential residual error. Block transmission delay is limited for the same reason. An established example using Raptor FEC codes ($\epsilon > 0$) is the multimedia broadcast multicast service "file delivery over unidirectional transport" (FLUTE) [21] in mobile networks as defined by the 3GPP.

6.5 Mobile Multicast

In development of the MBMS specification in UTRA networks, a number of HARQ FEC schemes have been considered for evaluation. Frenger et al. [103] have compared chase combining with incremental redundancy and they show that with equal transmit energy per packet, latter outperforms plain repetition. Apart from multicast file delivery using FLUTE, at the radio link control layer of LTE [104] the multimedia broadcast multicast services (MBMSs) in single-cell and single frequency networks (SFNs) implement an open-loop FEC system. The *unacknowledged mode* (UM) as defined in 3GPP UTRA is used, which enables detection of losses and packet reordering by sequence number stamping of the individual packets. The FEC coding scheme is overlaid at the application layer and a rateless Raptor code is used [22].

6.6 Broadcast Channels

The focus in this work is on point-to-multipoint transmission of services, such as digital television. The term *broadcast channel* [105] implies a multi terminal wireless network comprised of a base station (e.g. a WLAN access point) and a number of receivers. Specifically, Cover [105] has coined the term *degraded* broadcast channel, in which receivers can be ranked in terms of channel quality and consequently in achievable throughput. With multiple antennas per terminal and AWGN at the receiver, the Gaussian vector (MIMO) broadcast channel has been shown to provide a maximum achievable *sum-rate capacity* [106]. It is achieved by *dirty paper coding*, by which Costa et al. [107] have shown that channel capacity is independent of interference whenever the channel state is perfectly known at the transmitter. Hence, the normalized channel capacity remains $C = log_2(1 + SNR)$, i.e. the channel state can be compensated perfectly. Computation can be assumed expensive with frequent high quality CSI updates being required from all receivers.

6.6.1 Multi-User Diversity

In general, the term multi-user diversity (MUDiv) implies that different users experience different channels. Uplink TDMA with power control subject to frequency-flat fading has been shown to exhibit a significant MUDiv gain [108]. When perfect channel knowledge is available in a degraded broadcast channel, i.e. each station knows its momentary channel gain and that of every other station at any time, one of them is subject to the highest gain at some point in time. It is then referred to as the "best" station, and it is able to identify itself as such. A MUDiv gain is achieved when the "best" station continues to transmit as long as it remains in this rank. This gain is further increased by allocating more transmit power to the "best" receiver. For multi-antenna systems, water-filling is an optimal power allocation strategy which allocates more power on MIMO channels with high SNR, hence MUDiv gain and MIMO gain both exploit an increased capacity at higher SNR.

As in MIMO, a drawback is that if fading is fast, exploitation of a MUDiv gain may be infeasible due to excessive feedback in a real situation where stations are not omniscient with respect to channel quality. On the other hand, in case fading is slow, the "best" receiver will potentially stay the "best" for a too long time.

Conversely, when the base station transmits, but chooses a rate at which only the "best" receiver can receive, due to reciprocity a MUDiv gain is also achieved. In a multi-user unicast network, this implies simulcast when information shall be conveyed to more than a single receiver and a potentially large delay depending on the speed of fading. With multicast capability, this leads to the topic of "opportunistic multicasting".

6.6.2 Opportunistic Multicasting

In a publication with the same title, Gopala and Gamal [109] have coined the term *opportunistic multicasting*. They make the assumption that channel state information at the transmitter is perfectly known for the whole multicast group. A receiver in the multicast group is termed *user*. With perfect channel knowledge at all stations, several multicast transmission *schedulers* can be defined. Among those are:

- "best user" scheduling strategy

  transmission is done at a rate suitable for the "best user". If no two users experience the exact same channel condition, the strategy is identical to simulcast, and the multi-user diversity gain is maximally exploited. It can be shown that the delay grows exponentially with the number of users [110].

- "worst user" scheduling strategy

  the rate is chosen suitable for the "worst user". This is identical to serving all users. Hence, the multicast gain is maximally exploited.

When channels are varying over time, for each transmitted frame the user ranking may be a different one. With the schedulers as defined above, i.e. maximizing multicast gain or MUDiv gain, it has been shown [109] that there is a scheduler exploiting a maximum throughput.

Maximum throughput can be achieved by a "best users" scheduler with perfect channel state information at the sender. This scheduler transmits at a rate sufficient to be decoded by the best l out of L users for each channel access, i.e. transmitted frame, whereas L is the multicast group size and l is fixed. This implies inability of reception for receivers not in this set. The resulting packet loss is assumed compensated by a packet level overlay FEC code (cf. section 6.4) of rate l/L.

For a given fading scenario, it is necessary to find l, maximizing throughput. For i.i.d. Rayleigh fading, SNR x is exponentially distributed

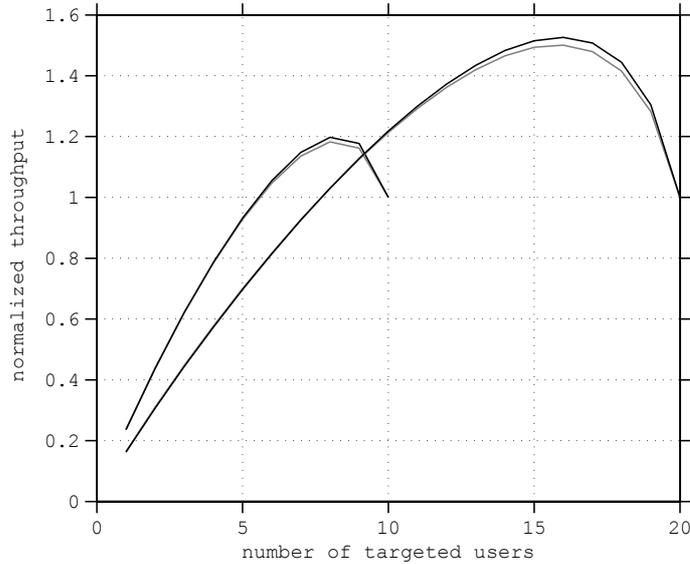$$p_{\mathrm{x}}(x) = 1 - e^{-\lambda x}$$

Figure 6.4: Opportunistic multicast gain with "best user" scheduling for 10 and 20 users. Black lines: i.i.d Rayleigh fading at a mean SNR of 100; Gray lines: i.i.d Rician fading at a mean SNR of $10 + K$, Rician $K \approx 2$ (3 dB).

and the mean throughput $\bar{\Psi}(l)$ for l "best users" scheduling is given as [111]

$$
\begin{aligned}
\bar{\Psi}(l) &= \frac{l}{L} \mathrm{E}\left[C_l\right] \\
&= \frac{l}{L \cdot ln(2)} \sum_{j=1}^{L} \binom{L}{j} \int_0^\infty \frac{[1 - p_{\mathrm{x}}(x)]^j [p_{\mathrm{x}}(x)]^{(L-j)}}{1 + x} dx
\end{aligned}
\tag{6.6.1}
$$

Exemplary results for multicast group sizes of 10 and 20 users in Rayleigh and Rician fading scenarios are depicted in figure 6.4, in which curves are normalized to an average throughput figure as obtained when all stations are jointly targeted for each and every channel access. In the literature, some authors prefer to normalize to the simulcast case, i.e. targeting the single "best user" per channel access. Delay in this scenario is quasi infinite by Monte-Carlo simulation over the respective fading RV. From this it can be observed that different fading scenarios may lead to approximately identical results. With numerical evaluation of (6.6.1) and the fading distribution explicitly part of formula 6.6.1, one can obtain results for different statistical fading characteristics and more complex, realistic channel models. Furthermore, correlated fading simulation is possible. In the chosen scenarios "i.i.d. Rayleigh with 20 dB mean" and "i.i.d. Rician with mean 12 (K=2)", a maximum in throughput is achieved for 8 (17) users and exceeds the "worst user" scheduler (for which $l = L$) by 20% (50%).

6.7 Opportunistic WLAN Multicasting

In case all users are targeted for transmission at each channel access in opportunistic multicasting, a broadcast scheme is implemented, albeit at variable bit rate decodable by the "worst user", and hence, by all. Throughput of opportunistic multicast with uncorrelated i.i.d. and non-i.i.d. Rayleigh fading normalized to the throughput in case $l = L$ has been evaluated numerically by Kozat et al. [111]. As described above, a long term gain in case of infinite delay (see above) as well as in the delay constrained case can be observed. When targeting e.g. the best $l = 7$ out of

$L = 10$ users, this gain is nearly 100% for i.i.d. Rayleigh distributed channel gain at 10dB mean. An important assumption is that any instantaneous channel gain due to slow fading results in an AWGN SNR at the receiver of γ, which itself becomes a random variable. This leads to a capacity of $C = log_2(1 + \gamma)$ per channel access. In practice, however, MCS bit rates are finite in number and are subject to a lower SNR limit, below which communication is impossible using this respective technology. This is evaluated herein by example of 802.11 WLAN.

Correlated Fading

Considering correlated fading is required when simulating the behavior of realistic rate adaptation and retransmission protocols. Opportunistic multicasting on the other hand considers very long codes, e.g. spanning hundreds of packets.

Generation of a correlated random process with Rayleigh or Rician distribution and arbitrary Doppler psd is out of the scope of this work. Solutions for simulation of correlated fading are readily available in MATLAB[6]. Correlated fading using the classical Doppler psd for simulation of very long codes and realistic (channel non-aware) rate adaptation (cf. LBP ARF below), is achieved.

As WLANs are typically used indoors, indoor channel modeling is included. For example bell shaped Doppler psd [47] can be applied due to the receivers mostly being stationary while there is motion in the environment [27] (as opposed to the classical shape) for simulation of indoor environments. Hence correlated single-cluster SISO Rayleigh fading, multi-cluster [45] SISO Rician/Rayleigh fading with bell shaped Doppler psd at a max. Doppler shift of less than 6Hz [47] (cf. TGn channel model B) are simulated. Rician fading K-factor herein is 1 on the first channel tap (cluster) and 0 elsewhere [36].

6.7.1 Rate Quantization

A simulation environment has been implemented to reproduce results as available in the literature [111]. The results are extended in this work by evaluation of quantization of the available rates in different and more realistic fading scenarios.

When the capacity is quantized at fine granularity, e.g. in 10^5 log-spaced steps ranging from $\bar{\gamma}[dB] - 100dB$ to $\bar{\gamma}[dB] + 30dB$, identical figures as in the continuous case are obtained. In case it is lower bounded by e.g. $\bar{\gamma}[dB] - 10dB$, a degradation in normalized throughput gain is observed, whereas the max. gain is achieved at the same number of targeted receivers. Both effects are shown in figure 6.5 for an example of 20dB mean i.i.d. Rayleigh fading. As individual deep fades are compensated at another time, whereas other users are served this time, intuitively, a lower limit reduces the number of users served per transmission. Reducing the number of steps results in a shift in the relative throughput maximum towards less targeted users. Note that the "best users" scheduler may actually serve more than the targeted l users per transmission (but never less than l) due to this quantization, hence the maximum gain is shifted to the left. This is done by design to keep the algorithm in line with what it has been proposed to do initially: For each transmission, the sender sorts the users according to their current channel gain and transmits at the highest possible rate suitable for the best l users (here: at least l). One could argue that the scheduler could refrain from transmitting as it knows when e.g. no user can receive even at the lowest rate. However, the goal is to keep the results comparable to a rate adaptation scheduler without channel knowledge.

6.7.2 802.11a Multicast Throughput Gain

According to 802.11a/g OFDM receiver sensitivity figures [64] (cf. section 5.2.3) and assuming 17dBm transmit power, further a 118 dB distance to the thermal noise floor and 10 dB noise figure at the receivers [54], one may obtain the SNR thresholds for 802.11a/g OFDM physical
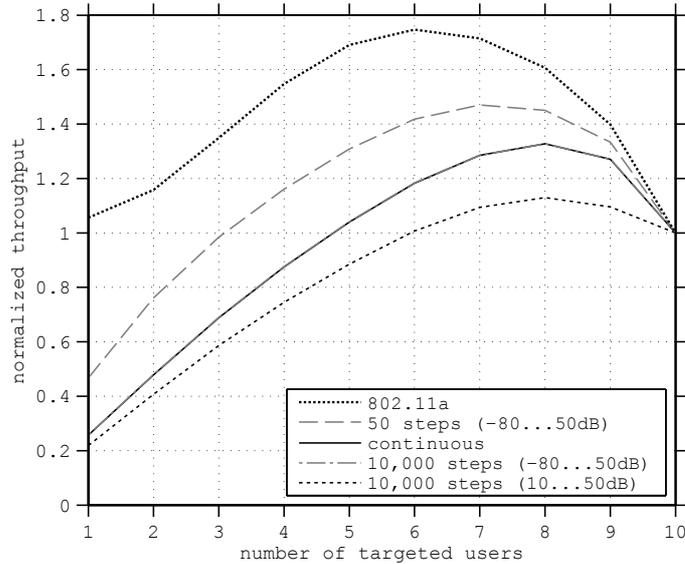
---

[6]www.mathworks.com (Communications Toolbox)

Figure 6.5: Opportunistic Multicast throughput gain due to "best users" scheduler at 20dB mean i.i.d. Rayleigh fading with and without quantization of the available throughput rates. Note that users are selected a-priori.

Table 6.1: 802.11a/g opportunistic "best users" multicast throughput (10 users, Rayleigh)

Mean SNR [dB]	14	17	20	23	26	29
Targeted users	4	5	6	6	6	7
Max. throughput [Mbps]	7.16	11	15.2	20.5	26.9	34.4
Min. redundancy spent	2.08	1.69	1.44	1.41	1.41	1.29

layer as given in table 5.3 on page 55. Although they do not exactly match the ones obtained in section 5.4, they serve as conservative figures.

Considering the set of MCSs as provided by OFDM based SISO 802.11, the multicast throughput gain of the opportunistic "best users" scheduler is of interest herein, whereas i.i.d. Rayleigh fading at the receivers is assumed. An exemplary result is depicted in figure 6.5 for 20 dB mean SNR. This indicates a shifted and increased maximum normalized throughput for 802.11a/g as compared to the ideal case, whereas the maximum is shifted from 8 to 6 users. Calculating the minimum throughput using raw bit rate figures as given in table 5.4 on page 61, throughput for $l = 6$ at 20 dB mean power and i.i.d. Rayleigh fading is approx. 15.2 MBps when 44% of redundancy (counted in packets) is provided to correct packet loss (due to targeting 6/10 users per transmission) for all users (i.e. for the worst user). In other words, 10 users receive at this rate without residual error. Compared to simulcast this is 152 Mbps, albeit using a single antenna at base station and user terminals.

It is important to note that the redundancy is not equal to $1/(l/L)$. Instead, it may be higher when targeted users are below the lowest threshold[7], while due to quantization, the scheduler may actually serve more than the targeted l users per transmission. In this section, reference figures for multicast throughput have been obtained. It is promising that for quantization of the available bit rates due to a finite number of MCSs, the maximum throughput is still almost fully achieved.

---

[7]In this scenario of 20dB mean i.i.d. Rayleigh fading, approx. 8% of residual error remains when targeting $l = L = 10$ users

6.8 Delay-Constrained Multimedia Multicast

As elaborated above, opportunistic multicasting aims at exploiting a multicast throughput gain by spatial diversity. The price paid for this gain certainly is delay. However, in delay-constrained multimedia multicast, such as in live TV, excessive delay would be a contradiction. Conversely, with a delay constraint, a multicast throughput gain may not be obtained. To stay with the example of television, the typical TV program is not entirely made up of live broadcast. In fact, major portions are pre-produced. With bidirectional and multi-purpose IP networks as transport vehicle, these portions of television content need not be provided at low delay. The system however needs to be capable of providing both.

In this section it has been shown that multicast throughput gain can be significant, but it is not always feasible or reasonable to aim at exploiting it. Nevertheless, it serves as a reference of maximum achievable throughput in case delay is not an issue. Key in transmitting AV streams efficiently in wireless multicast is the combination of available mechanisms depending on the situation. For increasingly large receiver groups, exploiting antenna diversity becomes infeasible. Low delay requirements as in live television may diminish the otherwise achievable multicast throughput gain. The focus of this work is thus on transmitting inelastic streams efficiently by rate adaptive multicast over wireless networks, by example of wireless LAN.

Multicast Feedback

In many wireless standards, such as IEEE 802.11 and those introduced by the Third Generation Partnership Project (3GPP), unicast feedback is implicitly polled by the data frame destined to a single receiver. In 802.11, upon reception of a unicast data frame an acknowledgement (ACK) is responded after a fixed medium idle time as specified by the standard, i.e. the short inter-frame space (SIFS). The SIFS is a gap introduced in order to enable the receiver to terminate reception, compute the cyclic redundancy check (CRC) and initiate ACK transmission in case of checksum match. The exact point in time of medium access for feedback transmission is subject to SIFS timing inaccuracy. Different variants of the standard specify different SIFS durations[1] and timing inaccuracy tolerances. Unicast data execution time, in case of successful reception, is composed of a variable frame duration and a constant C, the latter of which is composed of ACK duration, SIFS, SIFS tolerance and location dependent propagation time. In multicast, data execution time may additionally depend on the number of receivers from which feedback is acquired.

As stated above (cf. 5.5.2, 6.3), feedback may be conveyed in different forms but is in general used for the purpose of error control. A basic form of feedback is binary. More complex transmission algorithms make use of channel state information (CSI) feedback. Binary feedback can be implemented by an explicit ACK message, whereas absence thereof is taken as the semantic opposite. True binary feedback conveys both states (success/failure) by explicit positive and negative ACK. Both forms of binary feedback are semantically equivalent, they only differ in execution time and implementation complexity. More complex feedback can be given by the receiver in forms of e.g. history of previous transmit success (statistics) or channel quality indication (measurement). In this work, the focus is on binary feedback in multimedia broadcast multicast service (MBMS). An overview of feedback in multicast transmission schemes is given in the following. Analysis of the event of feedback jamming in time-division multiple access (TDMA) feedback aggregation is provided in section 8.1. Error control by feedback aggregation is covered in chapters 8 and following.

7.1 Open-Loop Broadcast/Multicast

In control theory an open-loop controller is a device operating without knowledge of its output. Hence, its decision and consequently the system output is solely based on some control input. In case measurement data of the control system output is fed back to the input, the loop is closed and the controller may become adaptive. A well-known example for open-loop broadcast of digital audio visual data is Digital Video Broadcast (DVB) television. In any equally complex system there may be a number of control variables, and the control target at the output is a matter of definition. In DVB the control input in terms of transmit power, forward error coding (FEC) coding rate, channel bandwidth, etc. is fixed and is chosen at the time DVB is physically deployed, subject to country specific regulations, service specific requirements and local wireless propagation conditions, to name a few.

---

[1]Example short inter-frame space conventions in WLAN standards: 802.11a: $9\,\mu s$, 802.11b: $20\,\mu s$

For which specific task a system is finally designed and deployed as open-loop or closed-loop may be a question of implementation complexity. With respect to feedback in closed-loop MBMS in general, the problem of *feedback implosion* [112] has to be solved. Implosion of feedback describes a situation in which feedback about a broadcast/multicast transmission event is issued by many receivers at the same time (in absence of mechanisms for feedback suppression). In case the feedback destination cannot reasonably handle the multitude of feedback, provision thereof is futile from the start. In systems like DVB for example, deployment with fixed parameters in an open-loop manner can be assumed less complex than gathering feedback from all users. Exclusive use of time and spectrum in such systems obviates the necessity of feedback from all users.

Other systems serve a more general purpose of digital data transmission and are thus variable in their input parameters. Examples are Long-Term Evolution (LTE) and wireless LAN, in which channel bandwidth, FEC coding parameters and modulation order are variable within some interoperability limits defined by the respective standard. By e.g. immediate acknowledgement of each successfully transmitted frame in unicast, the control algorithm operates in a closed-loop. Control parameters may be the FEC coding rate and modulation order per transmitted data frame. By example of WLAN, this is denoted as the momentary modulation and coding scheme (MCS). Feedback as introduced herein is used for MCS adaptation as well as adaptation of overlay FEC redundancy.

The multicast feedback implosion problem can be relaxed or even avoided in multiple ways. A probabilistic approach using timers and non-exhaustive feedback has initially been proposed by Erramilli and Singh [113] and was further developed [114, 115]. In this work the focus is on avoiding feedback implosion in MBMS by gathering feedback from the entire group of receivers at the same time. This is further denoted as feedback aggregation, as a single feedback time slot of a purely TDMA multiplexing system is used and feedback is transmitted concurrently. The scheme is based on a leader receiver that can be outvoted with respect to its feedback by the remaining group members and has been initially proposed by Kuri et al. [116]. By example of WLAN this is evaluated for immediate feedback which is either gathered per each transmitted frame or for groups of frames.

7.2 Closed-Loop Multicast

As opposed to fixed FEC systems, 802.11 is a multi user bidirectional system. Overlay FEC coding may be applied in open-loop multicast, however it is also important to transmit at the currently highest possible MCS in order to not waste transmission time, which is shared among potentially many services or users. If the rate for this particular multicast group of receivers is not correctly chosen, due to reception quality variations (over time and/or receiver location) this can potentially lead to situations in which most receivers are unable to successfully receive what is sent in multicast. It is well known that in absence of feedback (i.e. with open-loop error control), full reliability cannot be guaranteed. For some receivers in a multicast group, a large portion of transmission failures may remain uncorrected. This section gives an overview of closed-loop communication protocols in general and by example.

7.2.1 Sequential Feedback

Figure 7.1 depicts explicit group based sequential feedback polling in a multicast transmission. Herein, feedback about reception of the previous frame is requested from each receiver individually. This can be done by means of polling feedback from each receiver i with a dedicated request per receiver (REQ_i). In doing so, feedback medium access coordination is achieved, as it is clear which receiver is about to transmit in response, and at which point in time (cf. IEEE 802.11aa [117]). Compared to unicast data+ACK transmission time, multicast execution time is increased. When feedback is polled from all receivers, n times feedback request overhead (REQ frame) plus ACK duration (which may differ from unicast) is added, whereas n is the
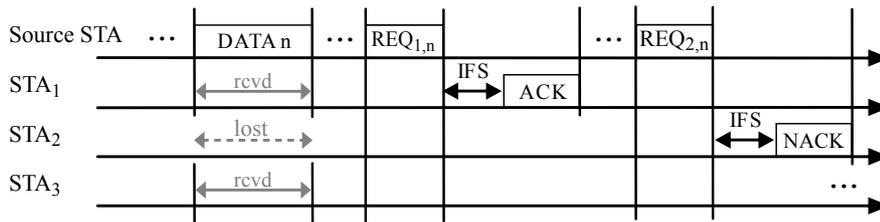
Figure 7.1: Individual feedback polling from multiple wireless stations receiving data frames of a multicast stream. A feedback request frame $REQ_{i,n}$ is issued per receiver i and n.

number of multicast receivers. In order to reduce the feedback overhead, a source may decide to poll only a subset of stations receiving respective multicast stream [118]. However, incomplete polling may result in a residual error at the stations outside the polling subset.

7.2.2 Multicast Feedback in 802.11

As elaborated in section 5.3.5, according to IEEE 802.11-2007 [64, (9.2.7)], no acknowledgement is issued following successful broadcast and multicast data exchange. The amendment 802.11aa [117] as formulated by IEEE 802.11 task group aa (TGaa) includes an implementation of explicit group based sequential feedback polling as depicted in figure 7.1. Feedback is polled from individual receivers that are part of a multicast group by means of a dedicated feedback request per receiver. The obtained information is used to schedule retransmissions, hence the algorithm is termed groupcast with retries (GCR). Feedback may be obtained for a group of previously transmitted frames, which decreases feedback overhead as compared to per-frame acknowledgement. A bit map is transmitted in response to an individual feedback request, in which the respective receiver signals which frames of the previously transmitted block of frames (indicated by sequence numbers), has been received correctly. When the sender has gathered this binary state per previously transmitted frame from every receiver explicitly (or optionally of a subset of receivers), it may schedule the set of hence determined lost frames for retransmissions. This is subject to a retransmission limit per frame as defined in 802.11aa. While above scheme can be assumed to work well for small receiver groups, the feedback overhead becomes increasingly large with increasing group size. Therefore, *unsolicited retries* have been introduced in 802.11aa. The access point (AP) may decide to refrain from gathering multicast feedback according to some not further specified measure (e.g. when the group size exceeds some threshold). It may then use unsolicited retries by transmitting frames multiple times in order to reduce the probability of loss at the multicast receivers.

With 802.11v [98] the IEEE has further standardized the *directed* multicast service (DMS) protocol. Strictly speaking this is not a multicast feedback protocol. Instead, in DMS a station may request the AP to convert a multicast stream (assume n receivers) into a unicast stream destined to this station. The protocol enables smooth transition between multicast, simulcast and a mix thereof. For each station requesting DMS, the order of simulcast is increased by one, resulting in $1 + n_{DMS}$, $n_{DMS} < n$ instances of the streams being transmitted until $n = n_{DMS}$, upon which the original IP multicast stream is shut down.

7.3 Representative Based Multicast

Representative based multicast protocols, often termed *leader* based, are a class of closed-loop protocols in which, strictly speaking, the loop is only closed for a single member of the group of receivers. The representative based approach typically requires a leader to be selected among the group of receivers, such that the remainder of the group is satisfied with the control loop
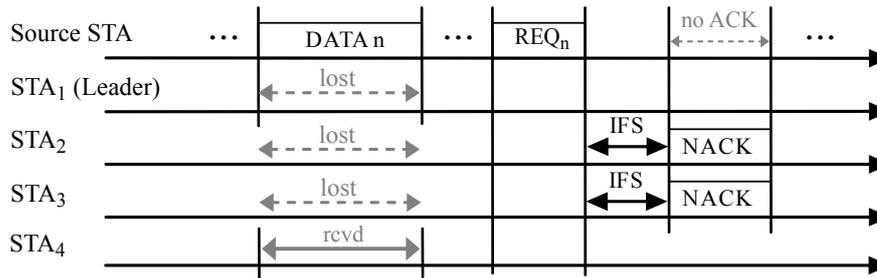
Figure 7.2: Aggregated feedback jamming scheme with feedback request frame, four receivers and one multicast group leader.

decisions made on behalf of them. An approach is presented by Dujovne and Turletti [119], in which the leader is selected to be the receiver with the "worst channel conditions", which implies some form of explicit CSI feedback from all receivers[2].

Feedback aggregation in a leader based protocol (LBP) has been initially proposed by Kuri and Kasera [116]. In the protocol specified therein, a leader receiver is responsible for acknowledging transmit success on behalf of the multicast group, i.e. the protocol is representative based. However, the protocol deliberately allows feedback from the leader and the non-leaders to collide. Non-leader receivers may not transmit positive ACKs but may issue negative feedback (NACK) as depicted in figure 7.2. Similarly, busy-tone based negative ACK has been evaluated by Gupta et al. [120]. Both describe leader-based feedback aggregation with jamming, whereas feedback from non-leaders is used as a joint jamming signal, i.e. their negative feedback shall cancel the leader's ACK. The proposals [116, 120] as presented above are what this work is based on.

In the scope of this work, leader (or representative) based multicast aggregates feedback from all receivers within a single feedback time slot. Thus, the time consumed for one round of feedback is independent of the number of receivers. For example, in OFDM based WLAN this may be the point in time of ACK frame transmission with duration of $44\mu s$ when the MCS resulting in 6 Mbps used. By contrast, the time required for polling feedback from each receiver individually grows linearly with the number of receivers and thus results in increasingly large feedback overhead. Full reliability on the other hand can only be achieved by exhaustive gathering of group feedback. Without additional FEC, feedback polling may thus provide reliability similar to unicast with some identical retransmission limit, albeit at the cost of throughput reduction. For increasingly large groups [121], feedback aggregation is an alternative with constant feedback overhead. A retransmission scheme with feedback aggregation is introduced in section 8.1. Rate adaptation based on feedback aggregation as well as a combination of incremental redundancy and rate adaptation are introduced in section 9.3 and following.

7.3.1   Selection of a Representative

For representative based multicast in which feedback is deliberately jammed by non-leader receivers in order to outvote a leader receiver, failure of jamming is a false positive. In this regard, false positive implies that the feedback destination gets a positive (ACK) response and is unaware of the failure of the outvoting attempt (and even of its existence). A scheme selecting the representative should thus minimize the false positive rate. The update frequency of a selection algorithm is assumed dependent on the speed of movement and the fading environment, and requires some signaling overhead in the form of CSI feedback. It has been stated that "the worst" receiver is a justified momentary representative [116]. In this work, however, homogeneous fading is assumed such that receivers are indistinguishable in their individual channel quality, such

---

[2]Proposal of Dujovne et al. involves the leader being served by unicast and the rest of the group "overhears" the communication (cf. promiscuous mode in IEEE 802 networks)

that a long term "worst receiver" is not present. In this regard, selection of a representative is infeasible and in the scope of this work, the leader is randomly chosen. In the following it will be elaborated how the protocol maintains its functionality still.

7.4 OFDM Multicast Feedback Capture

In wireless TDMA systems the so-called *capture effect* has an influence on system performance. Throughput analysis, if capture is not considered [68], has been shown to underestimate the real-world throughput [69, 70, 71], as collisions do not necessarily result in definite loss of the colliding signals. The capture effect describes the incident of successful reception of a strong signal in the presence of at least one other transmission at the same time and within the same frequency band. This is also referred to as *near-far effect*, as stronger signals in wireless communications typically come from transmitters that are closer to the receiver. In code-division multiple access (CDMA) transmission may take place simultaneously[3]. Conversely, time-division multiplexing shall avoid simultaneous transmission. However, it may still happen that multiple stations transmit at the same time, which is referred to as *medium access collision*. An algorithm susceptible to this problem is the decentralized medium access scheme distributed coordination function (DCF), an implementation of carrier sense multiple access with collision avoidance (CSMA/CA) (cf. section 5.3.4.1). In CSMA/CA there is, to a certain extent depending on the number of users, a probability of simultaneous channel access. Capture comes into effect whenever one of the transmitted signals has been correctly received *although* one or more interfering signals had been transmitted at the same time. Without loss of generality, one of the signals is regarded as the *desired signal*, while the rest are *interfering* signals. The probability of capture of the desired signal strongly depends on the compound interference power, as experienced at the receiver, compared to the power of the desired signal.

Consequently, power capture (on which the focus is herein, cf. section 7.4.2) may be seen as a capability of rejection of concurrently transmitted signals of the same type (frame format and carrier frequency). While interference may be assumed as additional white noise in some cases, within the scope of this work, it is evaluated whether interfering signals introduce a white noise interference. Literature references evaluating the performance of TDMA protocols such as the 802.11 DCF consider incoherent addition of signals [122] in case of collision. Coherent accumulation of signals on the other hand results in higher dynamic range [123] of interference. In this work the power capture effect is evaluated for time aggregated orthogonal frequency division multiplex (OFDM) multicast feedback. The conditions for coherent accumulation are [123]

- short observation time compared to the channel fluctuation rate

- approximately equal carrier frequency

- low phase modulation index

In the scope of this work, these are not entirely met for synchronous OFDM feedback using frames of few OFDM symbol lengths. OFDM in general can be considered as carrying approximately half of the information in the phase component. Consequently, phases of different OFDM signals can be assumed to differ significantly. In the following, feedback capture is evaluated by analysis of incoherent accumulation, simulation of concurrent transmission according to 802.11 as well as practical measurements.

7.4.1 Failure of Feedback Jamming

With respect to multicast feedback aggregation by feedback jamming it is important to include power capture in the analysis of the event of feedback jamming. A non-zero probability of capture

---

[3]In CDMA multiple stations transmit at the same time through orthogonal time signals. The *near-far effect* results in the *near-far problem*, as signals from different users should arrive at the base station at approximately the same power for successful decoding.

of the leader's acknowledgment (herein: the desired signal) amidst a multitude of non-leaders' negative acknowledgments (herein: the interference signals) results in a non-zero jamming failure probability. Consequently, failure of feedback jamming is a false-positive when interpreted at the feedback destination, which is assumed incapable of detecting jamming failure. By checksum comparison, it may only distinguish between a frame that is received error-free, and a checksum mismatch (cf. section 5.3.1) which implies some error. The cause or any other characteristics of the error that lead to a checksum mismatch are typically not conveyed.

In the following, a detailed distinction of delay capture [124] and power capture is omitted. Delay capture may occur when the desired signal arrives significantly before the interfering signals, or is of much greater signal strength than the interfering signals but arrives during reception of one of the interfering signals. It is assumed that inter-arrival delay times of feedback transmitted deliberately at the same time, especially if some synchronization mechanism is included, are small compared to the length of the feedback. In section 10.1.1 it is elaborated how, within the scope of this work, feedback is triggered by a broadcast signal from the base station and is consequently issued by all participating stations immediately afterwards. Feedback jamming failure probabilities are evaluated in the following under this premise.

7.4.2 Power Capture

Power capture is evaluated in fading channels (cf. section 3.2). Each receiver is subject to an instantaneous and independent fading gain due to the fading channel between itself and the feedback destination. The *power capture threshold* z is defined in evaluating the capture effect and is an implementation specific parameter. Herein z is defined such that the condition for feedback jamming $C_\mathrm{l}(z)$ is the condition that the leader's feedback is canceled whenever the sum fading gain of those non-leaders that did not successfully receive respective data frame exceeds a capture threshold that is $10 \cdot log_{10}(z)$ decibel (dB) below the fading gain of the leader $p_\mathrm{l,t}$.

$$C_\mathrm{l,t}(z) = p_\mathrm{l,t} > z \cdot \sum_{\mathrm{j}=1}^{n} I_\mathrm{j,t} \cdot p_\mathrm{j,t}$$

Herein, $I_\mathrm{j,t}$ is an indicator function which has a value of 0 or 1 for each user j at each transmit instant t. It indicates whether a non-leader transmits a NACK or not at this instant. In the following, the focus is on the capture effect and thus all participating stations transmit during the feedback aggregation phase. From this it can be deduced that an increased threshold z will result in a decreased capture probability, whereas a decreased threshold z will result in a decreased jamming probability.

7.4.3 Power Capture Probability

In the following it is assumed that an OFDM frame is transmitted by wireless station l, herein the source of the *desired signal*, in the presence of n interfering frames from n other wireless stations, at the same time. Probability of capture for $m = n + 1$ concurrent transmissions in fading channels was first described by Zorzi et al. [125, 126, 127]. Considering capture exclusively, the condition that the desired signal captures the receiver is

$$C_\mathrm{l}(z) \quad = \quad \sum_{\mathrm{j}=1}^{n} p_\mathrm{j} < \frac{p_\mathrm{l}}{z}$$

With the desired signal distributed as $f_\mathrm{p_l}(p_\mathrm{l})$, the probability of capture is

$$c_\mathrm{n}(z) = \int_{0}^{\infty} f_\mathrm{p_l}(p_\mathrm{l}) \cdot \mathrm{Prob}\left[C_\mathrm{l}(z)\right] dp_\mathrm{l}$$

The sum of random variables determining the interferer powers results in the compound probability density function (pdf)

$$f_{P_n}(p_n) = \text{Prob}\left[\sum_{j=1}^{n} p_j\right]$$

which is the n-fold convolution of the respective homogeneous fading pdfs assumed for each interferer, $f_{P_j}(p_j)$. Thus the integral limits (part A) of $c_n(z)$ become

$$c_n(z) = \int_0^\infty f_{P_l}(p_l) \underbrace{\int_0^{p_l/z} f_{P_n}(p_n) dp_n}_{A} \, dp_l \tag{7.4.1}$$

With the homogeneity assumption $f_{P_j}(p_j) = f_{P_l}(p_l)$, capture solely depends on the capture threshold z and the number of interferers n. While in the following some arbitrary capture threshold z is assumed, a practical example is given in section 7.5.1.

Rayleigh fading

Assuming independent and identically distributed (i.i.d.) Rayleigh fading for the n interferers, the compound pdf assuming equal mean power p_0 for all non-leaders such that these powers add up (incoherent addition) and thus $\bar{p}_n = n \cdot p_0$ is the mean of the interference power, is given as the Gamma distribution [123]

$$f_{P_n}(p_n) = \frac{1}{\bar{p}_n \cdot (n-1)!} \left(\frac{p_n}{\bar{p}_n}\right)^{n-1} exp\left(-\frac{p_n}{\bar{p}_n}\right)$$

for the inner part A of eq. 7.4.1 there is no known closed form solution. It can however be shown by change of variables [123] that $c_n(z)$ for equal mean i.i.d. Rayleigh fading simplifies to

$$c_n(z) = \left(\frac{1}{z+1}\right)^n$$

Rician fading

It can be shown, assuming equal $\bar{p}_n$ and equal Rician K for all receivers, that with i.i.d. Rician fading, the capture probability is, according to Sanchez-Garcia et al. [128],

$$c_n(z, K) = 1 - e^{-K(n+1)} \sum_{i=0}^{\infty} \frac{(nK)^i}{i!}$$
$$\cdot \sum_{k=0}^{n-1+i} \left(\frac{1}{z+1}\right)^k \sum_{j=0}^{\infty} \frac{K^j(j+k)!}{(j!)^2 \, k!} \left(\frac{z}{z+1}\right)^{j+1}$$

which simplifies with $K = 0$ (Rayleigh) by setting $0^0 = 1$ and $0! = 1$ to

$$c_n(z, 0) = 1 - z \sum_{k=1}^{n} \left(\frac{1}{z+1}\right)^k = \left(\frac{1}{z+1}\right)^n$$

For a set of different values of K and z, Rician power capture probabilities are plotted in figure 7.3.
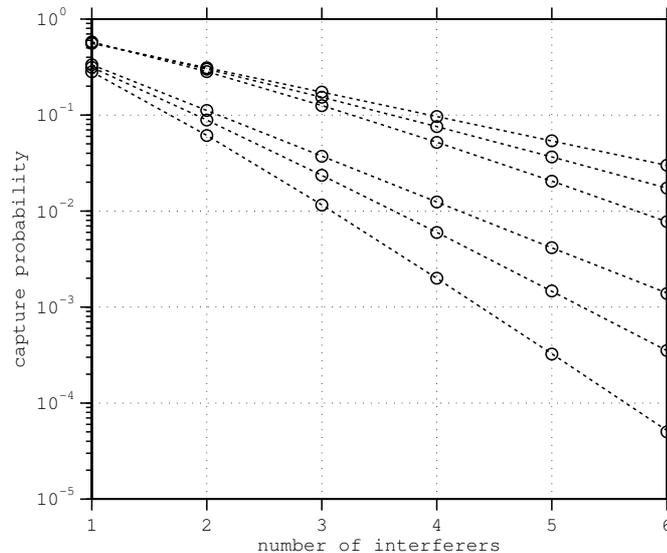
Figure 7.3: Rician power capture probabilities. Rician $K \in \{-1, 0, 3\}$ dB, capture threshold $z = -1$ dB (top bundle) and $z = 3$ dB (bottom bundle).

7.5 802.11 OFDM Feedback Capture

When dealing with ACK frame capture, or conversely, the probability of ACK jamming when one or more interfering negative acknowledgements are transmitted at the same time, realistic measurement data is of interest. What is more, obtaining measurement data from devices that are used in practice, i.e. consumer hardware, is both interesting and challenging. Typical TDMA wireless devices are specifically designed to avoid transmission at the same time. It is thus not straightforward to obtain such results.

In the course of this work, OFDM based ACK/NACK jamming in an Atheros[4] based testbed [129] has been evaluated by determining erasure rates of frames being transmitted at the same time. This kind of synchronous transmission has been possible even without full access to the medium access control (MAC) layer logic of the wireless interface[5]. According to 802.11 (cf. section 7.2.1), upon reception of a unicast frame a station shall reply a unicast ACK after a SIFS. Multiple stations may be forced to reply with this mandatory unicast ACK for the same preceding unicast data frame. In the testbed this was done by re-configuring each wireless network interface card to have the same MAC address (MAC address deceit). When unicast frames are transmitted to this address, each station will issue feedback by immediate ACK, unless a station failed to receive the data frame. Given all stations do receive each transmitted unicast frame without error, feedback is transmitted simultaneously. However, as there is only the sender and receiver MAC addresses conveyed in an 802.11 unicast acknowledgement and all receiving stations are configured to have the same MAC address, this feedback is perfectly identical, even after scrambling (cf. section 5.2.2). Rather than interfering with each other, transmitted signals would be conceived as echoes, increasing the receiver signal-to-noise ratio (SNR) [130] (cf. sections 3.2.2.2 and 4.2.3).

In order to evaluate feedback jamming probabilities by transmitting non-identical frames synchronously, the following property of 802.11 [7] can be exploited: A station may reply a unicast ACK at a physical layer MCS lower than or equal to the MCS at which the respective preceding

---

[4]Atheros, manufacturer of 802.11 network interfaces (http://www.atheros.com)

[5]MAC functionality is typically implemented an run on the wireless interface processor and thus externally inaccessible.
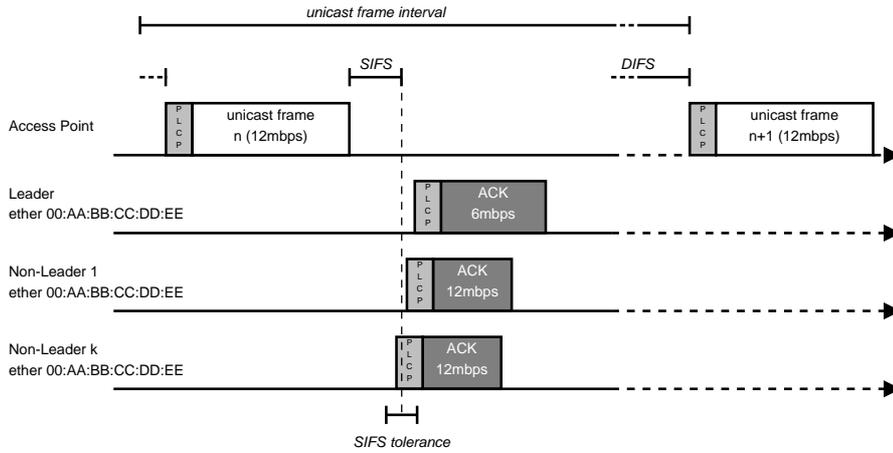
Figure 7.4: Timing diagram of feedback jamming measurements
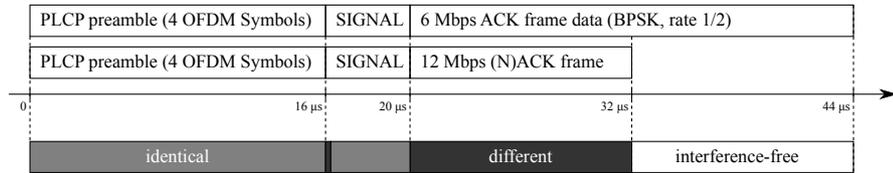
Figure 7.5: Difference in duration of simultaneously transmitted frames during ACK/NACK jamming tests. Note: SIGNAL differs in the leftmost bit.

unicast data frame has been received. Some consumer wireless LAN cards can be configured by enabling or disabling this feature. If this is disabled, the ACK is always transmitted at the lowest MCS instead.

For measurement data as provided herein and consequently in the following simulations, positive OFDM ACKs are transmitted at 6 Mbps while OFDM NACKs are transmitted at 12 Mbps. Latter is due to the preceding data frames also being transmitted at 12 Mbps, according to the above rule. This choice was made to ensure the highest probability of positive ACKs to be correctly received when no simultaneous NACK is present, minimizing the false negative rate. By configuring each non-leader to reply feedback at the higher of the two MCSs, while the leader's feedback is transmitted at the respective other, different frames are transmitted at the same time. Medium access is subject to the aforementioned timing inaccuracy. The SIFS is an idle time before MAC layer acknowledgement, for which IEEE mandates accuracy of ± 900 ns or less [7] for OFDM based transmission. Consequently, feedback jamming is evaluated as depicted in figure 7.4.

Note that although the information conveyed in both frames is identical, their signal shape is different due to binary phase shift keying (BPSK) on all OFDM subcarriers of the 6 Mbps frame, while the 12 Mbps OFDM frame has quarternary phase shift keying (QPSK) on all subcarriers. The difference in data rate results in a difference in duration of both types of feedback, due to the fact that the number of used OFDM symbols is greater than one in both cases. The differences of both frames are depicted in figure 7.5. Furthermore, the initial OFDM symbol after the fixed synchronization preamble (SIGNAL) is always transmitted at BPSK and not scrambled (cf. section 5.2.2). The SIGNAL symbol starts with the rate field, which is either $1101|_b$ for 6 Mbps or $0101|_b$ for 12 Mbps [7]. Thus, only the first bit of the first OFDM symbol and all the bits of the payload OFDM symbols differ.
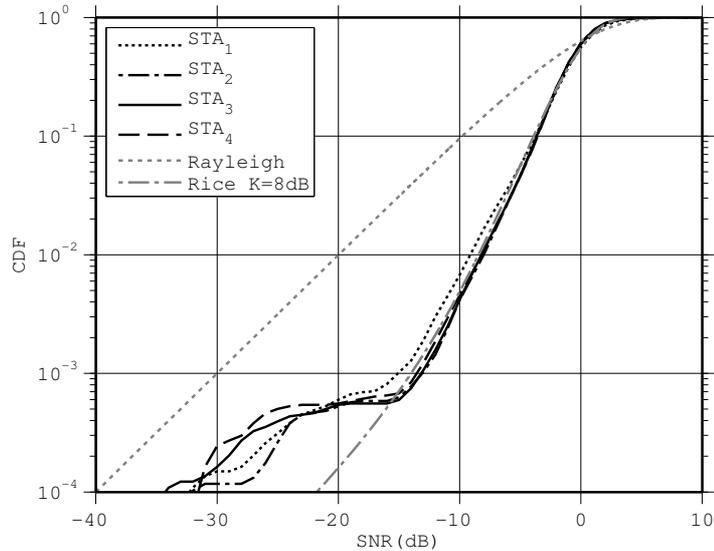
Figure 7.6: SNR distribution as measured at the wireless stations. Rayleigh and Rician ($K = 8\,\text{dB}$) cdfs are given for comparison.

7.5.1   Capture Results by Measurement

As described above, NACK versus ACK jamming probability results can be obtained by measurements using consumer hardware. A homogeneous fading environment was established among the participating wireless stations during the measurements described in the following. This is achieved by, on average, identical SNR at all receivers [129] during a measurement run. The obtained measurement results consequently are reproducible and can be verified by simulation, as elaborated in section 7.5.2 below. Fading distributions are measured at the receiving stations using built-in wireless interface provided mechanisms (subject to calibration, cf. section 5.5.1). They show a strong resemblance to a Rician power cumulative distribution function (cdf) with Rician K factor of 8 dB when the slow fading component in our measurement data is removed[6], as depicted in figure 7.6.

Due to the provisions made as described above, simultaneous channel access is assumed when stations are transmitting ACK and NACK OFDM frames. Apart from not differing completely nor being equal in duration (due to different MCS parameters), note that furthermore the NACK frame is not especially designed to achieve a high jamming probability. Figure 7.5 shows that during more than 50 % of the ACK signal there is an overlap with the NACK signal. Due to multiple NACKs being transmitted at the same time, they form a joint interference which can be assumed as a random signal with increasing number of interferers. Preambles are identical and apart from the first bit, the SIGNAL field is identical as it remains unscrambled. At the end of the ACK, for a duration of $12\,\mu s$ (three 802.11a OFDM symbols) there is no interference. Thus exactly half of the BPSK data symbols contained in the ACK are assumed to experience distortion in the presence of interfering NACK(s).

In a similar setup with two simultaneous and equally similar transmitted signal forms, Lee et al. [131] have shown the SIR required to decode a frame that arrived significantly earlier to be 1dB, while whenever it arrived later (after preamble decoding of the respective other frame had already passed), it is around 11dB. All of their frames and interfering frames were 1000 Bytes at 6 Mbps (BPSK, rate 1/2) OFDM. This is an implementation specific result, yet it is a practical result quantifying the capture effect of this specific consumer 802.11 hardware. In the scope of

---

[6]By FIR high-pass filtering after linear interpolation

Table 7.1: Capture threshold measurement setup and results

Parameter	Value
802.11 wireless channel	40
	(5.2 GHz)
AP transmit power setting	17 dBm
Station transmit power setting	8 dBm
Number of stations/non-Leaders	4/3
Frame rate	10 Hz
Frames transmitted	26,000
6 Mbps ACK received	10.61 %
12 Mbps (N)ACK received	14.59 %

this work, the probability of a single OFDM ACK becoming undecodeable at the feedback source in the presence of interference caused by multiple NACKs is evaluated.

7.5.1.1 Empirical Capture Threshold

When frames are transmitted sequentially and in absence of interference, it may be possible to deduce a channel quality indication at the receiver for each frame (e.g. as described in section 5.5.1). On the other hand, for transmission at the same time, this is not possible due to the unknown interference power level. However, on average a rate of successful reception of one or the other can be observed empirically when performing a sufficiently large number of trials within some measurement scenario. Results and parameters of a measurement run using 802.11a consumer devices are given in table 7.1, along with ACK and NACK success rates.

As stated above, preambles of transmitted feedback frames are identical in any case when using frame compatible WLAN. The channel quality may be estimated during the preamble as elaborated above. With identical preambles and simultaneous transmission, however, any interferer may contribute to a preamble determined SNR estimate. It is therefore impossible to determine individual ACK and NACK channel quality measurements during feedback jamming. At the multicast receivers, however, it is possible to record the channel quality in terms of SNR at data frame reception, which in turn triggers and thus immediately precedes the synchronous ACK transmission at the receivers (cf. figure 7.4). Consequently, at the source of the unicast data frames, ACK/NACK jamming rates are obtained, while at the receivers, SNR statistics are acquired. Under the assumption of reciprocal channel conditions maintained within the time of data frame and succeeding ACK transmission, SNR statistics at feedback stations translate to ACK and NACK power levels during jamming. By combination of both sets of measurement data, the capture threshold in this specific setup (specific with respect to herein described ACK/NACK frame structure, but independent of the environment) is determined as follows.

From the interference (NACK) power random variable (RV) Y_i^2 and ACK power random variable X^2 the random variable $Z = X^2 / \sum_{i=1}^{n-1} Y_i^2$ is of interest. Neither Y_i^2 nor X^2, and thus, nor Z, are known. However, signal-to-interference-plus-noise ratio (SINR) measurements are obtained at the receivers. A slow fading component is part of these measurements, which is maintained in the following in order to reproduce the actual SINR as would have been measured at the source during feedback capture, if it were possible. The MathWorks® Matrix Laboratory (MATLAB®) is used to replay the realizations of each of the random variables as recorded during data frame reception at the stations issuing feedback in direct consecution. Reciprocity of the channel within this time frame is assumed. While the exact pdfs of above said RVs are unknown, different permutations of the obtained realizations are generated, while it is observed that the outcome is not significantly different.

The realizations of the RVs X and Y_i represent a combination of fading effects and are thus only valid for this measurement. Additionally, ACK and NACK loss rates have been determined during above measurements, while signal-to-interference ratios for each channel access are de-
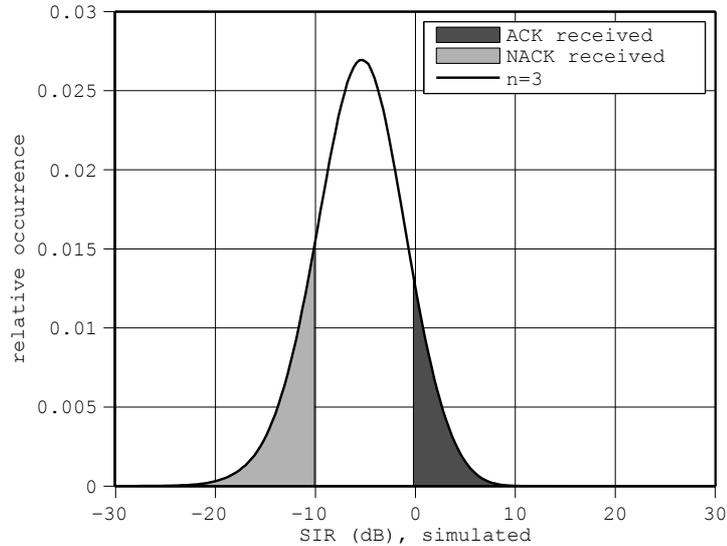
Figure 7.7: Simulated ACK signal-to-interference ratio during measurement (3 non-leaders). The SIR range of successful ACK (NACK) reception (as measured) are shaded in light (dark) gray. ACK (NACK) area is 10.8 % (14.9 %) of the total area under the curve.

termined by simulation. Considering the results in [131] and the herein given partial overlap in time of ACK and NACK the capture threshold is anticipated below 0 dB SIR, while neglecting the influence of other sources of noise. By use of completely identical hardware at the wireless stations it is assumed that all feedback arrives at the source at the same time. Specifically, 802.11a OFDM frames with a guard interval of 800 ns and a mandated maximum SIFS tolerance of ±900 ns [7] are transmitted.

7.5.1.2 Comparison of Results

By combination of the results as described above, the capture threshold may be deduced as follows. In attempting to obtain identical relative occurrence of ACK and NACK frames in the simulation as counted in above measurement, the ACK capture threshold is set to some value. Herein, figures match when it is set to $z = -0.3$ dB in the simulation. In the given setup the simultaneous presence of three simultaneous NACKs is ensured. The corresponding area under the simulated signal-to-interference ratio (SIR) pdf for $n = 3$ non-leaders (as in the performed measurement) is depicted in figure 7.7 as a shaded dark gray area (visible from -0.3 dB < SIR<10 dB). This is what could not be determined during synchronous ACK and NACK transmission as elaborated above. The pdf area of NACK reception is shaded light gray for SIR < $-10.3\,dB$. It can be observed that within an approximately 10 dB wide SIR range the collision of ACK and NACK results in destruction, i.e. neither ACK nor a NACK have been correctly decoded at the source. For the above chosen values, ACK and NACK reception rates very close to what had been measured on average (cf. table 7.1) are obtained.

7.5.1.3 Extrapolation

Figure 7.7 indicates that the simulation is valid and yields results for the jamming probability very close to the actual measurements with three non-leaders constantly transmitting NACKs. The simulation environment enables extrapolation to increased receiver group sizes, with some limitation. It can be observed how the feedback jamming rate is increased with increasing number of receivers. For example, roughly 97% successful jamming rate is obtained for five non-leaders.
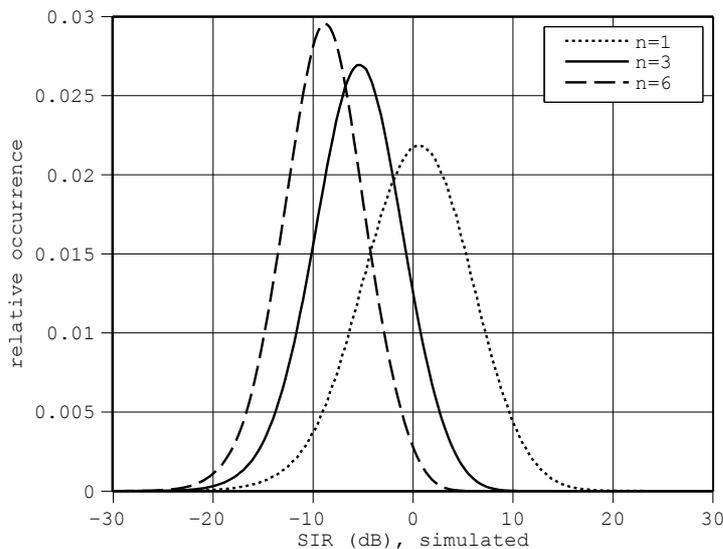
Figure 7.8: Simulated ACK signal-to-interference ratio for 1,3 and 6 non-leaders.

Increasing the number of non-leaders significantly is infeasible in this regard, as the RVs Y_i^2 and X^2 remain unknown and only the known realizations can be used for extrapolation. Respective curves of the relative occurrences of SINR for 1, 3 or 6 non-leaders are depicted in figure 7.8. Similarly as shown in figure 7.7 on the preceding page, respective probabilities of successful ACK/NACK reception could be deduced, albeit at increased error with increasing number of non-leaders.

7.5.1.4   Feedback Power Control

By power control of the ACK frame at the leader the probability of successful feedback jamming can be increased. For this, in the above given simulation the ACK transmit power at the leader is reduced by e.g. 3, 6 or 8 dB. The results are depicted in figure 7.9. Note that the capture threshold again is set to $z = -0.3$ dB, as it is universally valid for the used hardware and assumed independent of any other effects.

Due to homogeneity, the leader may be arbitrarily chosen. The results show that the jamming failure probability (i.e. the capture probability of the ACK frame) can be tuned at some granularity (depending on the power control capabilities at the leader) within predictable limits.

7.5.2   Capture Results by Simulation

As an example for frame capture, 802.11a/g acknowledgement frame capture in the presence of one or many interfering frames has been evaluated by measurement and power capture simulation above. One of the results has been the capture threshold of approximately $z = -0.3$ dB. In the following this result is reproduced by explicit synchronous transmission of the respective WLAN signals as described above in an OFDM baseband simulation environment. Relevant parts of the joint 802.11a/g physical layer (PHY) have been implemented in MATLAB®. Figure 7.10 depicts the implementation details.

A variable start time of the interfering signals is simulated. The delay of the interfering frames with respect to the point in time of the start of the desired signal (ACK) is simulated normally distributed within the 802.11 SIFS tolerance of ± 900 ns (cf. section 7.5). Without loss of generality, the ACK frame is assumed to arrive at the receiver exactly one SIFS after the
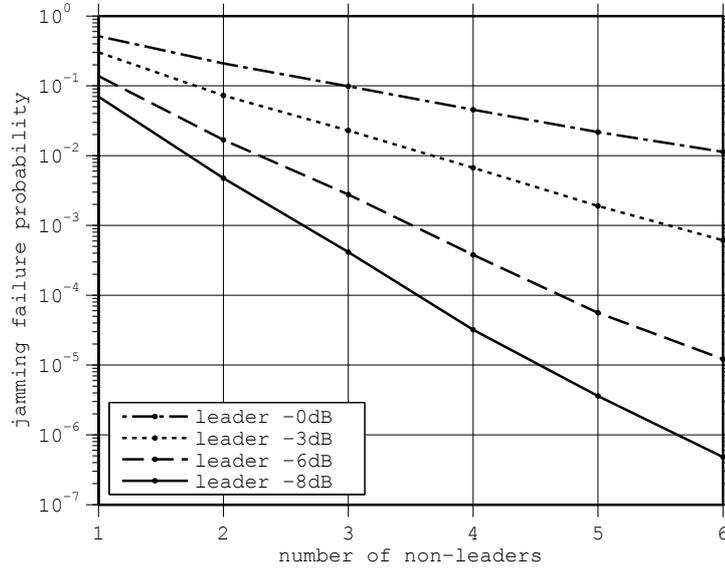
Figure 7.9: Simulated feedback jamming probability in a measurement that includes slow fading and with feedback power reduction at the leader.
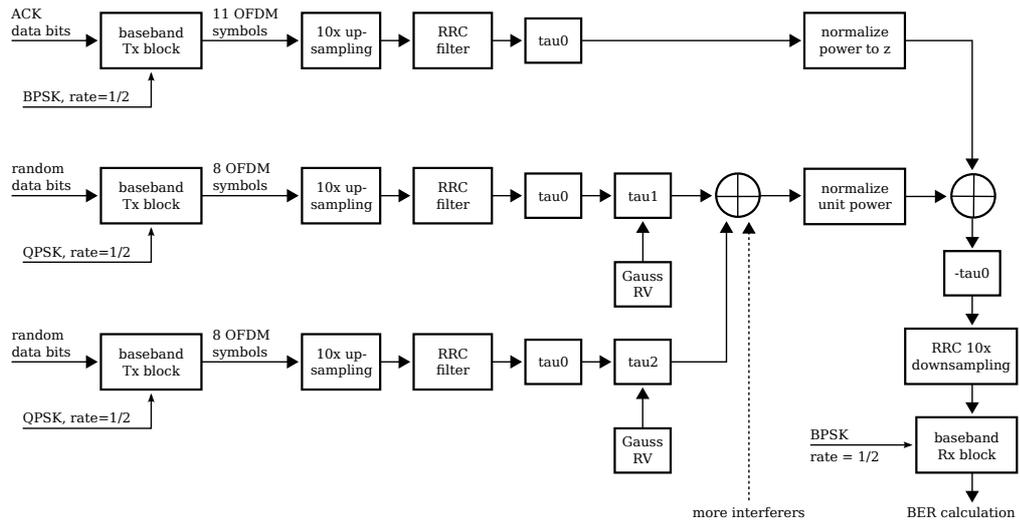
Figure 7.10: 802.11a/g OFDM ACK capture simulation block diagram

preceding data frame[7]. In order to achieve a fine granular resolution in delay time, all signals are upsampled by a factor of 10 by linear phase finite impulse response[8] frequency domain root-raised-cosine (RRC) filtering. The filter roll-off is parametrized such that none of the used carriers are attenuated (cf. section 5.2.4). After oversampling and application of a randomized delay, NACK frames are added in the complex baseband and their joint power is normalized to unit power. As above, the NACK frames are of MCS 12 Mbps. The ACK signal power is normalized to the desired SIR z and added to the sum interference. Figure 7.11 depicts the influence of 1, 3 and 10 interfering signals on the scatter plot per subcarrier of the ACK signal when the desired signal and the interference are of equal strength, i.e. the SIR is 0 dB. It is important to note that during suchlike OFDM feedback jamming, a Gaussian noise source may be assumed in the case of multiple interfering signals. For low numbers, such as 1 or 3 interferers as in the example of figure 7.11, however, it can be observed that the noise introduced by interfering transmissions may be non-Gaussian.

At the receiver the exact start time of the ACK is assumed known, excluding effects of an otherwise potentially imperfect synchronization. Soft decision as well as hard decision Viterbi decoding is executed and the resulting bit error rate is used to compute the corresponding ACK decoding success rate (by assumed checksum match) over 10,000 trials. Figure 7.12 on page 103 shows the results for ACK frame decoding failure with three interfering signals. Viterbi decoding is done using a trellis traceback length of 48 and 4-bit quantization for soft decision decoding. These values are chosen as an example that comes close to the above obtained results. It is observed that in the setup evaluated herein, the power capture threshold z may be as low as roughly -1 dB, at which the decoding failure probability steeply increases to 1 for soft decision decoding.

---

[7]Data frame transmission is not simulated as the focus is on the event of feedback collision
[8]FIR is chosen to preserve OFDM phase information
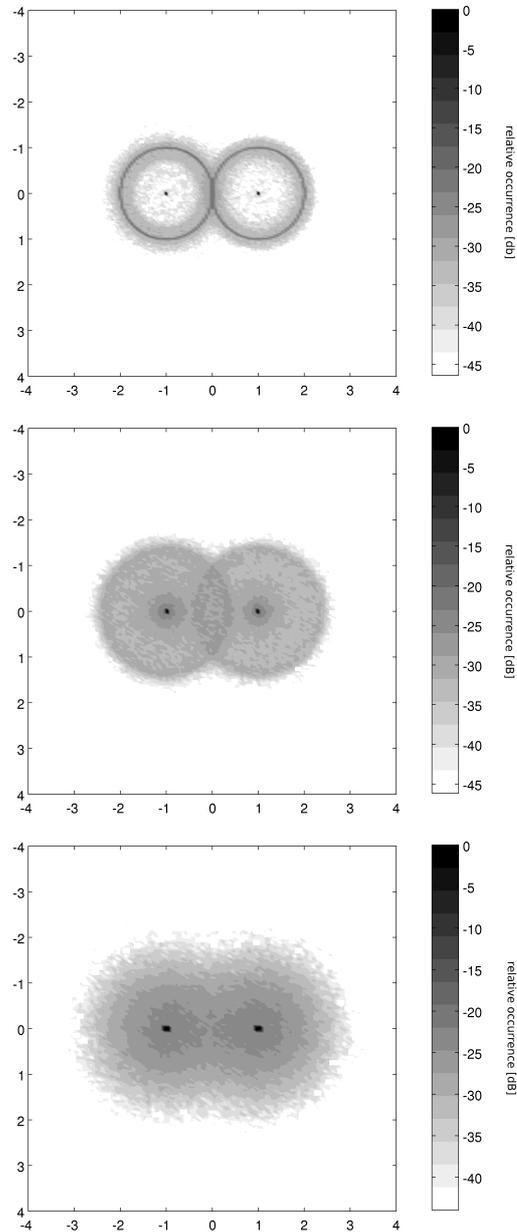
Figure 7.11: Scatter plot of QAM symbols on subcarriers of an 802.11 OFDM ACK (BPSK), averaged over all carriers, in the presence of interfering 802.11 OFDM signals with QPSK on all carriers. The interfering signals are active 50% of the ACK duration and the SIR is 0 dB.
top: single interferer, *center:* two interferers, *bottom:* ten interferers
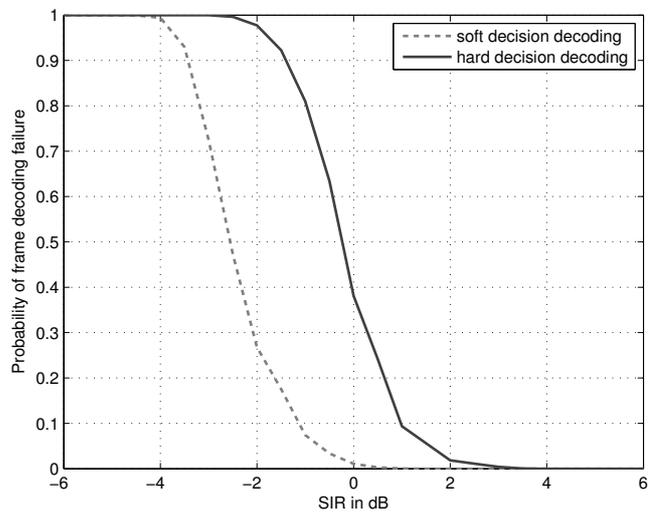
Figure 7.12: Probability of unsuccessful 802.11 OFDM ACK (6 Mbps) reception (checksum mismatch) in the presence of 3 independently delayed interfering signals (12 Mbps each) with Viterbi decoder traceback length of 48 states. Soft decision decoding is done at 4-bit quantization (16 levels). At positive SIR values, the ACK signal power exceeds the compound interference power level.

Error Correction with Feedback Aggregation

Feedback aggregation in a leader based protocol (LBP) for multicast error correction is subject to a false positive rate in practice, as elaborated above (cf. section 7.4.1). Full reliability can thus not be guaranteed. However, audio-visual multicast is typically regarded as error tolerant. While noticeable artefacts that occur seldomly may even remain unnoticed, error concealment techniques in audio-visual coding may hide transmission errors from the user. So-called partial (or imperfect) reliability is thus reasonable in the scope of this work, but it implies a residual error rate after error control coding. In this chapter, a residual error of retransmission based error correction for multicast audio-visual streaming with feedback aggregation by feedback jamming is evaluated in isolation from other effects. Particularily, an independent and constant data packet loss probability is assumed for each receiver, whereas for feedback transmission, independent and identically distributed (i.i.d.) fading is assumed. The evaluation is preceeded by a description of the feedback jamming retransmission protocol.

8.1 Feedback Jamming LBP

A frame exchange sequence of a feedback aggregation LBP is depicted in figure 8.1. Data frame n is transmitted in multicast to a number of wireless stations, some of which consequently transit to a state of having correctly received (cf. fig. 8.1 "rcvd") this data frame, others to a state of error (cf. fig 8.1 "lost"). As transmission is protected by frame individual forward error coding (FEC) and each frame is checksum validated as elaborated above, it is assumed that no other state is possible. In order to ensure state transition integrity at the receivers, a feedback request frame (REQ) is introduced. As opposed to unicast transmission, a dedicated and robust feedback request frame may reduce complexity with respect to medium access in multicast, cf. groupcast with retries (GCR) in IEEE 802.11aa [117]. In leader based protocols with feedback aggregation, the dedicated feedback request synchronizes the feedback aggregation phase. One protocol dependent inter-frame space (IFS) after the successive feedback request frame for data frame n:

- the leader shall reply an ACK *iff* data frame n is received correctly (possibly in a previous retransmission round)

Furthermore, for the rest of the multicast group:

- each non-leader shall reply a negated ACK (NACK) frame *iff* data frame n has not been received correctly (including previous retransmission rounds)

If at least one non-leader experiences data frame loss, a collision occurs whenever the leader does not experience loss. With a certain probability the leader's positive feedback is canceled (jammed by one or more NACKs), resulting in a timeout or reception of NACK. In both cases, the sender repeats the whole procedure until the retry limit is reached or an ACK is received, upon which it advances to the next data frame, if available. In order to distinguish new from
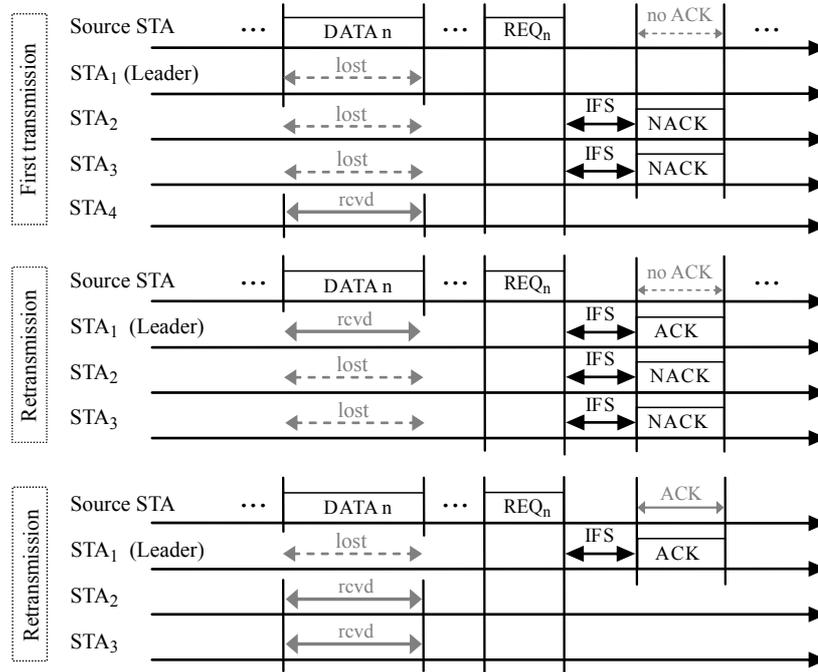
Figure 8.1: Aggregated feedback jamming scheme with a feedback request frame and one multicast leader, terminating retransmissions with an ACK.

repeated data frames, sequence numbering is required. The sequence number may be provided with the REQ frame, hence it is referred to as a SEQ frame[1].

8.2 Single Frame Residual Error

Above described LBP and its ACK/NACK jamming scheme may be assumed to work most reliably in case of correlated loss among the receivers. Correlated loss is not a pathological phenomenon as it may occur due to medium access collisions in time-division multiple access (TDMA) systems, which are e.g. inherent of the carrier sense multiple access with collision avoidance (CSMA/CA) protocol employed in 802.11. Concurrent transmission which is interfering with a multicast data frame transmission may result in failure of reception thereof for a large subset of the multicast group. In case of correlated loss, many, if not all of the non-leader receiver (nL) receivers will issue a NACK and the probability of jamming is largely increased. It is thus more interesting to evaluate the protocol performance in a more adverse situation with respect to feedback jamming. When multicast data frame erasure at the receivers is uncorrelated, participation of nLs in the event of feedback jamming is uncorrelated as well. In a real scenario, the situation may be highly complex with overlapping networks, hidden nodes, data frame capture etc., increasing with the size of the network in terms of potential receivers. With the focus on increasingly large multicast groups, the assumption of uncorrelated errors becomes increasingly realistic.

In the following it is assumed that a loss at the leader is always corrected[2] by retransmission, subject to a certain retransmission limit. Hence, a residual error at non-leader receivers due to feedback jamming failure is examined. Without loss of generality, this is done for an arbitrary

---

[1]Introduction of a feedback request frame is but one of many possibilities of signaling.

[2]Absence of an ACK from the leader results in a timeout or NACK reception. Both trigger a retransmission subject to a retransmission limit.

non-leader receiver. For this receiver the packet error probability (PEP) after the initial transmission of a data packet subject to a *packet erasure channel* is denoted by ρ. Consequently, after one (initial) round the residual error is $p_{\mathrm{r}} = \rho$.

In the analysis of feedback jamming LBP performance with respect to error correction by retransmission, independent data frame loss at constant and equal error probability is assumed for all receivers. Slow i.i.d. fading is assumed during feedback aggregation in order to evaluate the impact of the capture effect on error correction performance during feedback jamming. Herein, capture of the feedback destination (i.e. the multicast source) by a positive acknowledgement in the presence of negative feedback is a false positive. This event is further termed as *jamming failure*. The only degree of freedom of jamming failure is the capture threshold z (cf. section 7.4.2). Feedback power reduction at the leader is modeled by respective increase of the capture threshold.

8.2.1 Single Retransmission

In the following the *residual error due to jamming failure* probability for the i.i.d. packet erasure channel after one retransmission is deduced. For this, the joint loss at the nL receivers for i.i.d. packet error probability and consequently, the jamming failure probability, are derived.

Initial packet transmission

Herein, K is a binomially distributed random variable, $\rho \in [0, 1]$ is the PEP, $n > 0$ is the number of non-leader receivers (nLs), $k > 0$ is the number of nLs jointly loosing a packet and $\mathrm{E}\,[K]$ is the expected number of nL stations experiencing a loss jointly. In the event of feedback jamming, $p_{\mathrm{cap}}(k)$ is the jamming failure (i.e. ACK capture) probability when k nLs interfere in order to cancel the leader's acknowledgement.

$$
\begin{aligned}
K &\sim\ Binomial(n, \rho),\ n > 0 \\
p_{\mathrm{joint}}(n, k) &=\ Prob(K = k) = \binom{n}{k} \rho^k \,(1 - \rho)^{\,n-k},\ k > 0 \\
\mathrm{E}\,[K] &=\ n \cdot \rho \\
p_{\mathrm{cap}}(k) \in [0, 1] &:\quad \text{jamming failure probability for } k \text{ active jammers} \\
\rho_{\mathrm{L}} = \rho &:\quad \text{packet error probability at the leader} \tag{8.2.1} \\
p_{\mathrm{cf}}(n) &=\ \sum_{\mathrm{j}=0}^{n-1} p_{\mathrm{joint}}(n - 1, j) \cdot p_{\mathrm{cap}}(j + 1) \tag{8.2.2}
\end{aligned}
$$

Above given $p_{\mathrm{cf}}(n)$ is the conditional probability of failure to request a retransmission, under two conditions. Firstly, a condition is that the leader is issuing an ACK, and secondly, the observed nL for which the PEP is deduced, is issuing a negated acknowledgement (NACK) due to packet loss. Then, $0 \leq j \leq n - 1$ other nLs may simultaneously issue a NACK due to packet loss in the initial transmission.

For practical reasons, jamming failure probabilities may not be available for $k \leq n$ non-leader receivers experiencing packet loss jointly. Let $m \leq n$ be the number of nLs for which jamming success probability measurements (or capture probability results) are available. Then, an approximation extending the results from m to n values by

$$
\begin{aligned}
\tilde{p}_{\mathrm{cf}}(n)\big|_{\mathrm{m<n}} &=\ \sum_{\mathrm{j}=0}^{m-1} p_{\mathrm{joint}}(n - 1, j) \cdot p_{\mathrm{cap}}(j + 1) \\
&\quad + \sum_{\mathrm{i}=\mathrm{m}}^{n-1} p_{\mathrm{joint}}(n - 1, i) \cdot p_{\mathrm{cap}}(m) \tag{8.2.3}
\end{aligned}
$$

is feasible. Note that in case of i.i.d. packet loss, the approximation may be rarely used for low error rates as the jamming probability depends on the binomial event probability that m nLs jointly miss a data frame which the leader already received. Specifically, Under the assumption that, with increasing j the jamming failure probability for k active jammers, $p_{\mathrm{cap}}(j)$, decreases, it holds

$$\tilde{p}_{\mathrm{cf}}(n) > p_{\mathrm{cf}}(n) \tag{8.2.4}$$

Hence, the conditional probability of failure to request a retransmission is conservatively estimated.

Residual error

The residual error at any arbitrary non-leader out of the set of n non-leaders after the initial transmission and one potential consecutive retransmission round is denoted by $p_{\mathrm{r}}(n, 1)$. A retransmission is executed only in case the leader receiver experiences packet loss in the initial transmission or, whenever the leader receives the initial transmission correctly, in case feedback jamming is successful. Consequently, the residual error at any non-leader is

$$p_{\mathrm{r}}(n, 1) \quad = \quad \rho^2 \rho_{\mathrm{L}} + \rho\,\bar{\rho}_{\mathrm{L}}\,p_{\mathrm{cf}}(n) + \rho^2 \bar{\rho}_{\mathrm{L}}\,(1 - p_{\mathrm{cf}}(n)) \tag{8.2.5}$$

in which the subscript versions of $\rho_{\mathrm{L}} = \rho$ and $\bar{\rho}_{\mathrm{L}} = (1 - \rho)$ denote the respective probabilities at the leader in order to improve readability. Note the first term in eq. 8.2.5 is the case of loss in both rounds with loss at the leader in the initial round. The second term quantifies a premature end of the protocol after the initial transmission due to feedback jamming failure. Finally, the third term in eq. 8.2.5 quantifies the case of loss in both rounds albeit succesful jamming. In case of reliable jamming (i.e. reliable feedback), the residual error after transmitting each data packet exactly twice is

$$p_{\mathrm{r}}(n, 1) = \rho^2\big|_{\mathrm{p_{cf}(n)}=0\ \forall \mathrm{n}} \ .$$

Figure 8.2 depicts a flow graph for eq. 8.2.5 in two variants, forward and reverse, from which the residual error can be deduced graphically. In the reverse state graph, failure of reception at the observed nL station is used as starting states.

8.2.2 Multiple Retransmission Rounds

With introducing more rounds $r > 0$, whereas $r = 0$ is the initial round, K_{r} is a random variable in round r

$$
\begin{aligned}
K_{\mathrm{r}} \quad &\sim \quad Binomial\,(n, \rho^r) \\
E\,[K_{\mathrm{r}}] \quad &= \quad n \cdot \rho^r
\end{aligned}
$$

After each round the expected number of stations requiring a retransmission is decreased, and in the first retransmission round, $K_{\mathrm{r}} = K$. For the rth round one obtains due to the events of jamming success and frame loss being independent

$$p_{\mathrm{joint}}(n, k, r) \quad = \quad \binom{n}{k} (1 - \rho^r)^{n-k}\,\rho^{kr} \tag{8.2.6}$$

$$p_{\mathrm{cf}}(n, r) \quad = \quad \sum_{\mathrm{j}=0}^{n-1} p_{\mathrm{joint}}(n-1, j, r) \cdot p_{\mathrm{cap}}(j + 1) \tag{8.2.7}$$
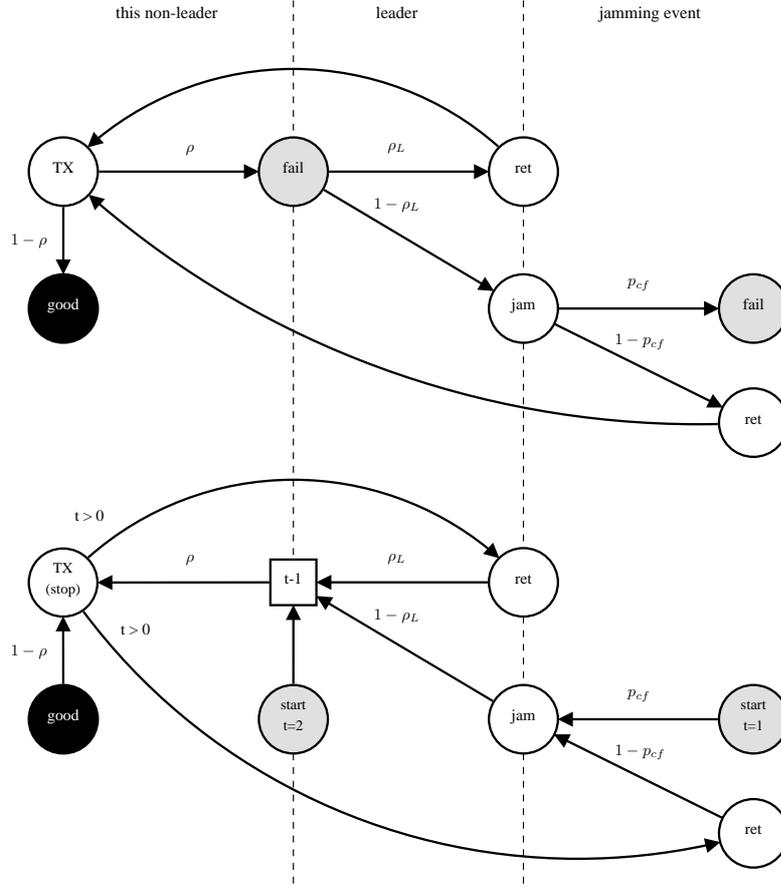
Figure 8.2: Residual error of LBP with retransmission. In states labeled *ret* a retransmission is triggered. *Top:* Starting in state *TX* and ending in *fail*; *Bottom:* Starting in states *start* and ending in *stop* when the counter t has reached zero.

Note that $p_{\text{joint}}(n-1, k, r)$ denotes the probability that, after r transmission rounds, k out of $n-1$ non-leaders participate in a jamming event. The residual error after the rth retransmission is composed of two recursive parts, one after which the next round is triggered

$$
\begin{aligned}
p_{\text{r,retx}}(n, r)\big|_{\text{r}=0} &= \rho \\
p_{\text{r,retx}}(n, r)\big|_{\text{r}>0} &= p_{\text{r,retx}}(n, r-1) \cdot [\rho_{\text{L}} \rho \\
&\quad + \bar{\rho}_{\text{L}} \, \rho \, (1 - p_{\text{cf}}(n, r-1))]
\end{aligned}
\tag{8.2.8}
$$

and one after which the next round is not triggered

$$
\begin{aligned}
p_{\text{r,stop}}(n, r)\big|_{\text{r}=0} &= 0 \\
p_{\text{r,stop}}(n, r)\big|_{\text{r}>0} &= p_{\text{r,stop}}(n, r-1) + p_{\text{retx}}(n, r-1) \, \bar{\rho}_{\text{L}} \, p_{\text{cf}}(n, r-1)
\end{aligned}
\tag{8.2.9}
$$

Thus the residual error $p_{\text{r}}(n, r)$ is

$$
\begin{aligned}
p_{\text{r}}(n, r)\big|_{\text{r}>0} &= p_{\text{r,stop}}(n, r-1) + p_{\text{r,retx}}(n, r-1) \cdot \\
&\quad [\rho_{\text{L}} \, \rho + \bar{\rho}_{\text{L}} \, p_{\text{cf}}(n, r-1) \\
&\quad + \bar{\rho}_{\text{L}} \, \rho \, (1 - p_{\text{cf}}(n, r-1))]
\end{aligned}
\tag{8.2.10}
$$

whereas $\tilde{p}_{\text{r}}(n, m, r)$ is the residual error after round r with $m < n$ joint capture probability values. In the special case of $p_{\text{cf}}(n, r) = 0$, the residual error is ρ^r.

Table 8.1: LBP with retransmissions – simulation parameters

Parameter	Value(s)
capture threshold	$z = 0\,\mathrm{dB}$
ACK attenuation	$0\,\mathrm{dB} - 20\,\mathrm{dB}$
fading (nLs)	i.i.d. Rayleigh
fading (leader)	i.i.d. Rayleigh, Rician $K = 8\,\mathrm{dB}$
receivers	$n \leq 51$
non-i.i.d. capture results	$m = 6$
packet error probability	$\rho = 0.1$
transmission rounds	$0 \leq r \leq 6$
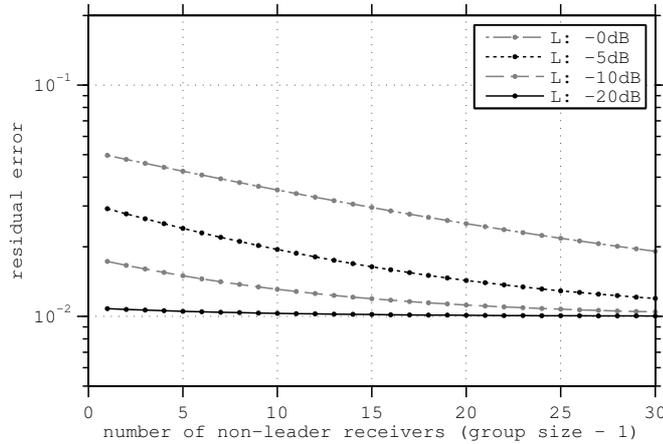
Figure 8.3: Residual error after one retransmission of the feedback jamming scheme with increasing group size and increasing ACK attenuation at the leader (L). Feedback jamming assumes i.i.d. Rayleigh fading.

8.2.3 Results

Figure 8.3 depicts the residual error after one retransmission (2nd transmission) $p_{\mathrm{r}}(n, 1)$ of the feedback aggregation and jamming scheme when the leader's ACKs are attenuated as given in table 8.1. In figure 8.4 the error floor is plotted and the maximum number of transmission rounds is set to a fixed value of seven, as defined in 802.11 [7]. With limited transmission rounds of a single data frame, a perfectly reliable feedback scheme directly depends on the PEP, yielding 10^{-7} with $\rho = 0.1$. It can be observed that both increasing the ACK attenuation as well as with increasing group size, the residual error is decreased. Note that due to imperfect jamming, spending more potential retransmission rounds does not improve the residual error. For example, in case of 3 receivers and an ACK attenuation at the leader of this group of $20\,\mathrm{dB}$, after 4 transmission attempts the error floor is reached at roughly 10^{-3}. However, due to the assumptions made, figures provided herein are worst-case results under especially adverse conditions.

The error floor of this LBP single frame retransmission scheme is determined by the non-zero feedback capture threshold (here: close to $0\,\mathrm{dB}$ as measured with consumer hardware [129] and as simulated above, cf. section 7.4). The protocol is thus useful for provision of multimedia broadcast multicast service (MBMS) when the audio visual coding scheme can tolerate a residual error. By ACK power control at the leader and additional selection of the multicast group representative (if possible), the residual error can be adjusted to some application defined requirement.

Figure 8.5 further shows the situation when the non-leader receivers are subject to i.i.d.
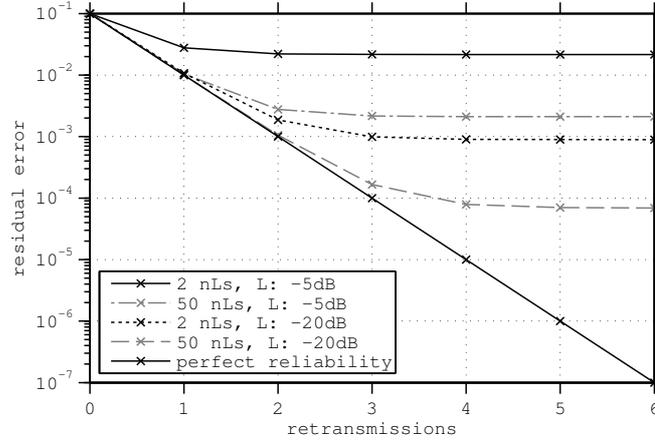
Figure 8.4: Error floor of the feedback jamming scheme with i.i.d. Rayleigh feedback fading at different group sizes and average ACK/NACK SIRs, as compared to perfectly reliable feedback.
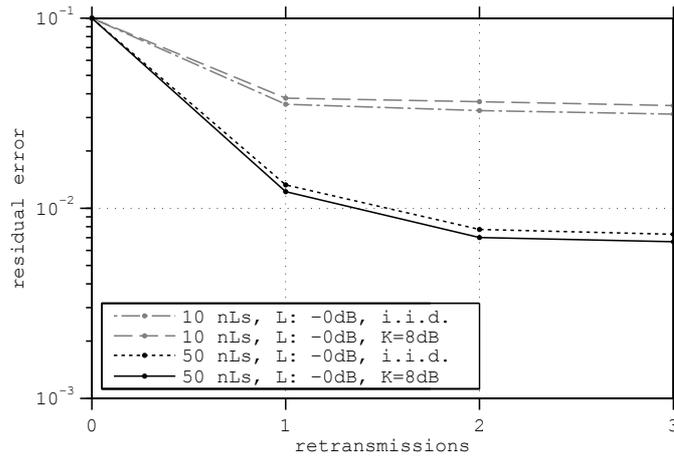
Figure 8.5: Comparison of the error floor due to feedback jamming under i.i.d. Rayleigh fading and for Rician fading ($\tilde{p}_\mathrm{r}(n,m,r)$, cf. table 8.1) at the leader, at different group sizes and in absence of leader (L) power reduction.

Rayleigh fading during feedback aggregation, whereas the leader is subject to Rician fading with $K = 8\,\mathrm{dB}$. Confer figure 7.6 in section 7.5.1 for the cumulative distribution functions (cdfs) of both of those fading random variables (RVs). The influence of a strong line-of-sight (LOS) component can be considered as low, albeit at identical average fading gain (herein normalized to 1) for all receivers. This is done in order to ensure a worst-case scenario in which a single on avereage "weakest" receiver can not be distinguished. From this it can also be concluded that an estimation of the strength of a LOS component in leader selection is ineffective. Since ACK power control at the leader is identical to selecting a leader according to a lower on average signal-to-noise ratio (SNR) (but subject to identical statistical fading properties), results provided herein also hold for leader selection in the given scenario.

8.3 Feedback and Frame Aggregation

Frame aggregation is a mechanism to reduce feedback overhead by aggregating feedback over multiple transmitted frames. It is referred to as block acknowledgement (BA) in 802.11 [7]. In a feedback jamming protocol, any information in the feedback is assumed to be canceled, hence it is not straightforward to extend this mechanism to frame aggregation. A hybrid LBP [132] (HLBP) proposal exists in the literature, in which the block of frames is subject to a frame level FEC, whereas k frames out of $k + m$ frames (k systematic, m parity frames) are sufficient to decode the whole block at the receiver. Then, each of the $k + m$ frames can replace any other potentially lost frame at one of the multicast receivers. As acknowledgment is requested for any k frames out of the previously sent multicast frames that comprise the current block, the LBP scheme is extended by frame aggregation. For an in-depth discussion on hybrid leader based protocols (HLBPs), the reader is referred to the work of Li [121]. Further results of a multicast HLBP with modulation and coding scheme (MCS) adaptation are presented in section 9.4. A prototype implementation using consumer hardware is presented in section 10.2.3.

The use of aforementioned algebraic maximum distance separable (MDS) codes in conjunction with virtual interleaving is advocated herein, as the receiver can perfectly determine decoding success from the number of received packets per hybrid FEC block. With knowledge of code rate and block boundaries when transmitting single IP packets within individual MAC layer frames as it is common in wireless LANs, feedback decisions can be made on the MAC layer. In general, feedback and frame aggregation are not strictly limited to former types of codes. Rateless codes such as the Raptor code is supported, albeit at increased complexity. A detailed feasibility analysis of overlay Raptor HLBP is beyond the scope of this work, as the focus herein is on medium access control (MAC) layer mechanisms.

Multicast Rate Adaptation

It has been elaborated above how multicast transmission can be achieved avoiding feedback implosion in general. While open loop implies no feedback (at least not in-band), closed loop multicast implies feedback from all receivers. The representative based multicast is a special case in which the feedback loop is closed only for the group representative. It has further been elaborated that these two kinds of (quasi) closed loop multicast behave differently with respect to reliability, which is due to different feedback properties. When the feedback loop is closed for any receiver in the multicast group, one may speak of receiver individual feedback polling. In time-division multiple access (TDMA) systems this further implies time sequential feedback from each receiver. In representative based multicast as elaborated herein on the other hand, feedback is aggregated in time.

9.1 Channel Knowledge at the Transmitter

The idea of having nearly perfect channel knowledge at the sender by means of high resolution channel quality feedback from each receiver may sound promising at first. In opportunistic multicast (cf. section 6.6.2), this channel state information (CSI) is assumed known at the transmitter at all times. For fading channels exhibiting a coherence time well above the time required to transmit several multicast data frames (i.e. quasi static channel conditions), it is evident that high resolution CSI could result in a high amount of redundant information at the transmitter. CSI at the transmitter is obtained by frequent CSI feedback, subject to quantization due to digital transmission thereof. At the most coarse level of quantization, binary feedback provides information about success or failure of some error control coding algorithm. By example of the momentary signal-to-noise ratio (SNR) as measured at the receiver, at some less coarse level of quantization, non-binary information can be conveyed.

With respect to unicast link adaptation, Camp and Knightly [80] conclude that loss-triggered rate adaptation mechanisms are typically overly conservative in selecting transmit bitrate as they require consecutive transmission success for switching to a higher data rate. Conversely, they find that SNR-based rate adaptation tends to overselect transmit bitrate when the coherence time is small. An SNR-based algorithm that is aware of the channel coherence time may perform satisfactory. For multicast however, the problem of gathering feedback from all receivers in case of SNR-based rate adaptation persists. In the following, multicast rate adaptation mechanisms as available in the literature are presented. Followed up by that is an alternative proposal that is loss-triggered as it is based on feedback aggregation, and it is reasoned why this approach may inherently exploit a multicast throughput gain, resulting in a scheme of low complexity, constant feedback overhead and high throughput.

9.2 Related Work

Explicit feedback by polling of multicast receivers via IEEE 802.11 collision avoidance mechanisms is done in rate adaptive multicast (RAM) as proposed by Basalamah et al., which has later

been extended by byte-level overlay FEC [99]. Request-to-send (RTS) and clear-to-send (CTS) medium access control (MAC) layer frames are used prior to multicast transmission, whereas SNR information is conveyed in CTS messages. Their proposal includes ACK/NACK jamming in which a dedicated feedback time slot is further sub divided by time offsets. The offset used for feedback by some receiver indicates a certain overlay FEC and modulation and coding scheme (MCS) rate request based on receiver determined SNR information.

In SNR-based auto rate for Multicast (SARM) as proposed by Park, Bonnin et al. [133], channel state feedback is obtained from all receivers via periodic channel measurement messages transmitted by an IEEE 802.11 access point (AP). Upon reception thereof, each multicast group member reports the SNR as measured during reception of this message back to the AP. Feedback is suppressed for a defined amount of time if the most recently measured SNR is greater than what was previously reported.

Periodic feedback about packet loss statistics is used in a proposal by Xi et al. [134]. Villalón, Turletti et al. [135] propose the use of SNR feedback from all receivers for MCS adaptation, while transmit success is signaled by a representative based protocol [116]. The CLARA [136] algorithm is used, which combines ARF and RBAR (cf. section 5.5.2.2).

All of the above mentioned proposals thus include some form of out of band CSI feedback with respect to the MAC layer multicast transmission. Another combination of LBP and ARF is proposed by Choi et al. [137], termed probing based ARF (PARF). In it, prior to switching to a higher MCS, a representative is informed about the new MCS and it may oppose to the change in bitrate if an anticipated error rate resulting from the switch exceeds an application defined limit.

In this work, a rate adaptive leader based protocol is proposed and evaluated, which includes rate probing transmissions when overlay forward error coding (FEC) is used to enable a simple cross layer hybrid leader based protocol (HLBP) for multimedia broadcast multicast services.

9.3   Rate Adaptation with Feedback Aggregation

In the following, rate adaptation performance of a single data frame multicast feedback protocol with aggregation by jamming (in the following for short: RA-LBP) is analyzed by example of OFDM based IEEE 802.11 WLAN. For reasons of separability of the observed effects, feedback is *solely* used for rate adaptation, and consequently, rate adaptation is based on binary transmit success information. A data frame is thus transmitted exactly once[1]. Identical instantaneous channel gain during the feedback aggregation phase and the immediately preceding data frame is further assumed for each receiver individually, i.e. independent and identically distributed (i.i.d.) channel conditions with full correlation of the channel for data and respective feedback. Any rate adaptation based on transmit success operates with past information. Therefore, correlated fading processes are generated for simulation of the protocol performance. Due to i.i.d. statistics, one of the receivers is randomly selected as the leader[2].

The rate adaptation scheme proposed herein is similar to the auto rate fallback (ARF) [82, 83] type of mechanisms, in which after a number of successful transmissions a (e.g. 3, 10), the next higher (less robust) rate is chosen, while after b unsuccessful transmissions, the next lower (more robust) rate is chosen. A value of $b = 2$ is considered as a reasonable choice as two consecutive medium access collisions under the 802.11 distributed coordination function (DCF) have been shown to be unlikely [138]. As opposed to the original ARF proposal, an additional timeout value triggering an MCS increase is omitted, as it is redundant for the assumed periodic channel access (due to streaming) under the assumption of solely fading induced errors. A sliding window of size a is used for keeping track of the number of successful transmissions. This implies that rates may be switched up multiple consecutive times in case of ongoing transmit success. Switching rates upwards and downwards may thus happen at nearly the same speed.

---

[1]Single transmission of data can be seen as a retry limit of 0 on the MAC layer

[2]For L receivers an average over L trials is computed, whereas a different leader is chosen in each trial

Table 9.1: LBP-ARF ($a = 10$, $b = 1$) rate adaptive multicast throughput under i.i.d. fading (10 users, Rayleigh fading, 6 Hz max. Doppler)

Mean SNR [dB]	20			23		
Capture z [dB]	0	3	6	0	3	6
Jamming failure rate	0.68	0.64	0.59	0.69	0.65	0.61
Avg. num. of targeted users	7.48	8.14	8.61	7.62	8.29	8.77
Throughput (nL receivers) [Mbps]	**12.1**	11.7	10.5	**16.7**	16.3	15.1
Min. Redundancy	1.38	1.26	1.18	1.36	1.23	1.16

Leader-Based Multicast Throughput

It is important to note that in a leader based protocol (LBP), due to the probability of feedback jamming being less than 1 (cf. section 7.4), rate adaptation based on feedback aggregation implicitly does not target all users with each transmission. Specifically, not all non-leader receivers (nLs) are targeted. As the jamming probability depends on ACK vs. NACK signal-to-interference ratio (SIR), the probability of jamming success decreases for comparatively weak non-leader receivers. Therefore, a direct comparison to the opportunistic "best users" scheduler as described above is reasonable. Throughput figures as given in the following are non-leader specific, unless otherwise noted. In the following, throughput for nL receivers has been validated to be approximately equal across nLs. The special role of the leader implies that for the leader (yet only for the leader) packet loss is signaled reliably. Hence, throughput at the leader, assuming absence of non-leader receivers, could be higher as compared to the nLs. However, in multicast the weakest receiver determines the throughput, as is the case for opportunistic multicast. In any rate adaptive LBP, this is a nL receiver. For comparison, a random rate adaptation algorithm as well as a static rate scheduler (which is set to the floor of the median of the available rates, here: 18 Mbps), are used. As opposed to scheduling with perfect channel knowledge, no channel knowledge is assumed prior to transmission. Results are obtained by first simulating i.i.d. fading and subsequent analysis of how many receivers have been served per transmission on average. Absolute throughput is compared to the theoretical maximum due to perfect multicast throughput gain exploitation by perfect channel knowledge and "best users" scheduling (cf. section 6.6.2).

9.3.1 Fading Scenarios

For the analysis of RA-LBP multicast rate adaptation performance under i.i.d. slow fading, the following scenarios are defined, whereas channel access intervals are unified for simplicity at 1 kHz independent of the physical layer rate chosen.

Fading scenario a) Rayleigh fading with classical Doppler power spectral density (psd) at 6 Hz max. Doppler shift is simulated. The 3 dB coherence time is about 65 ms. For each station, the fading gain random variable (RV) mean value is 20 dB. Except for time coherence, this scenario is directly comparable with that of section 6.6.2.

Fading scenario b) Rician fading with $K = 0$ dB and classical Doppler psd at 3 Hz max. Doppler shift, coherence time of about 150 ms and equal mean of 26 dB is simulated.

Due to the feedback jamming being imperfect, a subset of receivers will be served per transmission, whereas the same holds true naturally for the random and fixed rate selection mechanisms. The results for a set of parameter combinations is given in table 9.1, whereas after $b = 1$ transmit failures the PHY rate is decreased to emphasize the effect of the capture threshold z. The results for the random and fixed schedulers are given in table 9.2. Figures in parenthesis of table 9.2 are for uncorrelated i.i.d. Rayleigh for comparison. Note that with these figures it can be assumed that the correlated fading process is correctly modeled.

Table 9.2: Random RA vs. fixed rate multicast throughput (10 users, Rayleigh fading, 6 Hz max. Doppler)

Mean SNR [dB]	20		23	
RA scheduler	random	18 Mbps	random	18 Mbps
Avg. num. of targeted users	5.51	7.76	6.63	8.8
	(5.51)		(6.7)	
Throughput (all users) [Mbps]	7.96	3.07	11.39	3.5
	(8.2)		(12)	
Min. Redundancy	1.84	1.3	1.52	1.14
	(1.82)		(1.5)	
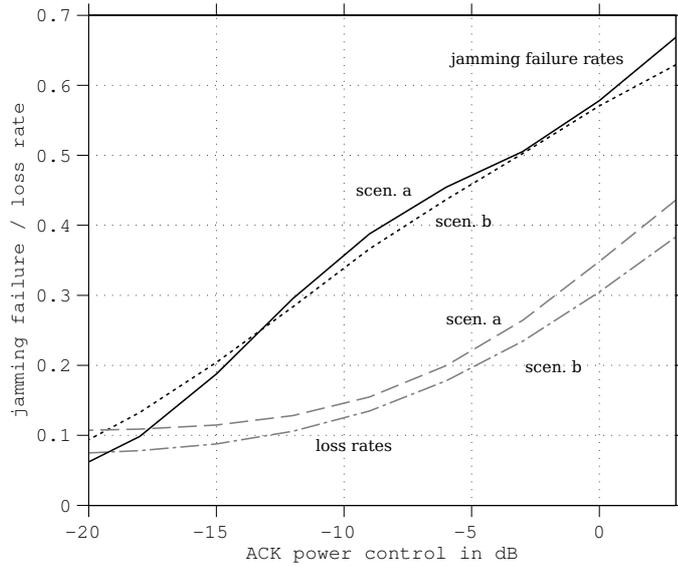
Figure 9.1: Feedback aggregation LBP-ARF jamming failure and loss rates (10 users) with increasing ACK power in two fading scenarios.

It can be seen that with a capture threshold of 0 dB for RA-LBP, as may be given in practice (cf. section 7.4), the described LBP-ARF multicast rate adaptation scheme achieves the highest throughput. Comparing this to the results in section 6.6.2 this is roughly 80% of the maximum "best users" opportunistic scheduler throughput gain. Random and fixed schedulers are outperformed by far.

Figure 9.1 depicts the jamming failure rate and loss rate increase with increasing ACK power in the two scenarios. Both rates are achieved by monte-carlo simulation and are averaged over the set of receivers. The jamming failure rate is determined by i.i.d. fading induced loss subject to the adaptively selected current MCS and frame capture in the event of jamming. With decreasing ACK power, due to the increased jamming failure rate, the loss rate converges to an error floor. This error floor is further determined by the fading RV, as any receiver may experience a fading gain below the lowest SNR threshold (cf. table 5.3 on page 55). Hence, for frames transmitted at those times, a receiver is unable to correctly decode. On average, this happens less frequently for scenario b as compared to scenario a due to the 6 dB increase in fading gain mean value. Note that ACK reception is assumed guaranteed regardless of the power reduction.

In figure 9.2 the achieved throughput of LBP-ARF, normalized to the case when jamming is perfectly reliable, is shown. A gain in multicast throughput is achieved depending on feedback power control at the leader receiver. In scenario b for example, the maximum throughput is achieved for ACK power reduction of 3 dB, whereas the packet loss $p_e = 0.234$ due to imperfect
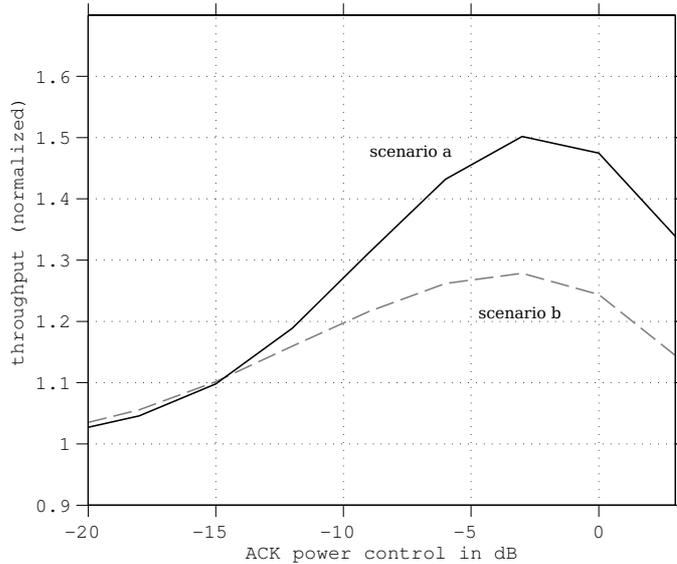
Figure 9.2: Feedback aggregation LBP-ARF throughput (10 users) with variable ACK transmit power in two fading scenarios, each normalized to the respective throughput under perfect feedback jamming.

Table 9.3: Random RA vs. LBP-ARF (10 users, 5% joint PEP, $z = 0\,\mathrm{dB}$, Rayleigh fading, $6\,\mathrm{Hz}$ max. Doppler)

RA scheduler	random		ARF, $b = 2$,			
			$a = 3$		$a = 10$	
Mean SNR [dB]	20	23	20	23	20	23
Jamming failure rate	-	-	0.5	0.49	0.57	0.56
Avg. num. of targeted users	5.2	6.3	6.79	6.93	7.77	8.03
Throughput [Mbps] (random: all)	7.5	10.8	**10.3**	**13.9**	8.44	10.8
Min. Redundancy	1.9	1.61	1.52	1.49	1.31	1.27

jamming is assumed compensated by an ideal capacity approaching packet erasure correcting code providing redundancy of at least $m = 1/(1 - p_\mathrm{e}) - 1 \approx 0.31$.

9.3.2 Joint Packet Erasures

The performance of multicast LBP-ARF may be reduced in presence of packet loss events that are common among all receivers, e.g. due to medium access collisions or other forms of sporadic interference. Results are provided for $5\,\%$ joint packet error probability (PEP) in table 9.3. Note that the jamming failure rate (again with $z = 0\,\mathrm{dB}$) is reduced due to the fact that any joint loss event results in perfect detection thereof. The ARF consecutive failure parameter is set to $b = 2$ here, as motivated above. It can be seen that with $a = 10$, LBP-ARF and random scheduler performance figures are similar. However, with $a = 3$, LBP-ARF at 5% loss still achieves roughly 68% of the maximum "best users" opportunistic scheduler throughput gain.

9.4 HLBP with Rate Adaptation

The LBP approach uses feedback aggregation and is extended to frame aggregation by HLBP [121] as described in section 8.3. Consequently, rate adaptation for HLBP is evaluated in the scope of this work. For practical reasons, a fixed overlay FEC code rate (R) and integer block length (n, k)

combination may need to be chosen. With fixed parameters a limited time delay is achieved, while some residual error must be tolerated. As this is the case in any practical scenario, it is simulated for the above introduced HLBP, including rate adaptation. The simulation is conducted as follows in order to obtain maximum throughput figures. Throughput is defined in the same way as above as the bit rate that can be transmitted (i.e. as seen by the application). Herein, medium access scheduling, data frame and packet headers as well as feedback overhead are not considered. While the aforementioned play a role in evaluation of throughput as seen by the application, concerning this matter an abstracted consideration is made herein. Furthermore, throughput as evaluated below is given as an average over the transmitted blocks, whereas per individual block, the minimum bit rate satisfying all users is selected. Latter is necessary due to the code block length being fixed and in the order of several tens of data frames, during which as many errors as possible need to be corrected.

9.4.1 Rate Adaptation Algorithm

For physical layer (PHY) layer rate adaptation combined with HLBP, ARF (cf. section 5.5.2.1) is applied to blocks of packets. In HLBP, feedback is obtained regarding the whole overlay FEC block, as opposed to individual frames in LBP. Live streaming implies comparatively short FEC blocks. Transmit duration of a block may e.g. in the order of (or less than) the coherence time of the channel. Therefore, a multicast throughput gain is not expected. Consequently it is reasonable to use the same MCS for all of the individual packets within a block, whereas the MCS defined bit rate satisfies all ($l = L$) receivers with respect to decodeability.

Similar to unicast ARF, in this work multicast rate adaptation shall switch to the next higher rate (if any) for the next block after a successfully transmitted blocks, while it switches down after a single failed block, denoted HLBP_a. Block transmit success is assumed when an acknowledgement (ACK) is received after $\lceil [0...(1-R)] \cdot k \rceil$ incremental redundancy packets of the overlay FEC code block, assuming an integer number of k systematic packets. Block decoding failure for the group of receivers is assumed in absence of an ACK. In that case, the available overlay FEC redundancy was not sufficient to correct all of the individual packet losses. Note that due to the redundancy and time budgets being fixed in advance, a residual error may be inevitable for a given fading scenario. Again, the leader of the multicast group is randomly chosen in prior as simulation is carried out under i.i.d. fading conditions with equal mean for all receiving users.

9.4.2 Performance Reference

For performance comparison, a fading-aware HLBP rate adaptation is simulated. It is fading-aware by having perfect and group comprehensive momentary fading gain knowledge. Perfect leader selection is simulated, as within a short interval of fading gain values comprising one FEC block the average gain over this block may vary. Herein, the on average weakest receiver per block is adaptively selected to be the leader. The per-block data MCS is chosen in advance such that this weakest user still correctly receives at least $r \cdot n$ packets in each block. The fading-aware HLBP rate adaptation jamming failure rate is set to 0 by an assumed ACK frame capture threshold of $z = \infty$. For reference, the opportunistic "best users" scheduler throughput is also given for the fading scenario simulated herein. Note that also this omniscient reference rate adaptation can not prevent packet loss, as a receiver may experience fading gains due to which the SNR during data frame transmission becomes lower than the bare minimum, i.e. the SNR threshold of the lowest MCS. For this purpose, evaluation is done in another fading scenario exhibiting an increased coherence time as compared to previous scenarios a) and b).

Fading scenario c) Performance comparison is done simulating TGn channel model B [36] (SISO, cf. section 3.6) at a max. Doppler shift of $1\,\text{Hz}$ ($3\,\text{dB}$ coherence time is around $410\,\text{ms}$)

Table 9.4: Opportunistic vs. fading-aware HLBP rate adaptation schedulers (10 users, 29 dB mean, i.i.d. TGn B, 1 Hz max. Doppler, 2 channel realizations)

RA scheduler	Opportunistic, fading-aware "best users"		HLBP, fading-aware "all users"	
Capture z	-		∞	
Block size	10^6	$5 \cdot 10^5$	30	
Channel realization	I	II	I	II
Fixed redundancy	42.7%	30.6%	200%	
Throughput [Mbps]	34.66	34.41	20.90	20.95
Targeted users	6/10	7/10	10/10	10/10
Redundancy spent	42.7%	30.6%	24.1%	23.8%
Residual loss	0%	0%	0.3%	0.27%

and at full angular spread.

Channel access intervals are again unified at 1 kHz independent of the physical layer rate chosen. As an example, the block size is fixed due to some delay constraint to 30 frames (and IP packets) and a FEC coding rate of $R = 1/3$ (in packets), hence the maximum redundancy m per block is 200%. With short overlay FEC coding blocks, live transmission is possible, but it is necessary to ensure that redundancy is provided timely, i.e. per individual FEC block. With an increase in the number of packets for which feedback is aggregated as well as increasing the capture threshold, feedback jamming failure is reduced significantly. Table 9.4 provides results according to the above parameters. Due to finite overlay FEC block lengths, HLBP cannot achieve an opportunistic throughput gain.

9.4.3 HLBP Rate Probing

As elaborated above, rate adaptation based on binary feedback adapts to varying channel conditions by trial-and-error. With the ARF applied directly to blocks of packets, trial and potential error may affect a whole FEC block, which would be excessive. In order to increase robustness, the $P_p HLBP_b$ algorithm uses p probing packets in the systematic part of the bth consecutively successfully transmitted FEC block (subject to jamming failure induced false positives) before switching to the next higher rate for the next block. In the previous $b - 1$ blocks, the amount of incrementally provided redundancy is recorded. For the probing block, the redundancy is compared to the mean redundancy of the previous $b - 1$ blocks. If it is larger than the mean plus one standard deviation, this is assumed due to probing, resulting in refraining from switching to the next higher rate.

Table 9.5 compares HLBP rate adaptation. The capture threshold is set to $z = 20\,\mathrm{dB}$, which may be achieved by power control. From the table it can be observed that, comparing $HLBP_5$ with $P_4 HLBP_5$, throughput is in all cases higher when probing packets are used, while residual error is in all cases lower.

Probing packets in the systematic part of the block introduce the possibility to restrict wasting the transmission of a complete block at a higher rate, resulting in an increased throughput and a decreased residual error rate. The effect can be assumed to increase when channel conditions are static over longer periods of time. In real environments, it may happen that any individual channel of each multicast receiver is static over some period of time due to virtually no movement in the environment. To model this, static periods are inserted (as repetition of the last fading value before the beginning of a static period) into the given fading scenario for all receivers at the same time. When static periods are of duration 2.5 s and make up 1/3 of the channel samples, results as given in table 9.6 are obtained.

The $P_4 HLBP_5$ cannot gain much throughput over the non-probing rate adaptation, however

Table 9.5: HLBP-ARF with and without probing transmissions (10 users, 29 dB mean, $z = 20$ dB, i.i.d. TGn B, 1 Hz max. Doppler)

RA scheduler	HLBP$_5$		P$_4$HLBP$_5$	
Block size [packets]	30		30	
Fixed redundancy	200%		200%	
Channel realization	I	II	I	II
Joint PEP	0		0	
Throughput [Mbps]	15.78	16.42	16.67	16.87
Redundancy spent	33.89%	33.96%	24.15%	23.94%
Residual loss	1.83%	1.33%	0.88%	0.85%
Jamming failure	3.03%	3.44%	4.07%	3.96%
Joint PEP	5%		5%	
Throughput [Mbps]	11.01	12.31	11.23	12.40
Redundancy spent	49%	43.92	39.77%	39.27%
Residual loss	2.56%	2.2%	1.67%	1.75%
Jamming failure	2.22%	2.52%	2.72%	2.75%

Table 9.6: HLBP-ARF (10 users, 29 dB mean, $z = 20$ dB, i.i.d. TGn B, 1 Hz max. Doppler) with 1/3 2.5 s static periods

RA scheduler	HLBP (fading-aware)		HLBP$_5$		P$_4$HLBP$_5$	
Channel realization	I	II	I	II	I	II
Throughput [Mbps]	21.823	21.832	16.708	16.762	17.918	17.931
Redundancy spent	18.07%	17.68%	34.94%	34.37%	19.75%	18.88%
Residual loss	0.323%	0.318%	2.154%	2.153%	0.692%	0.686%

the residual loss is reduced by a factor of roughly 1/3 in this case, while the incremental redundancy that is spent on average is very close to the fading aware HLBP redundancy figure. Consequently, the introduction of rate increased probing packets that may be compensated by incremental redundancy can improve multicast streaming of delay constrained inelastic multimedia flows.

Live-Streaming Prototype

A multimedia multicast streaming and feedback aggregation prototype implementation based on consumer WLAN hardware has been developed in the course of this work. Aggregation of positive and negative feedback in the time domain results in the event of feedback jamming under the same preconditions as elaborated for the case of time-division multiple access (TDMA) multicast WLAN above (cf. section 7.4). The implementation is capable of transmitting a leader based hybrid-error-coding protected multicast stream to an arbitrary large number of multicast receivers. Forward error coding (FEC) is provided on the transport layer by the predictably reliable real-time transport (PRRT) protocol. Incremental redundancy in case of transmission errors is provided by medium access control (MAC) mechanisms. Rate adaptation is implemented as described above for error correction according to the hybrid leader based protocol (HLBP) with probing transmissions (cf. section 9.4.3). For the prototype implementation, both at the access point and on receiver side, MAC functionality has been extended. Modification of the MAC layer firmware[1], however, has been infeasible by the lack of source code thereof. Therefore, some extensions have been integrated into the operating system kernel. In general, to the best knowledge of the author, none of the mechanisms are infeasible to implement as firmware. The rate adaptive HLBP state machines are implemented in the Linux operating system kernel.

10.1 Feedback Aggregation Implementation

10.1.1 Feedback Request Signaling

A dedicated feedback request frame synchronizes medium access for receiver individual feedback (cf. 802.11aa [117]) as well as for feedback aggregation based multicast TDMA protocols. The herein presented feedback aggregation prototype implementation is based on standard compliant IEEE 802.11 WLAN, thus an additional feedback request frame is introduced (cf. the REQ frame in fig. 8.1 on page 106). Upon receiving this frame, receivers are triggered to respond feedback. The operating system driver level state machine implementation, however, is unable to interpret the payload of the feedback request frame in time due to scheduling latencies in the order of milliseconds. Therefore, the FEC coding block parameters (i.e. sequence numbers, n and k) need to be announced to the receiving stations in-prior by means of an announcement frame as depicted in figure 10.1. Receiving stations evaluate it in the driver level and by means of a sufficient, a priori chosen delay (cf. "DIFS+delay" in figure 10.1), they become ready before the subsequent feedback request frame triggers the card's internal firmware to respond a *hardware acknowledgement*, as elaborated below.

10.1.2 Feedback Frames

Feedback regarding the ability to decode the current FEC block is transmitted in the form of *hardware acknowledgements*. Latter term is chosen due to the feedback frame being a unicast

---

[1]Medium access control software is typically running embedded in wireless interfaces.
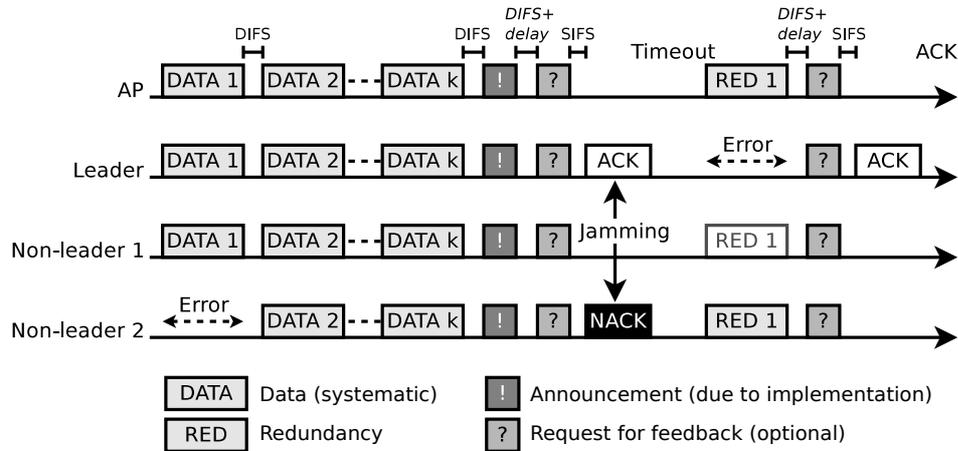
Figure 10.1: Protocol run of a WLAN HLBP prototype implementation with block announcement [79] and feedback request frames, providing incremental redundancy to a group of 3 multicast receivers.

WLAN acknowledgement (ACK) frame (cf. figure 5.7 on page 58), which is a functional element of the IEEE 802.11 MAC layer and thus abstracted by WLAN network interface hardware. Orthogonal frequency division multiplex (OFDM) unicast ACK frames, as responded by the group of OFDM WLAN multicast receivers, are transmitted either at the single-input single-output (SISO) modulation and coding scheme of 6 Mbps (taken as positive acknowledgement) or 12 Mbps (taken as negative acknowledgement). After one short inter-frame space (SIFS) as defined for the 802.11 OFDM physical layer (PHY) (cf. table 5.5 on page 63), these frames are transmitted subsequent to a feedback request frame. With the announcement frame prior to the request frame, the state machine is allowed to transit, within a large period of time as compared to the SIFS, from a previous state to the state in which a feedback decision has been made (either *ACK*, *NACK,* or *silence*, cf. section 8.1).

10.1.3   MAC Data Frame Buffering

In an HLBP prototype as well as in any non-prototype implementation, compared to unicast no additional MAC layer data frame buffer is required at the receivers. The sender on the other hand needs to buffer parity packets in order to be able to transmit them incrementally, but need not necessarily buffer systematic data frames. Each individual payload data unit traverses the protocol stack as a singular unit, whereas only state information needs to be kept at the participating stations. The state information is binary when erasure codes [139, 14] are used. This can be considered a benefit over 802.11 block-ACK [64] and groupcast with retries (GCR) block-ACK [117], in which due to a sequence number ordering preservation requirement, multiple MAC layer frames have to be buffered at sender and receiver(s), in addition to keeping state information. In the following, this feature is termed *passing-through* of data to the upper layers as it is received. Note that in feedback aggregation schemes, also no buffer size handshake (cf. TCP, block-ACK and GCR) is required prior to block transmission. For any HLBP implementation, the buffer for incremental redundancy at the sender is simply flushed by the next FEC block in case it has not been depleted. With low-cost consumer hardware, this may be an important benefit.

10.2   Cross-Layer Hybrid Error Correction Implementation

It has been elaborated above that with knowledge about the overlay FEC coding parameters, i.e. the block length and the number of systematic and parity packets, feedback on the MAC layer can be simplified to binary, also for block-based transmission. The remainder of this section covers the implementation details specific to the herein chosen approach.

10.2.1   Predictably Reliable Real-Time Transport

Block-of-packets based FEC by means of MDS codes and virtual interleaving is provided by the multicast capable transport layer protocol PRRT [14], which is based on UDP/IP. It is thus suitable for carriage of inelastic flows. Applications that are supported by PRRT are, among others, RTP/UDP/IP streaming (cf. section 2.4.2) as well as DVB-IPTV (cf. section 2.5.5) transport. A cross-layer implementation introduces the benefit of the application providing the overlay FEC block code being able to decide about the coding rate. Thus, the application, which potentially has knowledge about bit rate and delay requirements, can adapt the stream and the overlay FEC parameters to varying channel conditions by observation of the result at the receivers. The implementation presented herein detects the current overlay FEC parameters from a fixed header structure within the PRRT transport layer packets. Data and parity packet header field differences for PRRT are depicted along with virtual interleaving in figure 10.2.

10.2.2   Virtual Interleaving

The PRRT transport layer protocol error correcting code used herein is, as in DVB multiprotocol encapsulation (MPE) FEC, a Reed-Solomon RS(255,191) code. Virtual interleaving is done in order to expand the code to multiple Internet Protocol (IP) packets. Application and RS data tables carry systematic and parity information, respectively. As depicted in figure 10.2, each row of the combined tables contains one RS codeword. Some of the rightmost columns of the parity table may be discarded before transmission, enabling code puncturing of the interleaved transport layer code.

10.2.3   Protocol State Machines

Protocol state machines of the overlaid MAC layer protocol, herein given for the above described specific implementation, are simple. Transmitter state flow is depicted in figure 10.3 and receiver state flow in figure 10.4.

Part A: State Flow at the Sender

Data frame loop-through: For incoming PRRT/IP data packets (DATA), the sender encapsulates each in an LBP header according to the PRRT header fields as depicted in figure 10.2.

Incremental redundancy phase 1:   A diversion from the loop-through behavior is done starting from the first parity packets providing incremental redundancy (RED). The above justified announcement frame (ANN) is inserted into the packet stream at this point. The transmit queues of the wireless adaptor are monitored in order to ensure in-sequence delivery of the involved frames until this point. When the sender has gathered all RED packets for the current block, and a preconfigured constant delay has passed, the feedback request is assembled (indicated as QUES in figure 10.2) and transmitted. Aforementioned constant delay is required in this prototype implementation (cf. section 10.1.1) for the receivers to configure their respective response, depending on their status (leader, non-leader) and the number of received data frames of the current block.
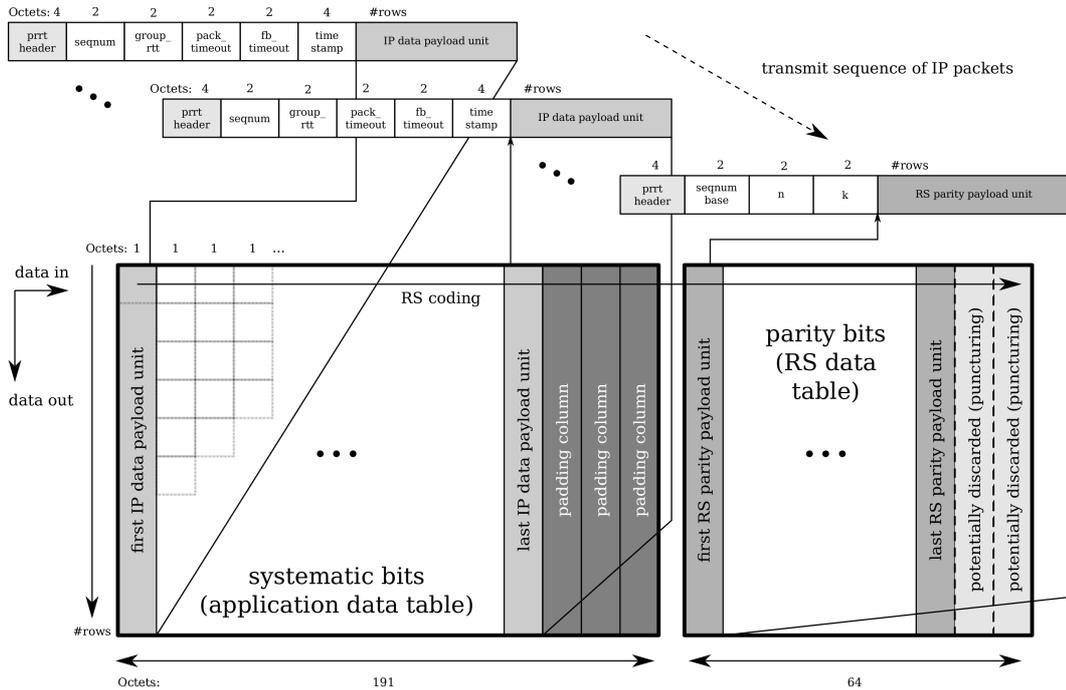
Figure 10.2: Virtual interleaving of MDS Reed-Solomon code and partition into application data and RS data tables as in DVB MPE-FEC [101]. Systematic and parity are transmitted via PRRT packets of respective different types and in the order given.

Incremental redundancy phase 2: The feedback request is transmitted initially after the announcement frame, upon which receivers respond with ACK, NACK or neither. In case the positive ACK is not decoded (potentially due to feedback jamming) at this point, incremental redundancy is provided. The process of feedback aggregation by request and response is then repeatedly initiated with each increment. When the retry limit is reached (by the stock of available redundancy packets for this block being depleted) or in case an ACK is decoded, the block is finished and the sender advances to the START state, awaiting a new block of packets.

Part B: State Flow at the Receivers

Data frame reception phase: As for the sender, the receiver provides DATA frames to the higher layers immediately. Sequence numbers are stored for determining data frame loss. Upon reception of the announcement frame, the potentially variable FEC block parameters (n,k) are read.

Incremental redundancy phase: Due to the overlay FEC implementation, the receiver may pass through any incremental redundancy (RED) packet as received. At the time of reception of a feedback request frame (QUES), the receiver has determined the number of frames it has gathered from the current block. No distinction between DATA and RED is made herein, as a number of k out of n packets is know to be sufficient for decoding the FEC block. Each receiver configures its feedback state according to this. Upon reception of a DATA frame in this phase, the receiver assumes the available redundancy at the sender to be depleted.
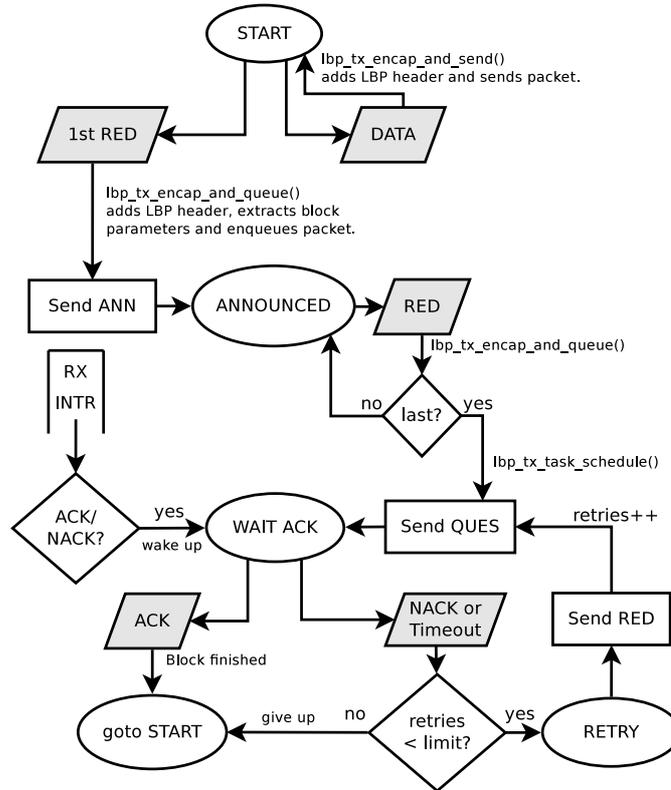
Figure 10.3: Prototype state flow diagram at the wireless multicast sender (WLAN access point)

10.3 Rate Adaptation

Rate adaptation for this hybrid overlay FEC multicast streaming prototype including feedback aggregation has been implemented including above proposed mechanism of rate probing (cf. section 9.4.3). Transmit success/failure based rate adaptation on a per-block basis is applied, whereas this decision is made on the MAC layer. The PRRT protocol provides systematic and parity packets, potentially in abundance. Consequently, the possibility of doing in-band rate probing transmissions is exploited, which is gained from overlay FEC. Note that the scheme is in general also applicable for unicast, whereas the complexity of overlay FEC is assumed more feasible in multicast (cf. section 6.6.1). Figure 10.5 depicts rate probing HLBP rate adaptation during operation, by example as measured in the vicinity of the leader receiver. Rate probing transmissions impede the success based adaptation from switching to higher modulation and coding scheme (MCS) bit rates in case the channel exhibits static periods.

Figure 10.5 further compares rate adaptation with zero and two probing packets. With probing packets, rate adaptation is more stable with long coherence times, as switching to a less robust rate is tested in advance and the probability of transmitting a block of packets at a rate unsuitable for the multicast group can be avoided. In order to show the effect visually, an artificial setting is chosen in which switching to a less robust rate is highly likely to result in packet loss, as intermediate PHY rates are omitted. As it is tedious to thoroughly examine the performance of a prototype, especially in case of multicast, the behavior has been studied by simulation as described in section 9.4.3.

Figure 10.4: Prototype state flow diagram at each wireless multicast receiver (WLAN station)

10.4 Experimental Evaluation

With a prototype rate adaptation implementation as described above, it is important to evaluate whether rate increase or decrease occurred due to potential implementation imperfectness, or whether adaptation is aligned to channel variations. In figure 10.6 it can be observed that rate adaptation as implemented herein is to a significant extent driven by channel variations. The signal-to-noise ratio (SNR) during multicast data frame reception is recorded at the receiving stations as described in sections 5.5.1 and 7.5.1. Furthermore, the sender chosen MCS is recorded for each data frame. The probability distribution of the used MCSs (here: 12 Mbps – 54 Mbps) over the channel SNR can be approximated by averaging over the measurements at each receiver. With the relative occurrence of the SNR values not being uniformly distributed for practical reasons, the rate adaptive MCS cdf exposes the rate adaptation algorithm to produce well separated curves per MCS.

In summary, the prototype implementation is capable of live audio/visual streaming using overlay FEC to provide incremental redundancy, and using feedback aggregation to achieve scalability with the number of multicast receivers. Figure 10.7 depicts the the scenario as described in use case 1 (cf. chapter 2.1): Local re-distribution of digital television by example of DVB-T. A conventional TV set and a number of wireless multicast receiver display the same TV program.

Figure 10.5: Multicast rate adaptation based on transmit failure in a prototype implementation. Top: No probing before rate switching and thus immediate switching back to the lower rate due to increased packet loss; Bottom: Two probing packets reduce rate adaptation failures. Note: SNR as reported by consumer WLAN hardware.
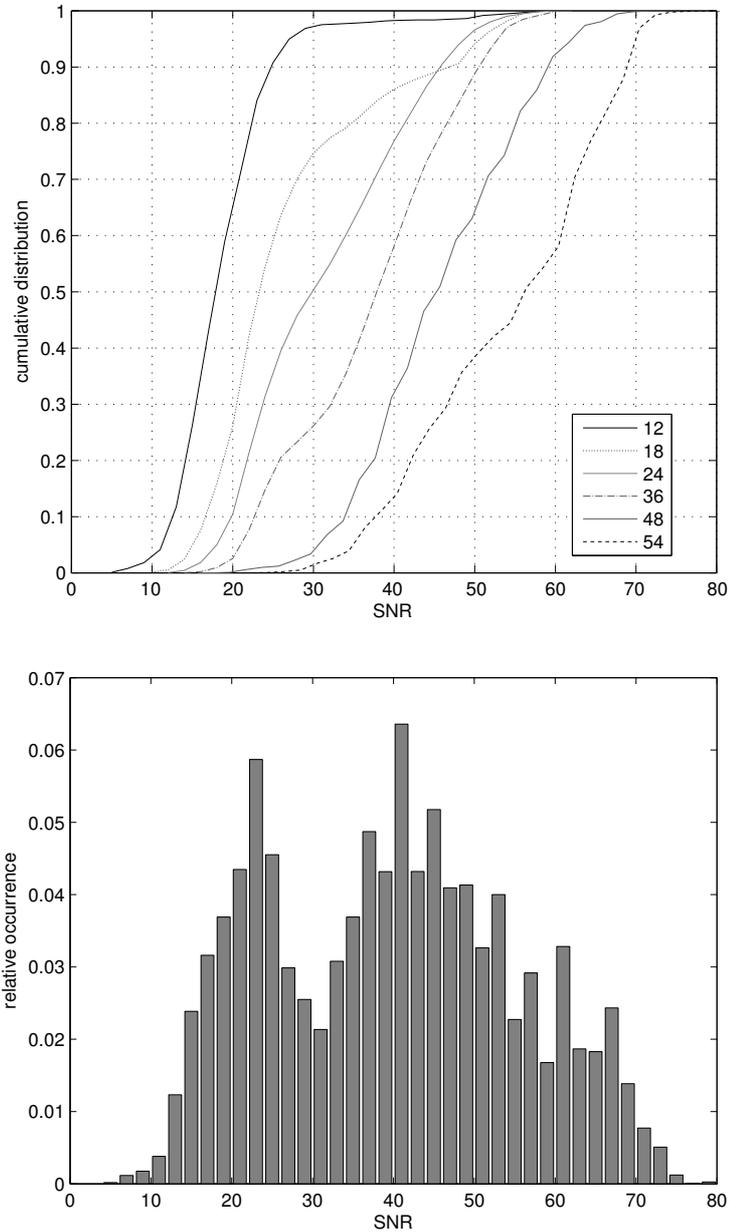
Figure 10.6: Probability distribution of WLAN card provided SNR measurements at one receiver in rate-adaptive feedback and frame aggregation multicast. Sender-receiver distance has been varied during measurements using herein described prototype. *Top:* evaluation of the cdf shows separation of the individual rates with increasing SNR. *Bottom:* SNR measurements have not been uniformly distributed due to limitations in varying the distances arbitrarily.

Figure 10.7: Prototype implementation used for local DVB-T redistribution to a group of receivers. *Top:* A leader receiver (top left) is placed deliberately further away from the base station (behind the camera); live DVB-T is shown on a TV set for comparison (top right). *Bottom:* All receivers are placed deliberately close together; the leader is randomly chosen and uses feedback power reduction.

11

Conclusion

This work has been motivated by the need for efficient multicast transmission of inelastic multimedia network streams over bidirectional and multi-user Internet protocol capable wireless networks. While the topic is broad, the focus in this work is on wireless LAN according to IEEE 802.11. Results as obtained herein are, however, not limited to aforementioned systems. Open loop multicast transmission is common for the wireless standards mentioned above, including WLAN, whereas multicast feedback was not included in the 802.11 standard until March 2012. With respect to this, an alternative leader based approach to multicast feedback is the basis for the considerations at hand. Use cases in the scope of this work are broadcast and, more generally, bidirectional audio/visual streaming. Low delay video coding enables audio/visual streaming in the order of several megabits per second. The focus of this work has been the downlink transmission of suchlike streams from the base station or access point to the user. Orthogonal frequency division multiplex is the predominant digital transmission technique at the time of writing, with several current standards that define the use of OFDM. For the reason of its predominance, OFDM has been described in relevant detail with respect to the scope of this work.

Multicast feedback which is aggregated in a single time slot of a TDMA system is the multicast feedback scheme advocated in this work. A benefit as compared to time sequential feedback is its scalability with the number of receivers due to constant feedback overhead. Furthermore, reliability of this scheme is improved with increasing number of receivers. The effect of frame capture in the process of feedback jamming during the phase of aggregation has been evaluated for synchronous OFDM feedback. The power spectral density of OFDM based systems, by example of 802.11a/g, has been examined. It is flat over the used parts of the spectrum except for a ripple due to the used guard interval. Hence, a conclusion may be that during feedback aggregation, interfering signals produce additional white noise. A reduction in AWGN SNR would be the result, independent of the number of interfering signals contributing to the feedback jamming attempt. The feedback destination may, however, not necessarily observe white noise on the individual OFDM subcarriers when the interfering signals are not specially designed. Herein, valid MAC layer frames have been used for jamming, albeit at different physical layer modulation order as compared to the positive acknowledgement. The interfering signals may hence not only destroy the positive acknowledgement, but may actually be decodable as valid OFDM frames instead. Semantically, this has been treated identically in the scope of this work.

The observations made in the course of this work have been conducted using single antenna OFDM systems in the scope of leader based multicast with feedback aggregation. Fading channels have been introduced in this regard. Multi-antenna systems have been introduced as alternatives to single antenna multicast. Specifically, those are simulcast multiple-input multiple-output and multi-user multiple-input multiple-output multicast. Both approaches have been shown to be outperformed with increasing numbers of multicast receivers. A diversity gain in multicast transmission in case of non delay constrained applications has been included in this comparison.

In this regard, the opportunistic behavior of rate adaptive multicast using feedback aggregation, resulting in an increased throughput as compared to fixed rate multicast, has been pointed out in this work. A comparison was done with respect to an opportunistic scheduler with perfect

channel knowledge. Feasibility of former mechanism is given regarding non-real time file delivery. The gain in multicast throughput by opportunistic scheduling has further been shown to increase when the available transmission bit rates are quantized. This has been evaluated by example of the available modulation and coding schemes of single-input single-output OFDM based WLAN.

With delay constrained streaming of inelastic flows, the implication was an overlay forward error coding code providing blocks of length in the order of several tens of IP packets. In this case, feedback jamming should be most effective in order to provide almost reliable per-block error correction feedback. The simple mechanism of feedback power control has been proposed herein in order to improve the jamming probability, and it is indispensable whenever a leader can not be selected among the receivers due to independent and identically distributed channel conditions. In both cases of delay consideration, rate adaptation mechanisms have been proposed. For delay constrained transmission, adaptation has been shown to be improved by rate probing transmissions. When switching the transmit bitrate downwards, transmission becomes both more robust and slower. In case switching downwards was not actually necessary, a lower efficiency is the result. Consequently, medium usage time is wasted, which potentially reduces throughput of any other wireless station in the vicinity. Switching down is thus proposed to be done only in case the transmitted data can no longer be decoded at the currently chosen modulation and coding scheme. The consequences of switching to the next faster modulation and coding scheme are much more severe. Reception is impeded with almost unit error probability below a certain, modulation and coding scheme dependent signal-to-noise ratio threshold, which depends on the chosen modulation and coding scheme (subject to the implementation complexity of the receiver). Rate probing may thus reduce redundancy in transmission. Herein proposed rate adaptation probes contain useful data, but loss thereof may be compensated by the overlay forward error coding code in case probing fails. In case probing is successful, the probing transmissions have been transmitted using less medium time, resulting in another small performance improvement. The packet level forward error coding coding scheme advocated in this context is maximum distance separable and systematic. This allows exact block-decodability checking at the medium access control layer by counting the number of received packets per block.

Last but not least, a prototype implementation comprises major parts of the above named aspects of delay constrained wireless audio/visual multicast. Implementation details and results as obtained with this prototype are presented herein. The prototype is assembled with OFDM based 802.11 consumer hardware and may thus serve as a platform for validation of the analytical and simulation results obtained in the course of this work.

Scientific Contribution

In the course of this work, a number of scientific contributions have been achieved. In the literature, the capture effect has been shown to have significant influence on the achievable throughput of distributedly coordinated medium access in TDMA systems. This work provides experimental results on the capture effect obtained with consumer hardware. Depending on frame structures and modulation and coding schemes involved in simultaneous transmission, capture has been shown to achieve sensitivity of $-0.3\,\mathrm{dB}$ in signal-to-interference-plus-noise ratio. With realistic capture effect figures, quantitative results on feedback jamming have been obtained. It has been shown that a leader based protocol may exhibit an error floor in the order of 10^{-2} for multicast groups of around 50 receivers. While these figures do not hold generally, scenarios that are particularly adverse with respect to feedback jamming probability have been chosen in order to provide conservative results. Furthermore, it has been shown that by feedback power control at one of the receivers (i.e. the leader receiver), the error floor is reduced. Nevertheless, a conclusion is that suchlike multicast transmission may not be feasible in any possible wireless scenario, making it of limited use.

With quantization of the available channel capacity by a limited number of available modulation and coding scheme combinations, as is the case e.g. in WLAN, it has been shown that an oppor-

tunistic scheduler may achieve a gain in throughput that is increased as compared to continuous instantaneously available channel capacity. Quantitative results are given by example, whereas due to selecting fading channel parameters as in the available literature, comparability is maintained.

In the final parts of this work, a feedback aggregation based rate adaptation scheme for WLAN is proposed. By monte-carlo simulation, it is shown how this scheme may behave opportunistically, achieving roughly 80 % of the throughput of an omniscient opportunistic scheduler for which the maximum number of targeted stations is fixed in advance, but chosen to achieve maximum throughput. Fixed and random MCS schedulers are shown to be outperformed. When transmission is delay constrained on the other hand, the herein provided rate adaptation proposal reduces redundant transmissions, especially for channels that exhibit static periods of significant duration, i.e. in the order of several ten FEC blocks. The above described prototype implementation is capable of showing the feasibility of latter proposal, whereas by the author, the implementation is regarded as unique in the literature.

Outlook

The choice of maximum distance separable codes for data frame transmission enables shorter blocks as compared to e.g. Fountain codes. The achieved delay may thus be lower, whereas decodability checking can be done at the MAC layer. However, in the scope of this work and especially in case of delay constrained transmission, the critical part of feedback aggregation based multicast is the event of feedback jamming when used in conjunction with either of the above. For delay constrained transmission, reliability of feedback jamming in case of only a single interfering signal determines the error floor. Reliability of jamming can be further increased in both single and multi-antenna systems. As shown herein, a signal that is not specifically designed for jamming of the positive acknowledgement may result in a capture threshold below 0 dB. Use of a white noise signal for jamming will thus increase this threshold, whereas binary phase shift keying on OFDM subcarriers of the positive ACK lends itself to jamming with an inverted signal. In multi-antenna systems, the use of multi-user multiple-input multiple-output multicast may be feasible in some scenario. In this case, the transmitter has acquired channel state information from the multicast group and consequently does multi-user transmit beamforming. Conversely, transmit beamforming may be used by multi-antenna non-leader receivers, decreasing the signal-to-noise ratio during the reception of the positive acknowledgement at the feedback destination in order to increase the propability of jamming success.

Bibliography

[1] U. Reimers, *DVB – The Family of International Standards for Digital Video Broadcasting.* Springer, 2nd ed., 2005.

[2] J. Qi, P. Neumann, and U. Reimers, "Dynamic broadcast," in *14th ITG Conference on Electronic Media Technology (CEMT)*, pp. 1–6, Mar. 2011.

[3] C. E. Shannon, "A Mathematical Theory of Communication," *Bell System Technical Journal*, vol. 27, pp. 379–423 and 623–656, 1948.

[4] ETSI, *TS 101 154 V1.2.1; Digital Video Broadcasting (DVB); Specification for the use of Video and Audio Coding in Broadcasting Applications based on the MPEG-2 Transport Stream.* European Telecommunications Standards Institute, 2009.

[5] ETSI, *TS 102 905 V1.1.1; Digital Video Broadcasting (DVB); Technical Specification for DVB Services in the Home Network Phase 1.* European Telecommunications Standards Institute, May 2010.

[6] LAN/MAN Standards Committee of the IEEE Computer Society, "Wireless LAN Medium Access Control (MAC) and Physical Layer (PHY) Specifications Amendment 8: Medium Access Control (MAC) Quality of Service Enhancements," *IEEE Std 802.11e™-2005 (Amendment to IEEE Std 802.11, 1999 Edition (Reaff 2003)*, 2005.

[7] LAN/MAN Standards Committee of the IEEE Computer Society, "IEEE Standard for Information technology – Telecommunications and information exchange between systems – Local and metropolitan area networks – Specific requirements – Part 11: Wireless LAN Medium Access Control (MAC) and Physical Layer (PHY) Specifications," *IEEE Std 802.11™-2012 (Revision of IEEE Std 802.11-1999)*, 2012.

[8] J.-R. Ohm, G. J. Sullivan, H. Schwarz, T. K. Tan, and T. Wiegand, "Comparison of the Coding Efficiency of Video Coding Standards – Including High Efficiency Video Coding (HEVC)," *IEEE Transactions on Circuits and Systems for Video Technology*, vol. 22, pp. 1669–1684, Dec. 2012.

[9] T. Wiegand, G. J. Sullivan, G. Bjø ntegaard, and A. Luthra, "Overview of the H.264/AVC Video Coding Standard," *IEEE Transactions on Circuits and Systems for Video Technology*, vol. 13, no. 7, pp. 560–576, 2003.

[10] A. Puri, X. Chen, and A. Luthra, "Video coding using the H.264/MPEG-4 AVC compression standard," *Signal Processing: Image Communication*, vol. 19, pp. 793–849, Oct. 2004.

[11] Telecommunication Standardization Sector of ITU, *ITU-T Recommendation H.222.0; SERIES H: AUDIOVISUAL AND MULTIMEDIA SYSTEMS. Infrastructure of audiovisual services – Transmission multiplexing and synchronization. Information technology – Generic coding of moving pictures and associated audio information: Systems.* International Telecommunications Union, May 2006.

[12] ETSI, *TS 126 606 V1.1.1; Digital Video Broadcasting (DVB); Generic Stream Encapsulation (GSE) Protocol.* European Telecommunications Standards Institute, Oct. 2007.

[13] A. Tanenbaum, *Computer Networks.* Prentice Hall Professional Technical Reference, 4th ed., 2002.

[14] M. Gorius, *Adaptive Delay-constrained Internet Media Transport.* Dissertation, Sept 2012.

[15] J. Iyengar, P. Amer, and R. Stewart, "Concurrent Multipath Transfer Using SCTP Multihoming Over Independent End-to-End Paths," *IEEE/ACM Transactions on Networking*, vol. 14, pp. 951–964, Oct. 2006.

[16] E. Kohler, M. Handley, and S. Floyd, "Designing DCCP: Congestion control without reliability," *ACM SIGCOMM Computer Communication Review*, 2006.

[17] A. M. Tekalp, E. Kurutepe, and M. R. Civanlar, "3DTV over IP," *IEEE Signal Processing Magazine*, vol. 24, pp. 77–87, Nov. 2007.

[18] M. Gorius, M. Karl, and T. Herfet, "Optimized Link-level Error Correction for Internet Media Transmission," in *NEM Summit*, 2009.

[19] M. Gorius, J. Miroll, M. Karl, and T. Herfet, "Predictable reliability and packet loss domain separation for IP media delivery," in *IEEE International Conference on Communications (ICC)*, 2011.

[20] ETSI, *TS 102 034 V1.4.1; Digital Video Broadcasting (DVB); Transport of MPEG-2 TS Based DVB Services over IP Based Networks*. European Telecommunications Standards Institute, Aug. 2009.

[21] M. Luby, M. Watson, T. Gasiba, and T. Stockhammer, "Raptor codes for reliable download delivery in wireless broadcast systems," *IEEE Consumer Communications and Networking Conference (CCNC)*, pp. 192–197, 2006.

[22] ETSI, *TS 126 346 V11.3.0; Universal Mobile Telecommunications System (UMTS); LTE; Multimedia Broadcast/Multicast Service (MBMS); Protocols and codecs (3GPP TS 26.346 version 11.3.0 Release 11)*. European Telecommunications Standards Institute, Jan. 2013.

[23] D. MacKay, "Fountain codes," *Capacity Approaching Codes Design and Implementation Special Section*, vol. 152, no. 6, 2005.

[24] ETSI, *TS 102 542 V1.3.2; Digital Video Broadcasting (DVB); Guidelines for the implementation of DVB-IPTV Phase 1 specifications; Part 3: Error Recovery; Sub-part 2: Application Layer - Forward Error Correction (AL-FEC)*. European Telecommunications Standards Institute, May 2011.

[25] H. Schmidt, *OFDM für die drahtlose Datenübertragung innerhalb von Gebäuden*. PhD thesis, University of Bremen, Germany, Aachen, Germany, June 2001.

[26] A. Goldsmith, *Wireless Communications*. Cambridge University Press, 2005.

[27] A. F. Molisch, *Wireless Communications*. Wiley-Blackwell, 2010.

[28] D. C. Cox, R. R. Murray, and A. W. Norris, "800-MHz attenuation measured in and around suburban houses," *AT&T Bell Laboratories technical journal*, vol. 63, no. 6, pp. 921–954, 1984.

[29] S. Y. Seidel and T. S. Rappaport, "914 MHz path loss prediction models for indoor wireless communications in multifloored buildings," *IEEE Transactions on Antennas and Propagation*, vol. 40, no. 2, pp. 207–217, 1992.

[30] K. W. Cheung, J. H. M. Sau, and R. D. Murch, "A new empirical model for indoor propagation prediction," *IEEE Transactions on Vehicular Technology*, vol. 47, pp. 996 –1001, Feb. 1998.

[31] F. Villanese, N. Evans, and W. Scanlon, "Pedestrian-induced fading for indoor channels at 2.45, 5.7 and 62 GHz," *IEEE Vehicular Technology Conference (VTC)*, vol. 1, pp. 41–43, Sept. 2000.

[32] K. Ziri-Castro, W. Scanlon, and N. Evans, "Characterisation of body-shadowing effects in the indoor environment at 5.2 GHz," *High Frequency Postgraduate Student Colloquium (Cat. No.03TH8707)*, pp. 2–5, 2003.

[33] C. Dillschneider, "Untersuchung drahtloser Kanalmodelle für In-Haus Netzwerke nach 802.11a," Master's thesis, Saarland University, 2008.

[34] R. H. Clarke, "A statistical theory of mobile-radio reception," *Bell System Technical Journal*, vol. 47, no. 6, pp. 957–1000, 1968.

[35] Q. Yao and M. Patzold, "Spatial-temporal characteristics of a half-spheroid model and its corresponding simulation model," *IEEE Vehicular Technology Conference (VTC)*, vol. 1, pp. 147–151, 2004.

[36] V. Erceg, L. Schumacher, P. Kyritsi, A. F. Molisch, D. S. Baum, A. Y. Gorokhov, C. Oestges, Q. Li, K. Yu, N. Tal, and B. Dijkstra, "IEEE P802.11 TGn Channel Models," *IEEE 802.11-03/940r4*, 2004.

[37] S. O. Rice, "Mathematical analysis of random noise," *Bell System Technical Journal*, vol. 24, pp. 46–156, January 1945.

[38] Bronstein, Semendjajew, Musiol, and Mühlig, *Taschenbuch der Mathematik*. 5th ed., 2001.

[39] P. Bello, "Characterization of Randomly Time-Variant Linear Channels," *IEEE Transactions on Communications Systems*, vol. 11, no. 4, pp. 360–393, 1963.

[40] H. Nuszkowski, *Digitale Signalübertragung im Mobilfunk*. Jörg Vogt Verlag, 2010.

[41] H. Hashemi, "The indoor radio propagation channel," *Proceedings of the IEEE*, vol. 81, no. 7, pp. 943–968, 1993.

[42] J. Medbo, H. Hallenberg, and J. Berg, "Propagation characteristics at 5 GHz in typical radio-LAN scenarios," in *IEEE Vehicular Technology Conference (VTC)*, vol. 1, pp. 185–189, IEEE, 1999.

[43] M.-S. Alouini and A. Goldsmith, "Capacity of Nakagami multipath fading channels," *IEEE Vehicular Technology Conference (VTC)*, vol. 1, pp. 358–362, 1997.

[44] S. Haykin and M. Moher, *Modern Wireless Communications*. Prentice Hall, 1 ed., Feb 2004.

[45] A. Saleh and R. Valenzuela, "A Statistical Model for Indoor Multipath Propagation," *IEEE Journal on Selected Areas in Communications*, vol. 5, pp. 128–137, Feb. 1987.

[46] LAN/MAN Standards Committee of the IEEE Computer Society, "Wireless LAN Medium Access Control (MAC) and Physical Layer (PHY) Specifications Amendment 4: Enhancements for Very High Throughput for Operation in Bands below 6 GHz," *IEEE Draft P802.11ac™2.1 (Amendment to IEEE Std 802.11-2012)*, March 2012.

[47] E. Perahia, A. Sheth, T. Kenney, R. Stacey, and D. Halperin, "Investigation into the Doppler Component of the IEEE 802.11n Channel Model," in *IEEE Global Telecommunications Conference (GLOBECOM)*, 2010.

[48] ETSI, *EN 302 755 V1.1.1; Digital Video Broadcasting (DVB); Frame structure channel coding and modulation for a second generation digital terrestrial television broadcasting system (DVB-T2)*. European Telecommunications Standards Institute, 2009.

[49] ETSI, *TS 136 211 V11.1.0; LTE; Evolved Universal Terrestrial Radio Access (E-UTRA); Physical channels and modulation (3GPP TS 36.211 version 11.1.0 Release 11)*. European Telecommunications Standards Institute, Feb. 2013.

[50] J. G. Proakis and M. Salehi, *Communication Systems Engineering*. Prentice Hall, 1994.

[51] K.-D. Kammeyer, *Nachrichtenübertragung*. B.G. Teubner, Reihe Informationstechnik, 4 ed., Mar 2008.

[52] W. H. Press, S. A. Teukolsky, W. T. Vetterling, and B. P. Flannery, *Numerical recipes in C (2nd ed.): the art of scientific computing*. New York, NY, USA: Cambridge University Press, 1992.

[53] T. V. Waterschoot, V. L. Nir, J. Duplicy, and M. Moonen, "Analytical Expressions for the Power Spectral Density of CP-OFDM and ZP-OFDM Signals," *IEEE Signal Processing Letters*, vol. 17, no. 4, pp. 371–374, 2010.

[54] A. P. Stephens *et al.*, "IEEE 802.11 TGn Comparison Criteria," *IEEE 802.11–03/813r31*, July 2004.

[55] T. Pollet, M. V. Bladel, and M. Moeneclaey, "BER sensitivity of OFDM systems to carrier frequency offset and Wiener phase noise," *IEEE Transactions on Communications*, vol. 43, no. 2, pp. 191–193, 1995.

[56] Y. Choi, P. Voltz, and F. Cassara, "On channel estimation and detection for multicarrier signals in fast and selective Rayleigh fading channels," *IEEE Transactions on Communications*, vol. 49, no. 8, pp. 1375–1387, 2001.

[57] M. Simon and M. Alouini, *Digital Communication over Fading Channels*. Wiley Series in Telecommunications and Signal Processing, Wiley, 2004.

[58] F. Peng, J. Zhang, and W. E. Ryan, "Adaptive Modulation and Coding for IEEE 802.11n," *2007 IEEE Wireless Communications and Networking Conference*, pp. 656–661, Mar. 2007.

[59] H. G. Myung, J. Lim, and D. J. Goodman, "Single carrier FDMA for uplink wireless transmission," *IEEE Vehicular Technology Magazine*, pp. 30–38, September 2006.

[60] LAN/MAN Standards Committee of the IEEE Computer Society, "Supplement to IEEE Standard for Information Technology- Telecommunications and Information Exchange Between Systems-Local and Metropolitan Area Networks- Specific Requirements- Part 11: Wireless LAN Medium Access Control (MAC) and Physical Layer (PHY) Specifications: Higher-Speed Physical Layer Extension in the 2.4 GHz Band," *IEEE Std 802.11b™-1999*, 2000.

[61] LAN/MAN Standards Committee of the IEEE Computer Society, "Wireless LAN Medium Access Control (MAC) and Physical Layer (PHY) Specifications Amendment 4: Further Higher Data Rate Extension in the 2.4 GHz Band," *IEEE Std 802.11g™-2003*, 2003.

[62] LAN/MAN Standards Committee of the IEEE Computer Society, "Supplement to IEEE Standard for Information Technology - Telecommunications and Information Exchange Between Systems - Local and Metropolitan Area Networks - Specific Requirements. Part 11: Wireless LAN Medium Access Control (MAC) and Physical Layer (PHY) Specifications: High-Speed Physical Layer in the 5 GHz Band," *IEEE Std 802.11a™-1999*, 1999.

[63] LAN/MAN Standards Committee of the IEEE Computer Society, "Wireless LAN Medium Access Control (MAC) and Physical Layer (PHY) Specifications Amendment 5: Enhancements for Higher Throughput," *IEEE Std 802.11n™-2009 (Amendment to IEEE Std 802.11-2007 as amended by IEEE Std 802.11k-2008, IEEE Std 802.11r-2008, IEEE Std 802.11y-2008, and IEEE Std 802.11w-2009)*, 2009.

[64] LAN/MAN Standards Committee of the IEEE Computer Society, "IEEE Standard for Information technology – Telecommunications and information exchange between systems – Local and metropolitan area networks – Specific requirements – Part 11: Wireless LAN Medium Access Control (MAC) and Physical Layer (PHY) Specifications," *IEEE Std 802.11™-2007 (Revision of IEEE Std 802.11-1999)*, 2007.

[65] E. Perahia and R. Stacey, *Next Generation Wireless LANs: Throughput, Robustness, and Reliability in 802.11n*. Next Generation Wireless LANs: Throughput, Robustness, and Reliability in 802.11n, Cambridge University Press, 2008.

[66] M. Morelli and C. Kuo, "Synchronization techniques for orthogonal frequency division multiple access (OFDMA): A tutorial review," *Proceedings of the IEEE*, vol. 95, pp. 1394–1427, July 2007.

[67] IEEE Computer Society, "Carrier sense multiple access with Collision Detection (CSMA/CD) Access Method and Physical Layer Specifications," *IEEE 802™ Part 3 (802.3™)*, 2008.

[68] G. Bianchi, "Performance analysis of the IEEE 802.11 distributed coordination function," *IEEE Journal on Selected Areas in Communications*, vol. 18, pp. 535–547, Mar. 2000.

[69] Z. Hadzi-Velkov and B. Spasenovski, "On the Capacity of IEEE 802.11 DCF with Capture in Multipath-Faded Channels," *International Journal of Wireless Information Networks*, vol. 9, no. 3, pp. 191–199, 2002.

[70] G. Xiaohu, Y. Dong, and Z. Yaoting, "Throughput analysis considering capture effect in IEEE 802.11 networks," *Proceedings of the 6th international IFIP-TC6 conference on Ad Hoc and sensor networks, wireless networks, next generation internet*, no. 60610106111, pp. 1165–1168, 2007.

[71] Z. Zeng, Y. Yang, and J. C. Hou, "How Physical Carrier Sense Affects System Throughput in IEEE 802.11 Wireless Networks," *IEEE International Conference on Computer Communications (INFOCOM)*, pp. 1445–1453, Apr. 2008.

[72] A. Mishra, M. Shin, and W. Arbaugh, "An empirical analysis of the IEEE 802.11 MAC layer handoff process," *ACM SIGCOMM Computer Communication Review*, vol. 33, pp. 93–102, Apr. 2003.

[73] R. Raghavendra, E. M. Belding, K. Papagiannaki, and K. C. Almeroth, "Unwanted Link Layer Traffic in Large IEEE 802.11 Wireless Networks," *IEEE Transactions on Mobile Computing*, vol. 9, pp. 1212–1225, Sept. 2010.

[74] M. Pursley and D. Taipale, "Error Probabilities for Spread-Spectrum Packet Radio with Convolutional Codes and Viterbi Decoding," *IEEE Transactions on Communications*, vol. 35, pp. 1–12, Jan. 1987.

[75] D. Haccoun and G. Begin, "High-rate punctured convolutional codes for Viterbi and sequential decoding," *IEEE Transactions on Communications*, vol. 37, no. 11, pp. 1113–1125, 1989.

[76] J. G. Proakis, *Digital Communications*. 2001.

[77] J. Lassing, T. Ottosson, and E. Strom, "On the union bound applied to convolutional codes," *IEEE 54th Vehicular Technology Conference. VTC Fall 2001. Proceedings (Cat. No.01CH37211)*, vol. 4, pp. 2429–2433.

[78] D. Qiao, S. Choi, and K. G. Shin, "Goodput analysis and link adaptation for IEEE 802.11a wireless LANs," *IEEE Transactions on Mobile Computing*, vol. 1, pp. 278–292, Oct. 2002.

[79] M. Beyer, "Real World Performance of Rate Adaptive OFDM Feedback Jamming based Wireless Multicast," Master's thesis, Saarland University, 2012.

[80] J. Camp and E. W. Knightly, "Modulation rate adaptation in urban and vehicular environments: cross-layer implementation and experimental evaluation," *Proceedings of the 14th ACM international conference on Mobile computing and networking*, pp. 315–326, 2008.

[81] I. Tinnirello and A. Sgora, "A Kalman Filter Approach for Distinguishing Channel and Collision Errors in IEEE 802.11 Networks," in *IEEE Global Telecommunications Conference (GLOBECOM)*, pp. 1–5, 2008.

[82] A. Kamerman and L. Monteban, "WaveLAN-II: A High-Performance Wireless LAN for the Unlicensed Band," *Bell Labs Technical Journal*, vol. 2, no. 3, pp. 118–133, 1997.

[83] M. Lacage, M. M. H. Manshaei, and T. Turletti, "IEEE 802.11 rate adaptation: a practical approach," *ACM international symposium on Modeling, analysis and simulation of wireless and mobile systems*, pp. 126–134, 2004.

[84] J. C. Bicket, *Bit-rate Selection in Wireless Networks*. PhD thesis, 2005.

[85] G. Holland, N. Vaidya, and P. Bahl, "A rate-adaptive MAC protocol for multi-Hop wireless networks," *Proceedings of the 7th annual international conference on Mobile computing and networking - MobiCom '01*, no. July, pp. 236–251, 2001.

[86] J. Kim, S. Kim, S. Choi, and D. Qiao, "CARA: Collision-Aware Rate Adaptation for IEEE 802.11 WLANs," *IEEE International Conference on Computer Communications (INFOCOM)*, pp. 1–11, Apr. 2006.

[87] F. Maguolo, M. Lacage, and T. Turletti, "Efficient collision detection for auto rate fallback algorithm," *IEEE Symposium on Computers and Communications (ISCC)*, pp. 25–30, 2008.

[88] S. H. Y. Wong, S. Lu, H. Yang, and V. Bharghavan, "Robust rate adaptation for 802.11 wireless networks," *Proceedings of the 12th annual international conference on Mobile computing and networking (MobiCom)*, pp. 146–158, 2006.

[89] D. Tse, "Optimal power allocation over parallel Gaussian broadcast channels," *International Symposium on Information Theory*, 1997.

[90] V. R. Cadambe and S. A. Jafar, "Interference Alignment and Spatial Degrees of Freedom for the," *IEEE International Conference on Communications (ICC)*, pp. 971 – 975, 2008.

[91] E. Telatar, "Capacity of Multi-antenna Gaussian Channels," *European transactions on telecommunications*, vol. 10, no. 6, pp. 585–595, 1999.

[92] G. Foschini, M. Gans, and J. Kahn, "Fading correlation and its effect on the capacity of multielement antenna systems," *IEEE Transactions on Communications*, vol. 48, pp. 502–513, Mar. 2000.

[93] C. Zimmermann, M. Paasch, O. Weikert, and U. Zölzer, "On Investigating Spatial Correlations of MIMO Indoor Channels," in *Proc. 12th International OFDM-Workshop 2007 (InOWo'07)*, 2007.

[94] L. Schumacher, K. Pedersen, and P. Mogensen, "From antenna spacings to theoretical capacities-guidelines for simulating MIMO systems," in *IEEE International Symposium on Personal, Indoor and Mobile Radio Communications*, vol. 2, pp. 587–592, IEEE, 2002.

[95] N. Czink, X. Yin, H. OZcelik, M. Herdin, E. Bonek, and B. Fleury, "Cluster Characteristics in a MIMO Indoor Propagation Environment," *IEEE Transactions on Wireless Communications*, vol. 6, pp. 1465–1475, Apr. 2007.

[96] H. Weingarten, Y. Steinberg, and S. Shamai, "The Capacity Region of the Gaussian Multiple-Input Multiple-Output Broadcast Channel," *IEEE Transactions on Information Theory*, vol. 52, pp. 3936–3964, Sept. 2006.

[97] I. Livni, A. Khina, A. Hitron, and U. Erez, "Space-time MIMO multicasting," *CoRR*, vol. abs/1204.1, 2012.

[98] LAN/MAN Standards Committee of the IEEE Computer Society, "Wireless LAN Medium Access Control (MAC) and Physical Layer (PHY) Specifications Amendment 8: IEEE 802.11 Wireless Network Management," *IEEE Std 802.11v™-2011 (Amendment to IEEE Std 802.11, 2007 Edition)*, 2011.

[99] A. Basalamah and T. Sato, "A Comparison of Packet-Level and Byte-Level Reliable FEC Multicast Protocols for WLANs," *IEEE Global Telecommunications Conference (GLOBECOM)*, pp. 4702–4707, Nov. 2007.

[100] L. Rizzo, "Effective erasure codes for reliable computer communication protocols," *ACM SIG-COMM Computer Communication Review*, vol. 27, pp. 24–36, Apr. 1997.

[101] ETSI, *EN 301 192 V1.4.2; Digital Video Broadcasting (DVB); DVB specification for data broadcasting.* European Telecommunications Standards Institute, Apr. 2008.

[102] ETSI, *EN 302 304 V1.1.1; Digital Video Broadcasting (DVB); Transmission System for Handheld Terminals (DVB-H).* European Telecommunications Standards Institute, Nov. 2004.

[103] P. Frenger, S. Parkvall, and E. Dahlman, "Performance comparison of HARQ with chase combining and incremental redundancy for HSDPA," in *IEEE Vehicular Technology Conference*, pp. 1829–1833, 2001.

[104] ETSI, *TS 136 322 V11.1.0; LTE; Evolved Universal Terrestrial Radio Access (E-UTRA); Radio Link Control (RLC) protocol specification (3GPP TS 36.322 version 11.0.0 Release 11).* European Telecommunications Standards Institute, Oct. 2012.

[105] T. Cover, "Comments on broadcast channels," *IEEE Transactions on Information Theory*, vol. 44, pp. 2524–2530, Oct. 1998.

[106] T. Marzetta and B. Hochwald, "Capacity of a mobile multiple-antenna communication link in Rayleigh flat fading," *IEEE Transactions on Information Theory*, vol. 45, no. 1, pp. 139–157, 1999.

[107] M. Costa, "Writing on dirty paper (corresp.)," *IEEE Transactions on Information Theory*, vol. 29, no. 3, pp. 439–441, 1983.

[108] R. Knopp and P. Humblet, "Information capacity and power control in single-cell multiuser communications," *IEEE International Conference on Communications (ICC)*, vol. 1, pp. 331–335, 1995.

[109] P. Gopala and H. El Gamal, "Opportunistic multicasting," *Asilomar Conference on Signals, Systems and Computers*, pp. 845–849, 2004.

[110] P. Gopala and H. El Gamal, "On the throughput-delay tradeoff in cellular multicast," in *International Conference on Wireless Networks, Communications and Mobile Computing*, vol. 2, pp. 1401–1406, IEEE, 2005.

[111] U. C. Kozat, "On the Throughput Capacity of Opportunistic Multicasting with Erasure Codes," *IEEE International Conference on Computer Communications (INFOCOM)*, pp. 520 – 528, 2008.

[112] P. B. Danzig, *Optimally Selecting the Parameters of Adaptive Backoff Algorithms for Computer Networks and Multiprocessors*. PhD thesis, 1989.

[113] A. Erramilli and R. Singh, "A reliable and efficient multicast protocol for broadband broadcast networks," *Proceedings of ACM SIGCOMM*, pp. 343–352, 1987.

[114] M. H. Ammar, "Probabilistic multicast: Generalizing the multicast paradigm to improve scalability," *13th Proceedings IEEE INFOCOM '94. Networking for Global Communications.*, vol. 2, pp. 848 – 855, 1994.

[115] J. Nonnenmacher and E. Biersack, "Optimal multicast feedback," *IEEE International Conference on Computer Communications (INFOCOM)*, pp. 964–971, 1998.

[116] J. Kuri and S. Kasera, "Reliable multicast in multi-access wireless LANs," *IEEE International Conference on Computer Communications (INFOCOM)*, vol. 7, no. 4, pp. 359–369, 1999.

[117] IEEE Computer Society, "Wireless LAN Medium Access Control (MAC) and Physical Layer (PHY) Specifications, Amendment 2: MAC Enhancements for Robust Audio Video Streaming," *IEEE 802.11aa™(Amendment to IEEE Std 802.11™-2012)*, 2012.

[118] Y. Cai, S. Lu, L. Zhang, C. Wang, P. Skov, Z. He, and K. Niu, "Reduced Feedback Schemes for LTE MBMS," *VTC Spring 2009 - IEEE 69th Vehicular Technology Conference*, pp. 1–5, Apr. 2009.

[119] D. Dujovne and T. Turletti, "Multicast in 802.11 WLANs: an experimental study," *ACM international symposium on Modeling analysis and simulation of wireless and mobile systems*, pp. 130–138, 2006.

[120] S. Gupta, V. Shankar, and S. Lalwani, "Reliable multicast MAC protocol for wireless LANs," in *IEEE International Conference on Communications (ICC)*, vol. 85287, pp. 93–97, Ieee, 2003.

[121] Z. Li, *Multicast MAC Extensions for High Rate Real-Time Traffic in Wireless LANs*. PhD thesis, Saarland University, 2011.

[122] Z. Hadzi-Velkov and B. Spasenovski, "Capture effect in IEEE 802.11 basic service area under influence of Rayleigh fading and near/far effect," *The 13th IEEE International Symposium on Personal, Indoor and Mobile Radio Communications*, no. 3, pp. 172–176, 2002.

[123] J. C. Arnbak and W. Van Blitterswijk, "Capacity of slotted ALOHA in Rayleigh-fading channels," *IEEE Journal on Selected Areas in Communications*, vol. 5, no. 2, pp. 261–269, 1987.

[124] D. Davis and S. Gronemeyer, "Performance of slotted ALOHA random access with delay capture and randomized time of arrival," *IEEE Transactions on Communications*, vol. 28, no. 5, pp. 703–710, 1980.

[125] M. Zorzi and R. Rao, "Capture and retransmission control in mobile radio," *IEEE Journal on Selected Areas in Communications*, vol. 12, no. 8, pp. 1289–1298, 1994.

[126] M. Zorzi, "Mobile radio slotted ALOHA with capture and diversity," *IEEE International Conference on Computer Communications (INFOCOM)*, vol. 1, no. 2, pp. 227–239, 1995.

[127] M. Zorzi, "Capture probabilities in random-access mobile communications in the presence of Rician fading," *IEEE Transactions on Vehicular Technology*, vol. 46, no. 1, pp. 96–101, 1997.

[128] J. Sanchez Garcia and D. R. Smith, "Capture probability in Rician fading channels with power control in the transmitters," *IEEE Transactions on Communications*, vol. 50, pp. 1889–1891, Dec. 2002.

[129] J. Miroll, Z. Li, and T. Herfet, "Wireless Feedback Cancellation for Leader-Based MAC Layer Multicast Protocols," in *IEEE International Symposium on Consumer Electronics (ISCE)*, 2010.

[130] J. Miroll and T. Herfet, "Efficient OFDM-based WLAN-Multicast with Feedback Aggregation, Power Control and Rate Adaptation," *Elsevier Computer Communications*, vol. 35, no. 18, 2012.

[131] J. Lee, W. Kim, S.-J. Lee, D. Jo, J. Ryu, T. Kwon, and Y. Choi, "An experimental study on the capture effect in 802.11a networks*+," *Proceedings of the the second ACM international workshop on Wireless network testbeds, experimental evaluation and characterization - WinTECH '07*, p. 19, 2007.

[132] Z. Li and T. Herfet, "MAC Layer Multicast Error Control for IPTV in Wireless LANs," *IEEE Transactions on Broadcasting*, vol. 55, pp. 353–362, June 2009.

[133] Y. Park, Y. Seok, T. Kwon, Y. Choi, and J.-M. Bonnin, "A Rate-Adaptive Multimedia Multicasting Mechanism in Multi-Rate 802.11 Wireless LANs," *IEEE Consumer Communications and Networking Conference (CCNC)*, pp. 23–35, 2008.

[134] C. Xi, W. YunHeng, and L. JianHua, "Cross-layer link rate adaptation for high performance multimedia broadcast over WLANs," in *IEEE GLOBECOM Workshops*, pp. 965–969, IEEE, 2010.

[135] J. Villalón, Y. Seok, T. Turletti, P. Cuenca, and L. Orozco-Barbosa, "ARSM: Auto Rate Selection Multicast Mechanism for Multi-Rate Wireless LANs," in *Personal Wireless Communications*, pp. 239–250, Springer, 2006.

[136] C. Hoffmann, M. Hossein, and T. Turletti, "CLARA: closed-loop adaptive rate allocation for IEEE 802.11 wireless LANs," *International Conference on Wireless Communications, Networking and Mobile Computing (WiCOM)*, vol. 1, pp. 668–673, 2005.

[137] N. Choi, Y. Seok, T. Kwon, and Y. Choi, "Multicasting multimedia streams in IEEE 802.11 networks: a focus on reliability and rate adaptation," *Springer Wireless Networks*, vol. 17, pp. 119–131, Aug. 2010.

[138] H. Kim, K.-y. Choi, H. Lee, and I. Kang, "A simple congestion-resilient link adaptation algorithm for IEEE 802.11 WLANs," in *IEEE Global Communication Conference (GLOBECOM)*, 2006.

[139] Z. Li and T. Herfet, "MAC Layer Support for High Rate Video Multicast Applications in Wireless LANs," in *7th International ITG Conference on Source and Channel Coding*, 2008.

Related Publications

- J. **Miroll** and T. Herfet, "Efficient OFDM-based WLAN-Multicast with Feedback Aggregation, Power Control and Rate Adaptation," *Elsevier Computer Communications*, vol. 35, no. 18, 2012.

- J. **Miroll**, M. Beyer, and T. Herfet, "An OFDM WLAN Multicast Hybrid Erasure Correction Prototype with Feedback Aggregation and Rate Adaptation," in *Proc. 17th International OFDM Workshop 2012 (InOWo'12)*, 2012.

- J. **Miroll** and T. Herfet, "On error correction based on feedback jamming in OFDM-based wireless MBMS systems," in *Proc. Consumer Communications and Networking Conference (CCNC)*, pp. 776–781, 2012.

- J. **Miroll**, Z. Li, and T. Herfet, "Efficient OFDM-based WLAN-Multicast with Feedback Aggregation and Power Control," in *Proc. Networked & Electronic Media (NEM) Summit*, 2011.

- M. Gorius, J. **Miroll**, and T. Herfet, "Service compatible efficient 3D-HDTV Delivery," in *Proc. 14. ITG Fachtagung für Elektronische Medien (Dortmunder Fernsehseminar)*, 2011.

- M. Gorius, J. **Miroll**, M. Karl, and T. Herfet, "Predictable reliability and packet loss domain separation for IP media delivery," in *Proc. IEEE International Conference on Communications (ICC)*, 2011.

- J. **Miroll**, Z. Li, and T. Herfet, "Wireless Feedback Cancellation for Leader-Based MAC Layer Multicast Protocols," in *Proc. IEEE International Symposium on Consumer Electronics (ISCE)*, 2010.

- Z. Li, J. **Miroll**, and T. Herfet, "Video transmission in IEEE 802.11aa," in *Proc. Networked & Electronic Media (NEM) Summit*, 2009.

- J. **Miroll** and T. Herfet, "On the applicability of predictive multicast rate adaptation for audiovisual streaming in WLANs," in *Proc. Networked & Electronic Media (NEM) Summit*, 2008.

- A. Spenst, J. **Miroll**, and T. Herfet, "An Implementation of the User-Centric QoS Management Approach in Wireless Home Networks," in *Proc. 4th International Symposium on Wireless Communication Systems*, pp. 107–112, IEEE, Oct. 2007.

List of Symbols

$S(f_\mathrm{d}, \tau)$	Doppler-variant impulse response
$H(f_\mathrm{d}, f)$	Doppler-variant transfer function
d_0	breakpoint distance
$h(t, \tau)$	time-variant impulse response
$T(t, f)$	time-variant transfer function
c	speed of light
z	capture threshold
$c(t)$	time-variant channel coefficient
R	code rate
B_coh	coherence bandwidth
T_coh	coherence time
τ	delay
T_ds	delay spread
μ_rms	delay spread (root-mean-squared)
$\delta(t)$	Dirac delta distribution
f_d	Doppler frequency
f_D	Doppler shift maximum
E	expected value of a random variable
f	frequency
n	forward error coding block length
m	forward error coding parity symbols
k	forward error coding systematic symbols
$\mathcal{F}\{s(t)\}$	Fourier transform of $s(t)$, where $s(t) \bullet\!\!-\!\!\circ\ S(f)$
L_fs	path loss in free space
T_GI	guard interval duration
T_GI2	doubled IEEE 802.11 guard interval duration
L_B	link budget
N_CBPS	number of coded bits per symbol
N_DBPS	number of data bits per symbol
N	number of FFT/IFFT samples
N_i	IFFT implementation size
$n(t)$	noise component
N_0	noise power
Δ_f	OFDM subcarrier spacing
p_cf	conditional probability of failure to request a retransmission
$p_\mathrm{x}(x)$	probability density function of x
ρ	packet erasure probability
ρ_L	packet erasure probability at the leader
L	path loss
n	path loss exponent
T_P	preamble duration
$\chi_\mathrm{rc}(t, r)$	raised cosine pulse with roll-off factor r
$r(t)$	received signal
$R(f)$	frequency spectrum of received signal

P_r	received signal power level
S_RX	receiver sensitivity
$\sqcap(t)$	rectangular pulse: $\sqcap(t) = \begin{cases} 1 & -1/2 \le t \le 1/2 \\ 0 & else \end{cases}$
K	Rician fading line-of-sight component ratio K
r	roll-off factor
T_s	sampling interval
$s(t)$	sent signal
$S(f)$	frequency spectrum of sent signal
T_sig	IEEE 802.11 signal field symbol duration
γ_req	signal-to-noise ratio requirement
γ	signal-to-noise ratio random variable
T_sym	symbol duration
E_s	symbol energy
T_FFT	fast Fourier transform and core symbol duration
$T_\mathrm{frame}(x)$	frame duration for x Bytes of data
t_RC	raised-cosine duration
P_t	transmit power
N_u	number of used OFDM subcarriers
$\Phi_\mathrm{h}(\Delta t, \tau)$	delay cross power spectral density
$\Phi_\mathrm{H}(f_\mathrm{d}, \Delta f)$	Doppler cross power spectral density
$\Phi_\mathrm{S}(f_\mathrm{d}, \Delta f)$	Doppler delay cross power spectral density
$\phi_\mathrm{T}(\Delta t, \Delta f)$	time frequency correlation function
$X(f)$	Fourier transform of $x(t)$

Index

The MathWorks® Matrix Laboratory, 97, 99